UC Berkeley
UC Berkeley Electronic Theses and Dissertations

Title

Intrinsic Regional Brain Dynamics in Health and Disease

Permalink

https://escholarship.org/uc/item/1q9138m3

Author

Lurie, Daniel Jonathan

Publication Date

2022

Peer reviewed|Thesis/dissertation

eScholarship.org Powered by the California Digital Library
University of California

Intrinsic Regional Brain Dynamics in Health and Disease

By

Daniel Jonathan Lurie

A dissertation submitted in partial satisfaction of the

requirements for the degree of

Doctor of Philosophy

in

Psychology

in the

Graduate Division

of the

University of California, Berkeley

Committee in charge:

Professor Mark D'Esposito, Chair
Professor Kevin Weiner
Professor Lexin Li

Fall 2022

Abstract

Intrinsic Regional Brain Dynamics in Health and Disease

By

Daniel Jonathan Lurie

Doctor of Philosophy in Psychology

University of California, Berkeley

Professor Mark D'Esposito, Chair

The brain is a complex dynamical system in which many different areas interact to process information in support of adaptive cognition and behavior. Just as brain areas vary in their local anatomical features and patterns of connectivity to remote regions, so too do their dynamics, and regional differences in intrinsic dynamics are a fundamental feature of functional brain organization. Here, I present the results of three studies which use resting fMRI to investigate how multiple features of intrinsic regional dynamics vary across the human brain, their relationship to the anatomical and connectomic properties of each area, and the extent to which these dynamics are disrupted in patients with focal brain lesions. First, I show that a key property of intrinsic regional dynamics—their timescale—is related to the topological role of each region within the modular community structure of functional and structural brain networks, and that cortical areas exhibit preferential functional connectivity to other regions with similar timescales. Second, I use a data driven time series "phenotyping" approach to characterize how multiple aspects of intrinsic dynamics vary across the cerebral cortex. I find that regional BOLD dynamics can be modeled as varying a long two spatial axes, each of which captures different time series features, and which exhibit distinct relationships to anatomical and connectomic hierarchies. Finally, given findings from my first two studies which suggest a robust relationship between regional timescales and network topology, I investigate whether alterations in network topology following focal brain lesions are associated with parallel alterations in the timescale of intrinsic dynamics. While I did not find the predicted effect, I nonetheless extend my findings from the first two studies by showing that timescales are related to multiple features of regional network topology both within and across individuals. Together, these results provide important new insights into a key feature of functional brain organization.

Dedicated to my parents, whose love and support knows no bounds.

Without you, none of this would be possible.

Acknowledgements

First, I would like to thank my advisor, Mark D'Esposito. Doing a PhD isn't easy for anyone, and life circumstances made things particularly difficult for me. Mark stood by me through thick and thin, and I will always be very grateful for his advice and support. I am also grateful for the support, advice, and encouragement I have received from other faculty mentors at UC Berkeley, in particular Kevin Weiner, Rich Ivry, Bob Knight, Lexin Li, Ann Kring, and Fritz Sommer. Thanks also to Mac Shine for his mentorship, and to Jennifer Mangels and Mike Milham for being living examples of the sentiment that a mentor's work doesn't end when a trainee leaves the lab.

I am also indebted to my colleagues in the D'Esposito lab. I am privileged to have had the opportunity to work with so many people who are not only smart, but also kind. I would particularly like to thank Ioannis Pappas for being such an enthusiastic mentor during my dissertation research. Special thanks also to Daniel Toker, Savannah Cookson, Justin Riddle, Elizabeth Lorenc, Raana Mohyee, Adam Eichenbaum, Jacob Miller, David Vogelsang, Daniella Furman, Regina Lapate, Arielle Tambini, Derek Nee, and JB Poline.

I am fortunate to have been involved in many collaborations during my PhD, and I am indebted to the brilliant colleagues who I worked with on these projects. In particular—in addition to the collaborators who I have already mentioned above—I would also like to specifically acknowledge Daniel Kessler, Vince Calhoun, Adam Kimbrough, Ben Fulcher, and Ben Inglis.

Last but not least, thank you to my friends and family. I could not have done this without you.

Table of Contents

Introduction	1
Cortical timescales and the multi-scale modular organization of structural and functional brain networks	3
Gradients of intrinsic dynamics show distinct relationships with anatomical and connectomic hierarchies in the cerebral cortex	46
Investigating the impact of focal brain lesions on regional dynamics and functional network topology	106
Conclusion	141

Introduction

The brain is a complex dynamical system in which over 80 billion neurons interact via trillions of synapses. Like all complex systems, these interactions give rise to emergent phenomena—sensory experience, complex behavior, thoughts and feelings—which are more than the simple sum of their parts, and which change continually from moment to moment. As such, any attempt to build a mechanistic understanding of brain function will necessarily require knowledge of how a multiplicity of factors interact to shape the neural dynamics underlying cognition and behavior. In this dissertation, I make my own small contribution to this enormous scientific undertaking.

In Chapter 1, I investigate the relationship between a key property of intrinsic regional brain activity and the organization of large-scale structural and functional connectivity networks. While there are many ways to characterize how brain areas differ in their dynamics, one measure in particular has garnered substantial scientific interest over the past decade. Specifically, multiple studies have found that the "timescale" of intrinsic brain activity—the degree to which activity is similar from one moment to the next—tends to increase along sensory processing hierarchies. This "hierarchy of timescales" is thought to reflect regional differences in information processing. Previous work suggests that the timescale of each cortical area may be related to the extent to which that area exhibits widespread connectivity to other parts of the brain, but past studies had so far failed to consider a key organizing principle which shapes the dynamics of biological systems: modularity. In modular systems, the underlying components form communities in which members of each community are more likely to interact with other members of the same community, and this architecture is seen across spatial and temporal scales ranging from genes and neurons in the brain to entire organisms within an ecosystem. Large-scale brain networks also exhibit a modular structure which can be seen in the presence of densely interconnected sets of brain areas. I demonstrate that cortical timescales—estimated from resting BOLD fMRI in human participants—are related to measures of regional connectivity which consider the role that each area plays within this modular network structure.

In Chapter 2, I move beyond the special case of timescales to explore the diversity of ways in which regional dynamics vary across cortical areas. In a data-driven analysis, I show that regional variation in intrinsic brian dynamics estimated from resting fMRI can be modeled as varying along two principal spatial axes, each of which captures a different property of dynamics. The first of these axes captures the timescale of intrinsic brain activity, while the second axis captures how the variability of intrinsic activity changes over time. Critically, I show that these axes are differentially related to regional differences in local anatomical features and inter-regional connectivity, as well as to information processing hierarchies in the cerebral cortex. I also replicate my findings from Chapter 1 that timescales are related to the modular architecture of large-scale brain networks.

In Chapter 3, I build on my prior observations of a relationship between timescales and connectivity by investigating whether intrinsic dynamics are altered in patients with focal brain lesions due to stroke. Prior work from our lab and others has found that focal brain lesions are associated with alterations in the functional connectivity of remote, undamaged brain areas, and in particular, their role within the larger network. As such, I hypothesized that cortical areas in patients would exhibit alterations in functional connectivity, and further, that these would be associated with parallel changes in timescale. While these predictions were not borne out by the data, I was able to demonstrate that previously observed associations between timescales and connectivity exist within both healthy individuals and patients with neurological illness, and that studying these associations in single-subjects can reveal additional effects beyond those visible in group-level analyses.

Together, the studies contained in this dissertation make a significant contribution to our understanding of how intrinsic brain dynamics relate to multiple other features of large-scale brain organization. I return to the implications of my findings in the Conclusion.

Cortical timescales and the multi-scale modular organization of structural and functional brain networks

Introduction

There are many different ways to characterize the properties of neural time series, ranging from simple, commonly used metrics such as amplitude and frequency, to complex, seemingly esoteric measures taken from statistical physics and chaos theory (Breakspear, 2017; Fulcher et al., 2013; Fulcher & Jones, 2017; Lubba et al., 2019; Toker et al., 2020). From this menagerie of measures, the past decade has seen estimates of neural "timescale" emerge as an increasingly popular way to study the dynamical properties of brain activity. While there are multiple ways to estimate the timescale of neural activity, their common goal is to characterize the degree to which brain activity (or the information it represents) is similar from one moment to the next. The literature on neural timescales ranges from studies using invasive recordings of individual neurons and population activity in animals (Cirillo et al., 2018; Maisson et al., 2021; Murray et al., 2014; Nougaret et al., 2021; Rossi-Pool et al., 2021; Runyan et al., 2017; Wasmuht et al., 2018) to BOLD fMRI and MEG/EEG in humans (Baldassano et al., 2017; Fallon et al., 2020; Golesorkhi et al., 2021; Hasson et al., 2008; Huang et al., 2018; Ito et al., 2020; Müller et al., 2020; Raut et al., 2020; Stephens et al., 2013; Watanabe et al., 2019; Wengler et al., 2020; Zilio et al., 2021), as well as computational models which seek to provide mechanistic explanations for regional differences in timescale (Chaudhuri et al., 2014, 2015; Demirtaş et al., 2019; Gollo et al., 2015; Li & Wang, 2022). Many of these studies suggest the presence of a "hierarchy of timescales" in the cerebral cortex which parallels information processing hierarchies, with shorter timescales in sensory and motor areas responsible for processing rapidly changing low-level sensory information and action sequences, and longer timescales in higher-order association regions which integrate information over longer periods in order to support more complex information processing (such as the construction and maintenance of increasingly abstract representations).

Computational models and emerging empirical work suggest that regional differences in neural timescales are shaped not only by heterogeneity in local circuit properties, but also the pattern of connections each region receives from distant brain areas (Baria et al., 2013; Chaudhuri et al., 2014, 2015; Demirtaş et al., 2019; Fallon et al., 2020; Gao et al., 2020; Gollo et al., 2015; Ito et al., 2020; Li & Wang, 2022; Müller et al., 2020; Sethi et al., 2017; Watanabe et al., 2019; Wengler et al., 2020). While some of this work has focused on specific aspects of inter-regional connectivity such as the proportion of feed-forward vs. feed-back connections (Chaudhuri et al., 2015) or the degree of innervation from particular thalamic populations (Müller et al., 2020), other studies have taken a more general view of the brain as a complex network. In particular, there is growing evidence that timescale hierarchies may follow connectomic hierarchies, with

highly connected "hub" regions tending to exhibit longer timescales than less topologically central areas (Baria et al., 2013; Fallon et al., 2020; Gollo et al., 2015; Sethi et al., 2017). However, these studies have so far failed to consider a key feature of how neural systems are organized: modularity.

Modularity is ubiquitous in biological systems (Wagner et al., 2007), and describes an architecture in which the system as a whole can be decomposed into multiple smaller communities with dense internal connectivity but relatively sparse connectivity to other communities (Girvan & Newman, 2002; Newman, 2006). In the context of brain networks, communities are commonly defined based on patterns of structural or functional connectivity (Sporns & Betzel, 2016). This modular organization has been shown to exist across multiple scales (Akiki & Abdallah, 2019; Ashourvan et al., 2019; Betzel & Bassett, 2017; Meunier et al., 2009) and is thought to play a key role in facilitating functional specialization and flexible reconfiguration by balancing the competing demands of integration and segregation (Bertolero et al., 2015, 2018; Bullmore & Sporns, 2009; Sporns, 2013; Sporns & Betzel, 2016). By considering this modular organization, we can take a much more nuanced view of the role each region plays within the larger network. In particular, beyond identifying "global" hubs (as has been done in prior studies of the relationship between timescales and network topology), we can characterize whether each brain area has widespread connectivity within its own community, or diverse connections across multiple communities (Guimerà & Amaral, 2005; Guimerà & Nunes Amaral, 2005; Power et al., 2013; van den Heuvel & Sporns, 2013a).

We hypothesized that regional differences in intrinsic brain dynamics would be associated with the modular organization of structural and functional brain networks, and specifically that brain areas with extensive within-community connectivity or diverse connectivity across communities would tend to have longer timescales, consistent with their putative roles in integrating information within and between network modules. To test this hypothesis, we first used resting fMRI to estimate timescales across the cerebral cortex of human participants, as well as in many subcortical structures. We show that cortical timescales estimated from BOLD fMRI exhibit multiple consistent features across independent datasets, but that timescales in subcortical areas are relatively less consistent. Further, we replicate prior observations that regions with long timescales tend to have extensive structural connectivity. Most significantly, we characterize the community structure of structural and functional brain networks across multiple scales and demonstrate that cortical timescales correlate with the extent of within-community functional connectivity and the diversity of regional structural connectivity. Finally, we show that functional connectivity between brain areas with similar timescales tends to be stronger than functional connectivity between areas with dissimilar timescales, and discuss the implications of these findings for our understanding of dynamical and connectomic hierarchies within the human brain. Our major methods and primary hypotheses were preregistered with the Open Science Framework (Lurie, 2018), all data used in our analyses are publicly available, and we provide software and scripts to fully and easily reproduce all of the reported results.

Methods

Resting BOLD fMRI data

For our initial ("discovery") analysis, we analyzed data from 93 healthy young individuals (ages 18-35) from the Enhanced Nathan Kline Institute-Rockland Sample (Nooner et al., 2012). These individuals were selected based on the absence of any history of psychiatric or neurological illness, as well as the presence of complete imaging data (i.e. no missing scans). Resting fMRI scans were 10 minutes in duration with TR/TE = 1400/30ms and 2mm isotropic voxels. Data were preprocessed using FMRIPRPEP (Esteban et al., 2019). GLM denoising was applied using Nilearn (Abraham et al., 2014) and included 24 motion parameters plus 6 aCompCor components containing nuisance signals from WM and CSF voxels (Behzadi et al., 2007), as well as the mean whole brain signal.

For our validation analysis, we selected a sample of 100 unrelated healthy young individuals (ages 21-35) from the Human Connectome Project (Van Essen et al., 2013) based on a subject list provided by (Shine et al., 2016). For each individual, we analyzed the first 15 minute resting fMRI scan (TR/TE = 720/33ms, 2mm isotropic voxels). We used minimally preprocessed data (Glasser et al., 2013) provided by HCP which had undergone ICA-FIX denoising (Griffanti et al., 2014) and global signal regression.

Functional connectivity network construction

For each participant, we estimated functional connectivity as the Pearson correlation between the time series of each pair of ROIs. We then applied the Fisher r-to-z transform to the correlations estimated from each individual before averaging edges across participants to create a group-level network. Due to uncertainties regarding the interpretation of negative correlations in studies of functional connectivity (Fox et al., 2009; Murphy et al., 2009; Rubinov & Sporns, 2010), all edges with negative z-scores were set to zero. Functional connectivity networks were otherwise un-thresholded. This process was repeated separately for the discovery and validation datasets. In order to identify common functional network communities across datasets, we combined the average FC networks from the discovery and validation data into a single common network prior to community detection. However, measures of regional network topology (i.e. degree, PC, and WD) were computed separately for each dataset based on its respective average FC network.

Structural connectivity network construction

We constructed a single structural connectivity network from a publicly available, expert-curated voxelwise "population-average" atlas of the human structural connectome (Yeh et al., 2018). This atlas was derived from high-resolution, multi-shell diffusion MRI images from 842 participants from the Human Connectome Project (Van Essen et al., 2013). Complete details of how the atlas was produced can be found in (Yeh et al., 2018), but we review them briefly here. Images for each participant were transformed to MNI space using q-space

diffeomorphic registration (Yeh & Tseng, 2011), which preserves spins and fiber geometry and estimates the spin distribution function (SDF) at each voxel. Voxelwise SDFs were averaged across participants to create a group-average template, after which multiple runs of deterministic tractography (Yeh et al., 2013) were used to estimate 550,000 streamlines describing connectivity across the entire brain. All streamlines were then reviewed and labeled by a team of expert neuroanatomists to identify fiber tracts, remove anatomically implausible (i.e. false positive) connections, and manually seed additional streamlines to identify known fascicles which were missing from the initial set of connections. The final atlas contains ~145,000 voxelwise streamlines describing the representative white matter connectivity of cortical and subcortical regions in the human brain.

Based on this atlas, we estimated structural connectivity as the number of streamlines connecting each pair of ROIs. The resulting whole-brain connectome had an edge density of 0.103, with all but two regions connected to the rest of the network by at least one streamline. However, because the distribution of streamline counts was highly skewed and spanned several orders of magnitude (0 to 1027), we followed the common practice of applying a log transformation to edge weights prior to subsequent analyses (Fornito et al., 2016). Due to the nature of the log transformation (i.e. log(1) = 0), edges with only a single streamline were set to zero, leading to four additional regions becoming disconnected (Fig. S1).

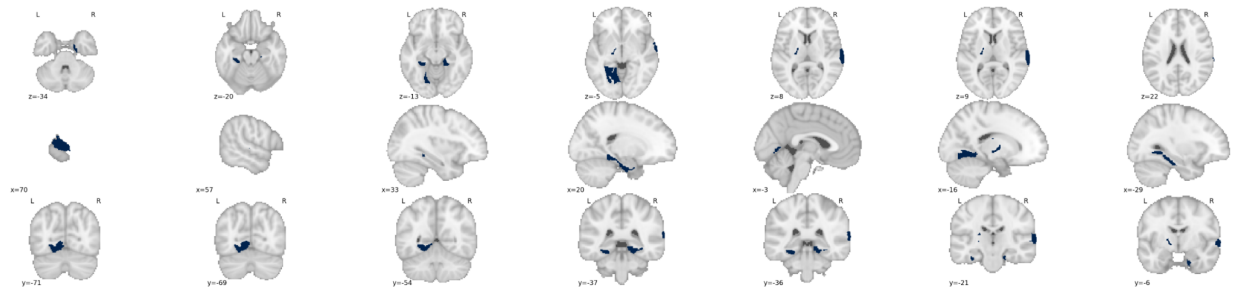


Figure S1: Regions of interest with no structural connections after log-transforming streamline counts.

Multiscale community detection

To identify network communities at multiple scales, we applied the Louvain algorithm (Blondel et al., 2008) to the structural and functional connectivity networks while varying the resolution parameter (γ) across a range of values (0.5 to 3.5, in increments of 0.1). As γ increases, the algorithm is biased toward detecting smaller and smaller communities, thus also increasing the number of communities identified. Like all community detection methods which rely on modularity maximization, the Louvain algorithm is stochastic, and the partitions it identifies are degenerate (i.e. many possible partitions will have approximately the same modularity) (Good et al., 2010). As such, we ran the algorithm 1,000 times for each value of γ and used consensus-based clustering (Bassett et al., 2013; Lancichinetti & Fortunato, 2012) to identify a single stable partition at each resolution. This resulted in 31 community partitions for each

network, with the number of non-singleton communities (# regions > 1) ranging from 3 to 21 for the functional connectivity network, and 2 to 13 for the structural connectivity network.

Identification of maximally representative community partitions

To identify the maximally representative partition (MRP) for each network, we first computed the variation of information (VI) (Meilă, 2003)—an information-theoretic measure of distance—between each pair of partitions across all 31 scales. We then identified the MRP for each network as the partition with the lowest median VI (and thus the highest similarity with the most other partitions). We note that our approach is conceptually different from how VI (and other measures of partition similarity, such as the Rand index) have most often previously been used to select brain network partitions (i.e. to select the scale at which stochastic runs of a community detection algorithm show the least variability (e.g. (Betzel et al., 2017; Betzel & Bassett, 2017; Shafiei et al., 2019)), and is more closely analogous to the approach taken by (He et al., 2018) and (Bazinet et al., 2021), who used partition similarity to identify domains of stability across scales. Our method builds on this work and is based on the idea that representative features of community structure should be present across a wide range of scales, particularly in a hierarchically organized system like the brain.

For the functional connectivity network, the community partition at γ = 1.8 (8 communities) exhibited the lowest median VI (Fig. S2A), and visual inspection of the pairwise VI matrix (Fig. S2B) confirmed that this partition had good similarity to other partitions across a wide range of scales, ranging from from γ = 1.3 (5 communities) to γ = 3.5 (21 communities). The selected partition at γ = 1.8 also occurs at the visual asymptote of the modularity maximization function (Fig. S2A), such that past this point, modularity (Q) only shows modest gains with increasing resolution. In agreement with prior studies of functional brain organization, the 8 communities identified at this resolution (Fig. S3) show excellent correspondence with "canonical" macro-scale human functional brain networks (Power et al., 2011; Smith et al., 2009; Uddin et al., 2019; Yeo et al., 2011).

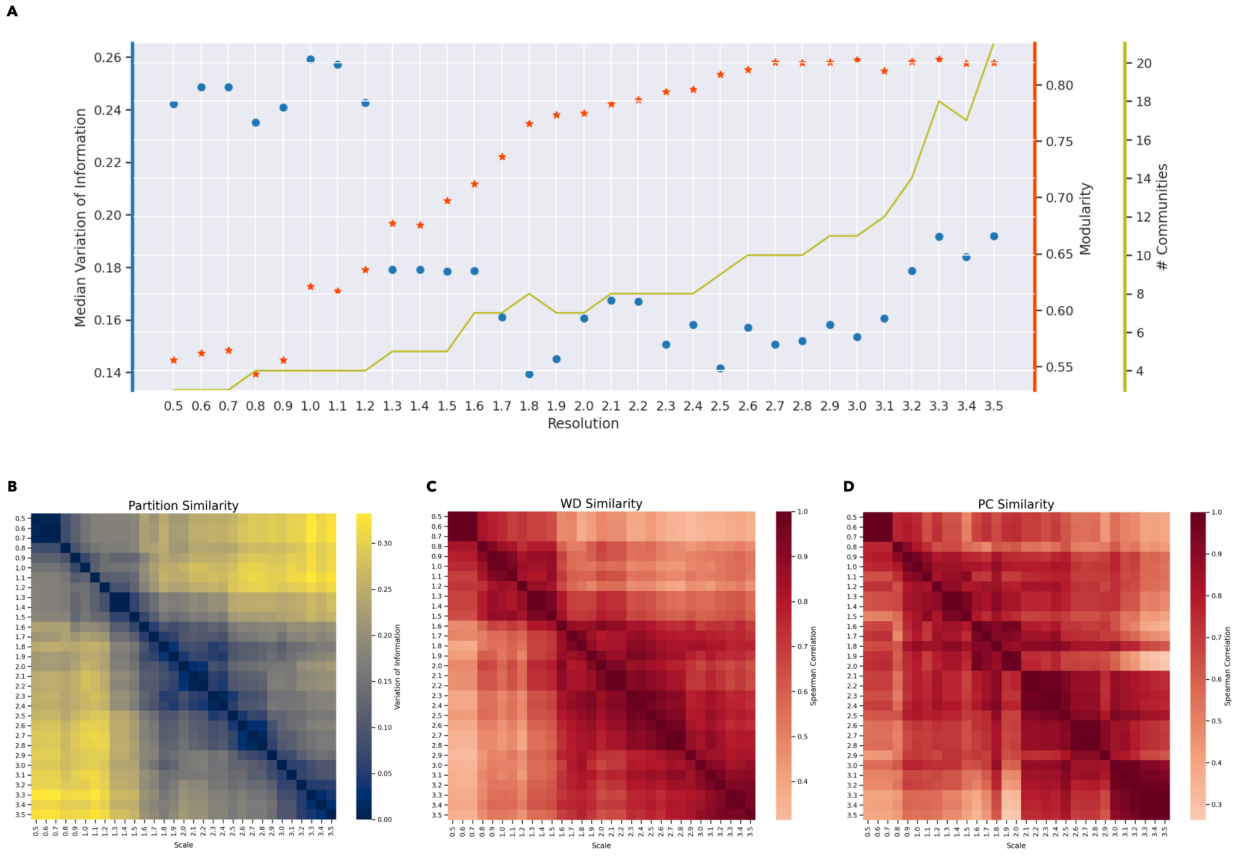


Figure S2: Multiscale community detection for the functional connectivity network.
The global minima for median VI was observed at γ = 1.8 (A), leading us to select that partition as being maximally representative of FC community structures across scales. Further support for this selection comes from the fact that this scale occurs at the asymptote of the modularity maximization function (A), and that PC values at this scale are highly similar to those across a wide range of other scales (D).

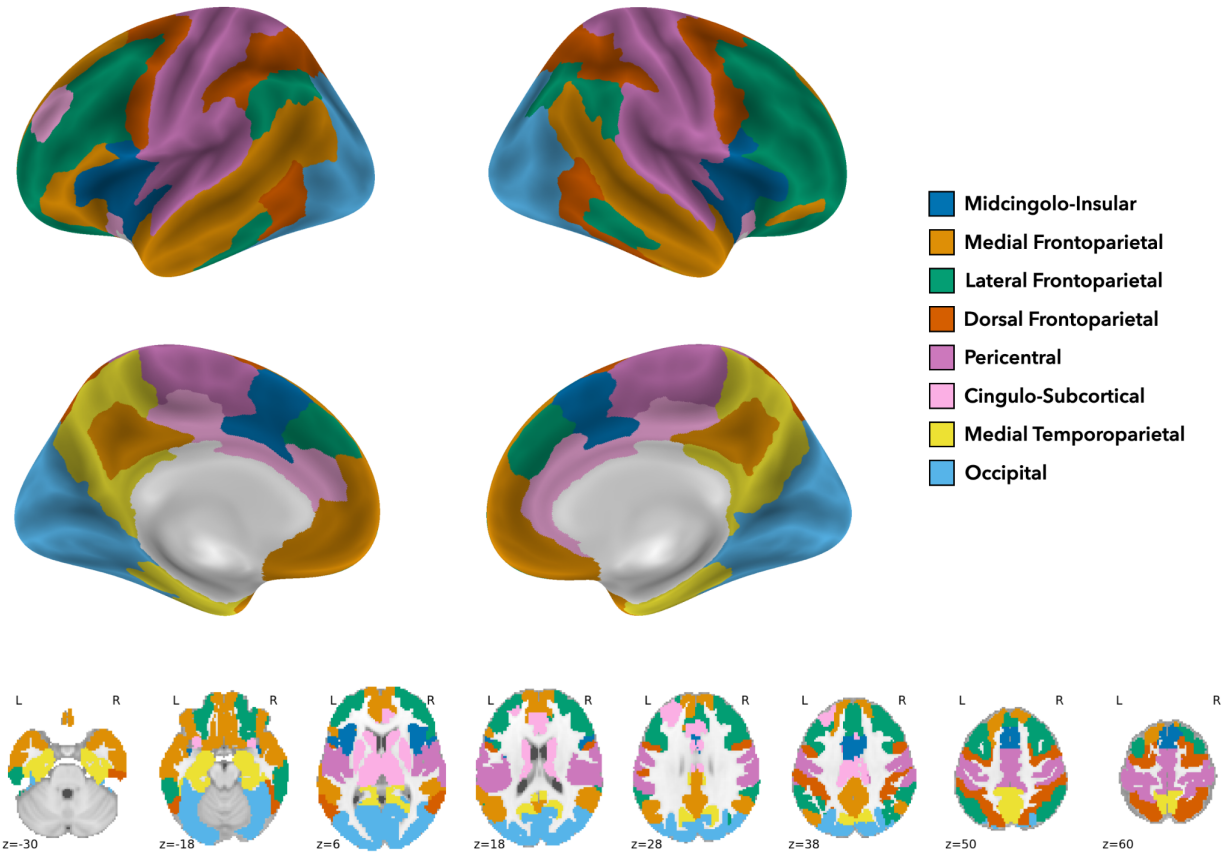


Figure S3: Maximally representative partition (γ = 1.8, 8 communities) of the functional connectivity network.
Community labels are based on the nomenclature proposed in (Uddin et al., 2019).

For the structural connectivity network, the partition at γ = 2.5 exhibited the lowest median VI (Fig. S4A). However, visual inspection of the pairwise VI matrix (Fig. S4B) revealed that while the partition at this resolution is highly similar to other partitions within the domain of resolutions $\gamma \geq 2.0$, it has relatively low similarity to partitions at coarser scales. In contrast, the partition at γ = 2.0 has only a marginally higher median VI than the global minima at γ = 2.5, while showing good similarity to partitions across a much wider range of resolutions (γ = 0.9 to γ = 3.0, 4 to 12 communities). Further, the partition at γ = 2.0 has the lowest total VI. For these reasons, we judged the partition at γ = 2.0 to be maximally representative. This partition contained 8 non-singleton (N regions > 1) communities (Fig S5).

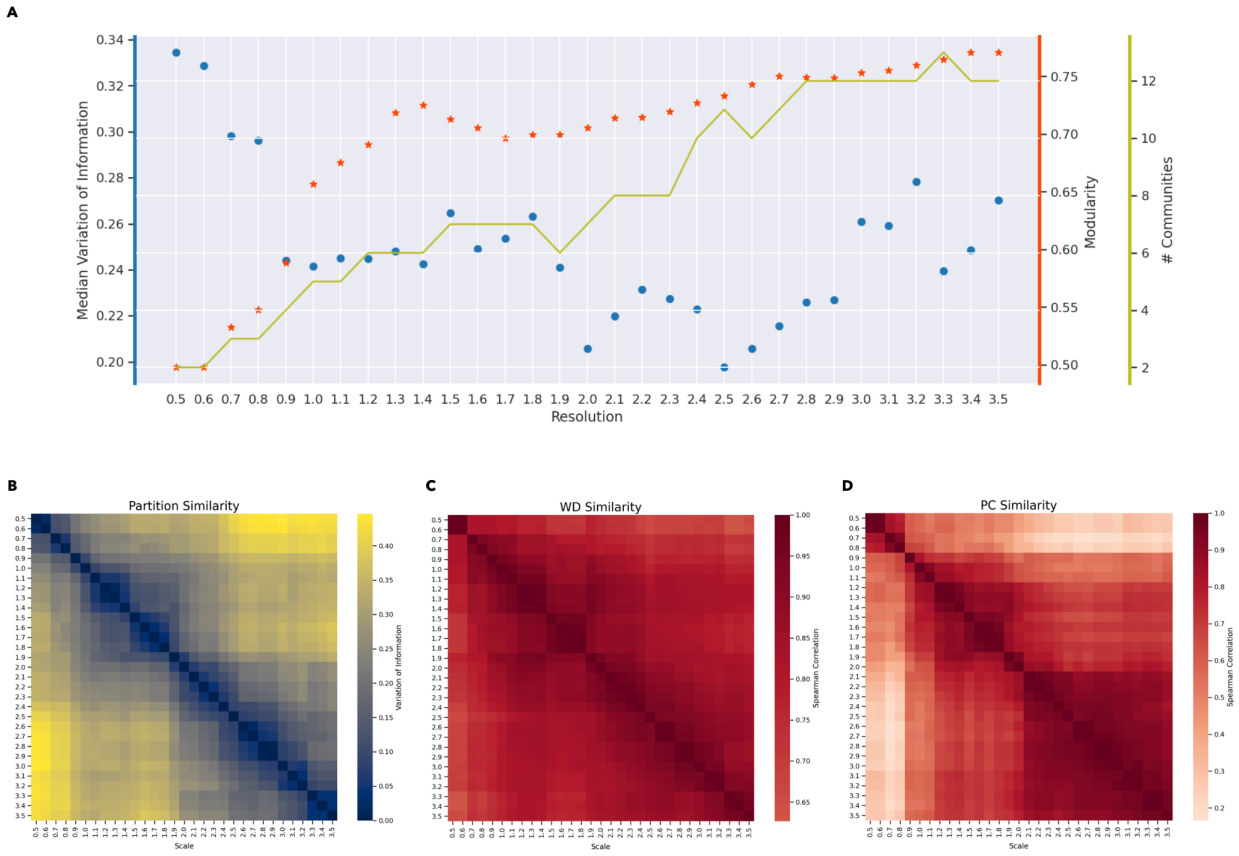


Figure S4: Multi-scale community detection for the structural connectivity network.
While the global minima for median VI was observed at $\gamma = 2.5$ (A), visual inspection of the partition similarity matrix (B) suggests that the partition at $\gamma = 2.0$ showed high similarity with a wider range of other scales while having only a slightly higher median VI. Thus, we selected $\gamma = 2.0$ as the scale with the Maximally Representative Partition (MRP).

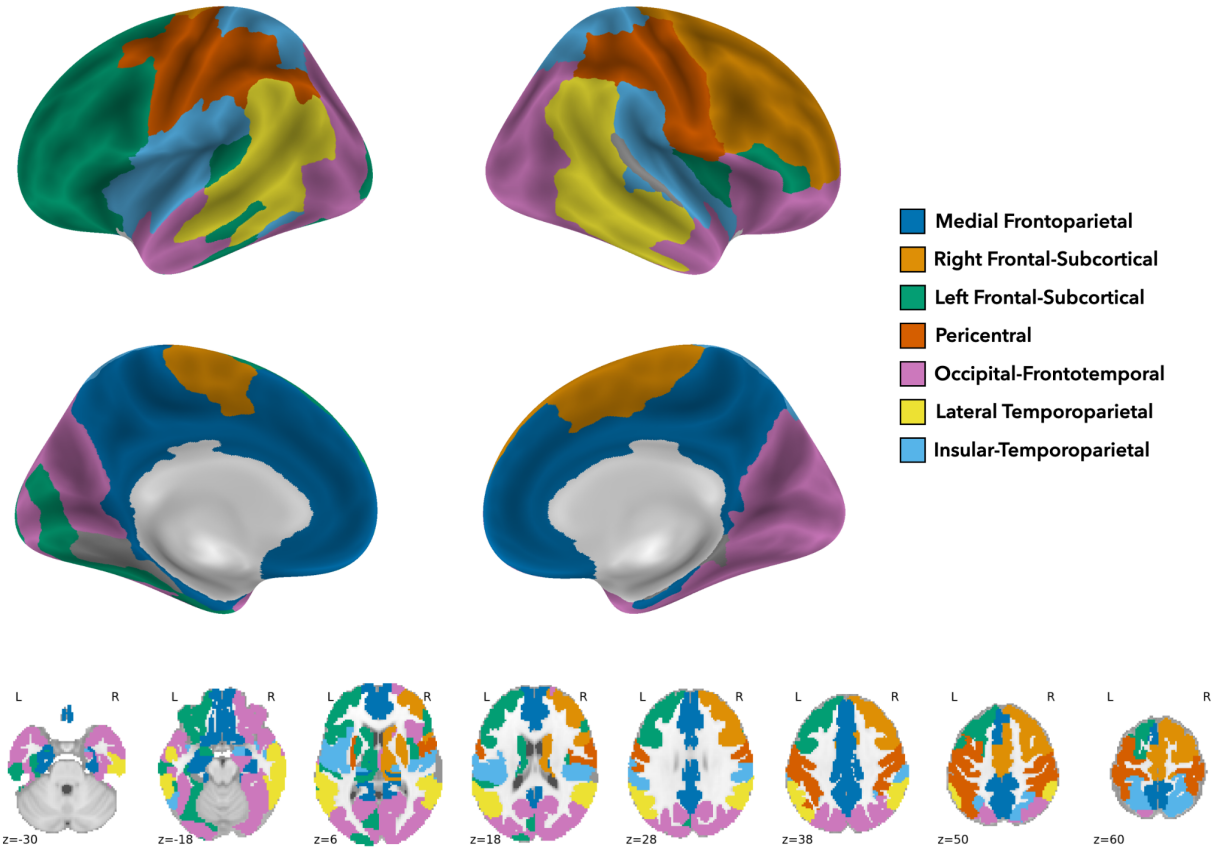


Figure S5: Maximally representative partition (γ = 2.0; 8 communities) of the structural connectivity network.
Regions assigned to singleton communities (due to disconnection from the larger network) are colored in gray.

The nuances of comparing brain maps

The statistical comparison of spatial maps describing different aspects of brain structure and function is a core practice in neuroimaging. However the spatial autocorrelation inherent in brain maps violates the assumptions of independent samples that are key to valid parametric statistical inference (Alexander-Bloch et al., 2018; Bartlett, 1935). This lack of independence inflates the variance of the sampling distribution of the test statistic (e.g. correlations, t-values, etc) and reduces the effective degrees of freedom, leading to inflated Z-scores and high rates of false-positives when using traditional parametric tests. As such, it is necessary to evaluate whether two brain maps show an association *above-and-beyond* that induced by their autocorrelation. To do this, we calculated p-values for all statistical tests using non-parametric permutation testing and 10,000 surrogate timescale maps generated using an autocorrelation-preserving spatial null model (Burt et al., 2020). These were implemented using a custom-developed Python package (https://github.com/danlurie/PyPALM) which facilitates the use of arbitrarily complex null models when evaluating multivariable linear models .

Correction for multiple comparisons

Given the large number of tests performed in this study, we take a multi-pronged approach to guarding against false-positive results. First, we use the Benjamini-Hochberg method (Benjamini & Hochberg, 1995) to control the False Discovery Rate (FDR) at q = 0.05 across all statistical tests in each dataset (with the exception of a small number of post-hoc tests conducted to evaluate the independence of predictors). We report corrected p-values as p_{perm}^{FDR}, and uncorrected p-values as p_{perm}. Second, while we report the results from each dataset separately, we require each effect to be significant in both datasets in order to reject the overall null hypothesis.

Comparing effects and correcting for selective inference

Inference regarding differences in effects necessitates formally testing these differences: it is not enough to simply observe that one effect is significant and the other isn't (Gelman & Stern, 2006; Nieuwenhuis et al., 2011). The classic example of such comparisons is checking for a significant interaction when conducting an analysis of variance, though our use of multiple models (one for each measure) rather than a single unified model (containing all measures) precludes a formal interaction test. As such, we rely on the method introduced by (Zou, 2007) for comparing correlations. In this approach, a confidence interval is computed for the difference in effects while accounting for dependence (i.e. measures estimated from the same data) and overlapping variables (e.g. X is overlapping in a comparison of $corr_{X,Y}$ and $corr_{X,Z}$). If the confidence interval includes zero, we are unable to reject the null hypothesis for a difference between correlations (and vice versa). Because we are primarily concerned with establishing whether one feature of network topology is more strongly associated with timescale than another (rather than whether the direction of the association differs between features), we computed confidence intervals using the absolute value of partial correlations. However, because we seek to compute confidence intervals for only a portion of the effects we have estimated (i.e. that subset of paired effects for which one effect is significant and the other is not), we are faced with an issue of selective inference (a.k.a circular inference, double-dipping, or "voodoo" statistics (Kriegeskorte et al., 2009; Vul et al., 2009)). Failing to account for such such selection risks biased inference. As such, we control the False Coverage-statement Rate (FCR) using the approach proposed by (Benjamini & Yekutieli, 2005) and adapted for neuroimaging by (Rosenblatt & Benjamini, 2014). This method is a generalization of the Benjamini-Hochberg FDR procedure (Benjamini & Hochberg, 1995) to the case of selected multiple CIs. As with correction for multiple testing, we apply the FCR adjustment across all comparisons within each dataset.

Results

Mapping cortical and subcortical intrinsic timescales with resting BOLD fMRI

Following preprocessing and denoising, we extracted the average resting BOLD time series from each of 246 cortical and subcortical regions of interest defined in the Brainnetome atlas (Fan et al., 2016). Intrinsic timescales are commonly estimated based on the autocorrelation properties of neurophysiological time series (e.g. (Gao et al., 2020; Murray et al., 2014; Raut et al., 2020; Watanabe et al., 2019)), with greater autocorrelation indicating longer timescales. Here, we use the lag-1 autocorrelation, a straightforward measure which has recently been shown to have higher test-retest reliability for fMRI data than alternative methods for estimating timescale (i.e. those based on the decay of the autocorrelation function) while retaining sensitivity to long-memory processes (Shinn et al., 2021). Group-level timescale maps were then created by taking the median of lag-1 autocorrelation values for each region across individuals in each dataset. Because ROI volume can bias timescale estimates by artificially inflating time series autocorrelation (Afyouni et al., 2019; Fallon et al., 2019; Sethi et al., 2017; Shinn et al., 2021), the number of voxels in each ROI was regressed from group-median timescale estimates prior to visualization and during further all analyses.

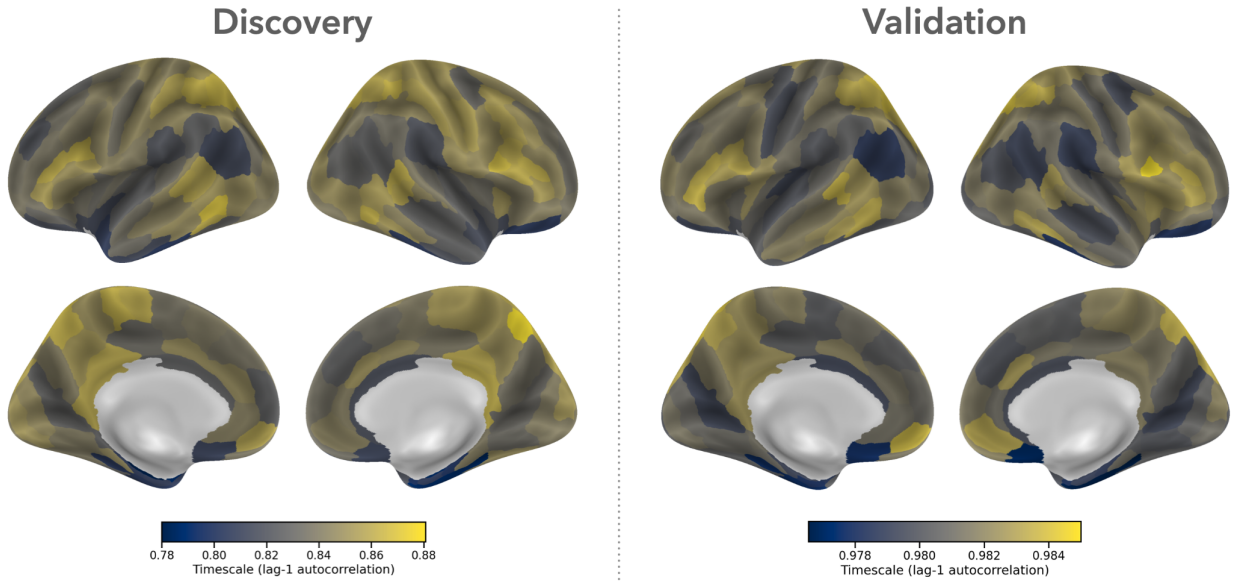


Figure 1: Cortical timescales exhibit consistent features across datasets.
We used lag-1 autocorrelation to estimate the intrinsic timescale of regional resting BOLD fMRI time series in two different datasets of healthy young adults. Our initial ("discovery") analysis used data from 93 participants taken from the Nathan Kline Institute-Rockland Sample. We then attempted to replicate our findings in a validation sample of 100 individuals taken from the Human Connectome Project. Timescales within the cerebral cortex exhibited multiple consistent features across datasets. The validation data exhibits overall higher values of lag-1 autocorrelation than the discovery data due to the significantly shorter TR (720ms vs. 1400ms).

Visual inspection of group-level timescale maps revealed multiple consistent features within the cerebral cortex (Fig. 1). Cortical areas with consistently *longer* timescales across both datasets include bilateral superior parietal lobule, inferior frontal gyrus, lateral posterior temporal lobe, and dorsal precuneus, as well as left anterior medial prefrontal cortex and retrosplenial cortex. Cortical areas with consistently *shorter* timescales include bilateral inferior parietal lobule, anterior temporal operculum, orbitofrontal cortex, medial temporal lobe, medial parieto-occipital sulcus, and limbic areas of the anterior cingulate cortex, as well as right dorsal precentral gyrus and anterior superior temporal sulcus.

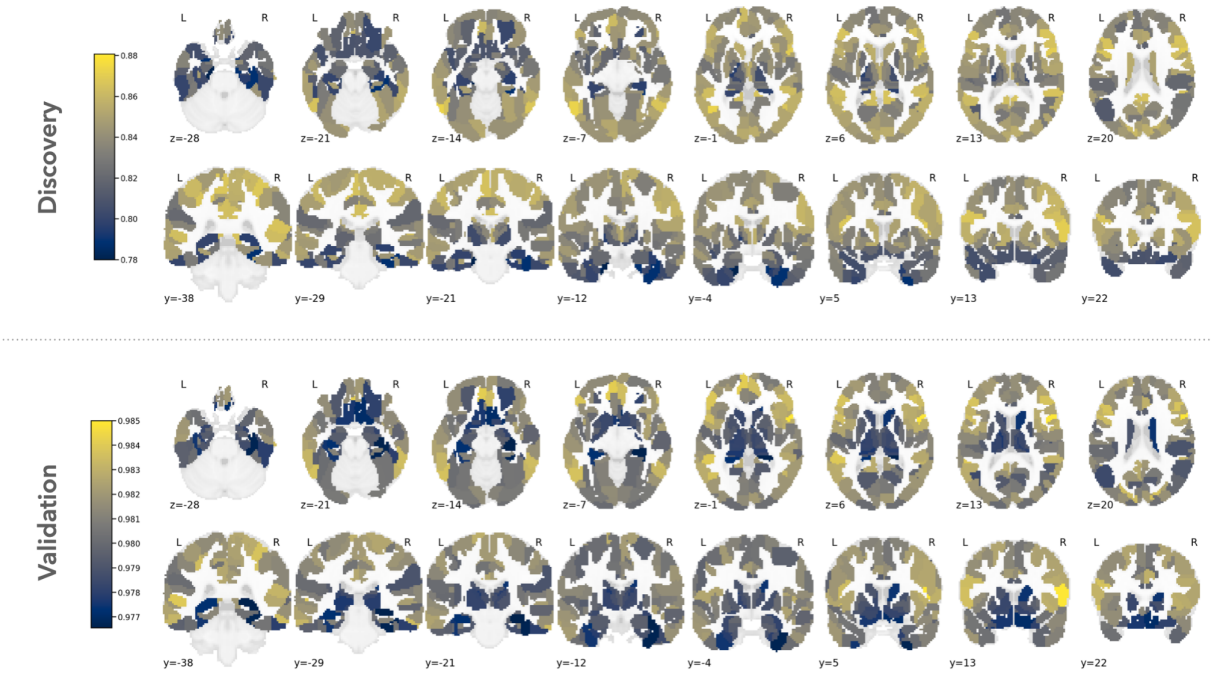


Figure 2: Subcortical timescales are generally shorter than cortical timescales.
Subcortical regions tend to have shorter timescales than cortical areas in both datasets, but this difference is substantially larger in the validation data.

In both datasets, subcortical areas tend to exhibit shorter timescales than cortical areas (discovery: t (51.4) = 4.22, $p < 0.0001$; validation: t (93.8) = 16.72, $p < 0.0001$), but the magnitude of this difference is over twice as large in the validation data than the discovery data (discovery: d = 0.7; validation: d = 1.9). As a result, subcortical timescales in the validation data appear largely undifferentiated from each other when visualized alongside cortical regions (Fig. 2). To better visualize differences in timescale within and between subcortical structures within each dataset, we created additional slice views of all subcortical regions after excluding cortical ROIs (Fig. 3), as well as separately for each group of subcortical ROIs (i.e. thalamus, basal ganglia, and medial temporal lobe; Fig. S6). This revealed some consistent features in the pattern of timescales among subcortical ROIs within each dataset, but also some notable differences. In both datasets, timescales lengthen along a ventrolateral to dorsomedial axis within the thalamus (Fig. 3, Fig. S6A/B). Timescales are also consistently longer in the medial versus

lateral amygdala and the anterior versus posterior hippocampus (Fig. 3, Fig. S6C/D), as well as the in dorsolateral putamen compared to the globus pallidus (Fig. 3, Fig. S6E/F). In contrast, timescales in the caudate differ considerably between datasets. In the discovery data, the caudate exhibits some of the longest timescales relative to the rest of the basal ganglia (Fig. S6E) as well as compared to the majority of other subcortical ROIs (Fig. 3). In the validation data, however, the opposite is true (i.e. shorter timescales in the caudate relative to both the rest of the basal ganglia (Fig. S6F) and other subcortical regions (Fig. 3)). Similarly, while the medial amygdala and dorsolateral putamen exhibit relatively middling timescales in the discovery data, they have the longest timescales among all subcortical regions in the validation data (Fig. 3).



Figure 3: Visualization of timescales across all subcortical ROIs.
Colors in each panel are scaled based on the maximum and minimum lag-1 autocorrelation among all subcortical ROIs in each dataset.

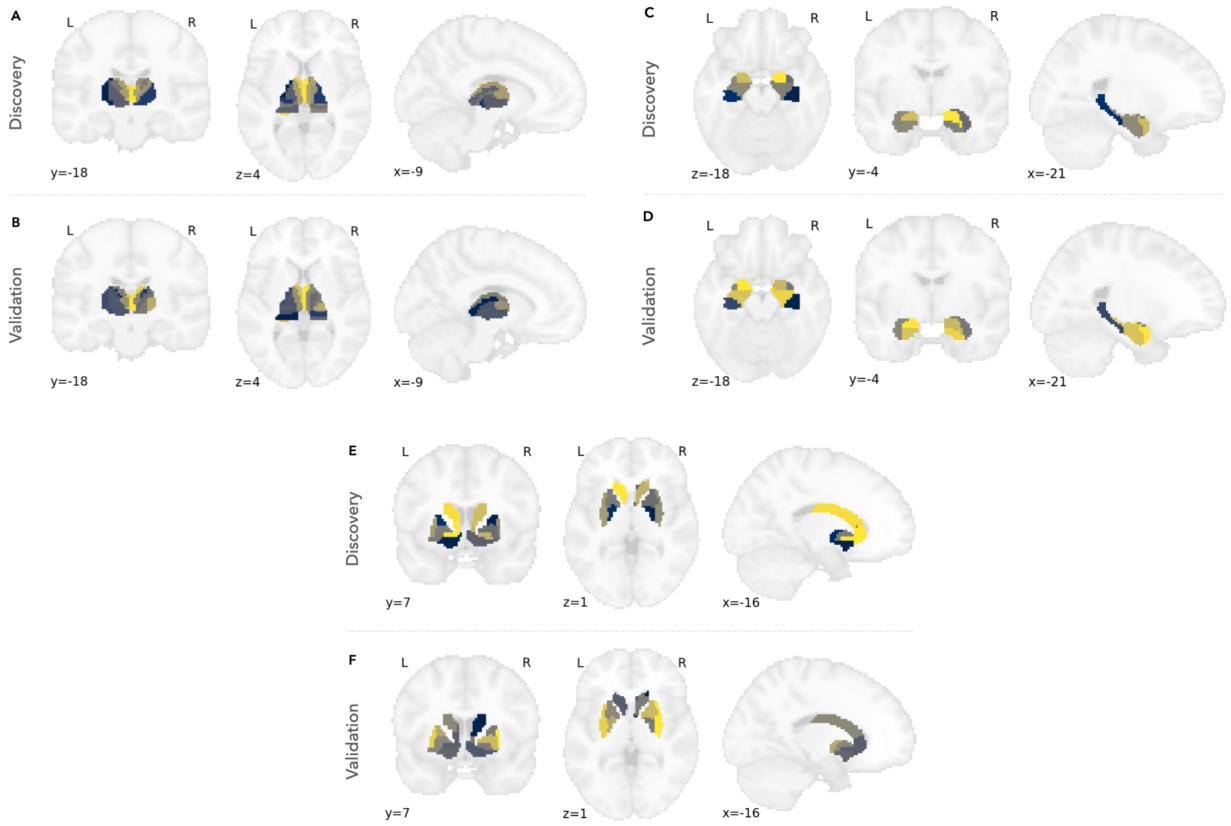


Figure S6: Visualization of timescales within each group of subcortical ROIs.
Colors in each panel are scaled based on the maximum and minimum lag-1 autocorrelation among each group of ROIs in each dataset.

Due to these inconsistencies in the timescales of subcortical regions (particularly relative to cortical areas), we decided to consider only cortical ROIs when investigating the relationship between timescales and regional connectivity. However, prior to proceeding with these analyses, we evaluated the possibility that timescale estimates may be confounded by regional differences in signal to noise ratio. For each participant, we calculated tSNR by dividing the temporal mean by the standard deviation of ROI time series from images which had undergone only basic preprocessing (e.g. volume realignment and global intensity normalization). We then calculated the median of these values across participants in each dataset and computed the correlation between timescale and tSNR across cortical ROIs. Because spatial autocorrelation can induce spurious correlations when comparing brain maps (Alexander-Bloch et al., 2018), we evaluated the significance of these effects (and all other effects in this paper) using permutation testing and a spatially-aware generative null model (Burt et al., 2020). In the discovery data, we found a weak positive correlation between timescale and tSNR, but this effect was not significant (r = 0.175, p_{perm} = 0.424). In the validation data, the correlation between timescale and tSNR was notably stronger (r = 0.374, p_{perm} = 0.058). This effect largely disappeared when excluding the 21 cortical areas with the lowest tSNR (i.e. the bottom decile) (r = 0.097, p_{perm} = 0.615). As such, while the main text presents analyses which include all cortical ROIs, we

confirmed that all key findings in the validation data were robust to the exclusion of low signal ROIs (see "Robustness to tSNR" in the Supplement). The only effect which failed to replicate in this control analysis was the relationship between timescale and functional connectivity degree, and we note this when reporting the results of that analysis.

Timescales are associated with multiple features of regional brain connectivity

Cortical areas with longer timescales tend to have greater structural connectivity

The simplest way to characterize and quantify the topology of a brain area is to simply count how many other areas it connects to, and how strong those connections are. In weighted networks (such as those used in this study), this measure is calculated as the sum of the weights of all connections to a region, and is referred to as the "strength" or "weighted degree" of a node. In the interest of brevity—and to avoid confusion when discussing the strength of connectivity between pairs of regions—we refer to this measure simply as "degree". In mammalian structural brain networks, high degree "hub" regions exhibit preferential connectivity to other highly connected regions, forming a "rich club" of topologically central brain areas whose connections play an important role in integrating information across the network (de Reus & van den Heuvel, 2013; Harriger et al., 2012; van den Heuvel et al., 2012; van den Heuvel & Sporns, 2011, 2013c). High degree hubs are also a key feature of functional brain networks (Achard et al., 2006; Buckner et al., 2009; Cole et al., 2010; Grayson et al., 2014; Tomasi & Volkow, 2011; Zuo et al., 2012). Based on prior investigations into the relationship between network topology and regional dynamics (Baria et al., 2013; Fallon et al., 2020; Gollo et al., 2015; Sethi et al., 2017; Shinn et al., 2021), we predicted that brain areas with higher degree in the functional and structural connectivity networks would exhibit longer timescales. This hypothesis was preregistered (Hypothesis 2; (Lurie, 2018)).

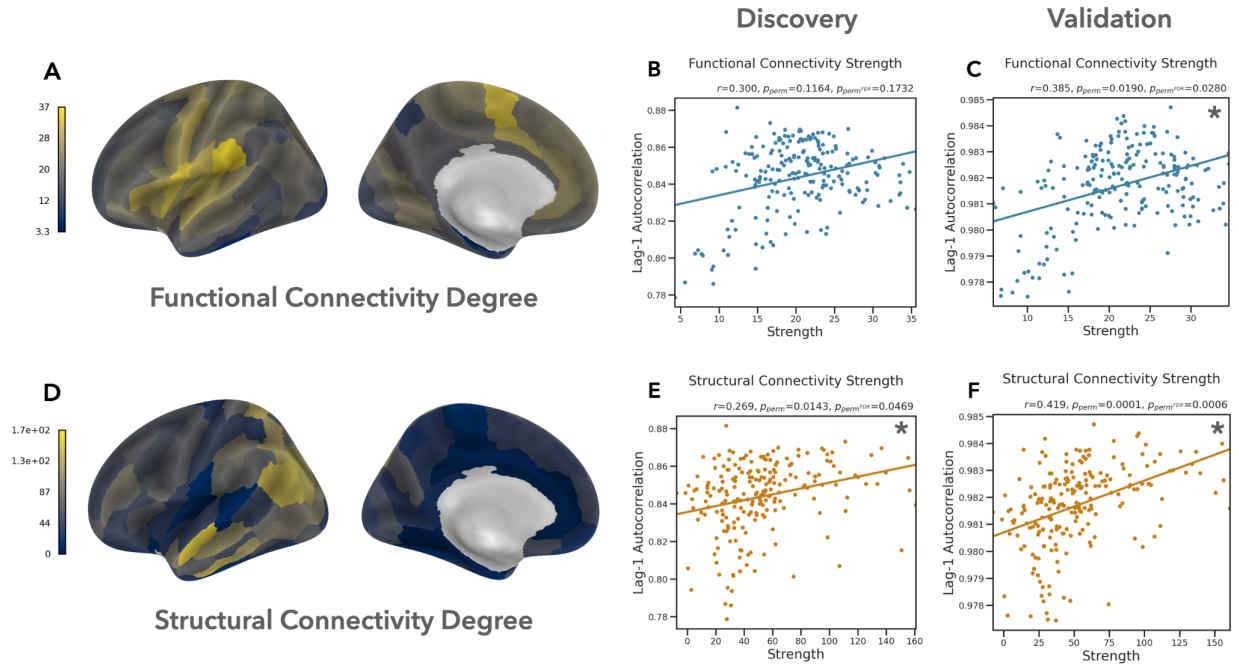


Figure 4: Cortical areas with longer timescales tend to have greater structural connectivity.
We found that functional connectivity degree (A) was positively correlated with regional timescale, but this effect was not significant in the discovery data (B) or in the validation data when excluding ROIs with low tSNR (Supplement: "Robustness to tSNR). In contrast, the relationship between timescale and structural connectivity degree (D) was significant in both the discovery (E) and validation datasets (F). Panel (A) visualizes FC degree in the discovery dataset. Asterisks highlight partial correlations that are significant at FDR q ≤ 0.05.

As predicted, we observed a positive partial correlation (covarying for ROI volume) between timescale and degree in both the functional and structural connectivity networks (Fig. 4). This relationship was significant in both datasets for structural connectivity degree (discovery: r = 0.269, p_{perm}^{FDR} = 0.0469; validation: r = 0.419, p_{perm}^{FDR} = 0.0006). In contrast, while the correlation between timescale and functional connectivity degree was significant in the validation data when including all cortical ROIs (r = 0.385, p_{perm}^{FDR} = 0.0280), this effect disappeared when excluding regions with low tSNR (r = 0.103, p_{perm}^{FDR} = 0.624), nor did it reach significance in the discovery data (r = 0.300, p_{perm}^{FDR} = 0.1732). These results replicate prior observations of a positive correlation between structural connectivity degree and the timescale of regional BOLD dynamics ((Baria et al., 2013; Fallon et al., 2020; Sethi et al., 2017), but fail to replicate reports of an analogous relationship in functional connectivity networks (Baria et al., 2013; Shinn et al., 2021).

The relationship between timescales and the modular structure of human brain networks

While degree is arguably the most fundamental measure of regional topology (and the network feature which has most consistently been associated with regional dynamics in prior studies), it fails to consider another key aspect of brain network topology. In particular, in addition to high degree hubs, an extensive literature in network neuroscience has demonstrated that brain

networks exhibit a modular community structure in which regions are more likely to connect to (or interact with) other regions in the same community than to regions in other communities (Girvan & Newman, 2002; Newman, 2006; Sporns & Betzel, 2016). This modular structure can be found at multiple scales, ranging from microscale neuronal populations (Lee et al., 2016; Schroeter et al., 2015; Shimono & Beggs, 2015) to macro-scale functional and structural brain networks (Crossley et al., 2013; Hagmann et al., 2008; He et al., 2009; Meunier et al., 2009; Power et al., 2011). This architecture is thought to play a key role in facilitating effective information processing, specialization of function, and flexible reconfiguration in support of adaptive behavior and cognition (Bertolero et al., 2015; Bullmore & Sporns, 2009; Sporns, 2013; Sporns & Betzel, 2016).

In the context of the brain's network community structure, a connection between two brain areas can be categorized as being either within-community (if the two brain regions are in the same network community), or between-community (if the two regions are members of different communities). Within-module degree (WD) and participation coefficient (PC) are two complementary measures of regional topology which consider the modular community structure of networks (Guimerà & Nunes Amaral, 2005), and thus provide important additional context about regional connectivity patterns above and beyond that provided by degree alone. In this way, they allow us to take a more nuanced view of the role each region plays in the larger network (Power et al., 2013).

Within-module degree quantifies the extent to which a region has a strong or widespread connectivity to other brain areas within the same network community. However, because communities often differ in size, raw WD values are z-scored across all regions in each community. This is necessary because the preferential within-community connectivity in modular networks will bias regions in larger communities to have a higher degree simply due to community size. Thus the normalized (z-scored) metric provides information about the extent of within-community connectivity of each region relative to other regions in the same community. As such, regions with high WD act as hubs within their respective communities, regardless of the extent to which they exhibit high overall degree. In contrast, participation coefficient provides a measure of the extent to which a region is diversely connected across multiple network communities. A low PC (approaching 0) indicates that a region connects only to other regions within the same network community, while a high value (approaching 1) indicates that connections are distributed evenly across communities. Regions with high PC act as "connectors" between network communities, and are thought to play an important role in coordinating activity or facilitating the integration or passage of information across communities (Bertolero et al., 2015, 2017, 2018).

Given their putative roles in integrating information within (WD) and between (PC) network communities, we predicted that brain areas with high PC and WD would exhibit longer intrinsic timescales. As with degree, we predicted that this relationship would exist in both the structural and functional connectivity networks. These predictions were preregistered (Hypothesis 1; (Lurie, 2018)).

Prior to calculating community-aware topological measures such as PC and WD, one must first identify (or impose) a "partition" which splits the network into communities and describes which regions belong to each community. While there are many different data-driven methods for identifying communities in complex networks, by far the most common are those which select an optimal partition based on modularity (Q), a mathematically defined quality function which describes the extent to which connections are concentrated within rather than between communities (Newman, 2006). However, all such "modularity maximization" algorithms suffer from a "resolution limit" such that they are unable to detect communities smaller than a given scale which depends on the size of the network and density of within-community connections (Fortunato & Barthélemy, 2007). To counter this limitation, methods have been developed (e.g. (Blondel et al., 2008)) that incorporate a "resolution parameter" (γ) which allows users to adjust the scale at which communities are identified (i.e. fewer larger communities vs. more smaller communities).

However, as noted above, the modular architecture of neural systems manifests at multiple scales, and this is true even for the macro-scale functional and structural brain networks amenable to investigation by human neuroimaging (Betzel & Bassett, 2017). For example, one might initially consider a coarse 2 community partition for human functional brain networks, composed of "task positive" and "task negative" subsystems (Fox et al., 2005). At finer scales, we might identify the "canonical" macroscale functional brain networks (e.g. default, frontoparietal, visual, somatomotor, etc. (Damoiseaux et al., 2006; Power et al., 2011; Smith et al., 2009; Uddin et al., 2019; Yeo et al., 2011)), each of which can in turn be further decomposed into multiple smaller communities (Akiki & Abdallah, 2019; Ashourvan et al., 2019; Meunier et al., 2009; Smith et al., 2009; Yeo et al., 2011). This sort of hierarchical community structure is consistent with a view of the brain as a complex dynamical system which operates across multiple spatial and temporal scales, but poses a challenge to researchers insofar as there is likely no single "correct" scale at which define network communities. Further, because participation coefficient and within-module degree are defined relative to a particular partition, there is no guarantee that these measures will show a consistent relationship across scales to other features of brain structure and function.

In light of these factors, we took a two-pronged approach to our investigation into the relationship between timescale and PC/WD. First, we identified communities in each network across a wide range of scales by varying the resolution parameter during community detection. We then selected a single partition for each network which was most similar to the community structure present at all other scales, and used this "maximally representative partition" (MRP) to compute PC and WD in an initial investigation into the relationship between these features and regional timescales. Second, we evaluated the degree to which each effect replicated at all other scales, thus allowing us to evaluate the robustness of our findings across multiple scales of network organization, as well as the opportunity to identify scale-specific effects (should they exist).

Longer timescales are associated with greater within-community functional connectivity across scales, and within-community structural connectivity at coarse scales

As predicted, we found that cortical areas with greater WD in the functional connectivity network tend to have longer timescales (Fig. 5). This relationship was significant in both datasets across the majority of network scales (Fig. 5D), including the scale which we identified as exhibiting the maximally representative community structure (discovery: $r = 0.368$, $p_{perm}^{FDR} = 0.0011$; validation: $r = 0.364$, $p_{perm}^{FDR} = 0.0006$; Fig. 5B/C). Regional timescales were also positively correlated with within-module connectivity in the structural connectivity network. This effect was significant in the validation data across the majority of scales, but only reached significance in the discovery data at the two coarsest scales (Fig. 5H). At these coarse scales, cortical areas were split between just two communities (Fig. S7). To investigate the possibility that the relationship between timescale and SC WD was scale-dependent, we compared correlations across scales by computing confidence intervals for the difference in absolute effect size (Zou, 2007). Effects were considered significantly different if the False Coverage-statement Rate (FCR) corrected (Benjamini & Yekutieli, 2005) 95% CI did not include zero. In the validation data, the strength of the relationship between timescale and SC WD was significantly stronger at the two coarsest scales ($\gamma = [0.5, 0.6]$) than at finer scales ($\gamma = [1.8, 2.5, 2.6, 2.7, 3.3, 3.4, 3.5]$), but there was no significant difference in effect size across scales in the discovery data. These results suggest that hubs of functional network communities tend to have longer timescales across multiple levels of network organization, and that a similar effect exists within structural connectivity networks at very coarse scales.

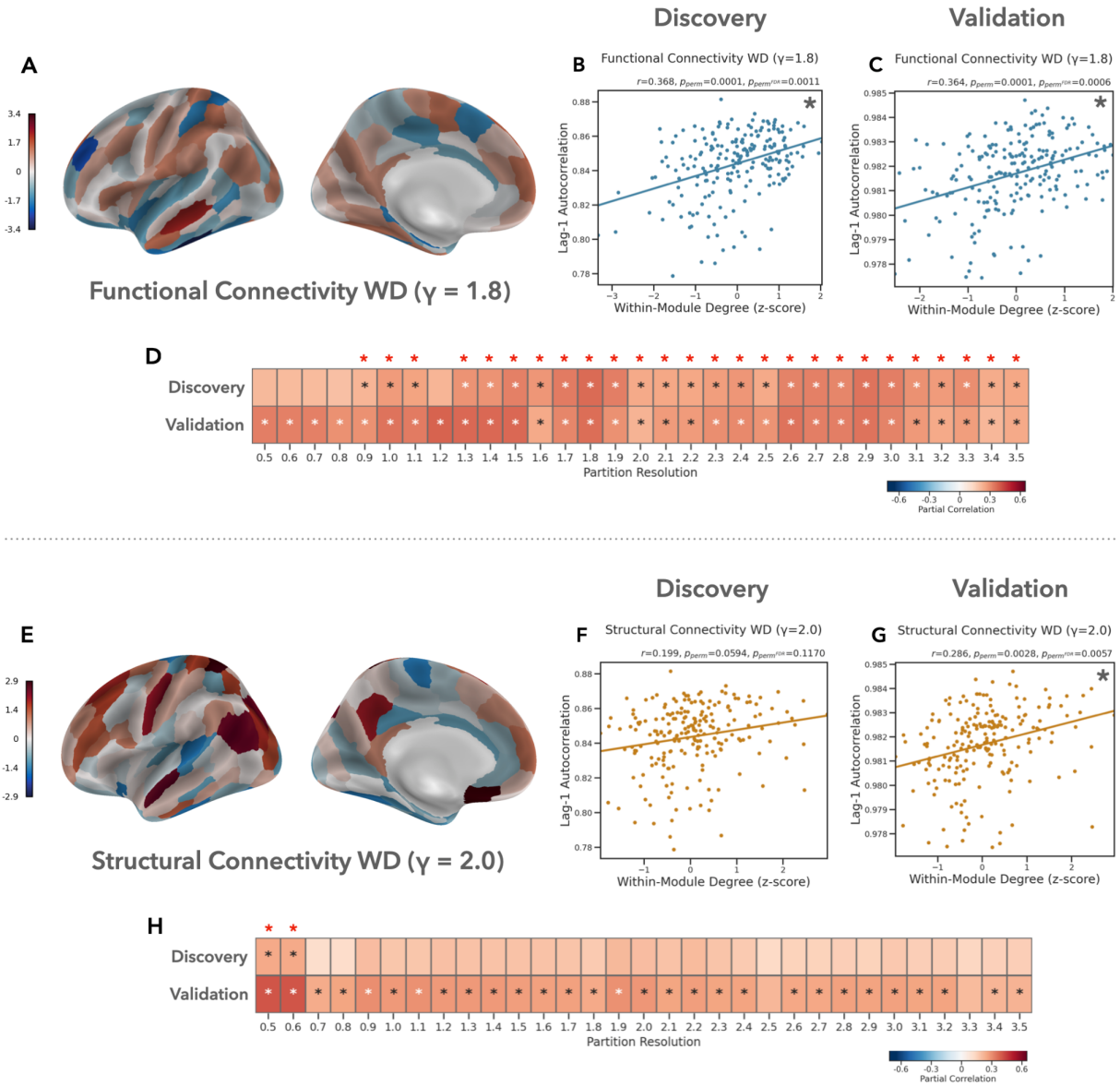


Figure 5: Longer timescales are associated with greater within-community functional connectivity across scales, and greater within-community structural connectivity at coarse scales.
(A-D) Brain areas with greater within-community functional connectivity tend to have longer timescales. This relationship was significant in both datasets across the majority of network scales. (E-H) Timescale was also positively correlated with within-community structural connectivity, but this effect only replicated at the two coarsest network scales. Panel (A) visualizes FC WD in the discovery dataset. Asterisks highlight partial correlations that are significant at FDR q ≤ 0.05.

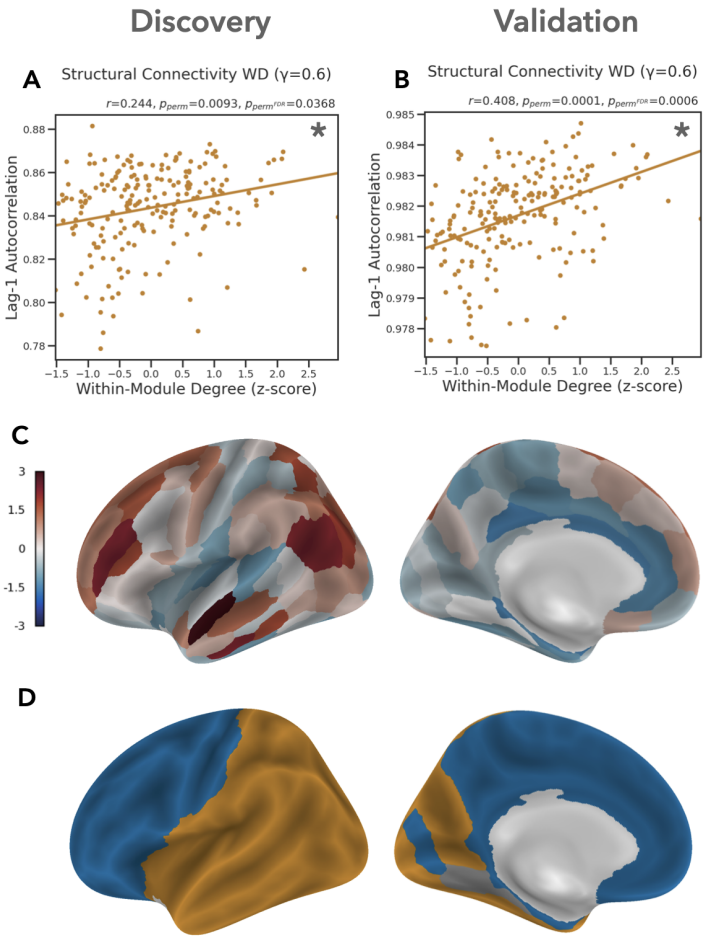


Figure S7: Correlation between cortical timescales and within-community structural connectivity at coarse scales.
(A-B) Partial correlation between timescale and SC WD at γ = 0.6. (C-D) SC WD and community structure at γ = 0.6.

Longer timescales are associated with diverse structural connectivity

We observed only a weak negative correlation between cortical timescales and FC participation coefficient at the majority of network scales, and these relationships did not reach significance at any scale in either dataset (Fig. 6A-D). At each network scale, we used confidence interval tests to compare the strength of these correlations to those we observed between timescale and FC WD. In both datasets, we found that the relationship between timescale and FC PC was significantly weaker than the relationship with FC WD at multiple scales (γ = [1.3, 1.4, 1.5, 3.0, 3.1, 3.2, 3.3, 3.4, 3.5]). This suggests that in functional connectivity networks, the extent of within-community connectivity, but not the diversity of between-community connectivity, is associated with longer timescales.

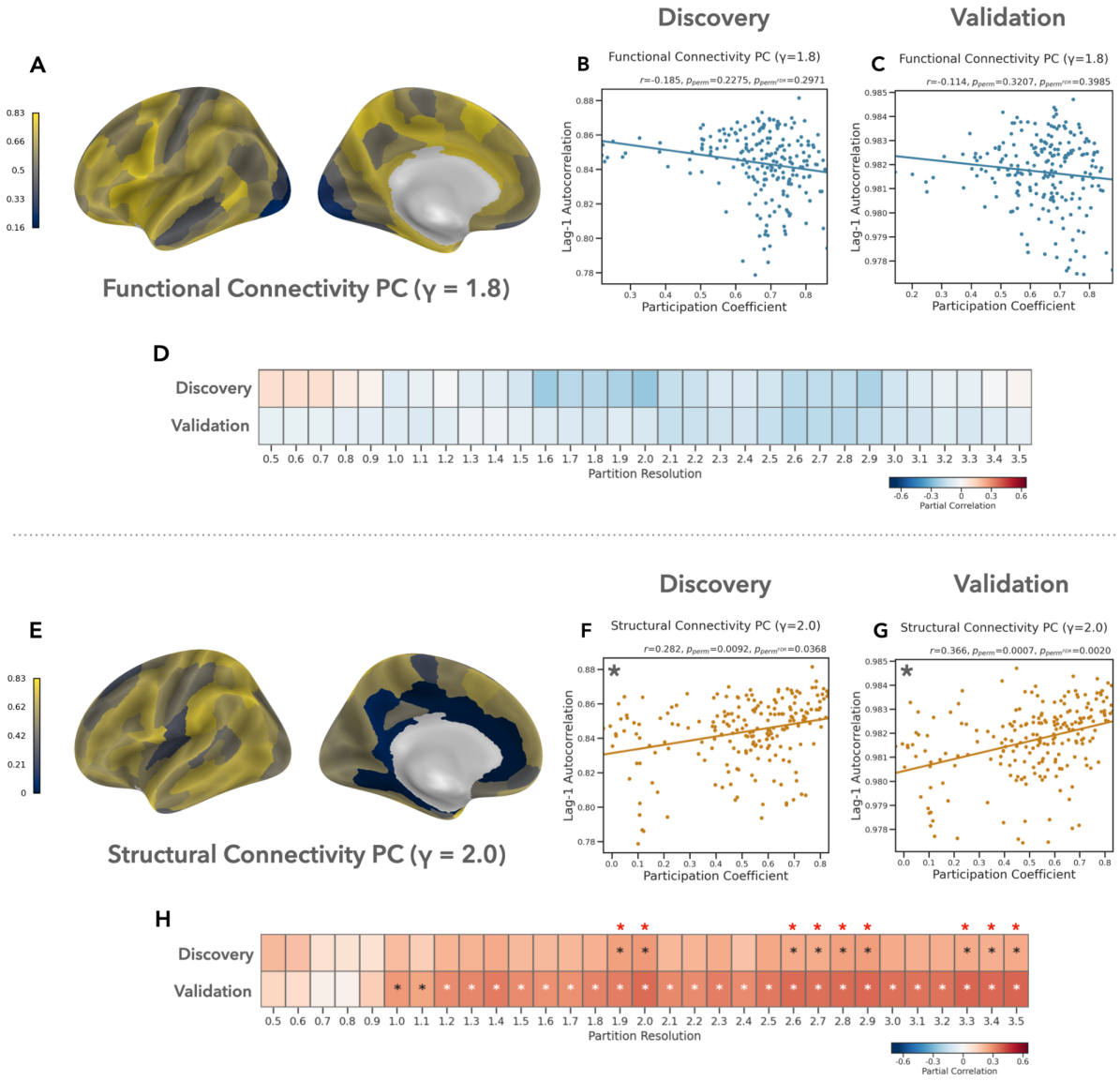


Figure 6: Longer timescales are associated with diverse structural connectivity.
(A-D) At most scales, we observed a weak negative correlation between cortical timescales and regional participation coefficient in the functional connectivity network, but this effect was not significant at any scale in either dataset. (E-H) In contrast, participation coefficient in the structural connectivity network exhibited a significant positive correlation with cortical timescales in both datasets across multiple scales. Panel (A) visualizes FC PC in the discovery dataset. Asterisks highlight partial correlations that are significant at FDR q ≤ 0.05.

In contrast, participation coefficient in the structural connectivity network showed a significant positive correlation with cortical timescales at multiple network scales (Fig. 6E-H), including when PC was computed relative to the maximally representative community structure (discovery: r = 0.282, p_{perm}^{FDR} = 0.0368; validation: r = 0.366, p_{perm}^{FDR} = 0.0020). In the validation data, this relationship was significantly stronger than the relationship between timescale and FC PC at multiple scales (γ = [1.9, 2.0, 2.9, 3.3, 3.4, 3.5]), but this difference was only significant

in the discovery data at the two finest scales (γ = [3.4, 3.5]). Together, these results suggest that longer timescales in the cerebral cortex are associated with greater diversity of between-community structural connectivity.

Functional connectivity WD and structural connectivity PC capture distinct aspects of brain organization

Our observation that cortical timescales exhibit a significant positive correlation with both FC WD and SC PC could in theory result from a correlation between the two measures of regional network topology. To evaluate this possibility, we first calculated the correlation between FC WD and SC PC at each network scale. This revealed that these two measures are only weakly correlated (discovery: mean (SD) = 0.085 (0.048), validation: 0.128 (0.051)). Second, we tested whether the relationship between timescale and SC PC remained significant when controlling for FC WD (and vice versa). For these control analyses, we focused on SC PC and FC WD calculated relative to the maximally representative community partition of each network (γ = 2.0 and γ = 1.8, respectively). The correlation between timescale and SC PC remained significant when controlling for FC WD (discovery: r = 0.268, p_{perm} = 0.0119; validation: r = 0.363, p_{perm} = 0.0019) as did the correlation with FC WD when controlling for SC PC (discovery: r = 0.358, p_{perm} = 0.0009; validation: r = 0.361, p_{perm} = 0.0009). Similarly, we evaluated the possibility that the relationship between timescale and within-community functional connectivity could be explained by overall functional connectivity degree. We found that the relationship between timescale and functional connectivity WD remained significant in both datasets when controlling for FC degree (discovery: r = 0.287, p_{perm} = 0.0009; validation: r = 0.255, p_{perm} = 0.0099).

Preferential functional connectivity between regions with similar timescales

Brain areas with similar properties (e.g. in terms of their anatomy (Barbas & Rempel-Clower, 1997; Wei et al., 2019), function (Smith et al., 2009; Yeo et al., 2016), or topology (Bertolero et al., 2017; van den Heuvel & Sporns, 2011)) preferentially connect to each other. Based on this principle of "similar prefers similar" (Goulas et al., 2016), we tested whether regions with similar timescales are more strongly connected than regions with dissimilar timescales, as well as if timescales are more similar between pairs of regions in the same network community compared to pairs belonging to different communities. Because brain areas are more likely to connect to other nearby regions compared to more distant areas (Alexander-Bloch et al., 2013; Bullmore & Sporns, 2012; Ercsey-Ravasz et al., 2013), both of these analyses accounted for the potentially confounding effect of Euclidean distance between regions.

To test for preferential connectivity between regions with similar timescales, we first calculated the difference in timescale between each pair of cortical areas. We then calculated the partial correlation (covarying for Euclidean distance) between the absolute value of pairwise timescale differences and the strength of functional and structural connectivity between each pair. We found a small but significant negative correlation between pairwise functional connectivity and timescale differences in both datasets (Table 1), suggesting that cortical areas tend to exhibit

marginally stronger functional connectivity to other areas with similar timescales. Given the positive correlation we observed between timescale and degree, we conducted a control analysis to ensure that preferential connectivity between regions with similar timescales was not a byproduct of the "rich club" phenomenon (i.e. preferential connectivity between high degree hubs). To do this, we regressed degree from timescale estimates prior to calculating pairwise differences. As before, we observed a significant negative correlation in both datasets.

Table 1: Preferential connectivity

Model	Discovery	Validation
FC strength	r = -0.182 **(0.0005)**	r = -0.151 **(0.0005)**
FC strength (adj. degree)	r =-0.165 **(0.0005)**	r =-0.159 **(0.0005)**
SC strength	r =-0.027 (0.6143)	r =-0.100 **(0.0288)**
SC strength (adj. degree)	r =-0.016 (0.6978)	r =-0.062 (0.1472)
SC conn. vs. not	t = -9.797 (0.2259)	t = -9.82 (0.1235)
SC conn. vs. not (adj. degree)	t = -8.618 (0.2935)	t = -9.054 (0.1236)

Parentheses contain p_{perm}^{FDR}
Significant effects are highlighted in bold.

Because the population structural connectome we analyzed is sparse (i.e. only ~10% of possible edges are present), we undertook two complementary analyses of preferential connectivity in the SC network. First, we evaluated the correlation between pairwise structural connectivity strength and timescale differences, but limited this analysis to region pairs connected by at least one streamline. We observed a significant relationship between timescale similarity and structural connectivity strength in the validation dataset, but this effect did not replicate in the discovery data or when accounting for SC degree (Table 1). Second, we binarized the structural connectivity network and tested whether the distribution of timescale similarities was different for connected vs. unconnected pairs of brain areas. As with the correlation analysis, we did not find evidence of preferential structural connectivity between areas with similar timescales. When controlling for regional degree, functional connectivity strength had a significantly stronger correlation with timescale similarity than did structural connectivity strength in both datasets (discovery: Δr = -0.149, FCR-adjusted 95% CI = [-0.206, -0.092]; validation: Δr = -0.097, FCR-adjusted 95% CI = [-0.154, -0.041]). Together, these results suggest that there is preferential functional connectivity but not preferential structural connectivity between cortical areas with similar timescales.

To test whether timescales were more similar within vs. between communities, we compared the distribution of timescale differences for pairs of regions in the same community to the distribution of differences for pairs where each region belonged to a different community. We repeated this analysis at every network scale. In the validation data, we found that timescales were significantly more similar within vs. between communities of the functional connectivity network at multiple scales, but none of these effects were significant in the discovery data (Fig. 7). In the structural connectivity network, we did not find evidence of greater within-community timescale similarity at any scale in either dataset.

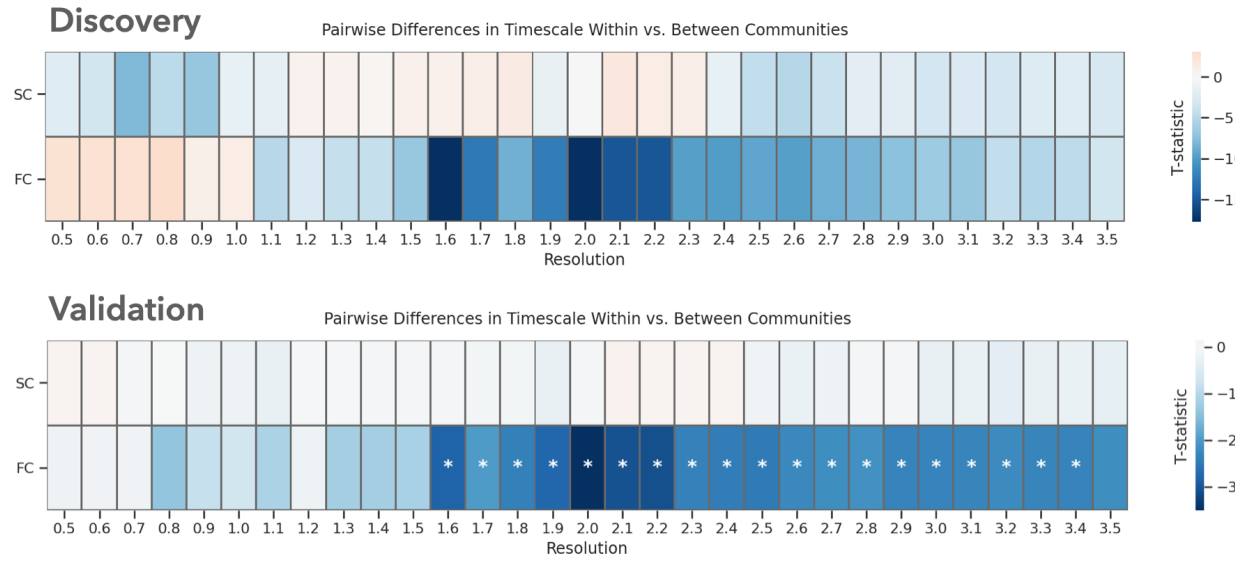


Figure 7: Similarity of timescales within versus between communities.
In the validation data, timescales were more similar between pairs of regions in the same functional network communities than for pairs where each region was in a different community. However, this effect did not replicate in the discovery data. We did not observe any evidence in either dataset for greater within-community timescale similarity in the structural connectivity network.

Discussion

In an analysis of resting BOLD fMRI data, we demonstrate that a fundamental property of regional brain dynamics—intrinsic timescale—is associated with multiple features of macro-scale brain connectivity. By considering the multi-scale modular organization of neural systems, our results provide new insights into the relationship between connectivity and dynamics in the cerebral cortex. We find that cortical regions with longer timescales tend to have extensive structural connectivity, as well as connectivity which is more diversely distributed across network communities. Longer timescales are also associated with greater within-community functional connectivity, and we show that functional connectivity between brain areas with similar timescales tends to be stronger than functional connectivity between areas with dissimilar timescales. These effects replicate across two different datasets and a wide range of topological scales.

The topography of timescales we observe in the cerebral cortex is largely consistent with the results of previous studies which have mapped timescales in the primate brain using BOLD fMRI (Baria et al., 2013; Fallon et al., 2020; Ito et al., 2020; Manea et al., 2022; Müller et al., 2020; Raut et al., 2020; Shafiei et al., 2020; Shinn et al., 2021; Watanabe et al., 2019; Wengler et al., 2020). That said, our observation of consistently short rather than long timescales in the inferior parietal lobule departs from the results from the majority of previous studies (though we note that there is substantial heterogeneity in this literature). All of the cortical areas we found to have consistently longer timescales are regions whose activity and functional connectivity have been associated with higher-order cognitive functions rather than low-level sensory and motor processes (Smith et al., 2009; Uddin et al., 2019; Yeo et al., 2016). However, not all higher-order cortical areas had consistently long timescales, and we found that many regions which sit near the top of canonical information processing hierarchies (e.g. limbic areas (Mesulam, 1998)) consistently exhibit some of the shortest timescales in the cerebral cortex. Similarly, we did not find consistently short timescales in the majority of sensory and motor regions. As such, our results (and those from numerous other studies (Baria et al., 2013; Fallon et al., 2019; Manea et al., 2022; Shafiei et al., 2020; Shinn et al., 2021; Wengler et al., 2020)) fail to support the view that BOLD timescales are shortest in unimodal sensory areas and longest in heteromodal association regions (though see (Raut et al., 2020) and (Ito et al., 2020)).

Given the sparse spatial sampling found in the majority of studies which used invasive electrophysiology to study neural timescales (typically only a handful of recording sites at most) (Maisson et al., 2021; Murray et al., 2014; Nougaret et al., 2021; Rossi-Pool et al., 2021; Wasmuht et al., 2018), it is difficult to determine the extent to which BOLD timescales conform to or depart from much of the broader literature on neural timescales. However, (Watanabe et al., 2019) found very good correspondence between timescales estimated from simultaneously recorded EEG-fMRI, and recent work by (Manea et al., 2022) was able to directly replicate many electrophysiology-based timescale hierarchies using high-resolution fMRI in macaques. However, results from another recent study which mapped timescales across the human cerebral cortex using invasive recordings found both similarities and notable differences compared to maps of BOLD timescales (Gao et al., 2020), suggesting that the relationship between neural timescales and hemodynamic timescales may be spatially heterogeneous.

We are aware of only three prior studies which have investigated differences in timescales across subcortical regions, and while we found subcortical timescales to be less consistent across datasets than cortical timescales, the consistent features we *did* observe largely replicate the findings from these prior reports. In particular, a recent analysis by (Raut et al., 2020) estimated voxelwise BOLD timescales in subcortical regions and found the same ventrolateral to dorsomedial gradient within the thalamus as we observe when using regions of interest. Our results similarly replicate Raut et al.'s finding of longer timescales in the anterior versus posterior hippocampus, and suggest that this gradient continues into the amygdala. The lack of consistency we observed for timescales in the basal ganglia makes it difficult to compare our results to prior work. That said, we did observe consistently longer timescales in the dorsolateral putamen compared to the globus pallidus, and this finding appears to replicate two

recent studies which found shorter timescales in the GP than the striatum using invasive electrophysiological recordings (Nougaret et al., 2021) and BOLD fMRI (Manea et al., 2022) in macaques. Raut and colleagues did not include the GP in their analysis, though they did observe a posterolateral to anteromedial timescale gradient within the striatum. More generally, our observation that BOLD timescales tend to be shorter in subcortical areas than in the cerebral cortex is consistent with the studies by (Raut et al., 2020) and (Manea et al., 2022).

Prior work suggests that brain areas with greater inter-regional structural connectivity (i.e. greater degree) tend to exhibit slower BOLD dynamics (Baria et al., 2013; Fallon et al., 2019; Sethi et al., 2017). Our work replicates and extends these findings in important ways. Most significantly, our analyses considered structural connections both within and between cortical hemispheres, as well as between cortical and subcortical regions. In contrast, the studies by (Baria et al., 2013) and (Fallon et al., 2020) both focused exclusively on connections between cortical areas within each hemisphere[1]. In the population-average structural connectome we analyzed here, interhemispheric connections make up almost half (46%) of all edges present in the network, while connections between cortical areas and subcortical regions make up almost a third (29%). As such, failing to consider these connections when analyzing the topology of structural connectivity networks will inherently provide an incomplete picture of brain network organization and the extent to which each region exhibits strong or widespread connectivity. Further, we believe ours is the first study on the relationship between regional dynamics and structural connectivity degree to consider and correct for the potentially confounding effects of both ROI volume and spatial autocorrelation. These corrections are far more than a formality; the majority of the null effects we report are significant when failing to correct for one or the other of these confounds. Overall, our results demonstrate that this relationship is replicable, statistically robust, and not unique to the special case of intra-hemispheric connectivity between cortical areas. Possible mechanistic explanations for this relationship come from computational models, which suggest that widespread inputs may stabilize the dynamics of high degree regions (Gollo et al., 2015), and that local synaptic integration may act as a low pass filter on these inputs (Baria et al., 2013).

In contrast to our findings for structural connectivity, we did not observe a significant correlation between timescale and functional connectivity degree in either dataset[2]. That said, we caution readers against drawing any strong conclusions based on these results, as the magnitude of the effects we *did* observe are comparable to those for structural connectivity. As such, our findings on the relationship between timescale and functional connectivity degree sit in an ambiguous statistical "limbo" (de Hollander et al., 2014); not themselves significant, but not significantly weaker than the significant effects we did observe. We are aware of two

[1] The work by (Sethi et al., 2017) similarly focused on a single hemisphere, but included connections to and from subcortical areas. That said it should be noted that this study differs from our work and the studies by Baria and Fallon insofar as it analyzed a directed network derived from tract-tracing in mice rather than undirected connectivity estimated from diffusion tractography in humans.

[2] This effect was significant in the validation data in our initial analysis, but became substantially weaker and failed to reach significance when excluding cortical ROIs with low tSNR.

previous human resting fMRI studies which found a tendency for regions with slower dynamics to exhibit greater functional connectivity degree (Baria et al., 2013; Shinn et al., 2021). While additional work is needed to determine exactly which factors are driving the discrepancy between our current findings and those in prior reports, we note that our use of weighted degree and consideration of all positive connections differs from the methods used by (Baria et al., 2013) and (Shinn et al., 2021), both of whom estimated degree as the number of connections exceeding a given threshold.

A major contribution of this work is our demonstration that cortical timescales are related to features of network topology which consider the modular organization of structural and functional brain networks. We show that brain areas with long timescales also tend to have higher within-community functional connectivity, and that this effect is at least partially independent of the extent to which these regions also exhibit high overall functional connectivity degree. Within the modular community structure of functional brain networks, these hubs are topologically positioned to facilitate segregated processing by integrating information within functionally specialized subsystems (Bertolero et al., 2018; Sporns, 2013; van den Heuvel & Sporns, 2013b), and our results suggest that this role is reflected in their dynamics. In contrast, we did not find evidence for a relationship between timescales and the extent to which each cortical area exhibits diverse functional connectivity across communities. This finding runs counter to our initial predictions, but is consistent with the fact that regions with diverse connectivity do not necessarily also exhibit widespread connectivity (i.e. regions with high PC do not necessarily also have high within-community or overall degree; (Oldham et al., 2019)). Indeed, we found that FC PC was negatively correlated with FC WD across scales in both datasets (Fig. S8). Together, these results suggest that long timescales may reflect topologically local rather than global integration within functional connectivity networks. Further, they are consistent with the possibility that timescale hierarchies may exist *within* each functionally specialized network module, though further work is needed to directly test this hypothesis.

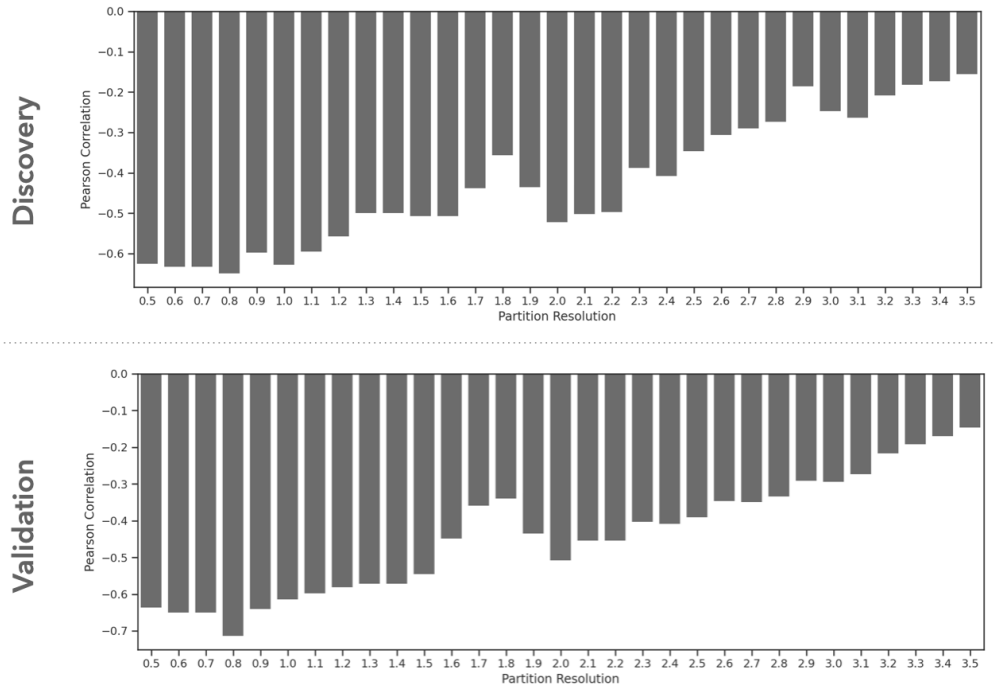


Figure S8: Correlation between WD and PC in the functional connectivity network.

We also found that regions with longer timescales tend to have more diverse structural connectivity. This finding stands in contrast to the lack of an association between timescale and participation coefficient in the functional connectivity network[3], and underscores the fact that functional connectivity patterns do not necessarily mirror the organization of the underlying structural connectome. The relationship between structural connectivity and functional connectivity is complex and spatially heterogeneous, and many areas with highly correlated brain activity do not have direct anatomical connections (Suárez et al., 2020; Vázquez-Rodríguez et al., 2019; Zamani Esfahlani et al., 2022). Similarly, as evidenced in our results, network communities in the structural connectome do not necessarily correspond to functionally specialized information processing modules. As such, the functional significance of structural connectome topology is not always readily apparent, and must often be discovered iteratively through experimentation rather than intuition. Our results add to this literature. Recent work suggests that regions with diverse structural connectivity have a topology which favors global multi-synaptic interactions (Bazinet et al., 2021). Further, many the regions identified by Bazinet and colleagues as having the strongest preference for topologically global multi-synaptic interactions overlap with areas we found to have consistently long timescales, while many of the areas with the strongest preference for topologically local mono-synaptic interactions overlap with regions we identified as having the shortest timescales. This suggests that long timescales in regions with diverse structural connectivity may reflect the integration

[3] Though we note that the difference in effects between FC PC and SC PC was only significant in both datasets at the two finest scales.

of signals across a wide range of remote brain areas, including regions to which they exhibit no direct anatomical connections. Our results may also provide insight into recent reports of timescale disruption in psychiatric disorders (Watanabe et al., 2019; Wengler et al., 2020), as regions with diverse structural connectivity are also more likely to exhibit disrupted activity in these conditions (Crossley et al., 2014).

Finally, we found a weak but significant correlation between the strength of functional connectivity between brain areas and the extent to which they exhibit similar timescales. The magnitude of this effect is comparable to that found in a recent report by (Shafiei et al., 2020), who found stronger structural connectivity between regions with similar time series properties. In contrast, we did not find evidence for preferential structural connectivity between cortical areas with similar timescales. These results suggest that functional assemblies may exhibit similar timescales, though we only found evidence for greater timescale similarity within versus between functional network communities in one of the two datasets we analyzed.

This study has at least seven limitations. First, while we analyzed fMRI data from multiple datasets, we compared timescales estimated from those data to a single common structural connectome. As such, our analyses of each dataset are not fully independent. Second, our analysis focused on group-level estimates of timescale and connectivity, and the effects we observe may not fully generalize in individual participants (Fisher et al., 2018). Third, we used only a single parcellation of cortical and subcortical areas, and it is possible that our results might differ when using alternative region definitions or when investigating timescales and connectivity at the level of individual voxels. Fourth, the parcellation we chose did not include any cerebellar regions. Fifth, recent work suggests that the generative null model to account for spatial autocorrelation may not exactly control the false positive rate (Markello & Misic, 2021). Sixth, we focused exclusively on communities identified through modularity maximization, and thus did not consider other kinds of network organization such as core-periphery or disassortative community structure (Betzel et al., 2018; Faskowitz et al., 2018). Seventh, we did not account for the potential confounding effect of time series autocorrelation on functional connectivity estimates (Afyouni et al., 2019; Bartlett, 1935). Our findings should be considered in light of these limitations.

Supplemental Information

Robustness to tSNR

To ensure the observed associations between cortical timescales and network topology were not confounded by tSNR, we repeated our analyses of the validation data after excluding the 21 cortical ROIs (i.e. the bottom decile) with the lowest tSNR. The only effect which was not robust to these exclusions was the correlation between timescale and FC degree, which became substantially weaker (r = 0.103, p_{perm}^{FDR} = 0.624). The relationship between timescale and SC degree remained highly significant (r = 0.429, p_{perm}^{FDR} = 0.003). The relationships between timescale and FC WD, SC WD, and SC PC also remained significant at multiple scales (Fig. S9)



Figure S9: Modular topology associations in validation data after excluding regions with low tSNR. Asterisks highlight correlations that are significant at FDR q ≥ 0.05.

References

Abraham, A., Pedregosa, F., Eickenberg, M., Gervais, P., Mueller, A., Kossaifi, J., Gramfort, A., Thirion, B., & Varoquaux, G. (2014). Machine learning for neuroimaging with scikit-learn. *Frontiers in Neuroinformatics*, *8*, 14. https://doi.org/10.3389/fninf.2014.00014

Achard, S., Salvador, R., Whitcher, B., Suckling, J., & Bullmore, E. (2006). A resilient, low-frequency, small-world human brain functional network with highly connected association cortical hubs. *The Journal of Neuroscience: The Official Journal of the Society for Neuroscience*, *26*(1), 63–72. https://doi.org/10.1523/JNEUROSCI.3874-05.2006

Afyouni, S., Smith, S. M., & Nichols, T. E. (2019). Effective degrees of freedom of the Pearson's correlation coefficient under autocorrelation. *NeuroImage*, *199*, 609–625. https://doi.org/10.1016/j.neuroimage.2019.05.011

Akiki, T. J., & Abdallah, C. G. (2019). Determining the Hierarchical Architecture of the Human Brain Using Subject-Level Clustering of Functional Networks. *Scientific Reports*, *9*(1), 19290. https://doi.org/10.1038/s41598-019-55738-y

Alexander-Bloch, A. F., Shou, H., Liu, S., Satterthwaite, T. D., Glahn, D. C., Shinohara, R. T., Vandekar, S. N., & Raznahan, A. (2018). On testing for spatial correspondence between maps of human brain structure and function. *NeuroImage*, *178*, 540–551. https://doi.org/10.1016/j.neuroimage.2018.05.070

Alexander-Bloch, A. F., Vértes, P. E., Stidd, R., Lalonde, F., Clasen, L., Rapoport, J., Giedd, J., Bullmore, E. T., & Gogtay, N. (2013). The Anatomical Distance of Functional Connections Predicts Brain Network Topology in Health and Schizophrenia. In *Cerebral Cortex* (Vol. 23, Issue 1, pp. 127–138). https://doi.org/10.1093/cercor/bhr388

Ashourvan, A., Telesford, Q. K., Verstynen, T., Vettel, J. M., & Bassett, D. S. (2019). Multi-scale detection of hierarchical community architecture in structural and functional brain networks. *PloS One*, *14*(5), e0215520. https://doi.org/10.1371/journal.pone.0215520

Baldassano, C., Chen, J., Zadbood, A., Pillow, J. W., Hasson, U., & Norman, K. A. (2017).

Discovering Event Structure in Continuous Narrative Perception and Memory. *Neuron*, *95*(3), 709–721.e5. https://doi.org/10.1016/j.neuron.2017.06.041

Barbas, H., & Rempel-Clower, N. (1997). Cortical structure predicts the pattern of corticocortical connections. *Cerebral Cortex* , *7*(7), 635–646. https://doi.org/10.1093/cercor/7.7.635

Baria, A. T., Mansour, A., Huang, L., Baliki, M. N., Cecchi, G. A., Mesulam, M. M., & Apkarian, A. V. (2013). Linking human brain local activity fluctuations to structural and functional network architectures. *NeuroImage*, *73*, 144–155. https://doi.org/10.1016/j.neuroimage.2013.01.072

Bartlett, M. S. (1935). Some Aspects of the Time-Correlation Problem in Regard to Tests of Significance. In *Journal of the Royal Statistical Society* (Vol. 98, Issue 3, p. 536). https://doi.org/10.2307/2342284

Bassett, D. S., Porter, M. A., Wymbs, N. F., Grafton, S. T., Carlson, J. M., & Mucha, P. J. (2013). Robust detection of dynamic community structure in networks. *Chaos* , *23*(1), 013142. https://doi.org/10.1063/1.4790830

Bazinet, V., Vos de Wael, R., Hagmann, P., Bernhardt, B. C., & Misic, B. (2021). Multiscale communication in cortico-cortical networks. *NeuroImage*, *243*, 118546. https://doi.org/10.1016/j.neuroimage.2021.118546

Behzadi, Y., Restom, K., Liau, J., & Liu, T. T. (2007). A component based noise correction method (CompCor) for BOLD and perfusion based fMRI. *NeuroImage*, *37*(1), 90–101. https://doi.org/10.1016/j.neuroimage.2007.04.042

Benjamini, Y., & Hochberg, Y. (1995). Controlling the false discovery rate: A practical and powerful approach to multiple testing. *Journal of the Royal Statistical Society*, *57*(1), 289–300. https://doi.org/10.1111/j.2517-6161.1995.tb02031.x

Benjamini, Y., & Yekutieli, D. (2005). False Discovery Rate–Adjusted Multiple Confidence Intervals for Selected Parameters. *Journal of the American Statistical Association*, *100*(469), 71–81. https://doi.org/10.1198/016214504000001907

Bertolero, M. A., Yeo, B. T. T., Bassett, D. S., & D'Esposito, M. (2018). A mechanistic model of connector hubs, modularity and cognition. *Nature Human Behaviour*, *2*(10), 765–777. https://doi.org/10.1038/s41562-018-0420-6

Bertolero, M. A., Yeo, B. T. T., & D'Esposito, M. (2015). The modular and integrative functional architecture of the human brain. *Proceedings of the National Academy of Sciences of the United States of America*, *112*(49), E6798–E6807. https://doi.org/10.1073/pnas.1510619112

Bertolero, M. A., Yeo, B. T. T., & D'Esposito, M. (2017). The diverse club. *Nature Communications*, *8*(1), 1277. https://doi.org/10.1038/s41467-017-01189-w

Betzel, R. F., & Bassett, D. S. (2017). Multi-scale brain networks. *NeuroImage*, *160*, 73–83.

https://doi.org/10.1016/j.neuroimage.2016.11.006

Betzel, R. F., Medaglia, J. D., & Bassett, D. S. (2018). Diversity of meso-scale architecture in human and non-human connectomes. *Nature Communications*, *9*(1), 346. https://doi.org/10.1038/s41467-017-02681-z

Betzel, R. F., Medaglia, J. D., Papadopoulos, L., Baum, G. L., Gur, R., Gur, R., Roalf, D., Satterthwaite, T. D., & Bassett, D. S. (2017). The modular organization of human anatomical brain networks: Accounting for the cost of wiring. *Network Neuroscience (Cambridge, Mass.)*, *1*(1), 42–68. https://doi.org/10.1162/NETN_a_00002

Blondel, V. D., Guillaume, J. L., & Lambiotte, R. (2008). Fast unfolding of communities in large networks. *Journal of Statistical*. https://iopscience.iop.org/article/10.1088/1742-5468/2008/10/P10008/meta

Breakspear, M. (2017). Dynamic models of large-scale brain activity. *Nature Neuroscience*, *20*(3), 340–352. https://doi.org/10.1038/nn.4497

Buckner, R. L., Sepulcre, J., Talukdar, T., Krienen, F. M., Liu, H., Hedden, T., Andrews-Hanna, J. R., Sperling, R. A., & Johnson, K. A. (2009). Cortical hubs revealed by intrinsic functional connectivity: mapping, assessment of stability, and relation to Alzheimer's disease. *The Journal of Neuroscience: The Official Journal of the Society for Neuroscience*, *29*(6), 1860–1873. https://doi.org/10.1523/JNEUROSCI.5062-08.2009

Bullmore, E., & Sporns, O. (2009). Complex brain networks: graph theoretical analysis of structural and functional systems. *Nature Reviews. Neuroscience*, *10*(3), 186–198. https://doi.org/10.1038/nrn2575

Bullmore, E., & Sporns, O. (2012). The economy of brain network organization. *Nature Reviews. Neuroscience*, *13*(5), 336–349. https://doi.org/10.1038/nrn3214

Burt, J. B., Helmer, M., Shinn, M., Anticevic, A., & Murray, J. D. (2020). Generative modeling of brain maps with spatial autocorrelation. *NeuroImage*, *220*, 117038. https://doi.org/10.1016/j.neuroimage.2020.117038

Chaudhuri, R., Bernacchia, A., & Wang, X.-J. (2014). A diversity of localized timescales in network activity. *eLife*, *3*, e01239. https://doi.org/10.7554/eLife.01239

Chaudhuri, R., Knoblauch, K., Gariel, M.-A., Kennedy, H., & Wang, X.-J. (2015). A Large-Scale Circuit Mechanism for Hierarchical Dynamical Processing in the Primate Cortex. *Neuron*, *88*(2), 419–431. https://doi.org/10.1016/j.neuron.2015.09.008

Cirillo, R., Fascianelli, V., Ferrucci, L., & Genovesio, A. (2018). Neural Intrinsic Timescales in the Macaque Dorsal Premotor Cortex Predict the Strength of Spatial Response Coding. *iScience*, *10*, 203–210. https://doi.org/10.1016/j.isci.2018.11.033

Cole, M. W., Pathak, S., & Schneider, W. (2010). Identifying the brain's most globally connected

regions. *NeuroImage*, *49*(4), 3132–3148. https://doi.org/10.1016/j.neuroimage.2009.11.001

Crossley, N. A., Mechelli, A., Scott, J., Carletti, F., Fox, P. T., McGuire, P., & Bullmore, E. T. (2014). The hubs of the human connectome are generally implicated in the anatomy of brain disorders. *Brain: A Journal of Neurology*, *137*(Pt 8), 2382–2395. https://doi.org/10.1093/brain/awu132

Crossley, N. A., Mechelli, A., Vértes, P. E., Winton-Brown, T. T., Patel, A. X., Ginestet, C. E., McGuire, P., & Bullmore, E. T. (2013). Cognitive relevance of the community structure of the human brain functional coactivation network. *Proceedings of the National Academy of Sciences of the United States of America*, *110*(28), 11583–11588. https://doi.org/10.1073/pnas.1220826110

Damoiseaux, J. S., Rombouts, S. A. R. B., Barkhof, F., Scheltens, P., Stam, C. J., Smith, S. M., & Beckmann, C. F. (2006). Consistent resting-state networks across healthy subjects. *Proceedings of the National Academy of Sciences of the United States of America*, *103*(37), 13848–13853. https://doi.org/10.1073/pnas.0601417103

de Hollander, G., Wagenmakers, E.-J., Waldorp, L., & Forstmann, B. (2014). An antidote to the imager's fallacy, or how to identify brain areas that are in limbo. *PloS One*, *9*(12), e115700. https://doi.org/10.1371/journal.pone.0115700

Demirtaş, M., Burt, J. B., Helmer, M., Ji, J. L., Adkinson, B. D., Glasser, M. F., Van Essen, D. C., Sotiropoulos, S. N., Anticevic, A., & Murray, J. D. (2019). Hierarchical Heterogeneity across Human Cortex Shapes Large-Scale Neural Dynamics. *Neuron*. https://doi.org/10.1016/j.neuron.2019.01.017

de Reus, M. A., & van den Heuvel, M. P. (2013). Rich club organization and intermodule communication in the cat connectome. *The Journal of Neuroscience: The Official Journal of the Society for Neuroscience*, *33*(32), 12929–12939. https://doi.org/10.1523/JNEUROSCI.1448-13.2013

Ercsey-Ravasz, M., Markov, N. T., Lamy, C., Van Essen, D. C., Knoblauch, K., Toroczkai, Z., & Kennedy, H. (2013). A predictive network model of cerebral cortical connectivity based on a distance rule. *Neuron*, *80*(1), 184–197. https://doi.org/10.1016/j.neuron.2013.07.036

Esteban, O., Markiewicz, C. J., Blair, R. W., Moodie, C. A., Isik, A. I., Erramuzpe, A., Kent, J. D., Goncalves, M., DuPre, E., Snyder, M., Oya, H., Ghosh, S. S., Wright, J., Durnez, J., Poldrack, R. A., & Gorgolewski, K. J. (2019). fMRIPrep: a robust preprocessing pipeline for functional MRI. *Nature Methods*, *16*(1), 111–116. https://doi.org/10.1038/s41592-018-0235-4

Fallon, J., Ward, P. G. D., Parkes, L., Oldham, S., Arnatkevičiūtė, A., Fornito, A., & Fulcher, B. D. (2020). Timescales of spontaneous fMRI fluctuations relate to structural connectivity in the brain. *Network Neuroscience (Cambridge, Mass.)*, *4*(3), 788–806. https://doi.org/10.1162/netn_a_00151

Fallon, J., Ward, P., Parkes, L., Oldham, S., Arnatkevičiūtė, A., Fornito, A., & Fulcher, B. D. (2019).

Timescales of spontaneous activity fluctuations relate to structural connectivity in the brain. In *bioRxiv* (p. 655050). https://doi.org/10.1101/655050

Fan, L., Li, H., Zhuo, J., Zhang, Y., Wang, J., Chen, L., Yang, Z., Chu, C., Xie, S., Laird, A. R., Fox, P. T., Eickhoff, S. B., Yu, C., & Jiang, T. (2016). The Human Brainnetome Atlas: A New Brain Atlas Based on Connectional Architecture. *Cerebral Cortex* , *26*(8), 3508–3526. https://doi.org/10.1093/cercor/bhw157

Faskowitz, J., Yan, X., Zuo, X.-N., & Sporns, O. (2018). Weighted Stochastic Block Models of the Human Connectome across the Life Span. *Scientific Reports*, *8*(1), 12997. https://doi.org/10.1038/s41598-018-31202-1

Fisher, A. J., Medaglia, J. D., & Jeronimus, B. F. (2018). Lack of group-to-individual generalizability is a threat to human subjects research. *Proceedings of the National Academy of Sciences of the United States of America*, *115*(27), E6106–E6115. https://doi.org/10.1073/pnas.1711978115

Fornito, A., Zalesky, A., & Bullmore, E. T. (Eds.). (2016). Chapter 4 - Node Degree and Strength. In *Fundamentals of Brain Network Analysis* (pp. 115–136). Academic Press. https://doi.org/10.1016/B978-0-12-407908-3.00004-2

Fortunato, S., & Barthélemy, M. (2007). Resolution limit in community detection. *Proceedings of the National Academy of Sciences of the United States of America*, *104*(1), 36–41. https://doi.org/10.1073/pnas.0605965104

Fox, M. D., Snyder, A. Z., Vincent, J. L., Corbetta, M., Van Essen, D. C., & Raichle, M. E. (2005). The human brain is intrinsically organized into dynamic, anticorrelated functional networks. *Proceedings of the National Academy of Sciences of the United States of America*, *102*(27), 9673–9678. https://doi.org/10.1073/pnas.0504136102

Fox, M. D., Zhang, D., Snyder, A. Z., & Raichle, M. E. (2009). The global signal and observed anticorrelated resting state brain networks. *Journal of Neurophysiology*, *101*(6), 3270–3283. https://doi.org/10.1152/jn.90777.2008

Fulcher, B. D., & Jones, N. S. (2017). hctsa: A Computational Framework for Automated Time-Series Phenotyping Using Massive Feature Extraction. *Cell Systems*, *5*(5), 527–531.e3. https://doi.org/10.1016/j.cels.2017.10.001

Fulcher, B. D., Little, M. A., & Jones, N. S. (2013). Highly comparative time-series analysis: the empirical structure of time series and their methods. *Journal of the Royal Society, Interface / the Royal Society*, *10*(83), 20130048. https://doi.org/10.1098/rsif.2013.0048

Gao, R., van den Brink, R. L., Pfeffer, T., & Voytek, B. (2020). Neuronal timescales are functionally dynamic and shaped by cortical microarchitecture. *eLife*, *9*. https://doi.org/10.7554/eLife.61277

Gelman, A., & Stern, H. (2006). The Difference Between “Significant” and “Not Significant” is

not Itself Statistically Significant. *The American Statistician*, *60*(4), 328–331. https://doi.org/10.1198/000313006X152649

Girvan, M., & Newman, M. E. J. (2002). Community structure in social and biological networks. *Proceedings of the National Academy of Sciences of the United States of America*, *99*(12), 7821–7826. https://doi.org/10.1073/pnas.122653799

Glasser, M. F., Sotiropoulos, S. N., Wilson, J. A., Coalson, T. S., Fischl, B., Andersson, J. L., Xu, J., Jbabdi, S., Webster, M., Polimeni, J. R., Van Essen, D. C., & Jenkinson, M. (2013). The minimal preprocessing pipelines for the Human Connectome Project. *NeuroImage*, *80*, 105–124. https://doi.org/10.1016/j.neuroimage.2013.04.127

Golesorkhi, M., Gomez-Pilar, J., Tumati, S., Fraser, M., & Northoff, G. (2021). Temporal hierarchy of intrinsic neural timescales converges with spatial core-periphery organization. *Communications Biology*, *4*(1), 277. https://doi.org/10.1038/s42003-021-01785-z

Gollo, L. L., Zalesky, A., Hutchison, R. M., van den Heuvel, M., & Breakspear, M. (2015). Dwelling quietly in the rich club: brain network determinants of slow cortical fluctuations. *Philosophical Transactions of the Royal Society of London. Series B, Biological Sciences*, *370*(1668). https://doi.org/10.1098/rstb.2014.0165

Good, B. H., de Montjoye, Y.-A., & Clauset, A. (2010). Performance of modularity maximization in practical contexts. *Physical Review. E, Statistical, Nonlinear, and Soft Matter Physics*, *81*(4 Pt 2), 046106. https://doi.org/10.1103/PhysRevE.81.046106

Goulas, A., Werner, R., Beul, S. F., Säring, D., van den Heuvel, M., Triarhou, L. C., & Hilgetag, C. C. (2016). Cytoarchitectonic similarity is a wiring principle of the human connectome. In *bioRxiv* (p. 068254). https://doi.org/10.1101/068254

Grayson, D. S., Ray, S., Carpenter, S., Iyer, S., Dias, T. G. C., Stevens, C., Nigg, J. T., & Fair, D. A. (2014). Structural and functional rich club organization of the brain in children and adults. *PloS One*, *9*(2), e88297. https://doi.org/10.1371/journal.pone.0088297

Griffanti, L., Salimi-Khorshidi, G., Beckmann, C. F., Auerbach, E. J., Douaud, G., Sexton, C. E., Zsoldos, E., Ebmeier, K. P., Filippini, N., Mackay, C. E., Moeller, S., Xu, J., Yacoub, E., Baselli, G., Ugurbil, K., Miller, K. L., & Smith, S. M. (2014). ICA-based artefact removal and accelerated fMRI acquisition for improved resting state network imaging. *NeuroImage*, *95*, 232–247. https://doi.org/10.1016/j.neuroimage.2014.03.034

Guimerà, R., & Amaral, L. A. N. (2005). Cartography of complex networks: modules and universal roles. *Journal of Statistical Mechanics* , *2005*(P02001), nihpa35573. https://doi.org/10.1088/1742-5468/2005/02/P02001

Guimerà, R., & Nunes Amaral, L. A. (2005). Functional cartography of complex metabolic networks. *Nature*, *433*(7028), 895–900. https://doi.org/10.1038/nature03288

Hagmann, P., Cammoun, L., Gigandet, X., Meuli, R., Honey, C. J., Wedeen, V. J., & Sporns, O.

(2008). Mapping the Structural Core of Human Cerebral Cortex. *PLoS Biology*, *6*(7), e159. https://doi.org/10.1371/journal.pbio.0060159

Harriger, L., van den Heuvel, M. P., & Sporns, O. (2012). Rich club organization of macaque cerebral cortex and its role in network communication. *PloS One*, *7*(9), e46497. https://doi.org/10.1371/journal.pone.0046497

Hasson, U., Yang, E., Vallines, I., Heeger, D. J., & Rubin, N. (2008). A hierarchy of temporal receptive windows in human cortex. *The Journal of Neuroscience: The Official Journal of the Society for Neuroscience*, *28*(10), 2539–2550. https://doi.org/10.1523/JNEUROSCI.5487-07.2008

He, Y., Lim, S., Fortunato, S., Sporns, O., Zhang, L., Qiu, J., Xie, P., & Zuo, X.-N. (2018). Reconfiguration of Cortical Networks in MDD Uncovered by Multiscale Community Detection with fMRI. *Cerebral Cortex* , *28*(4), 1383–1395. https://doi.org/10.1093/cercor/bhx335

He, Y., Wang, J., Wang, L., Chen, Z. J., Yan, C., Yang, H., Tang, H., Zhu, C., Gong, Q., Zang, Y., & Evans, A. C. (2009). Uncovering intrinsic modular organization of spontaneous brain activity in humans. *PloS One*, *4*(4), e5226. https://doi.org/10.1371/journal.pone.0005226

Huang, Z., Liu, X., Mashour, G. A., & Hudetz, A. G. (2018). Timescales of Intrinsic BOLD Signal Dynamics and Functional Connectivity in Pharmacologic and Neuropathologic States of Unconsciousness. *The Journal of Neuroscience: The Official Journal of the Society for Neuroscience*, *38*(9), 2304–2317. https://doi.org/10.1523/JNEUROSCI.2545-17.2018

Ito, T., Hearne, L. J., & Cole, M. W. (2020). A cortical hierarchy of localized and distributed processes revealed via dissociation of task activations, connectivity changes, and intrinsic timescales. *NeuroImage*, *221*(117141), 117141. https://doi.org/10.1016/j.neuroimage.2020.117141

Kriegeskorte, N., Simmons, W. K., Bellgowan, P. S. F., & Baker, C. I. (2009). Circular analysis in systems neuroscience: the dangers of double dipping. *Nature Neuroscience*, *12*(5), 535–540. https://doi.org/10.1038/nn.2303

Lancichinetti, A., & Fortunato, S. (2012). Consensus clustering in complex networks. *Scientific Reports*, *2*, 336. https://doi.org/10.1038/srep00336

Lee, W.-C. A., Bonin, V., Reed, M., Graham, B. J., Hood, G., Glattfelder, K., & Reid, R. C. (2016). Anatomy and function of an excitatory network in the visual cortex. *Nature*, *532*(7599), 370–374. https://doi.org/10.1038/nature17192

Li, S., & Wang, X.-J. (2022). Hierarchical timescales in the neocortex: Mathematical mechanism and biological insights. *Proceedings of the National Academy of Sciences of the United States of America*, *119*(6). https://doi.org/10.1073/pnas.2110274119

Lubba, C. H., Sethi, S. S., Knaute, P., Schultz, S. R., Fulcher, B. D., & Jones, N. S. (2019). catch22:

CAnonical Time-series CHaracteristics. *Data Mining and Knowledge Discovery*, *33*(6), 1821–1852. https://doi.org/10.1007/s10618-019-00647-x

Lurie, D. (2018). *Exploring the relationship between regional connectivity profile and activity dynamics*. Open Science Framework. https://doi.org/10.17605/OSF.IO/T42PD

Maisson, D. J.-N., Cash-Padgett, T. V., Wang, M. Z., Hayden, B. Y., Heilbronner, S. R., & Zimmermann, J. (2021). Choice-relevant information transformation along a ventrodorsal axis in the medial prefrontal cortex. *Nature Communications*, *12*(1), 4830. https://doi.org/10.1038/s41467-021-25219-w

Manea, A. M. G., Zilverstand, A., Ugurbil, K., Heilbronner, S. R., & Zimmermann, J. (2022). Intrinsic timescales as an organizational principle of neural processing across the whole rhesus macaque brain. *eLife*, *11*. https://doi.org/10.7554/eLife.75540

Markello, R. D., & Misic, B. (2021). Comparing spatial null models for brain maps. *NeuroImage*, *236*, 118052. https://doi.org/10.1016/j.neuroimage.2021.118052

Meilă, M. (2003). Comparing Clusterings by the Variation of Information. *Learning Theory and Kernel Machines*, 173–187. https://doi.org/10.1007/978-3-540-45167-9_14

Mesulam, M. M. (1998). From sensation to cognition. *Brain: A Journal of Neurology*, *121 (Pt 6)*, 1013–1052. https://doi.org/10.1093/brain/121.6.1013

Meunier, D., Lambiotte, R., Fornito, A., Ersche, K. D., & Bullmore, E. T. (2009). Hierarchical modularity in human brain functional networks. *Frontiers in Neuroinformatics*, *3*, 37. https://doi.org/10.3389/neuro.11.037.2009

Müller, E. J., Munn, B., Hearne, L. J., Smith, J. B., Fulcher, B., Arnatkevičiūtė, A., Lurie, D. J., Cocchi, L., & Shine, J. M. (2020). Core and matrix thalamic sub-populations relate to spatio-temporal cortical connectivity gradients. *NeuroImage*, *222*, 117224. https://doi.org/10.1016/j.neuroimage.2020.117224

Murphy, K., Birn, R. M., Handwerker, D. A., Jones, T. B., & Bandettini, P. A. (2009). The impact of global signal regression on resting state correlations: are anti-correlated networks introduced? *NeuroImage*, *44*(3), 893–905. https://doi.org/10.1016/j.neuroimage.2008.09.036

Murray, J. D., Bernacchia, A., Freedman, D. J., Romo, R., Wallis, J. D., Cai, X., Padoa-Schioppa, C., Pasternak, T., Seo, H., Lee, D., & Wang, X.-J. (2014). A hierarchy of intrinsic timescales across primate cortex. *Nature Neuroscience*, *17*(12), 1661–1663. https://doi.org/10.1038/nn.3862

Newman, M. E. J. (2006). Modularity and community structure in networks. *Proceedings of the National Academy of Sciences of the United States of America*, *103*(23), 8577–8582. https://doi.org/10.1073/pnas.0601602103

Nieuwenhuis, S., Forstmann, B. U., & Wagenmakers, E.-J. (2011). Erroneous analyses of

interactions in neuroscience: a problem of significance. *Nature Neuroscience*, *14*(9), 1105–1107. https://doi.org/10.1038/nn.2886

Nooner, K. B., Colcombe, S. J., Tobe, R. H., Mennes, M., Benedict, M. M., Moreno, A. L., Panek, L. J., Brown, S., Zavitz, S. T., Li, Q., Sikka, S., Gutman, D., Bangaru, S., Schlachter, R. T., Kamiel, S. M., Anwar, A. R., Hinz, C. M., Kaplan, M. S., Rachlin, A. B., … Milham, M. P. (2012). The NKI-Rockland Sample: A Model for Accelerating the Pace of Discovery Science in Psychiatry. *Frontiers in Neuroscience*, *6*, 152. https://doi.org/10.3389/fnins.2012.00152

Nougaret, S., Fascianelli, V., Ravel, S., & Genovesio, A. (2021). Intrinsic timescales across the basal ganglia. *Scientific Reports*, *11*(1), 21395. https://doi.org/10.1038/s41598-021-00512-2

Oldham, S., Fulcher, B., Parkes, L., Arnatkevic Iūtė, A., Suo, C., & Fornito, A. (2019). Consistency and differences between centrality measures across distinct classes of networks. *PloS One*, *14*(7), e0220061. https://doi.org/10.1371/journal.pone.0220061

Power, J. D., Cohen, A. L., Nelson, S. M., Wig, G. S., Barnes, K. A., Church, J. A., Vogel, A. C., Laumann, T. O., Miezin, F. M., Schlaggar, B. L., & Petersen, S. E. (2011). Functional network organization of the human brain. *Neuron*, *72*(4), 665–678. https://doi.org/10.1016/j.neuron.2011.09.006

Power, J. D., Schlaggar, B. L., Lessov-Schlaggar, C. N., & Petersen, S. E. (2013). Evidence for Hubs in Human Functional Brain Networks. *Neuron*, *79*(4), 798–813. https://doi.org/10.1016/j.neuron.2013.07.035

Raut, R. V., Snyder, A. Z., & Raichle, M. E. (2020). Hierarchical dynamics as a macroscopic organizing principle of the human brain. *Proceedings of the National Academy of Sciences of the United States of America*, *117*(34), 20890–20897. https://doi.org/10.1073/pnas.2003383117

Rosenblatt, J. D., & Benjamini, Y. (2014). Selective correlations; not voodoo. *NeuroImage*, *103*, 401–410. https://doi.org/10.1016/j.neuroimage.2014.08.023

Rossi-Pool, R., Zainos, A., Alvarez, M., Parra, S., Zizumbo, J., & Romo, R. (2021). Invariant timescale hierarchy across the cortical somatosensory network. *Proceedings of the National Academy of Sciences of the United States of America*, *118*(3). https://doi.org/10.1073/pnas.2021843118

Rubinov, M., & Sporns, O. (2010). Complex network measures of brain connectivity: uses and interpretations. *NeuroImage*, *52*(3), 1059–1069. https://doi.org/10.1016/j.neuroimage.2009.10.003

Runyan, C. A., Piasini, E., Panzeri, S., & Harvey, C. D. (2017). Distinct timescales of population coding across cortex. *Nature*, *548*(7665), 92–96. https://doi.org/10.1038/nature23020

Schroeter, M. S., Charlesworth, P., Kitzbichler, M. G., Paulsen, O., & Bullmore, E. T. (2015). Emergence of rich-club topology and coordinated dynamics in development of hippocampal functional networks in vitro. *The Journal of Neuroscience: The Official Journal of the Society for*

Neuroscience, *35*(14), 5459–5470. https://doi.org/10.1523/JNEUROSCI.4259-14.2015

Sethi, S. S., Zerbi, V., Wenderoth, N., Fornito, A., & Fulcher, B. D. (2017). Structural connectome topology relates to regional BOLD signal dynamics in the mouse brain. *Chaos* , *27*(4), 047405. https://doi.org/10.1063/1.4979281

Shafiei, G., Markello, R. D., Vos de Wael, R., Bernhardt, B. C., Fulcher, B. D., & Misic, B. (2020). Topographic gradients of intrinsic dynamics across neocortex. *eLife*, *9*. https://doi.org/10.7554/eLife.62116

Shafiei, G., Zeighami, Y., Clark, C. A., Coull, J. T., Nagano-Saito, A., Leyton, M., Dagher, A., & Mišic, B. (2019). Dopamine Signaling Modulates the Stability and Integration of Intrinsic Brain Networks. *Cerebral Cortex* , *29*(1), 397–409. https://doi.org/10.1093/cercor/bhy264

Shimono, M., & Beggs, J. M. (2015). Functional Clusters, Hubs, and Communities in the Cortical Microconnectome. *Cerebral Cortex* , *25*(10), 3743–3757. https://doi.org/10.1093/cercor/bhu252

Shine, J. M., Bissett, P. G., Bell, P. T., Koyejo, O., Balsters, J. H., Gorgolewski, K. J., Moodie, C. A., & Poldrack, R. A. (2016). The Dynamics of Functional Brain Networks: Integrated Network States during Cognitive Task Performance. *Neuron*, *92*(2), 544–554. https://doi.org/10.1016/j.neuron.2016.09.018

Shinn, M., Hu, A., Turner, L., Noble, S., Achard, S., Anticevic, A., Scheinost, D., Todd Constable, R., Lee, D., Bullmore, E. T., & Murray, J. D. (2021). Spatial and temporal autocorrelation weave human brain networks. In *bioRxiv* (p. 2021.06.01.446561). https://doi.org/10.1101/2021.06.01.446561

Smith, S. M., Fox, P. T., Miller, K. L., Glahn, D. C., Fox, P. M., Mackay, C. E., Filippini, N., Watkins, K. E., Toro, R., Laird, A. R., & Beckmann, C. F. (2009). Correspondence of the brain's functional architecture during activation and rest. *Proceedings of the National Academy of Sciences of the United States of America*, *106*(31), 13040–13045. https://doi.org/10.1073/pnas.0905267106

Sporns, O. (2013). Network attributes for segregation and integration in the human brain. *Current Opinion in Neurobiology*, *23*(2), 162–171. https://doi.org/10.1016/j.conb.2012.11.015

Sporns, O., & Betzel, R. F. (2016). Modular Brain Networks. *Annual Review of Psychology*, *67*, 613–640. https://doi.org/10.1146/annurev-psych-122414-033634

Stephens, G. J., Honey, C. J., & Hasson, U. (2013). A place for time: the spatiotemporal structure of neural dynamics during natural audition. *Journal of Neurophysiology*, *110*(9), 2019–2026. https://doi.org/10.1152/jn.00268.2013

Suárez, L. E., Markello, R. D., Betzel, R. F., & Misic, B. (2020). Linking Structure and Function in Macroscale Brain Networks. *Trends in Cognitive Sciences*, *24*(4), 302–315. https://doi.org/10.1016/j.tics.2020.01.008

Toker, D., Sommer, F. T., & D'Esposito, M. (2020). A simple method for detecting chaos in nature. *Communications Biology*, *3*, 11. https://doi.org/10.1038/s42003-019-0715-9

Tomasi, D., & Volkow, N. D. (2011). Functional connectivity hubs in the human brain. *NeuroImage*, *57*(3), 908–917. https://doi.org/10.1016/j.neuroimage.2011.05.024

Uddin, L. Q., Yeo, B. T. T., & Spreng, R. N. (2019). Towards a Universal Taxonomy of Macro-scale Functional Human Brain Networks. *Brain Topography*, *32*(6), 926–942. https://doi.org/10.1007/s10548-019-00744-6

van den Heuvel, M. P., Kahn, R. S., Goñi, J., & Sporns, O. (2012). High-cost, high-capacity backbone for global brain communication. *Proceedings of the National Academy of Sciences of the United States of America*, *109*(28), 11372–11377. https://doi.org/10.1073/pnas.1203593109

van den Heuvel, M. P., & Sporns, O. (2011). Rich-Club Organization of the Human Connectome. *The Journal of Neuroscience: The Official Journal of the Society for Neuroscience*, *31*(44), 15775–15786. https://doi.org/10.1523/JNEUROSCI.3539-11.2011

van den Heuvel, M. P., & Sporns, O. (2013a). Network hubs in the human brain. *Trends in Cognitive Sciences*, *17*(12), 683–696. https://doi.org/10.1016/j.tics.2013.09.012

van den Heuvel, M. P., & Sporns, O. (2013b). Network hubs in the human brain. *Trends in Cognitive Sciences*, *17*(12), 683–696. https://doi.org/10.1016/j.tics.2013.09.012

van den Heuvel, M. P., & Sporns, O. (2013c). An anatomical substrate for integration among functional networks in human cortex. *The Journal of Neuroscience: The Official Journal of the Society for Neuroscience*, *33*(36), 14489–14500. https://doi.org/10.1523/JNEUROSCI.2128-13.2013

Van Essen, D. C., Smith, S. M., Barch, D. M., Behrens, T. E. J., Yacoub, E., Ugurbil, K., & WU-Minn HCP Consortium. (2013). The WU-Minn Human Connectome Project: an overview. *NeuroImage*, *80*, 62–79. https://doi.org/10.1016/j.neuroimage.2013.05.041

Vázquez-Rodríguez, B., Suárez, L. E., Markello, R. D., Shafiei, G., Paquola, C., Hagmann, P., van den Heuvel, M. P., Bernhardt, B. C., Spreng, R. N., & Misic, B. (2019). Gradients of structure-function tethering across neocortex. *Proceedings of the National Academy of Sciences of the United States of America*, *116*(42), 21219–21227. https://doi.org/10.1073/pnas.1903403116

Vul, E., Harris, C., Winkielman, P., & Pashler, H. (2009). Puzzlingly High Correlations in fMRI Studies of Emotion, Personality, and Social Cognition. *Perspectives on Psychological Science: A Journal of the Association for Psychological Science*, *4*(3), 274–290. https://doi.org/10.1111/j.1745-6924.2009.01125.x

Wagner, G. P., Pavlicev, M., & Cheverud, J. M. (2007). The road to modularity. *Nature Reviews. Genetics*, *8*(12), 921–931. https://doi.org/10.1038/nrg2267

Wasmuht, D. F., Spaak, E., Buschman, T. J., Miller, E. K., & Stokes, M. G. (2018). Intrinsic neuronal dynamics predict distinct functional roles during working memory. *Nature Communications*, *9*(1), 3499. https://doi.org/10.1038/s41467-018-05961-4

Watanabe, T., Rees, G., & Masuda, N. (2019). Atypical intrinsic neural timescale in autism. *eLife*, *8*. https://doi.org/10.7554/eLife.42256

Wei, Y., Scholtens, L. H., Turk, E., & van den Heuvel, M. P. (2019). Multiscale examination of cytoarchitectonic similarity and human brain connectivity. *Network Neuroscience (Cambridge, Mass.)*, *3*(1), 124–137. https://doi.org/10.1162/netn_a_00057

Wengler, K., Goldberg, A. T., Chahine, G., & Horga, G. (2020). Distinct hierarchical alterations of intrinsic neural timescales account for different manifestations of psychosis. *eLife*, *9*. https://doi.org/10.7554/eLife.56151

Yeh, F.-C., Panesar, S., Fernandes, D., Meola, A., Yoshino, M., Fernandez-Miranda, J. C., Vettel, J. M., & Verstynen, T. (2018). Population-averaged atlas of the macroscale human structural connectome and its network topology. *NeuroImage*, *178*, 57–68. https://doi.org/10.1016/j.neuroimage.2018.05.027

Yeh, F.-C., & Tseng, W.-Y. I. (2011). NTU-90: a high angular resolution brain atlas constructed by q-space diffeomorphic reconstruction. *NeuroImage*, *58*(1), 91–99. https://doi.org/10.1016/j.neuroimage.2011.06.021

Yeh, F.-C., Verstynen, T. D., Wang, Y., Fernández-Miranda, J. C., & Tseng, W.-Y. I. (2013). Deterministic diffusion fiber tracking improved by quantitative anisotropy. *PloS One*, *8*(11), e80713. https://doi.org/10.1371/journal.pone.0080713

Yeo, B. T. T., Krienen, F. M., Eickhoff, S. B., Yaakub, S. N., Fox, P. T., Buckner, R. L., Asplund, C. L., & Chee, M. W. L. (2016). Functional Specialization and Flexibility in Human Association Cortex. *Cerebral Cortex* , *26*(1), 465. https://doi.org/10.1093/cercor/bhv260

Yeo, B. T. T., Krienen, F. M., Sepulcre, J., Sabuncu, M. R., Lashkari, D., Hollinshead, M., Roffman, J. L., Smoller, J. W., Zöllei, L., Polimeni, J. R., Fischl, B., Liu, H., & Buckner, R. L. (2011). The organization of the human cerebral cortex estimated by intrinsic functional connectivity. *Journal of Neurophysiology*, *106*(3), 1125–1165. https://doi.org/10.1152/jn.00338.2011

Zamani Esfahlani, F., Faskowitz, J., Slack, J., Mišić, B., & Betzel, R. F. (2022). Local structure-function relationships in human brain networks across the lifespan. *Nature Communications*, *13*(1), 2053. https://doi.org/10.1038/s41467-022-29770-y

Zilio, F., Gomez-Pilar, J., Cao, S., Zhang, J., Zang, D., Qi, Z., Tan, J., Hiromi, T., Wu, X., Fogel, S., Huang, Z., Hohmann, M. R., Fomina, T., Synofzik, M., Grosse-Wentrup, M., Owen, A. M., & Northoff, G. (2021). Are intrinsic neural timescales related to sensory processing? Evidence from abnormal behavioral states. *NeuroImage*, *226*, 117579. https://doi.org/10.1016/j.neuroimage.2020.117579

Zou, G. Y. (2007). Toward using confidence intervals to compare correlations. *Psychological Methods*, *12*(4), 399–413. https://doi.org/10.1037/1082-989X.12.4.399

Zuo, X.-N., Ehmke, R., Mennes, M., Imperati, D., Castellanos, F. X., Sporns, O., & Milham, M. P. (2012). Network Centrality in the Human Functional Connectome. *Cerebral Cortex* , *22*(8), 1862–1875. https://doi.org/10.1093/cercor/bhr269

Gradients of intrinsic dynamics show distinct relationships with anatomical and connectomic hierarchies in the cerebral cortex

Introduction

The brain is an inherently dynamic system. Fundamental to this dynamism are the time-varying patterns of activity exhibited by brain areas as they process and integrate neural signals in support of flexible cognition and adaptive behavior. Shaped by almost innumerable factors at multiple scales, these precise temporal patterns of firing and quiescence are where the rubber of neurophysiology meets the road of information processing. Building a robust science of brain function will necessarily require understanding how these dynamics vary across brain areas and behavioral contexts, as well as the anatomical and connectomic properties which give rise to these differences.

Just as the physical properties of brain areas vary in multiple ways, so too do their dynamics. However, studies of brain dynamics typically investigate only one time series property at a time. Similarly, the majority of these studies focus on time series features sensitive to a handful of common properties, such as spectral content, autocorrelation, and variability. As such, while these efforts have made important contributions to our understanding of brain function—such as the importance of variability for cognitive performance (Uddin, 2021; Waschke et al., 2021) and the discovery of a hierarchy of timescales in the primate cerebral cortex (Gao et al., 2020; Murray et al., 2014)—important questions remain about the characteristic features of regional brain dynamics, the relationships between these features, and their association with other aspects of brain structure and function.

Here, we use a data-driven "time series phenotyping" approach to characterize multiple properties of intrinsic regional brain dynamics recorded from resting fMRI in human participants. We show that a diverse set of 22 time series features vary along a small number of axes, and that these axes can be modeled as two spatial gradients, each of which has a distinct topography and captures different aspects of intrinsic dynamics. These gradients show distinct relationships to anatomical and connectomic hierarchies in the cerebral cortex, and together define a low-dimensional subspace which allows us to study and visualize how multiple time series properties vary within and between microstructurally defined cortical zones and functionally specialized subsystems. Our results replicate in an independent sample, and provide new insights into both the functional organization of the human brain as well as the methods used to study BOLD time series.

Results

Time series phenotyping of intrinsic regional brain dynamics

Following preprocessing and denoising, we extracted and z-scored the average BOLD time series from each of 400 functionally defined cortical regions (Schaefer et al., 2018). From each regional time series, we then computed 22 features (Table 1) sensitive to diverse time series properties including linear and nonlinear autocorrelation, the timing of extreme events, spectral content, and fractal scaling, as well as features based on the distribution of time series values, successive differences between neighboring time points, and symbolic transformations of the original time series. Together, these features allow us to characterize the complex multi-dimensional "phenotype" of intrinsic regional brain dynamics (B. D. Fulcher et al., 2013; B. D. Fulcher & Jones, 2017), similar to how one might measure multiple physical or psychological traits when studying individual differences in humans. This "time series phenotyping" approach produces, for each individual, a 22 x 400 (features x regions) time series feature matrix which captures how multiple aspects of intrinsic dynamics vary across the cerebral cortex. From these, we created a group-level feature matrix by calculating the median value for each feature and cortical area, and used this group-level matrix in subsequent analyses.

The 22 time series features we use here are a subset of a much larger (n > 7000) library of univariate time series features (B. D. Fulcher et al., 2013), and were selected in a data-driven manner by (Lubba et al., 2019). Specifically, Lubba and colleagues first evaluated the ability of each feature to accurately classify over 140,000 individual time series in 93 data sets taken from diverse fields including physics, engineering, finance, ecology, linguistics, and physiology (Bagnall et al., 2017). Features were then clustered based on their classification performance across data sets, and a single top performing feature was selected from each cluster. In this way, Lubba et al. identified a minimally redundant set of interpretable time series features which are maximally sensitive to differences in dynamics across domains while remaining representative of the diversity of methods used to study empirical time series.

To gain initial insight into the diversity and spatial distribution of time series phenotypes in the cerebral cortex, we used hierarchical clustering to group and order the 22 time series features based on the degree to which they produce similar results across regions. We then visualized the full 22 x 400 group-level feature matrix (Fig. 1), with brain areas arranged by hemisphere and functional connectivity network (Yeo et al., 2011). This revealed that 18 of the 22 features can be assigned to one of four clusters, each defined by a distinct pattern of variation across brain areas and functional networks. This cluster structure was replicated in the validation sample (Fig. S1).

Table 1: Time series features.

Distribution: Properties of the data distribution (which are insensitive to the time-ordering of values in the time series).
DN_HistogramMode_5: Mode of the distribution estimated using a 5-bin histogram.
DN_HistogramMode_10: Mode of the distribution estimated using a 10-bin histogram.
Extreme Events: Direction and timing of extreme events.
DN_OutlierInclude_p_001_mdrmd: Timing of extreme events above the mean.
DN_OutlierInclude_n_001_mdrmd: Timing of extreme events below the mean.
Symbolic: Features that involve symbolic transformations of a real-valued time series to a set of discrete symbols.
SB_BinaryStats_mean_longstretch1: Longest period of consecutive values above the mean.
SB_BinaryStats_diff_longstretch0: Longest period of successive incremental decreases.
SB_MotifThree_quantile_hh: Shannon entropy of two successive letters in an equiprobable 3-letter symbolization.
SB_TransitionMatrix_3ac_sumdiagcov: Trace of the covariance of the transition matrix between symbols in a 3-letter symbolization.
Linear autocorrelation and periodicity: Linear autocorrelation properties of the time series.
CO_f1ecac: First 1/*e* crossing of the autocorrelation function.
CO_FirstMin_ac: First minimum of the autocorrelation function.
FC_LocalSimple_mean3_stderr: Standard deviation of the residuals from a rolling 3-sample mean forecasting model.
PD_PeriodicityWang_th0_01: Periodicity (lag at which the autocorrelation function exhibits the first clear peak).
Nonlinear autocorrelation: Nonlinear autocorrelation properties of the time series.
CO_HistogramAMI_even_2_5: Automutual information calculated using a lag of 2 and a 5 bin histogram.
IN_AutoMutualInfoStats_40_gaussian_fmmi: First minimum of the automutual information function.
Spectral content: Statistics extracted from the power spectrum of the time series.
SP_Summaries_welch_rect_area_5_1: Total power in the lowest fifth of frequencies.
SP_Summaries_welch_rect_centroid: Centroid of the power spectrum (value at which the cumulative sum of the PSD is ½ of its maximum).
Successive differences: Statistics based on the first derivative of the time series (the time series of incremental differences).
MD_hrv_classic_pnn40: Proportion of successive differences exceeding 0.04 standard deviations.
FC_LocalSimple_mean1_tauresrat: Change in correlation length after differencing (x_{t-1}–x_t).
CO_Embed2_Dist_tau_d_expfit_meandiff: Exponential fit to successive distances in 2-dimensional time- delay embedding space.

CO_trev_1_num: Mean cubed successive differences.
Fractal scaling: Statistics of the long-range (self-affine) scaling of temporal fluctuations.
SC_FluctAnal_2_dfa_50_1_2_logi_prop_r1: Crossover point between scaling regimes in a Detrended Fluctuation Analysis (50% sampling).
SC_FluctAnal_2_rsrangefit_50_1_logi_prop_r1: Crossover point between scaling regimes in a Rescaled Range Analysis.

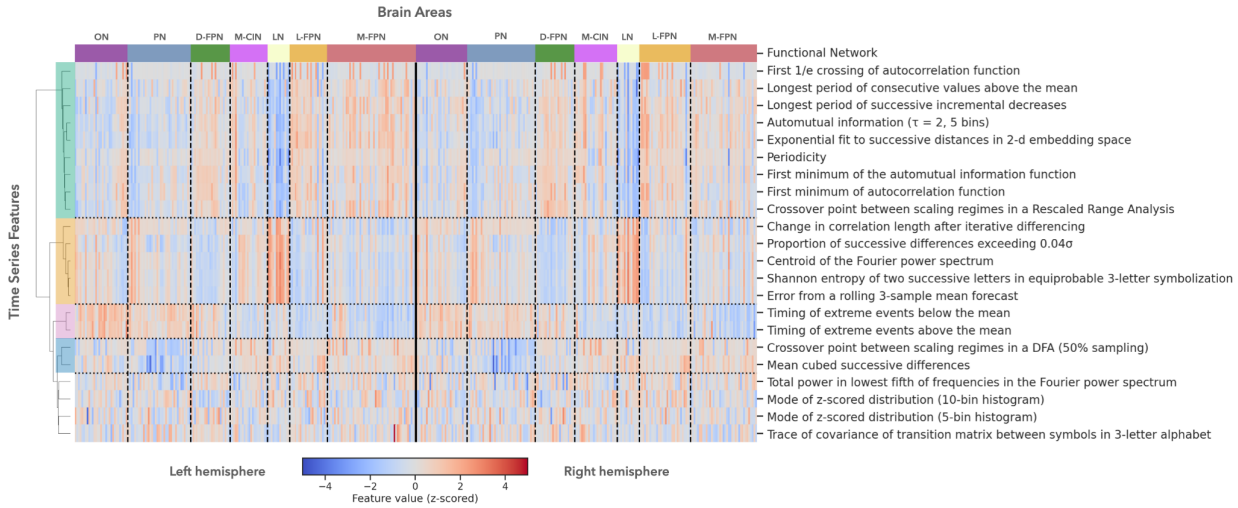


Figure 1: Time series phenotyping reveals the structure of intrinsic brain dynamics.
To characterize the dynamical properties of intrinsic BOLD activity in each cortical area (columns), we computed 22 time series features (rows) previously shown to be highly discriminative across a wide range of time-series classification tasks. Together, these features allow us to describe the multi-dimensional "time series phenotype" of intrinsic dynamics in each brain area. We then used hierarchical clustering to identify groups of features which exhibit similar patterns of variation across regions, and visualized these patterns relative to the large-scale functional architecture of the cerebral cortex (colored bar, top). We found that 18 of the 22 features can be assigned to one of four clear clusters (colored dendrogram, left). The two largest clusters (green and orange) both contain features sensitive to the "timescale" (autocorrelation) of intrinsic dynamics. Features in the third (pink) cluster capture information about the timing of extreme events, while features in the fourth (blue) cluster describe fractal scaling properties of regional time series and the symmetry of successive differences. Dotted horizontal lines delineate the four feature clusters. Left and right hemisphere regions are separated by the solid vertical line, while dashed vertical lines delineate functional connectivity networks. Network definitions are taken from (Yeo et al., 2011) and have been re-labeled using the anatomy-based taxonomy proposed by (Uddin et al., 2019): ON, occipital; PN, pericentral; D-FPN, dorsal frontoparietal; M-CIN, midcingulo-insular; LN, limbic; L-FPN, lateral frontoparietal; M-FPN, medial frontoparietal).

The two largest clusters (green and orange) both contain features sensitive to time series autocorrelation, and thus capture information about the "timescale" of intrinsic brain dynamics. These features cluster separately depending on whether they produce higher (green cluster) or lower values (orange cluster) for time series with high autocorrelation. As such, they follow two highly similar but opposite patterns of variation across brain areas. These features suggest that the shortest timescales (lowest autocorrelation) can be found in limbic regions,

while the longest timescales (highest autocorrelation) can be found in portions of the dorsal, lateral, and medial frontoparietal networks.

The two features in the third (pink) cluster are both sensitive to the timing of "extreme" events (i.e. timepoints which exceed a given threshold above or below the mean). Specifically, these features quantify the extent to which extreme events tend to occur more frequently towards the beginning (values approaching -1; Fig. 2D) or end (values approaching 1; Fig. 2C) of the resting scan. As such, these features capture information related to the "stationarity"[1] of extreme events. Both features produce a positive value for most brain areas (Fig. S2, O/P), and this tendency for extreme events to occur more frequently towards the end of the scan is most pronounced for regions in the occipital, pericentral, and dorsal frontoparietal networks (Fig. 1).

The fourth (blue) cluster contains two features which broadly distinguish regions in the pericentral network from the rest of the cortex (Fig. 1). The first of these features characterizes the symmetry of the distribution of successive differences in regional time series (i.e. increases and decreases in BOLD signal from one time point to the next). It is calculated as the mean of cubed[2] successive differences (MCSD) and produces a negative value for most brain areas (Fig. S2R), indicating an asymmetry towards sudden large decreases and more gradual increases (Fig. 2E). The second feature in this cluster uses a modification of Detrended Fluctuation Analysis (DFA) (Hardstone et al., 2012; Peng et al., 1994) to characterize the "multifractal" scaling properties of regional BOLD time series. In DFA, a scaling rule is estimated to describe the rate at which time series fluctuations grow when estimated over increasingly long timescales (window sizes). However, many real-world time series (including BOLD fMRI data) exhibit "multifractal" scaling in which there are different scaling rules across different ranges of timescales (Churchill et al., 2016; Müller et al., 2020; Peng et al., 1995; Talkner & Weber, 2000). The method used here assumes the presence of two distinct scaling regimes, and attempts to identify the "crossover" point at which scaling behavior changes (Fig. 2, G/H).

Together, our clustering results suggest that properties of intrinsic brain dynamics captured by the 22 time series features vary along a handful of common axes, each of which follows a distinct pattern of variation across cortical areas. As such, we sought to formally model this low-dimensional structure to better understand the relationships between time series features and how they interact to produce a diversity of time series phenotypes.

[1] A statistical property of a time series (here, the frequency of occurrence for extreme events) is said to be stationary if it does not change over time.

[2] Cubing has the effect of magnifying the influence of large successive differences.

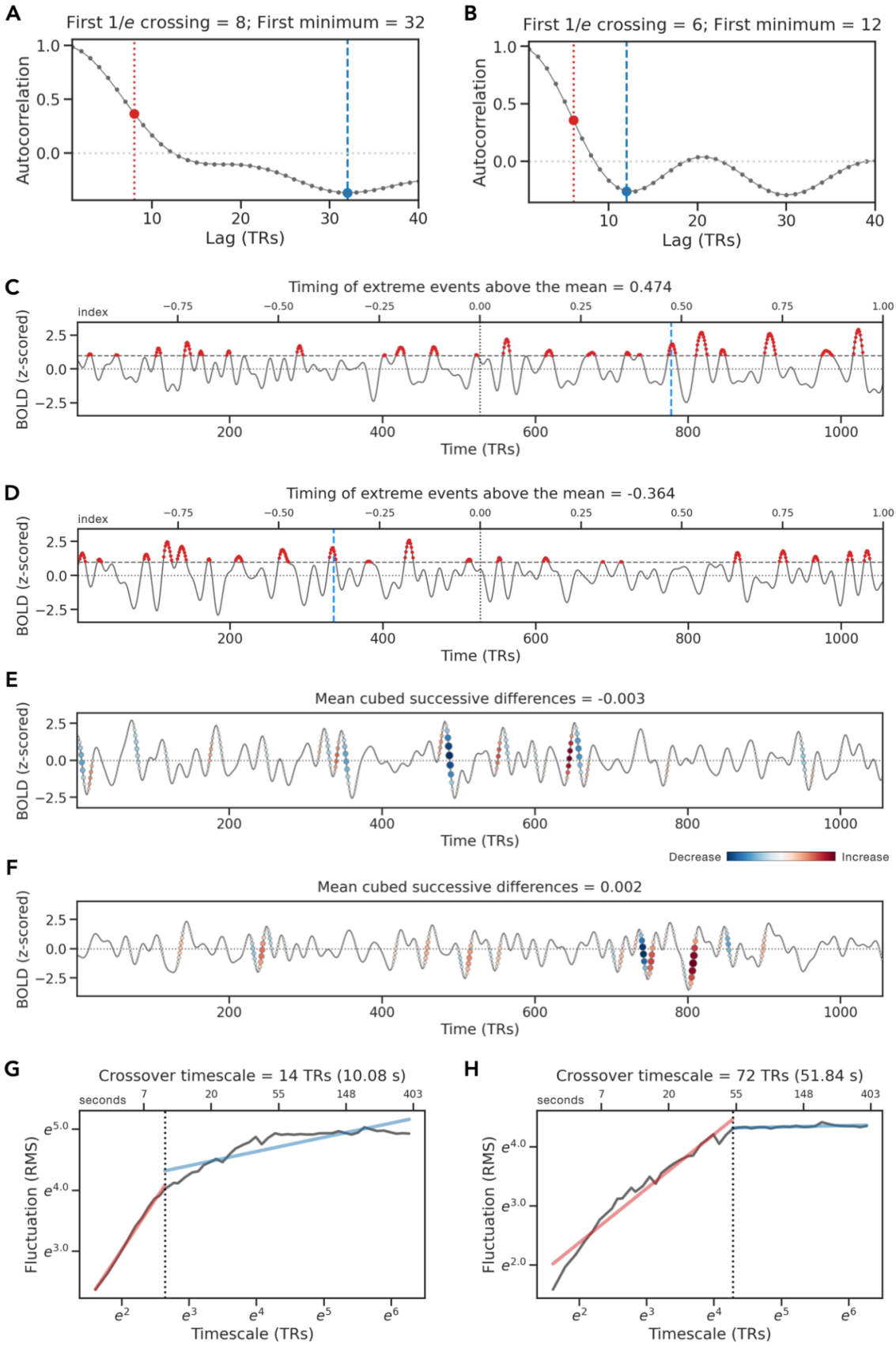

A
First 1/e crossing = 8; First minimum = 32
Autocorrelation
Lag (TRs)
B
First 1/e crossing = 6; First minimum = 12
Autocorrelation
Lag (TRs)
C
Timing of extreme events above the mean = 0.474
index
BOLD (z-scored)
Time (TRs)
D
Timing of extreme events above the mean = -0.364
index
BOLD (z-scored)
Time (TRs)
E
Mean cubed successive differences = -0.003
BOLD (z-scored)
Time (TRs)
Decrease
Increase
F
Mean cubed successive differences = 0.002
BOLD (z-scored)
Time (TRs)
G
Crossover timescale = 14 TRs (10.08 s)
seconds
Fluctuation (RMS)
Timescale (TRs)
H
Crossover timescale = 72 TRs (51.84 s)
seconds
Fluctuation (RMS)
Timescale (TRs)

Figure 2: Illustration of key time series properties and features.
The majority of the features which load significantly on the primary and secondary gradients capture regional differences in just four key time series properties: autocorrelation, the timing of extreme events, the symmetry of successive differences, and multifractal scaling. Here, we visualize these properties and provide illustrative examples of how they are characterized and quantified. (A, B) The primary gradient is characterized by significant loading from multiple features sensitive to the autocorrelation or "timescale" of intrinsic brain dynamics, which we visualize in panels A and B by plotting the autocorrelation function (ACF, gray line) of two regional BOLD time series. Time series from regions with long timescales produce an ACF which decays gradually (A), while autocorrelation decays more rapidly in regions with short timescales (B). The decay behavior of regional ACFs forms the basis of two features with strong positive loading on the primary gradient: the first $1/e$ crossing (i.e. the first lag for which autocorrelation ≤ 0.3679; red circle and dotted vertical line) and first minimum (blue circle and dashed vertical line). (C, D) The two features with the strongest positive loading on the secondary gradient are sensitive to the timing of "extreme" events (i.e. time points whose value exceeds a given threshold above or below the mean). These features first identify extreme events across a range of thresholds, and then compute the median index of these events at each threshold. Medians are rescaled such that the midpoint of the time series has an index of 0 (vertical dotted line), and the final statistic is calculated as the median of medians across all thresholds (vertical blue dashed line). For illustrative purposes, extreme events in panels C and D (red dots) are visualized relative to a single threshold (+1 SD; horizontal dashed line). These features produce increasingly positive values (approaching 1) for regions in which extreme events tend to occur more frequently towards the end of the scan (C), and increasingly negative values (approaching -1) for regions in which extreme events tend to occur more frequently towards the beginning of the scan (D). (E, F) The feature with the strongest negative loading on the secondary gradient is the mean of cubed successive differences (MCSD). Time points in panels E and F are scaled and colored based on the magnitude and direction of the (cubed) difference relative to the previous time point, $(t_n - t_{n-1})^3$. Some brain areas exhibit an asymmetry towards sudden large decreases and more gradual increases (E), while others exhibit the opposite tendency (F). (G, H) The other feature with significant negative loading on the secondary gradient uses Detrended Fluctuation Analysis (DFA) to characterize the multifractal scaling properties of regional BOLD time series. DFA first computes the cumulative sum of a time series and then splits this sequence into multiple equally sized windows. The cumulative sum is detrended within each window, and the level of fluctuation is calculated as the root-mean-square deviation (RMS) across windows. This process is then repeated across a range of timescales (window sizes), and scaling rules are estimated as the slope (in a log-log plot, G and H) with which the RMS grows with increasingly long timescales. The method used here assumes the presence of two distinct scaling regimes (red and blue lines) and identifies the "crossover" point where scaling behavior changes (vertical dotted line). In some brain areas, fluctuations scale consistently across a relatively narrow range of shorter timescales (G), while other areas exhibit consistent scaling behavior through longer timescales (H). Note that for illustration purposes we have expressed crossover points here in terms of their actual timescale, rather than as a percentile of all timescales (as in Fig. S2). Time series visualized above were selected by identifying regions with the maximum and minimum value of each feature from a randomly chosen participant. e (as in $1/e$ and e^x) is Euler's number, the base of the natural logarithm.

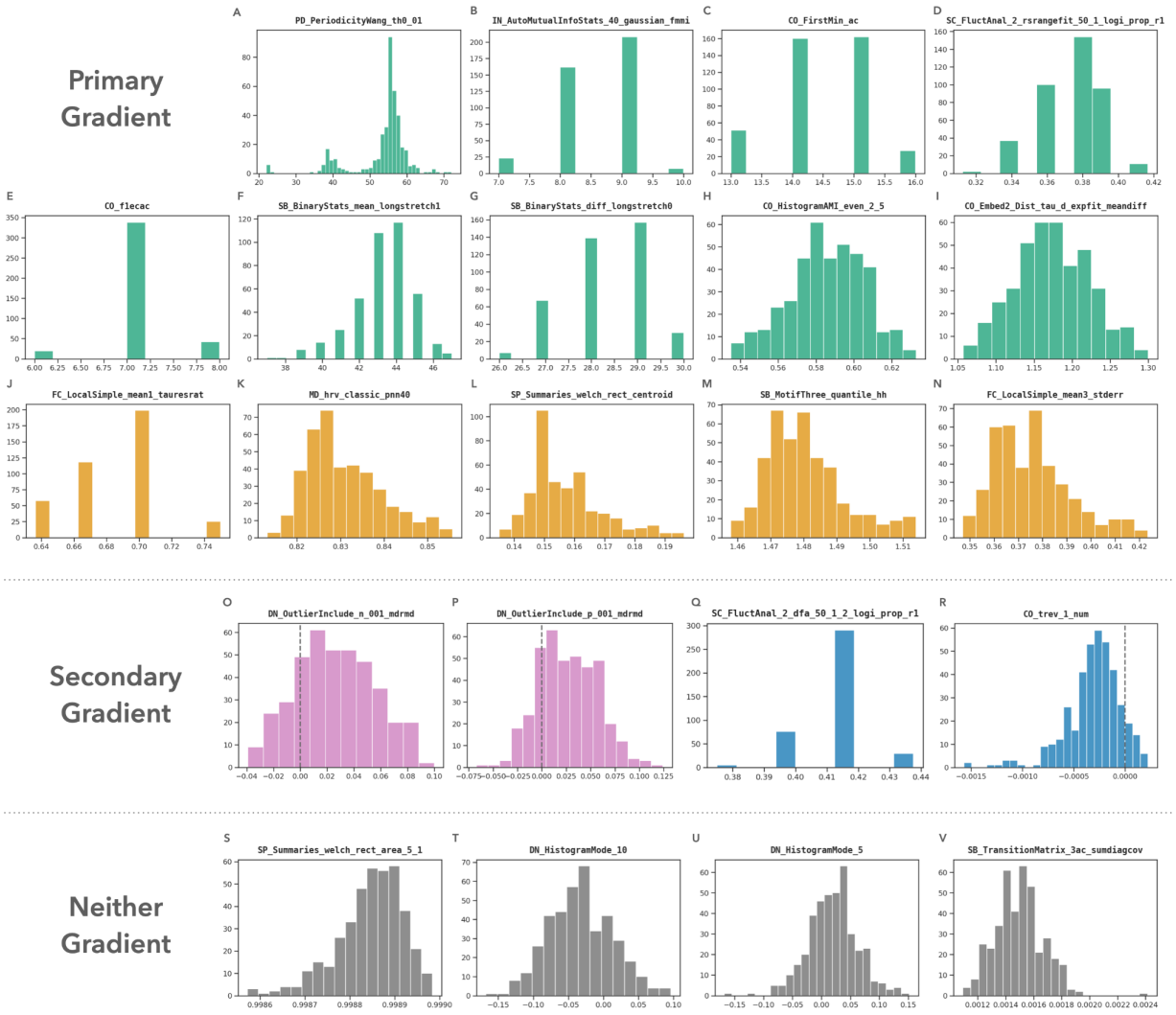


Figure S2: Distributions of group-median feature values across 400 cortical ROIs.
Features are grouped based on their loading on the first two principal components (gradients), and colored by their cluster membership from Figure 1. Readers are directed to Table 1 for a mapping between feature names (used here and in Fig. S3, and taken directly from the *catch22* code) and feature descriptions (used elsewhere in the paper).

Identifying gradients of intrinsic brain dynamics

To formally model the low-dimensional structure observed in our clustering results, we used principal components analysis (PCA) to identify a small number of "gradients" which capture common axes of variation among the 22 time series features. Each principal component defines a gradient, which consists of a spatial map (the PC scores for each brain area; Fig. 4B/D) and a set of feature loadings (Fig. 4A/C). The PC score for each cortical area is a weighted linear combination of the original 22 features, while feature loadings quantify the magnitude and direction with which each feature contributes to variation along the gradient. Feature loadings range from -1 to 1, and are equivalent to the correlation between each feature and the gradient axis defined by the principal component. In this way, the gradients identified via PCA allow us

to concisely describe and visualize how high-dimensional time series phenotypes vary across the cerebral cortex, while providing a direct mapping between the 22 time series features and a low-dimensional subspace of intrinsic brain dynamics. This approach is analogous to other recent studies which have used gradients to gain insight into diverse aspects of brain organization, including patterns of whole-brain functional connectivity (Margulies et al., 2016), cortical depth-dependent myelination (Paquola et al., 2019), gene expression (Burt et al., 2018), and the distribution of neurotransmitter receptors (Froudist-Walsh et al., 2021).

We used two complementary methods to determine the appropriate number of principal components to keep (and thus the number of gradients). First, we used 10-fold cross-validation (Bro et al., 2008; Krzanowski, 1987; Stacklies et al., 2007) to identify the dimensionality at which the PCA model most accurately predicted the dynamics of held out regions (Fig. 3A). Second, we generated 1000 surrogate null data sets in which the values for each feature had been randomly permuted across brain areas, and tested whether the proportion of variance explained by each component in the real data was significantly greater than in the surrogate data (Fig. 3B). This permutation testing approach (Camargo, 2022; Peres-Neto et al., 2003, 2005; Vitale et al., 2017) was also used to evaluate the significance of feature loadings (Fig. S3). We found that cross-validation error was minimized with two principal components, and that the first two PCs each explained significantly more variance (PC 1: 50.09%, PC 2: 11.85%) than expected under the null ($p = 0.001$ for both PCs). Together, these results suggest that regional differences in time-series phenotype can be well described by variation along just two spatial axes. We refer to these axes as the primary and secondary gradients of intrinsic brain dynamics.

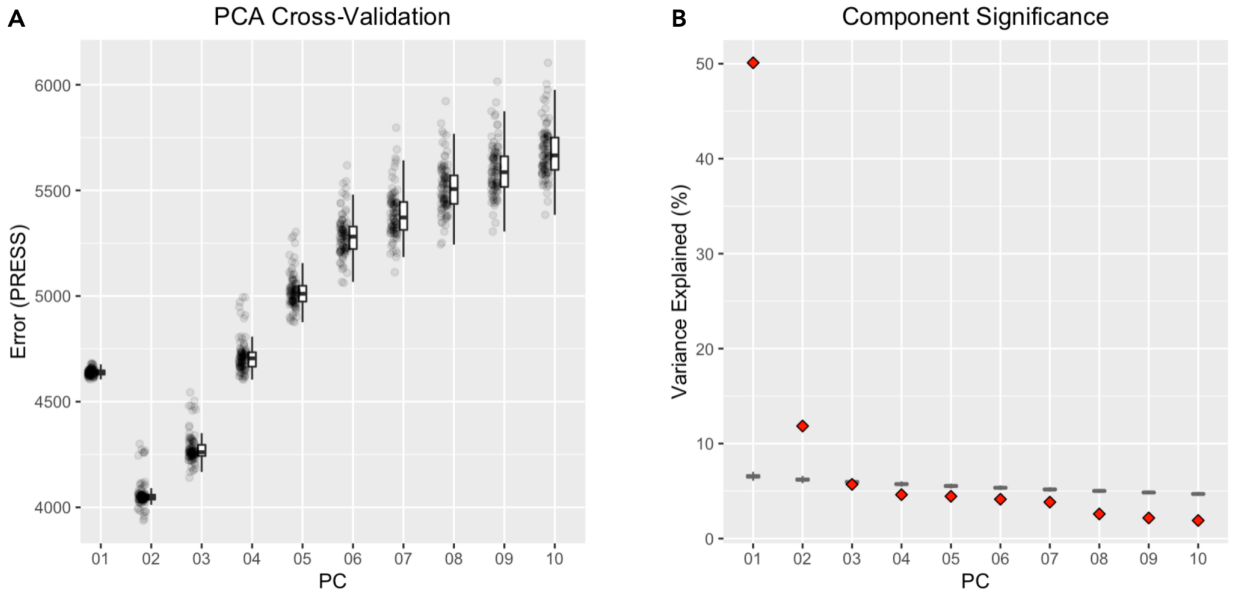


Figure 3: Intrinsic regional brain dynamics vary along two principal axes.
We used principal components analysis (PCA) to identify axes of variation ("gradients") which best explain regional differences in intrinsic brain dynamics as characterized by the 22 time series features. We used two complementary methods to determine the number of gradients to keep. (A) Cross-validation error is minimized with two principal components. Each data point is the average error (Predicted Residual Sum of Squares; PRESS) from one of 100 iterations of 10-fold cross-validation across regions. (B) The first two principal components also explain significantly more variance than expected under the null ($p = 0.001$ for PCs 1 and 2; $p > 0.99$ for all other PCs). Red diamonds indicate the proportion of variance explained (VE) by each component in the observed data. Gray boxes and whiskers show the null distribution of VE from 1000 random permutations of feature values across regions. In both panels, boxes cover the interquartile range, with the median indicated by a horizontal line. Whiskers extend 1.5 IQR above and below the 75th and 25th percentiles, respectively.

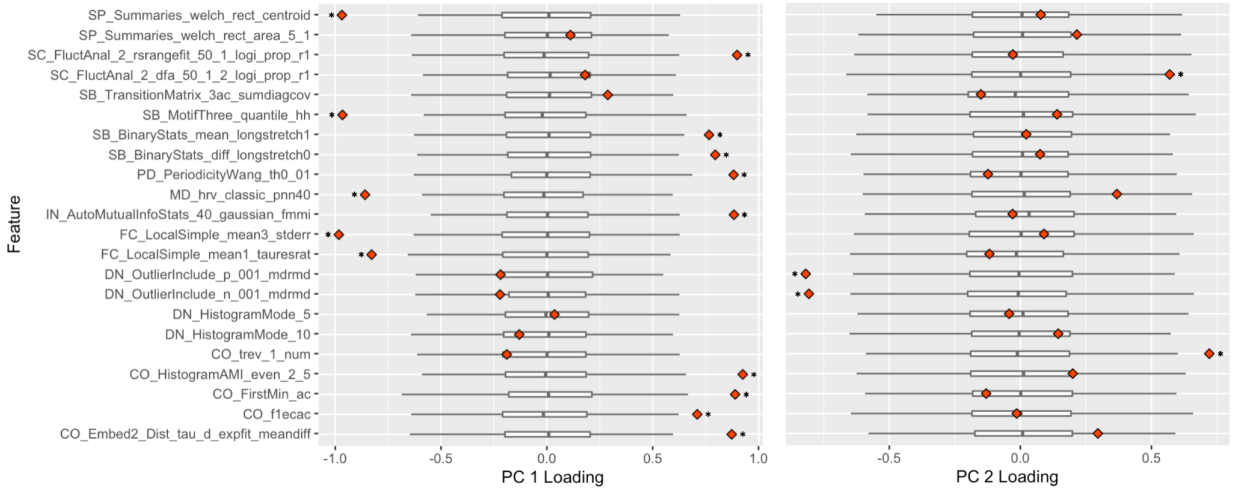


Figure S3: Permutation testing of feature loadings.
Features with significant loadings on each gradient were identified by comparing the observed loadings (red diamonds) to loadings from 1000 surrogate null data sets generated by randomly permuting feature values across brain areas (gray box plots). Black asterisks indicate loadings for which $p^{FDR} \leq 0.05$. Boxes and whiskers are as described in the caption for Figure 3. Readers are directed to Table 1 for a mapping between feature names (used here and in Fig. S2, and taken directly from the *catch22* code) and feature descriptions (used elsewhere in the paper).

The primary gradient effectively acts to summarize and collapse across multiple features sensitive to regional variation in the autocorrelation properties of regional BOLD time series (Fig. 4A; Fig. S3, left). Specifically, features which load positively on the primary gradient produce larger values for time series with higher levels of autocorrelation, while the opposite is true for features with negative loadings. As such, higher scores on the primary gradient reflect longer timescales (i.e. more gradually decaying autocorrelation; Fig. 2A), while lower scores reflect shorter timescales (i.e. more rapidly decaying autocorrelation; Fig. 2B). Scores on the primary gradient are generally higher in posteromedial areas and much of the lateral surface of the cortex, and generally lower in medial and inferior temporal and occipital areas, the insula and operculum, orbitofrontal cortex, the dorsal cingulate and paracentral lobule. The primary gradient peaks (longest timescales) in the inferior parietal lobule, middle and superior frontal gyrus, and posteromedial cortex, while the lowest scores (shortest timescales) can be found in the medial temporal lobe, orbitofrontal cortex, and dorsal cingulate.

In contrast to the primary gradient—which captures shared variation among features sensitive to the same underlying time series property (autocorrelation)—the secondary gradient is characterized by significant loadings from features sensitive to multiple different aspects of intrinsic dynamics: the timing of extreme events, the symmetry of successive differences, and the crossover point between scaling regimes (Fig. 4C; Fig. S3, right). Scores on the secondary gradient are generally lower in transmodal association areas (i.e. the majority of the frontal lobe, cingulate and posteromedial cortex, inferior parietal lobule, insula/operculum, medial and lateral temporal cortex) generally higher in sensory and motor regions (i.e. medial and lateral occipital cortex, occipitotemporal cortex, superior temporal gyrus, central sulcus and postcentral gyrus), and are highest in ventral aspects of the central sulcus (Fig. 4D). As such, the axis of the secondary gradient appears to closely follow well established anatomically and functionally defined cortical hierarchies (Burt et al., 2018; Hilgetag & Goulas, 2020; Margulies et al., 2016; M. Mesulam, 2000; M. M. Mesulam, 1998).

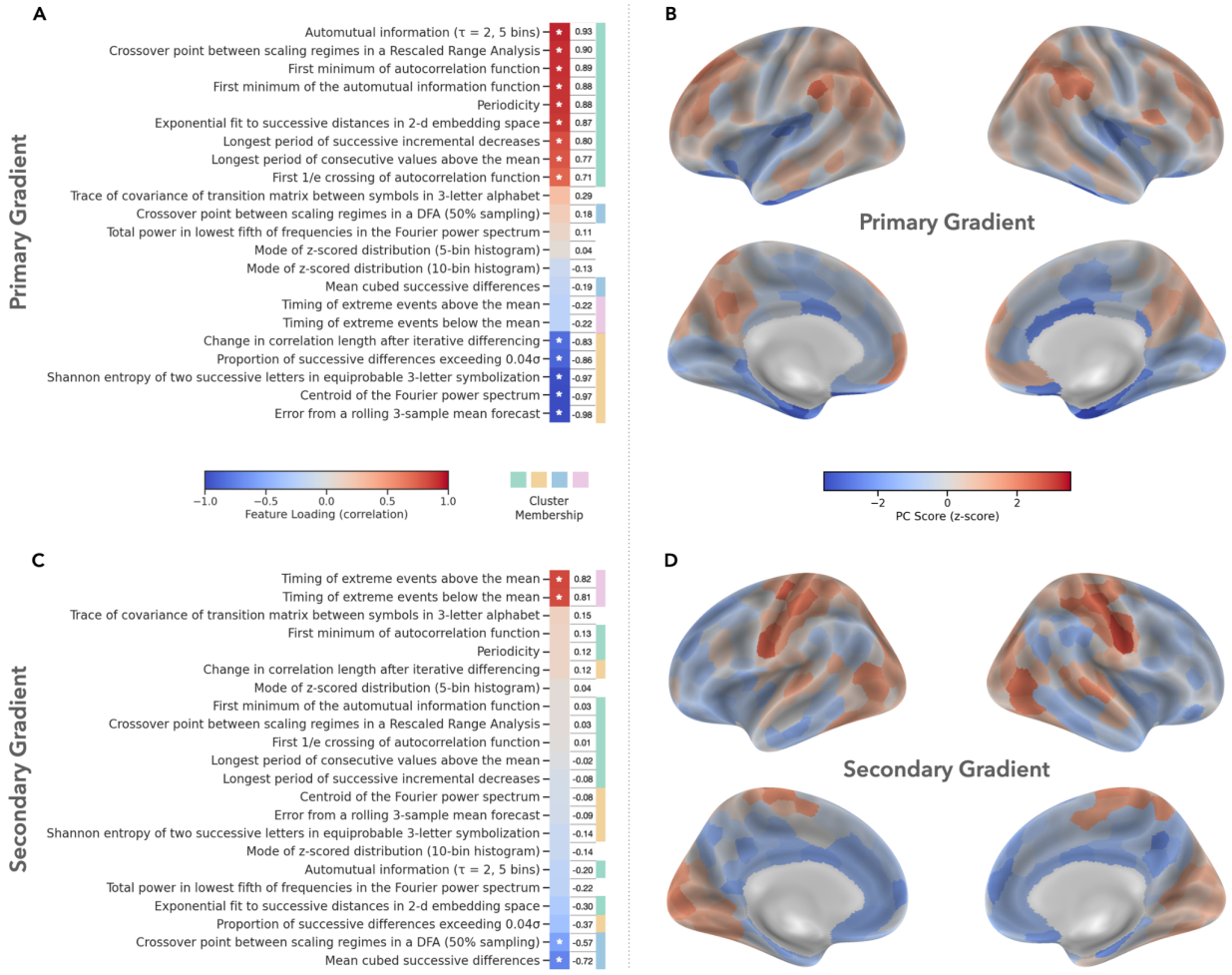


Figure 4: Primary and secondary gradients of intrinsic brain dynamics.
Feature loadings (A/C) describe the magnitude and direction (correlation) of the relationship between each of the 22 time series features and the gradients identified via PCA, while spatial maps of PC scores (B/D) provide a visualization of how these features vary across the brain. The primary gradient is defined by features sensitive to the autocorrelation properties of intrinsic brain dynamics (A) and peaks in the inferior parietal lobule, middle and superior frontal gyrus, and posteromedial cortex (B). These regions exhibit longer timescales (higher autocorrelation) than regions with lower scores on the primary gradient. (C) In contrast, the secondary gradient is characterized by features sensitive to the timing of extreme events, the symmetry of successive differences, and the multifractal scaling properties of regional BOLD time series. (D) Scores on the secondary gradient broadly distinguish between sensorimotor areas (higher scores) and transmodal association regions (lower scores). Colored bars on the right side of panels A and C indicate time series features assigned to one of the four clusters from Figure 1, while asterisks indicate features with significant loadings as determined through permutation testing.

Feature loadings suggest that the secondary gradient captures information about the dynamics the BOLD signal at both very short (i.e. volume-to-volume; MCSD) and very long timescales (i.e. over the course of an entire scan; timing of extreme events), as well as how dynamics differ across timescales (multifractal DFA). However, whereas building an intuition about the relationship between PC scores and underlying dynamics was relatively straightforward for the primary gradient (i.e. higher PC scores indicate longer timescales), two factors make this process significantly more difficult for the secondary gradient. First, whereas the primary gradient effectively acts to collapse across a set of highly similar features and preserves their existing common axis of variation, the secondary gradient captures shared variance among a more heterogeneous set of features. As a result, most feature loadings on the secondary gradient are weaker than those for the primary gradient, and thus the PC scores are less informative about each individual feature (and vice-versa)[3]. Second, the three features which load most strongly on the secondary gradient all produce values which must be interpreted relative to zero. For these features, it is not enough to know simply that one region produces a higher value than another. For example, given two time series A and B, an observation that A has a higher mean cubed successive differences (MCSD) than B could reflect five qualitatively different scenarios: 1) MCSD is positive for both A and B, 2) MCSD is negative for both A and B, 3) MCSD is positive for A but negative for B, 4) MCSD is positive for A but near zero for B, 5) MCSD is near zero for A but negative for B. These five scenarios are meaningfully different because positive, negative, and zero values of MCSD indicate qualitatively different kinds of dynamics (i.e. asymmetry towards sudden large increases, asymmetry towards sudden large decreases, or a symmetric distribution of cubed successive differences). The same issue arises for the two measures which characterize the timing of extreme events. These three "zero-anchored" features do not pose any particular challenge when working directly with the "raw" feature values, but complicate the interpretation of PC scores on the secondary gradient. Specifically, because feature values must be mean centered prior to PCA (and because PC scores are a weighted sum of multiple features), a positive PC score does not necessarily indicate a positive raw feature value, even for features which exhibit a significant positive correlation (positive loading) with the gradient axis. As such, scores on the secondary gradient do not on

[3] For example, gradient scores explain 96.6% of variance in the feature with the strongest loading on the primary gradient, but only 67.2% of variance for the equivalent feature on the secondary gradient (a difference of almost 30%).

their own provide sufficient information to qualitatively characterize the timing of extreme events or the symmetry of successive differences.

In light of the challenges to direct interpretation posed by zero-anchored features and weaker loadings, we visualized the "raw"[4] group-level maps for each feature with a significant loading on the secondary gradient and used these maps to help inform our understanding of how gradient scores relate to the underlying dynamics. This revealed that the majority of regions with a positive score on the secondary gradient (i.e. sensory and motor areas) exhibit a tendency for extreme events to occur more frequently towards the end of the resting scan (i.e. a positive value on the extreme event measures), while only a handful of regions with the most strongly negative scores (located in the medial and lateral frontoparietal networks) exhibit the opposite tendency (Fig. S4 B/C). Similarly, while almost all cortical areas exhibit a tendency towards sudden decreases and more gradual increases (i.e. negative MCSD), this asymmetry is notably stronger in areas with the very highest gradient scores (central sulcus and postcentral gyrus; Fig. S4D). These areas are also distinguished from the rest of the brain by an earlier crossover between scaling regimes, while a subset of areas with negative gradient scores (primarily in the medial frontoparietal and midcingulo-insular networks) exhibit consistent scaling behavior through longer timescales (Fig. S4E).

[4] Residualized relative to ROI volume, but not z-scored or mean centered.

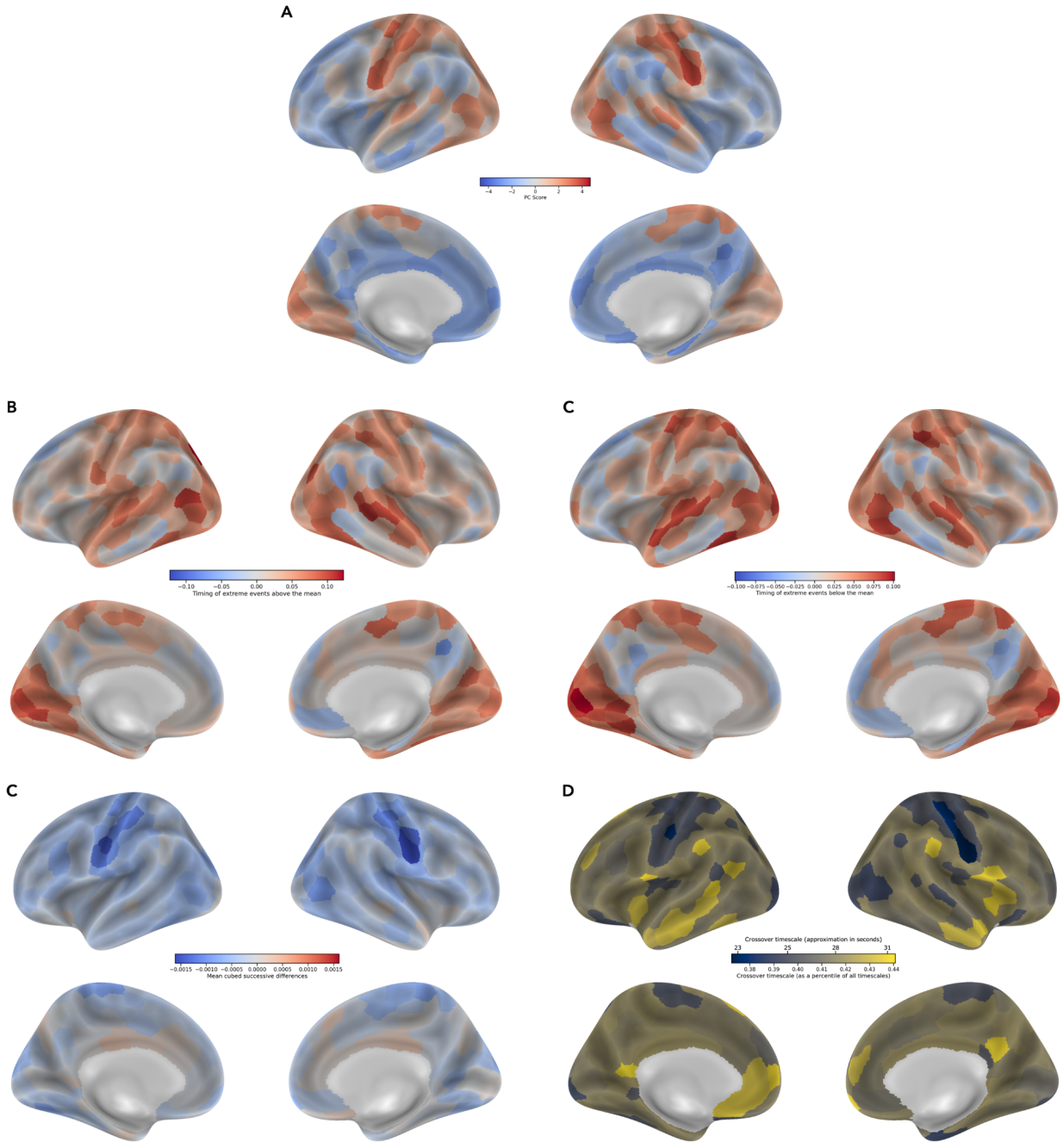


Figure S4: Secondary gradient and associated features.
(A) Secondary gradient. (B) Timing of extreme events above the mean. (C) Timing of extreme events below the mean. (D) Mean cubed successive differences. (E) Crossover timescale from a multifractal DFA.

Following the principle of parsimony (i.e. that one should seek the simplest explanation that fits the data), we hypothesized that the two extreme event measures (and thus much of the variance in the secondary gradient) might reflect more general nonstationarities in the distribution of time series values. To evaluate this hypothesis, we split the resting scan into

multiple shorter windows (100 time points per window, with 50 time points of overlap between windows), and computed the standard deviation (SD) and kurtosis (K) of each regional time series within each window. This sliding window analysis produced a series of 23 SD and K values for each cortical area. We then fit a linear trend to these series, and used the slope of this trend to characterize how SD and K change over the course of the resting scan. We refer to these trends as m_{SD} and m_K, respectively. As predicted, we found that m_{SD} and m_K were highly correlated with each other (r = 0.89), as well as with both the extreme event measures (r > 0.82) and scores on the secondary gradient (m_{SD}: r = 0.74; m_K: r = 0.77) (Fig. S5). These results indicate that m_{SD} and m_K explain almost as much variance in scores on the secondary gradient (m_{SD}: r^2 = 0.55; m_K: r^2 = 0.62) as the extreme event measures (r^2 = 0.66, r^2 = 0.67), roughly the same amount of variance as MCSD (r^2 = 0.52), and substantially more variance than crossover timescale (r^2 = 0.32). The strength of these associations is particularly notable because while the extreme events measures, MCSD, and crossover timescale are *necessarily* correlated with the secondary gradient (i.e. because their values contribute directly to the gradient scores), no such circularity exists for m_{SD} and m_K. All of these relationships replicate in the validation sample (Fig. S6).

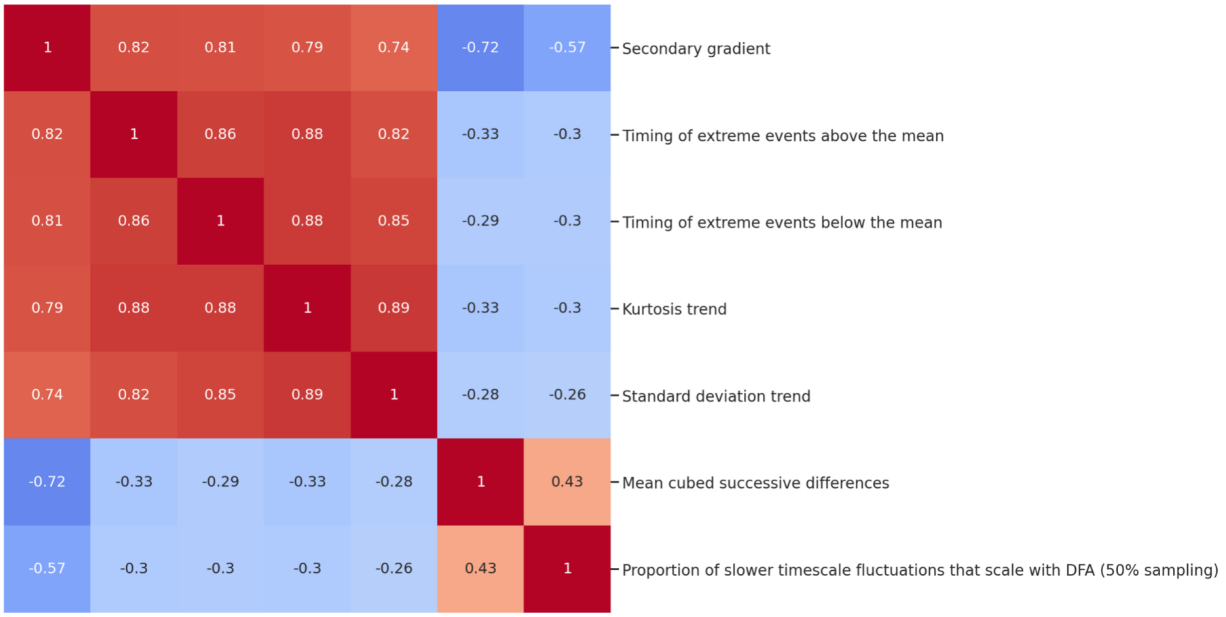


Figure S5: Correlation of m_{SD} and m_K with the secondary gradient and associated features.
The value in each cell is the Pearson correlation coefficient, which is equivalent to PCA feature loading.

As with the frequency of extreme events, the standard deviation and kurtosis of intrinsic brain activity tends to increase in most cortical areas over the course of the resting scan, but the magnitude of these increases is greatest in sensorimotor areas (Fig. S7, A/B). Similarly, only a small number of brain areas (particularly in the medial frontoparietal network) decrease their standard deviation and kurtosis over time. As such, these results allow us to (to some extent)

re-frame and simplify our interpretation of scores on the secondary gradient in terms of familiar statistical features and how they change over time.

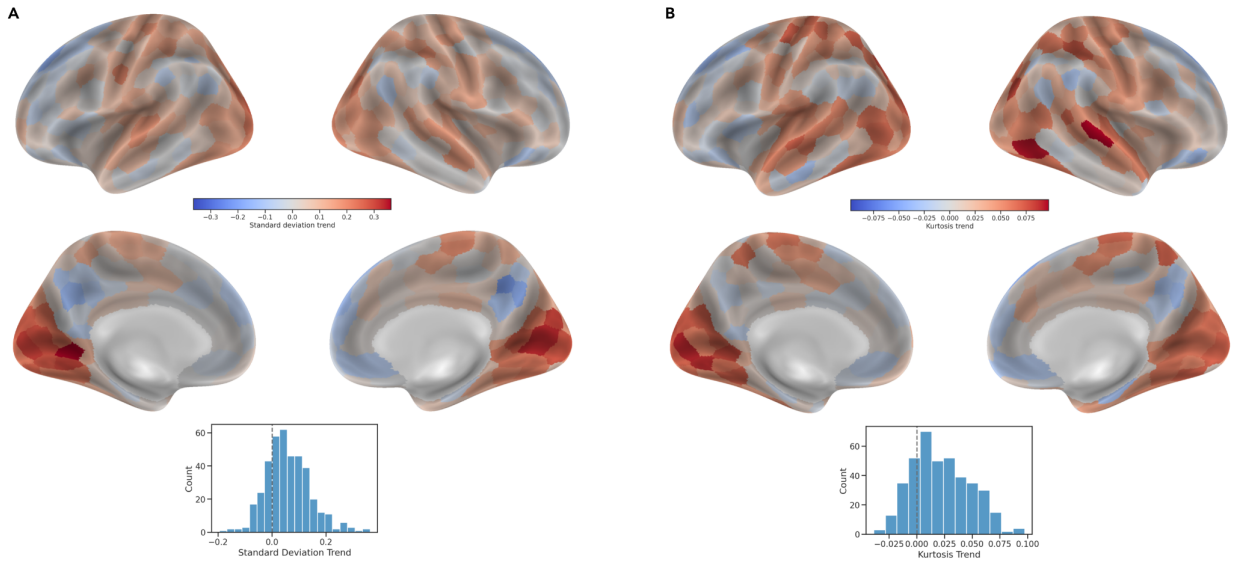


Figure S7: Trend of sliding-window standard deviation (m_{SD}; A) and kurtosis (m_K; B).

Together, the results of our gradient analysis suggest that multidimensional time series phenotypes can be modeled as varying along two spatial axes, each of which is defined by regional differences in distinct aspects of intrinsic brain dynamics. Scores on the primary gradient reflect the autocorrelation properties (timescale) of regional BOLD dynamics, while scores on the secondary gradient capture the degree to which the variance and kurtosis of intrinsic brain activity tend to increase or decrease over the course of the resting scan, as well as the symmetry of moment-to-moment increases and decreases in the BOLD signal, and the fractal scaling behavior of these fluctuations. We found nearly identical gradients in the validation sample, both in their pattern of feature loadings and the topography of PC scores (Fig. S8). Having identified these gradients and characterized their spatial and temporal properties, we sought to quantitatively evaluate their relationship with other features of large-scale cortical organization.

Gradients follow anatomical and connectomic hierarchies

Anatomical markers of cortical hierarchy: T1w/T2w MRI and cortical thickness

Anatomical hierarchies within the cerebral cortex have historically been defined based primarily on regional differences in microarchitecture (e.g. (M. Mesulam, 2000; von Economo & Koskinas, 1925)). While post-mortem histology remains the gold standard for mapping these features (Amunts et al., 2013, 2020; Amunts & Zilles, 2015), recent work suggests that measures derived from high-resolution structural MRI may serve as non-invasive proxies for many aspects of cortical microstructure, including intracortical myelin content, laminar

differentiation, the proportion of feed-forward vs. feed-back inputs to a region, and levels of recurrent excitation gene expression (Burt et al., 2018; Glasser & Van Essen, 2011; Gomez et al., 2019; Wagstyl et al., 2015, 2020; Whitaker et al., 2016). Of these measures, the ratio of T1w to T2w MRI signal (T1w/T2w) has been shown to be negatively correlated with anatomical hierarchies (Burt et al., 2018; Gomez et al., 2019), while cortical thickness shows the opposite relationship and increases along sensory processing hierarchies (Burt et al., 2018; Gomez et al., 2019; Wagstyl et al., 2015, 2020). To investigate how different aspects of intrinsic brain dynamics relate to these hierarchies, we calculated the Spearman correlation (r_s) between group-average maps of these two complementary anatomical measures and scores on the primary and secondary gradient. Because spatial autocorrelation can artificially inflate measures of association when comparing brain maps (Alexander-Bloch et al., 2018), we evaluated the significance of these and all other effects using non-parametric permutation testing and a spatial null model (Burt et al., 2020).

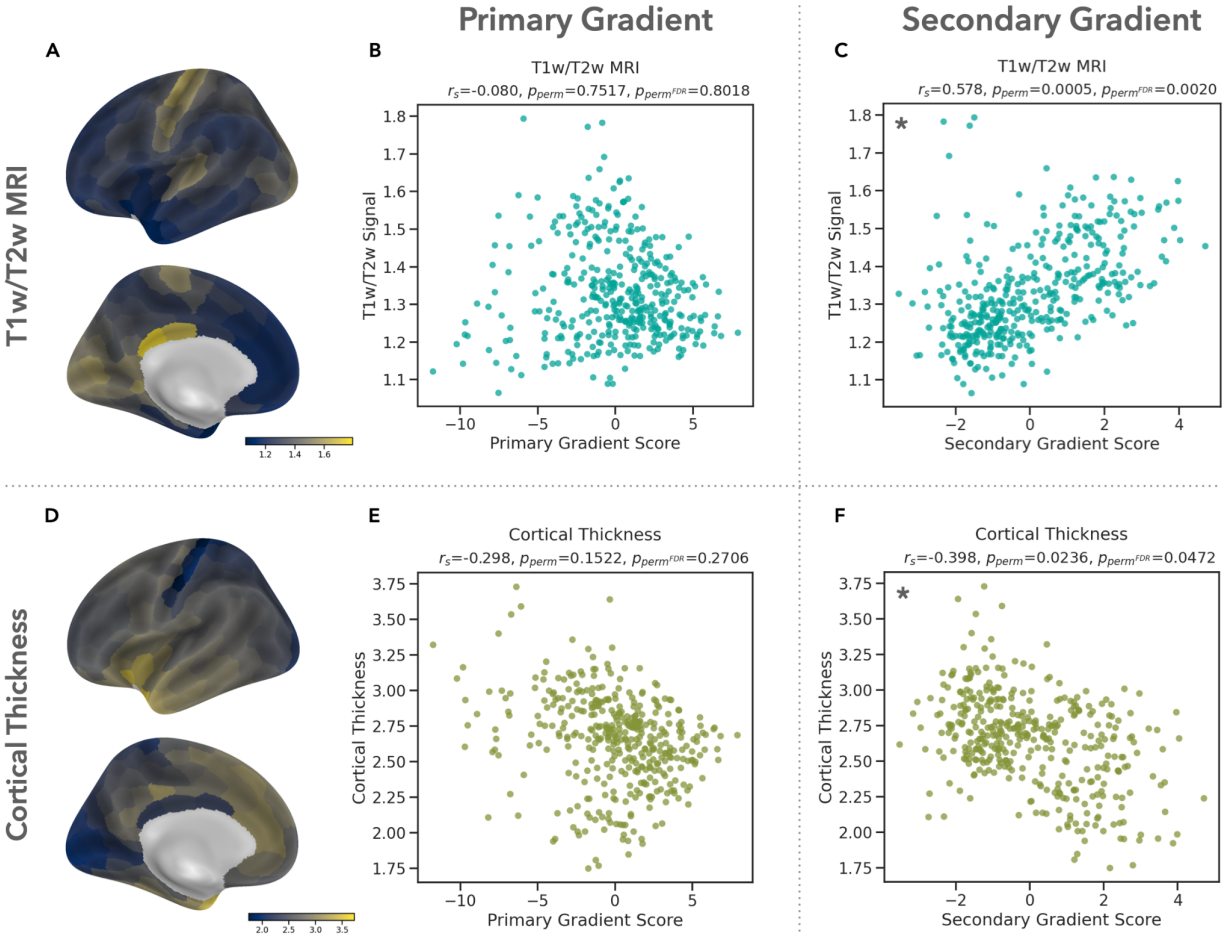


Figure 5: The secondary gradient of intrinsic dynamics follows anatomical markers of cortical hierarchy.
To investigate the relationship between intrinsic brain dynamics and anatomical hierarchies, we computed the Spearman correlation between the PC scores for each gradient and two non-invasive proxies for cortical microstructure, T1w/T2w MRI (A) and cortical thickness (D). The primary gradient did not show a significant relationship with either measure (B/E), while the secondary gradient was significantly correlated with both T1w/T2w (C) and cortical thickness (F). Asterisks indicate correlations which are significant at FDR $q \leq 0.05$.

Scores on the primary gradient were not correlated with T1w/T2w ($r_s = 0.080$, $p_{perm}^{FDR} = 0.8018$; Fig. 5B), nor were they significantly correlated with cortical thickness ($r_s = -0.298$, $p_{perm}^{FDR} = 0.2706$; Fig. 5E). In contrast, the secondary gradient showed a significant positive correlation with T1w/T2w ($r_s = 0.478$, $p_{perm}^{FDR} = 0.0020$; Fig. 5C), and a significant negative correlation with cortical thickness ($r_s = -0.398$, $p_{perm}^{FDR} = 0.0472$; Fig. 5F). Given the lack of a significant association between the primary gradient and either anatomical measure, we used confidence intervals to formally compare correlations (Zou, 2007). This revealed that the correlation between T1w/T2w and the secondary gradient was significantly stronger than between T1w/Tw2 and the primary gradient (Δr_s 95% CI = [0.36 – 0.63]). The strength of association with cortical thickness did not differ significantly between gradients (Δr_s 95% CI = [−0.04 – 0.24]), but the secondary gradient was more strongly correlated with T1w/T2w than cortical thickness (Δr_s 95% CI = [0.09 – 0.27]). These results fully replicated in the validation sample (Fig. S9), and suggest that regions at lower levels of anatomically defined cortical hierarchies (i.e. areas with high T1w/T2w signal or low cortical thickness) tend to exhibit greater increases in variance and kurtosis over the course of a resting scan than higher-order areas. In contrast, the timescale of intrinsic BOLD activity does not appear to vary systematically along these hierarchies.

Topological hierarchies in the structural and functional cortical connectome

In addition to variation in local anatomical features, brain areas can differ greatly in their inter-regional connectivity. Arguably the most fundamental way to characterize the connectivity of a brain area is to simply count how many other areas it connects to, and how strong those connections are. This measure, known as "strength" (or weighted degree) can be used to identify connectomic hierarchies which distinguish topologically central "hub" areas from less widely connected peripheral regions (Bullmore & Sporns, 2009; Rubinov & Sporns, 2010; van den Heuvel & Sporns, 2013). Large-scale brain connectivity is most often estimated based on the correlation between regional time series (functional connectivity) or the number of diffusion tractography streamlines connecting each pair of regions (structural connectivity). These two modalities offer complementary perspectives on large-scale brain connectivity, with functional connectivity capturing patterns of coordinated activity which are shaped by the underlying scaffold of direct axonal connections measured by structural connectivity. As such, we estimated the strength of each brain area based on both its functional and structural connectivity to other cortical regions, and assessed the extent to which these measures of connectomic hierarchy were related to scores on the primary and secondary gradient.

We found that the primary and secondary gradients were differentially related to functional and structural connectivity strength. Functional connectivity strength (Fig. 6A) was uncorrelated with the primary gradient ($r_s = 0.096$, $p_{perm}^{FDR} = 0.7169$; Fig. 6B), but showed a significant

positive correlation with the secondary gradient (r_s = 0.560, p_{perm}^{FDR} = 0.0005; Fig. 6C). Structural connectivity strength (Fig. 6D) exhibited the opposite relationship, showing a significant positive correlation with the primary gradient (r_s = 0.340, p_{perm}^{FDR} = 0.0005; Fig. 6E) but no correlation with the secondary gradient (r_s = 0.097, p_{perm}^{FDR} = 0.3630; Fig. 6F). The correlations between connectivity strength and gradient scores were significantly different both between modalities for each gradient (PC1: Δr_s 95% CI = [0.10 – 0.38]; PC2: Δr_s 95% CI =[0.33 – 0.59]) and between gradients for each modality (FC: Δr_s 95% CI = [0.33 – 0.59]; SC: Δr_s 95% CI = [0.09 – 0.39]). These effects fully replicated in the validation sample (Fig. S10).

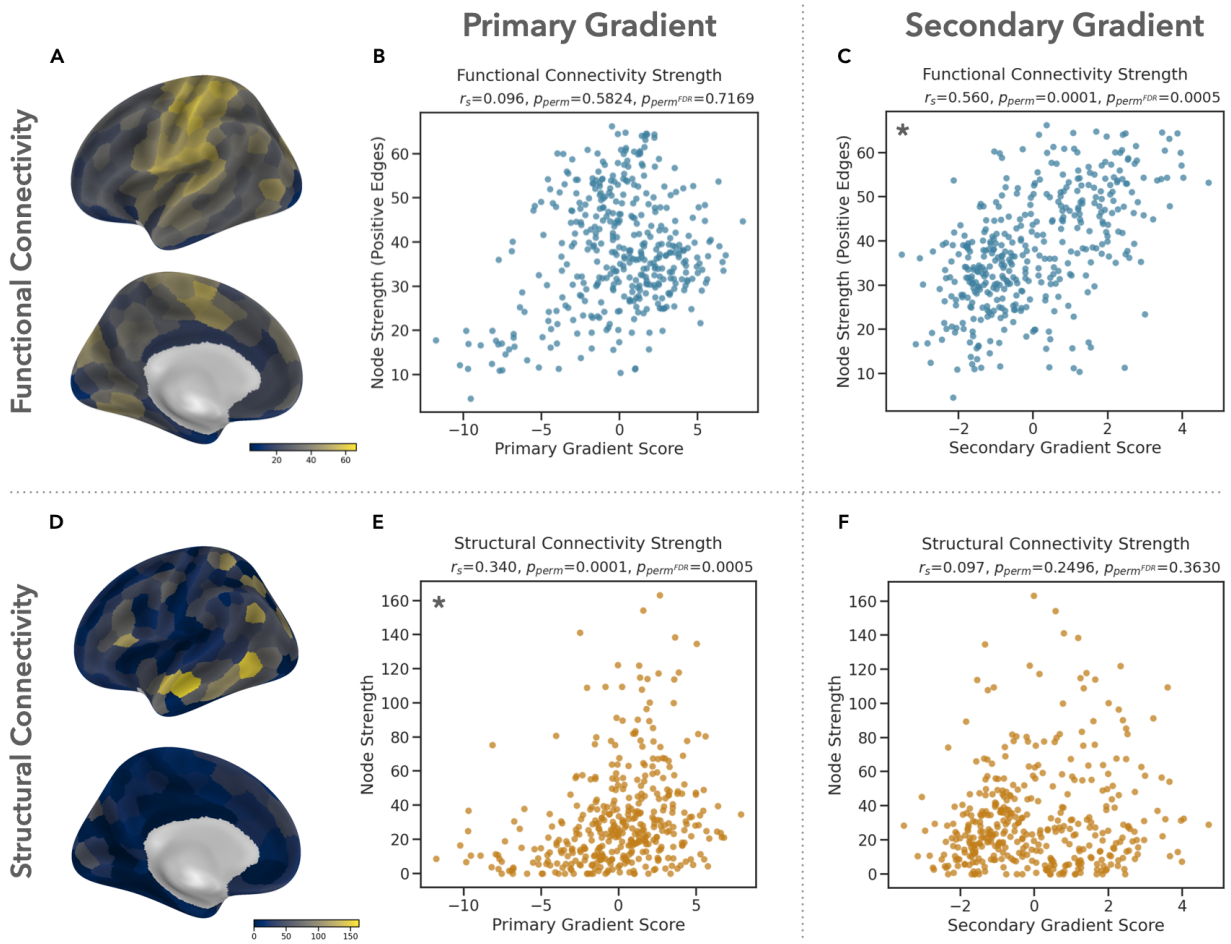


Figure 6: Gradients exhibit distinct relationships with functional and structural connectivity strength.

Functional connectivity strength (A) is uncorrelated with the primary gradient (B), but shows a significant positive correlation with the secondary gradient (C). In contrast, structural connectivity strength (D) shows a significant positive correlation with the primary gradient (E), but is uncorrelated with the secondary gradient (F). Asterisks indicate correlations which are significant at FDR q ≤ 0.05.

Our observation that scores on the primary gradient are positively correlated with structural connectivity strength is consistent with the results of a prior study by our group (Chapter 1), in

which we also found an association between BOLD timescales and measures of regional network topology which consider the modular community structure of human brain networks. As such, we additionally computed the within-module degree (WD) and participation coefficient (PC) (Guimerà & Amaral, 2005; Guimerà & Nunes Amaral, 2005) of each cortical area relative to the 7 functional networks identified by (Yeo et al., 2011). Within-module degree quantifies the extent to which each region exhibits widespread connectivity to other areas in the same network module, while accounting for differences in module size. In contrast, participation coefficient characterizes the degree to which a region's connections are concentrated within its own module (values approaching zero) or diversely distributed across multiple modules (values approaching 1). As with strength, we calculated these measures based on both functional connectivity and structural connectivity.

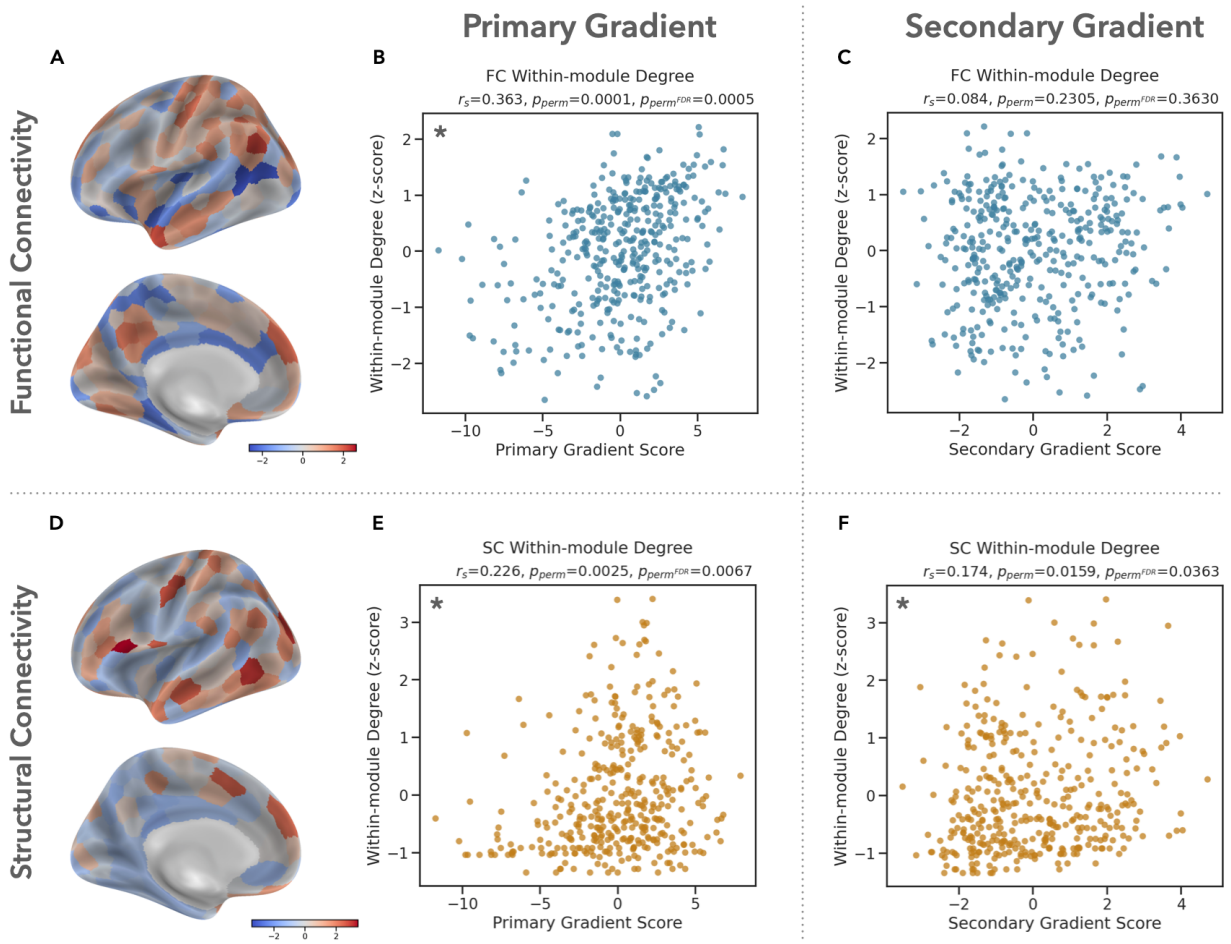


Figure 7: Relationship between gradient scores and within-module degree.
Within-module degree (z-scored) computed based on functional connectivity (A) showed a significant positive correlation with scores on the primary gradient (B), but was not correlated with scores on the secondary gradient (C). In contrast, within-module degree computed based on structural connectivity (D) exhibited a significant correlation with scores on both the primary (E) and secondary gradient (F). Asterisks indicate correlations which are significant at FDR q ≤ 0.05.

We found a significant positive correlation between the primary gradient and FC within-module degree (r_s = 0.363, p_{perm}^{FDR} = 0.0005; Fig. 7B), but no relationship between FC WD and scores on the secondary gradient (r_s = 0.084, p_{perm}^{FDR} = 0.3630; Fig. 7C; Δr_s 95% CI = [0.13 – 0.42]). In contrast, SC within-module degree exhibited a significant positive correlation with both the primary (r_s = 0.226, p_{perm}^{FDR} = 0.0067; Fig. 7E) and secondary gradient (r_s = 0.174, p_{perm}^{FDR} = 0.0363; Fig. 7F). These relationships replicated in the validation sample for the primary gradient, but not for the secondary gradient (Fig. S11).

Functional connectivity participation coefficient was not correlated with either gradient (primary gradient: r_s = −0.086, p_{perm}^{FDR} = 0.4646; secondary gradient: r_s = −0.031, p_{perm}^{FDR} = 0.8018; Fig. 8B/C), while structural connectivity PC was positively correlated with the primary gradient (r_s = 0.273, p_{perm}^{FDR} = 0.0051; Fig. 8E) but uncorrelated with the secondary gradient. (r_s = 0.015, p_{perm}^{FDR} = 0.8611; Fig. 8F; Δr_s 95% CI = [0.11 – 0.40]). These effects fully replicated in the validation sample (Fig. S12).

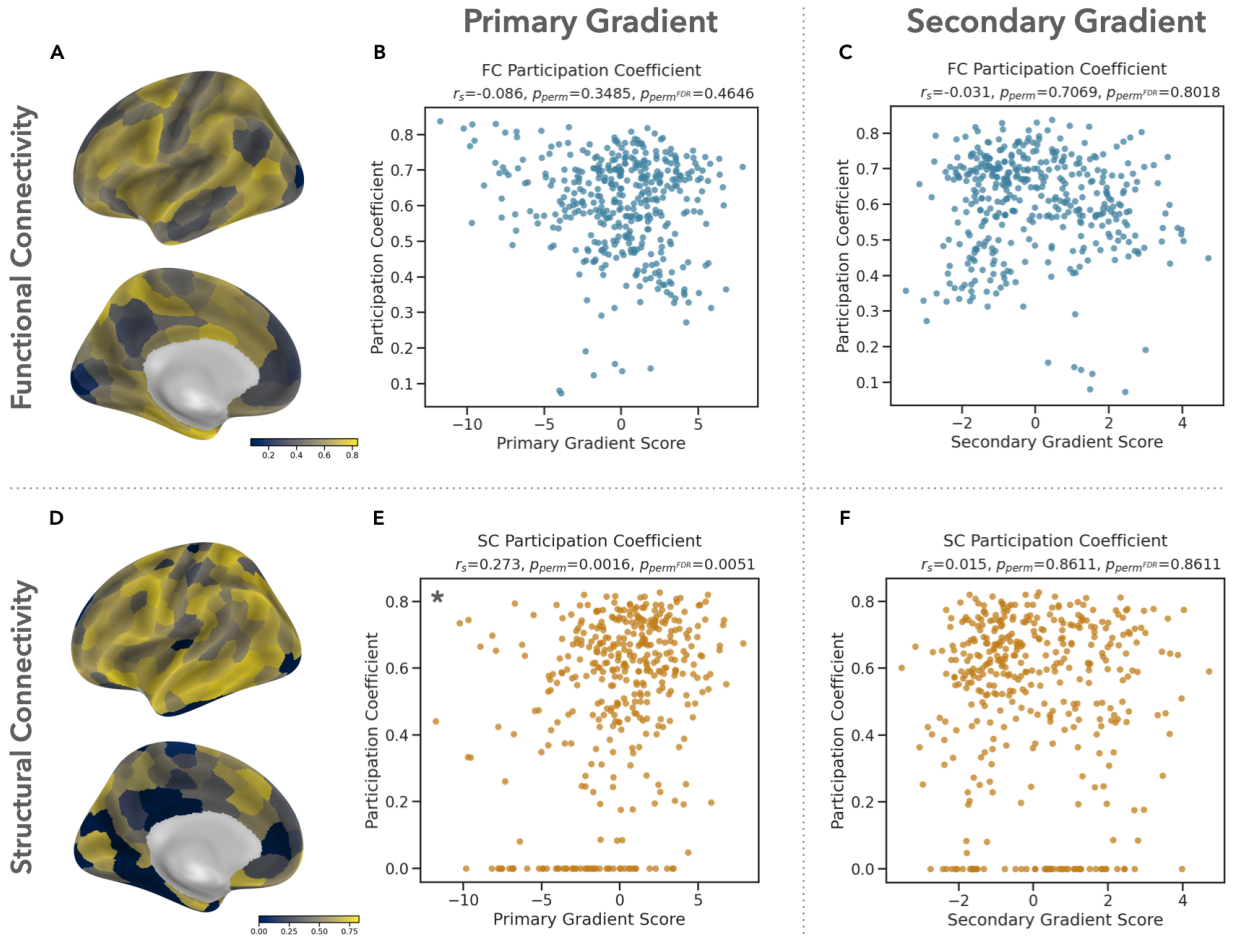


Figure 8: Relationship between gradient scores and participation coefficient.
Participation coefficient computed based on functional connectivity (A) was not correlated with scores on either gradient (B/C). In contrast, participation coefficient computed based on structural connectivity (D) showed a significant positive correlation with scores on the primary gradient (E), but was not correlated with scores on the secondary gradient (F). Asterisks indicate correlations which are significant at FDR $q \leq 0.05$.

Our results suggest that the primary and secondary gradients exhibit distinct relationships with topological hierarchies in the structural and functional cortical connectome. Specifically, cortical areas with long timescales tend to have widespread structural connectivity both in general (high SC strength) and specifically to other regions in the same functional network (high SC WD), as well as diverse structural connectivity to regions in other modules (high SC PC). Long timescale regions also tend to exhibit extensive within-module functional connectivity (high FC WD), but not necessarily high overall FC strength or diverse FC to other modules. In contrast, regions with high scores on the secondary gradient *do* tend to exhibit high overall FC strength, but do not show replicable associations with structural connectivity features.

Distinct relationships to local anatomy and inter-regional connectivity

Local circuit properties and patterns of long-range axonal connectivity have both been associated with regional differences in intrinsic dynamics (Anderson et al., 2020; Baria et al., 2013; Chaudhuri et al., 2014, 2015; Demirtaş et al., 2019; Fallon et al., 2020; Gao et al., 2020; Gollo et al., 2015; Ito, Hearne, et al., 2020; Li & Wang, 2022; Mahjoory et al., 2020; Sethi et al., 2017; Watanabe et al., 2019; Wengler et al., 2020). However, our results suggest that the primary and secondary gradient show distinct relationships with these features. Specifically, T1w/T2w and cortical thickness are more strongly correlated with the secondary gradient, while structural connectivity features (strength, WD, and PC) are more strongly correlated with the primary gradient (Fig. 9A). These differences are significant for T1w/T2w, strength, and participation coefficient. Similarly, the primary gradient shows a significantly stronger relationship with SC strength and PC than it does with T1w/T2w, while the secondary gradient shows a significantly stronger relationship with T1w/T2w and cortical thickness than it does with structural connectivity features (Fig. 9B/C). With the exception of the difference in correlations between T1w/T2w and SC PC for the primary gradient, all of these effects replicate in the validation sample (Fig. S13).

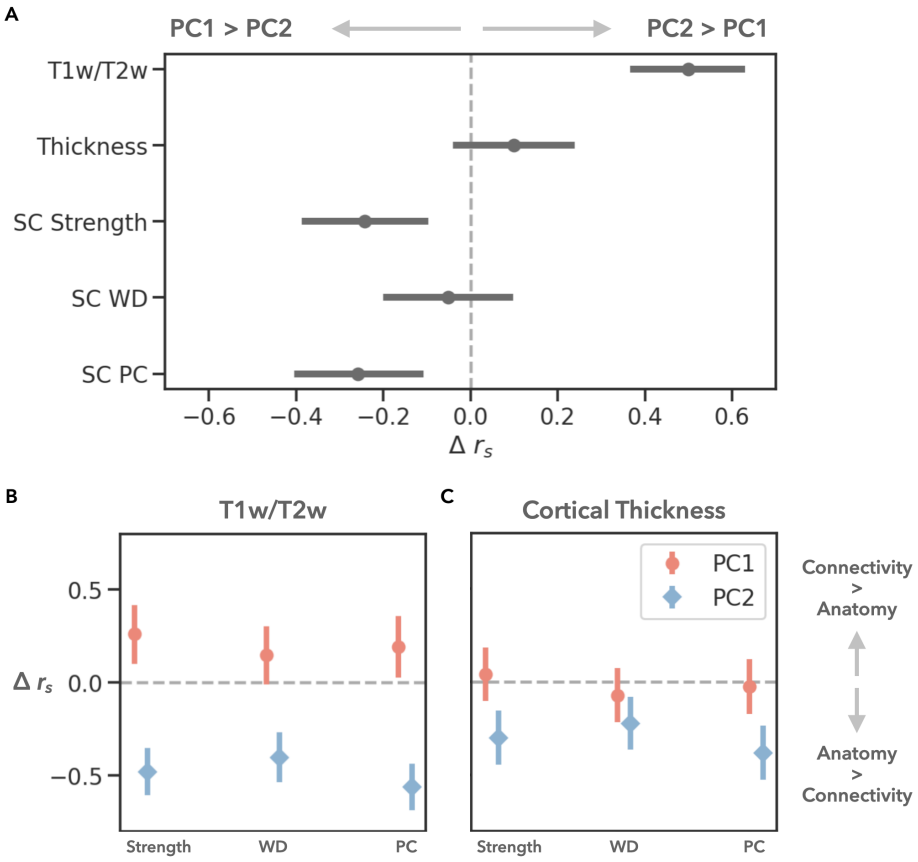


Figure 9: The primary and secondary gradient show distinct relationships to anatomy- and connectivity-based hierarchies.
(A) To visualize differences in the degree to which each gradient was related to features of regional anatomy and structural connectivity, we subtracted the absolute value of the correlation between each feature and the primary gradient from that for the secondary gradient (Δ r_s = $|r_s|$ PC2 − $|r_s|$ PC1). Structural connectivity features are more strongly correlated with the primary gradient (negative values of Δ r_s), while anatomical features are more strongly correlated with the secondary gradient (positive values of Δ r_s). Bars show the 95% CI for the difference in correlations. (B-C) This distinction can also be seen when comparing effects between features within each gradient. Panels (B) and (C) plot the difference in effect size between each structural connectivity feature and the two measures of regional anatomy (e.g. Δ r_s = $|r_s|$ SC WD − $|r_s|$ T1w/T2w). Negative values indicate a stronger correlation with the anatomical feature, while positive values indicate a stronger correlation with each structural connectivity feature.

Microstructurally defined cortical zones and functionally specialized subsystems

The regional differences in local anatomy and inter-regional connectivity discussed in previous sections ultimately exist to facilitate functional specialization and the information processing hierarchies necessary for adaptive behavior and cognition. Because brain function is inherently dynamic, we hypothesized that regional differences in functional specialization would manifest as differences in the dynamics of regional brain activity. As such, we sought to investigate how scores on the primary and secondary gradients differed across regions with different functional roles.

One of the simplest and most common ways to describe differences in function across the cerebral cortex is the distinction between unimodal sensory and motor areas on one hand, and transmodal association regions on the other. A more nuanced view of this distinction can be found in the functional zones of the cerebral cortex proposed by Mesulam (M. Mesulam, 2000; M. M. Mesulam, 1998). Each zone contains cortical regions with similar microarchitecture, and zones are organized along a sensory-fugal axis which begins in highly differentiated "idiotypic" primary sensory and motor areas, proceeds through increasingly undifferentiated unimodal and heteromodal association regions, and ends in paralimbic mesocortex and limbic allocortex (Fig. 10A). Critically, regions within each cortical zone are similar not only in their microarchitecture, but also their role within an information processing hierarchy which transforms low-level sensory features from the external environment into into progressively more complex (and more abstract) multi-modal internal representations which form the building blocks of higher order cognition. To investigate how different aspects of intrinsic dynamics vary along this hierarchy, we used a Welch's ANOVA to quantify the extent to which scores on the primary and secondary gradient differ between cortical zones.

We observed a significant main effect of cortical zone for both the primary ($F(3, 174.3) = 69.1$, $p_{perm} = 0.0001$) and secondary gradient ($F(3, 186.9) = 102.1$, $p_{perm} = 0.0001$), and effect sizes suggest that the two gradients show roughly equivalent levels of differentiation across levels of the cortical information processing hierarchy (primary gradient: $\eta^2 = 0.39$, secondary gradient: $\eta^2 = 0.40$). As suggested by the results presented in previous sections, post-hoc pairwise comparisons (Tables 2 and 3) and visualization of gradient scores across cortical zones (Fig. 10B and 10C) indicate that the primary and secondary gradients show both similarities and differences in their pattern of variation along the sensory-fugal axis. Specifically, neither gradient differs significantly between idiotypic primary sensory and motor areas and unimodal association regions, while both gradients exhibit significantly different scores in heteromodal association regions compared to the two earlier cortical zones. However, while scores on the secondary gradient continue to decrease along the sensory-fugal axis from heteromodal to paralimbic areas (Fig. 10B), scores on the primary gradient are actually significantly lower in paralimbic areas than all other cortical zones (Fig. 10C). All of these effects were replicated in the validation sample (Fig. S14, Tables S1 and S2).

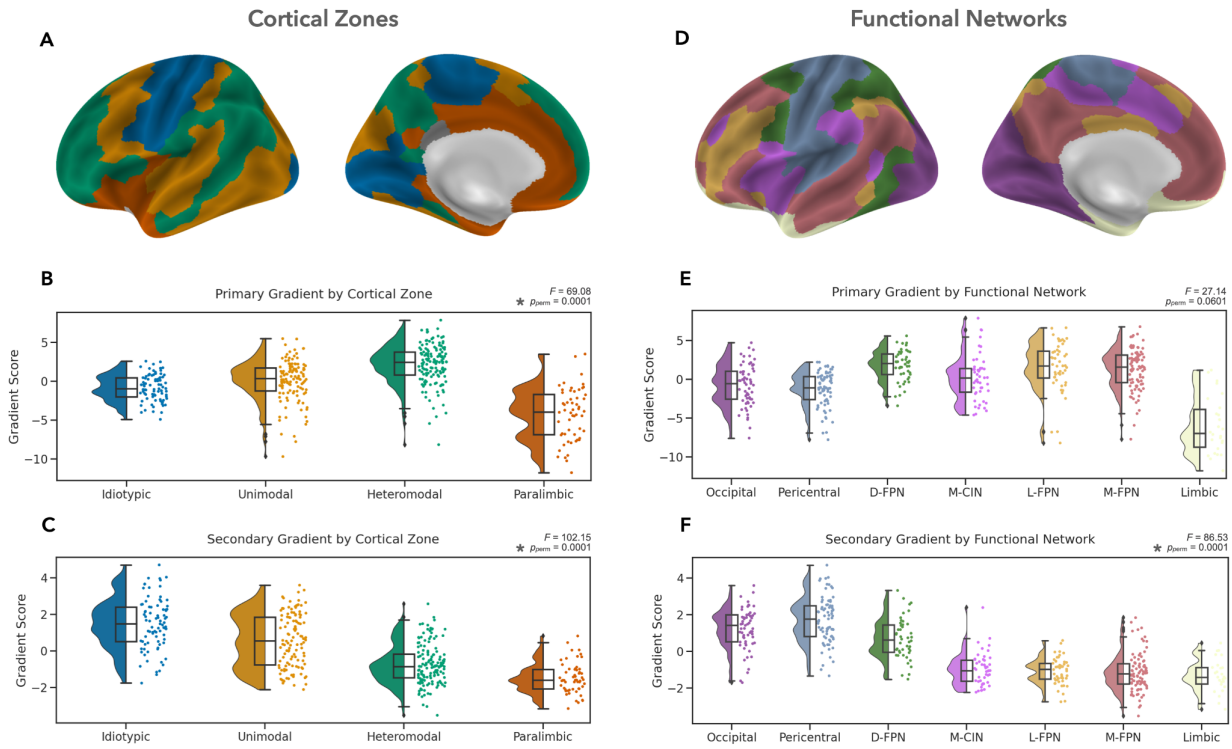


Figure 10: Gradient scores vary between microstructurally defined cortical zones and functional connectivity networks.

(A-C) Scores on both the primary and secondary gradient differ significantly between microstructurally defined zones of the cerebral cortex. Scores on the primary gradient increase from idiotypic and unimodal sensory areas to heteromodal association regions, but are lower in paralimbic areas than all other cortical zones. In contrast, scores on the secondary gradient continually decrease along a sensory-fugal axis. (D-F) Scores on the secondary gradient—but not the primary gradient—differ significantly between functional connectivity networks. Asterisks indicate a significant main effect.

Table 2: Post-hoc pairwise comparisons of primary gradient scores across cortical zones.

A	B	mean(A)	mean(B)	diff	SE	T	df	p_{perm}	Hedges' g
Heteromodal	Idiotypic	2.170	-0.822	2.991	0.285	10.481	218.359	0.002	1.447
Heteromodal	Paralimbic	2.170	-4.260	6.429	0.501	12.834	81.491	0.001	2.021
Heteromodal	Unimodal	2.170	0.090	2.079	0.329	6.319	245.555	0.021	0.786
Idiotypic	Paralimbic	-0.822	-4.260	3.438	0.488	7.038	73.786	0.006	1.211
Idiotypic	Unimodal	-0.822	0.090	-0.912	0.310	-2.945	197.976	0.265	-0.420
Paralimbic	Unimodal	-4.260	0.090	-4.350	0.515	-8.444	89.288	0.002	-1.362

Table 3: Post-hoc pairwise comparisons of secondary gradient scores across cortical zones.

A	B	mean(A)	mean(B)	diff	SE	T	df	p_{perm}	Hedges' g
Heteromodal	Idiotypic	-0.739	1.472	-2.211	0.179	-12.323	143.416	0.001	-1.701

Heteromodal	Paralimbic	-0.739	-1.486	0.747	0.146	5.103	132.898	0.041	0.804
Heteromodal	Unimodal	-0.739	0.568	-1.307	0.163	-8.012	218.388	0.001	-0.996
Idiotypic	Paralimbic	1.472	-1.486	2.958	0.190	15.588	135.547	0.001	2.681
Idiotypic	Unimodal	1.472	0.568	0.905	0.203	4.458	181.277	0.070	0.635
Paralimbic	Unimodal	-1.486	0.568	-2.054	0.174	-11.776	165.747	0.001	-1.900

Within each level of the cortical information processing hierarchy, brain areas can be further differentiated based on their participation in functionally specialized subsystems which support different aspects of cognition and behavior (e.g. visual processing, selective attention, working memory and executive control). To evaluate whether intrinsic dynamics differ between these subsystems, we compared gradient scores across seven large-scale functional connectivity networks ((Yeo et al., 2011); Fig. 10D) which have previously been shown to recapitulate assemblies of regions which co-activate during task engagement and stimulus processing, and which are differentially engaged across cognitive domains (Bertolero et al., 2015; Cole et al., 2014; Crossley et al., 2013; Krienen et al., 2014; Smith et al., 2009). We observed a significant main effect of functional network for scores on the secondary gradient ($F(6, 145.9) = 86.5$, $p_{perm} = 0.0001$), and this effect appears to be driven by differences in dynamics *between* rather than *within* levels of the sensory-fugal information processing hierarchy (Fig. 10F). Specifically, post-hoc tests (Table 4) revealed that secondary gradient scores were significantly higher in the occipital and pericentral networks than in the limbic, midcingulo-insular, medial and lateral frontoparietal networks. The four "higher order" networks (M-CIN, L-FPN, M-FPN, and LN) also tended to have lower scores than the dorsal frontoparietal network; this effect was significant for the L-FPN and M-FPN, and was of comparable size for the LN and M-CIN (Hedges' $g > 1.6$ for all four networks). In contrast, scores on the secondary gradient did not differ significantly between these four networks, nor between the three "lower order" networks (ON, PN, and D-FPN), and the effect sizes for pairwise differences *within* each set of networks were on average 6 times smaller than those *between* higher order and lower order networks (Fig S15). The main effect of functional network and the majority pairwise differences replicated in the validation sample (Figs. S14/S17, Table S3). We did not observe a significant main effect of functional network for scores on the primary gradient ($F(6, 141.3) = 27.1$, $p_{perm} = 0.0601$), and the effect we did observe was 70% smaller than that for the secondary gradient (primary gradient: $\eta^2 = 0.35$, secondary gradient: $\eta^2 = 0.59$), suggesting that functional networks are better differentiated along the secondary gradient than the primary gradient.

Table 4: Post-hoc pairwise comparisons of secondary gradient scores across functional networks.

A	B	mean(A)	mean(B)	diff	se	T	df	p_{perm}	Hedges' g
D-FPN	L-FPN	0.691	-1.080	1.771	0.192	9.232	75.044	0.036	1.854
D-FPN	Limbic	0.691	-1.309	2.000	0.239	8.354	61.957	0.068	2.028
D-FPN	M-CIN	0.691	-0.955	1.646	0.209	7.863	85.997	0.082	1.617
D-FPN	M-FPN	0.691	-1.152	1.842	0.196	9.382	84.293	0.033	1.688
D-FPN	Occipital	0.691	1.239	-0.549	0.218	-2.521	97.153	0.569	-0.489
D-FPN	Pericentral	0.691	1.721	-1.031	0.219	-4.713	104.565	0.297	-0.873
L-FPN	Limbic	-1.080	-1.309	0.229	0.201	1.142	41.690	0.788	0.272
L-FPN	M-CIN	-1.080	-0.955	-0.125	0.163	-0.765	88.253	0.873	-0.153
L-FPN	M-FPN	-1.080	-1.152	0.071	0.146	0.486	135.458	0.916	0.084
L-FPN	Occipital	-1.080	1.239	-2.319	0.174	-13.338	103.523	0.004	-2.500
L-FPN	Pericentral	-1.080	1.721	-2.802	0.175	-15.984	123.615	0.001	-2.852
Limbic	M-CIN	-1.309	-0.955	-0.354	0.217	-1.629	51.798	0.691	-0.394
Limbic	M-FPN	-1.309	-1.152	-0.158	0.205	-0.770	45.904	0.871	-0.170
Limbic	Occipital	-1.309	1.239	-2.549	0.225	-11.311	58.809	0.006	-2.626
Limbic	Pericentral	-1.309	1.721	-3.031	0.226	-13.388	61.612	0.004	-3.014
M-CIN	M-FPN	-0.955	-1.152	0.196	0.169	1.163	105.555	0.784	0.208
M-CIN	Occipital	-0.955	1.239	-2.194	0.193	-11.368	105.850	0.006	-2.191
M-CIN	Pericentral	-0.955	1.721	-2.677	0.194	-13.778	119.520	0.002	-2.535
M-FPN	Occipital	-1.152	1.239	-2.391	0.179	-13.363	121.493	0.004	-2.200
M-FPN	Pericentral	-1.152	1.721	-2.873	0.180	-15.939	145.919	0.001	-2.457
Occipital	Pericentral	1.239	1.721	-0.482	0.203	-2.373	134.467	0.596	-0.405

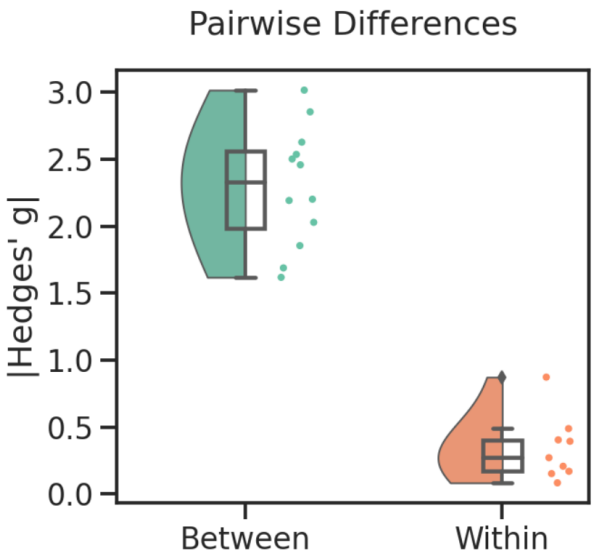


Figure S15: Pairwise differences in secondary gradient scores between functional networks.
Effect sizes for pairwise comparisons between the four "higher order" (limbic, mid-cingulo insular, medial and lateral frontoparietal) and three "lower order" (occipital, pericentral, and dorsal frontoparietal) networks were uniformly higher (on average 6 times higher) than comparisons within each group.

Situating cortical areas in a low-dimensional subspace of intrinsic brain dynamics

In previous sections, we sought to characterize the relationship between the dynamical properties captured by each gradient and multiple other features of cortical anatomy, connectivity, and function. However, just as no individual feature (or cluster of similar behaving features) is sufficient to describe the myriad ways in which intrinsic dynamics vary across the cortex, neither is either gradient in isolation. Instead, a more complete picture of regional variation in intrinsic dynamics requires considering both gradients simultaneously. To this end, we can use the gradient axes to construct an embedding space in which the location of each brain area depends on its score on each of the two gradients. By definition, the principal components used to define each gradient provide a low-dimensional representation of the 22 time series features, and as such allow us to project multidimensional time series phenotypes onto just two spatial dimensions (Fig. 11). We can then color each point (region) in this space based on its cortical zone (Fig. 11A) or functional network membership (Fig. 11B). These visualizations reveal that time series phenotypes are not uniformly distributed throughout the embedding space, but rather appear to sit between three poles, each of which is located at the extreme of one or both gradients. The first of these poles is located at the top of the secondary gradient and the middle of the primary gradient. Idiotypic and unimodal cortical areas in the occipital (visual) and pericentral (somatomotor) networks tend to cluster towards this pole. The second pole is located at the top of the primary gradient and the bottom of the secondary gradient. Regions near this pole tend to be heteromodal association areas and belong to the medial and lateral frontoparietal networks, as well as the midcingulo-insular network. The

third pole is located at the bottom of both gradients, and is anchored by limbic and paralimbic cortical areas. These results suggest that regions with different functional properties tend to sit in different parts of the subspace.

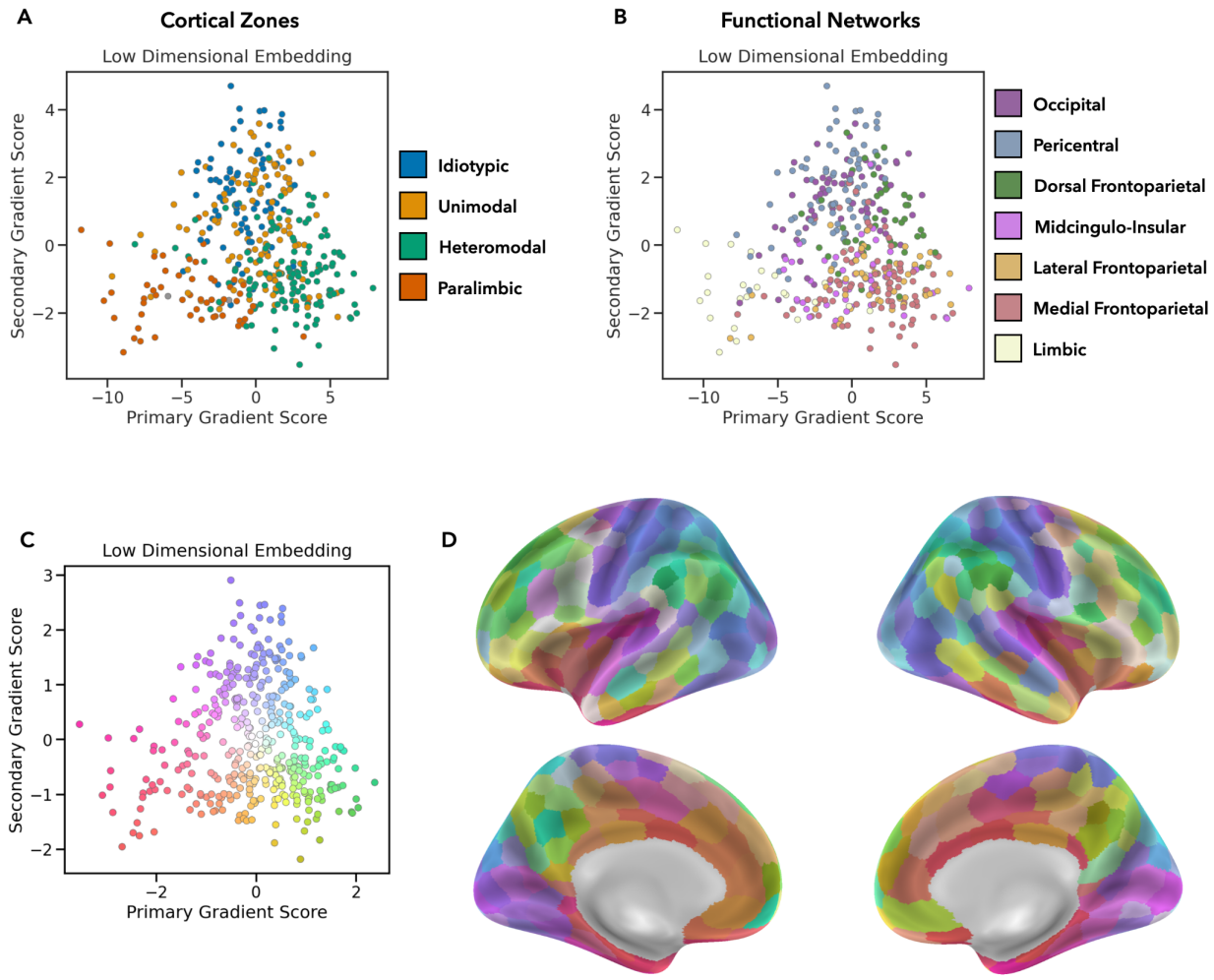


Figure 11: Defining a low-dimensional subspace of intrinsic brain dynamics.
(A-B) Plotting the two gradients against each other allows us to define a low-dimensional embedding space in which the location of each brain region depends on its multidimensional time series phenotype. This novel subspace facilitates comparison between brain areas based on multiple aspects of their intrinsic dynamics, and reveals how these dynamics differ within and between cortical zones and functional networks. (C) We can also color each brain area based on its angle (hue) and distance (saturation) from the center of the embedding space (i.e. a score of zero on both gradients). (D) Colors from C projected onto the cortical surface facilitate visualization of how multidimensional time series phenotypes vary across the brain.

As an alternative to coloring each data point in an embedding plot based on some other feature of brain organization (e.g. cortical zone or functional network membership, as in Fig. 11A and 11B), we can instead color each brain area based on its location within the low-dimensional subspace (Fig. 11C), thus effectively "color coding" time series phenotypes. By projecting these

colors onto the cortical surface (Fig. 11D), we can visualize the spatial organization of multidimensional time series phenotypes. This approach has previously been used to visualize a variety other of high-dimensional features of cortical organization, including patterns of whole-brain functional connectivity (Margulies et al., 2016), the content of semantic representations (Huth et al., 2016), as well as inter-regional structural connectivity and microstructural similarity (Paquola et al., 2020).

Discussion

Summary

In a data-driven analysis, we used a time series phenotyping approach to characterize multiple properties of intrinsic BOLD dynamics, and investigated how these dynamics vary across the cerebral cortex. We found that a diverse set of time series features vary along a small number of axes, and used principal components analysis to identify spatial gradients which capture these patterns of variation. This revealed a primary gradient defined by regional differences in the autocorrelation properties of BOLD time series, and a secondary gradient which captures the degree to which variance and kurtosis change over the course of a resting scan. As such, whereas the primary gradient provides information about the timescale of fluctuations in intrinsic brain activity, the secondary gradient provides complementary information about the characteristics of these fluctuations. Further, we find that these gradients are differentially related to the anatomical and connectomic properties of each cortical area, with the primary gradient exhibiting a stronger association with topological hierarchies within the structural connectome, and the secondary gradient showing a stronger association with non-invasive markers of anatomical hierarchy. Scores on the primary and secondary gradient also differ between microstructurally defined cortical zones and functional connectivity networks, and can be used to define a low-dimensional subspace of intrinsic brain dynamics.

The primary gradient captures regional differences in timescale and follows connectomic hierarchies

In line with a robust and rapidly growing literature suggesting that a hierarchy of timescales is a key feature of functional brain organization (e.g. (Gao et al., 2020; Hasson et al., 2015; Honey et al., 2012; Kiebel et al., 2008; Manea et al., 2022; Murray et al., 2014; Raut et al., 2020; Shafiei et al., 2020; Shinn et al., 2021)), the primary gradient identified by our PCA analysis captures regional variation in the autocorrelation properties of intrinsic brain dynamics. We observed the longest timescales in heteromodal association areas, intermediate timescales in sensorimotor areas, and the shortest timescales in paralimbic regions. This overall topography is broadly consistent with our own past work (Chapter 1), as well work from other groups which has mapped autocorrelation and related time series properties in the primate brain using BOLD fMRI (Baria et al., 2013; Fallon et al., 2020; Manea et al., 2022; Müller et al., 2020; Raut et al., 2020; Shafiei et al., 2020; Shinn et al., 2021; Watanabe et al., 2019; Wengler et al., 2020). While a complete review of this literature is beyond the scope of this article, we note that there is substantial heterogeneity in the literature on BOLD timescales, and future work is needed to identify the factors driving this variability.

Our finding that heteromodal association regions exhibit significantly longer timescales than idiotypic and unimodal sensory areas is in agreement with both theoretical models and empirical work which suggest that timescales lengthen along sensory processing hierarchies (Chaudhuri et al., 2015; Hasson et al., 2008, 2015; Honey et al., 2012; Kiebel et al., 2008; Manea et al., 2022; Murray et al., 2014; Stephens et al., 2013; Wengler et al., 2020). However, it is also clear that the primary gradient does not follow a 'canonical' axis of organization through all parts of the cerebral cortex. In particular, the fact that we observe the shortest (rather than longest) timescales in paralimbic regions is not only inconsistent with the notion that timescales lengthen along a sensory-fugal axis, but also more generally the idea that transmodal association areas tend to exhibit longer timescales than primary sensorimotor regions. Notably, the presence of short timescales in paralimbic areas (particularly the orbitofrontal cortex, subgenual and dorsal cingulate, insula, and medial temporal lobe) is not unique to the current study, but is in fact one of the most consistently replicated features of timescale maps estimated from BOLD fMRI (e.g. (Baria et al., 2013; Fallon et al., 2019; Manea et al., 2022; Müller et al., 2020; Raut et al., 2020; Shafiei et al., 2020; Shinn et al., 2021; Wengler et al., 2020), see also Chapter 1). Given this topography, it is perhaps unsurprising that we failed to observe a significant correlation between scores on the primary gradient and either T1w/T2w MRI or cortical thickness. These null effects are consistent with the results of other recent studies which have investigated relationship between BOLD timescales and non-invasive markers of anatomical hierarchy (i.e. (Shafiei et al., 2020) and (Wengler et al., 2020)[5], though see (Ito, Hearne, et al., 2020)[6] and (Watanabe et al., 2019)[7]). In contrast, we found a significant positive correlation between the primary gradient and multiple features of regional structural connectivity, and these results replicate findings from multiple prior studies (including the analyses we present in Chapter 1) which have found an association between BOLD timescales and topological hierarchies within the structural connectome (Baria et al., 2013; Fallon et al., 2019; Sethi et al., 2017). More generally, they are consistent with computational and empirical work which suggests that patterns of inter-regional connectivity play a key role in shaping cortical timescales ((Chaudhuri et al., 2014, 2015; Gollo et al., 2015; Li & Wang, 2022; Müller et al., 2020). Together, our results suggest that BOLD timescales may follow a distinct (and potentially novel) axis of organization across the cerebral cortex, and that this topography is more closely associated with regional differences in inter-regional connectivity than it is with local anatomical properties.

[5] While Wengler and colleagues did not find a significant correlation between these measures and BOLD timescales when the relationships were evaluated across the entire cortex, they did observe that BOLD timescales lengthened along specific auditory and somatosensory (though not visual) hierarchies defined based on T1w/T2w MRI and cortical thickness.

[6] Ito et al. report a significant negative correlation between BOLD timescales and T1w/T2w MRI. However, it should be noted that the timescale topography they observe departs from (to our knowledge) all other published maps of BOLD timescales. In particular, they found the longest timescales in the orbitofrontal cortex, medial temporal lobe, and temporal pole. This discrepancy is especially puzzling considering the fact that Ito et al. analyzed the same dataset used here (as well as in the studies by Shafiei and Wengler), and even used the same cortical parcellation as Wengler et al.

[7] Watanabe et al. observed a significant positive correlation between BOLD timescale and gray matter volume (GMV). This relationship was found both across cortical areas in group-level maps, as well as across individuals in a subset of regions. However, it should be noted that while cortical thickness and GMV are conceptually similar, the association between these measures varies markedly across brain areas, and overall they exhibit only a weak to moderate correlation (Panizzon et al., 2009; Winkler et al., 2010).

The secondary gradient follows a sensory-fugal axis and may reflect extrinsic influences on intrinsic dynamics

In contrast to the somewhat puzzling topography of the primary gradient, the secondary gradient closely follows a well established sensory-fugal axis of cortical organization. This topography is clearly visible when inspecting the map of scores on the secondary gradient, and is further evidenced by the significant correlation between scores on the secondary gradient and two non-invasive markers of anatomical hierarchy (T1w/T2w MRI and cortical thickness), as well as significant differences in gradient scores between microstructurally defined cortical zones. The secondary gradient is also associated with a hierarchy within the cortical functional connectome, with topologically central areas tending to exhibit higher scores than more peripheral regions. However, while our results suggest that the topography of the secondary gradient does reflect regional differences in anatomy and function, the dynamics underlying this topography are likely better understood in terms of a distributed process occuring at the level of the individual participant. In particular, scores on the secondary gradient can be described in terms of extent to which distributional properties (i.e. variance and kurtosis) tend to increase or decrease over the course of the resting scan. In the same way that the statement "brain area X tends to increase its activity" is largely meaningless without information about the context in which that increase occurs, so too is our observation of spatially heterogeneous changes in variance and kurtosis. As such, we hypothesize that the dynamics underlying the secondary gradient may result from the scanning experience itself, and specifically fluctuations in cognitive state and/or level of arousal.

In the absence of external task demands (such as during a "resting" fMRI scan), the contents of cognition shift away from the external world and towards internal representations (Christoff et al., 2016; Smallwood, 2013; Smallwood & Schooler, 2015). This transition from stimulus-related to stimulus-independent thought is accompanied by reduced processing of external stimuli and reduced activity in sensorimotor areas, but increased or sustained activity in a wide range of transmodal association regions (Baird et al., 2014; Benedek et al., 2016; Christoff et al., 2009; Cohen et al., 2022; K. C. R. Fox et al., 2015; Kam et al., 2011; C. Murphy et al., 2018, 2019; Schooler et al., 2011; Smallwood et al., 2008, 2021; Turnbull et al., 2019). Quiet rest is also associated with greater BOLD variability in most brain areas when compared to periods of active engagement in an externally oriented task, and the degree to which brain areas increase their variability from task to rest is spatially heterogeneous (Duff et al., 2008; Gaut et al., 2019; He, 2011; Ito, Brincat, et al., 2020; Millar et al., 2021; Rieck et al., 2022)[8]. In particular, a recent study by (Rieck et al., 2022) found that increases in BOLD variability from task to rest are significantly larger in the occipital, pericentral, and dorsal frontoparietal networks than in the medial and lateral frontoparietal networks. Critically, this pattern of results not only mirrors the topography of scores on the secondary gradient (i.e. highest in sensorimotor areas), but also the dynamics these scores represent (i.e. increases in variability). More generally, the findings reviewed above are consistent with our observation that most brain areas increase their variability over time, while only a subset of regions (located in the medial frontoparietal "default" network) decrease their variability. As such, we suggest that the dynamics underlying the secondary gradient may be driven in part by changes in activity and variability associated with gradual shifts in cognitive state which occur over the course of the resting scan (i.e. decreases in externally oriented attention and increases in self-generated thought). While tracking the dynamics of

[8] See also (Fegen, 2012), who found a negative correlation between BOLD task activation and variability.

self-generated, stimulus-independent cognition is notoriously difficult, studies using methods such as experience sampling and thought probes may help to evaluate this hypothesis (Christoff et al., 2009; Kucyi et al., 2021; Smallwood et al., 2008; Turnbull et al., 2019).

Decreasing arousal and eyelid closures due to fatigue or boredom during scanning offer another possible explanation for the dynamics underlying the secondary gradient. Like mind wandering, fluctuations in arousal are common during resting fMRI scans (for recent reviews, see (Gu et al., 2019; Liu & Falahpour, 2020; Martin et al., 2021)). Levels of arousal tend to decrease over the course of a scan session, and it is not uncommon for participants to close their eyes or even fall asleep during scanning (Allen et al., 2018; Laumann et al., 2017; Olbrich et al., 2009; Tagliazucchi & Laufs, 2014). Prolonged eyelid closures and periods of low arousal have consistently been associated with increased BOLD variability relative to wakeful eyes-open rest (Bianciardi et al., 2009; Fukunaga et al., 2006; Horovitz et al., 2008; Jao et al., 2013; Larson-Prior et al., 2009; McAvoy et al., 2008, 2012; Tagliazucchi & Laufs, 2014; Wong et al., 2016). Critically, as with the dynamics underlying the secondary gradient, these increases in variance tend to be largest in sensorimotor areas (Horovitz et al., 2008; Jao et al., 2013; McAvoy et al., 2008, 2012; Tagliazucchi & Laufs, 2014). As such, it is plausible that the spatially heterogeneous changes in variance captured by the secondary gradient may be driven by gradually decreasing arousal and more frequent eyelid closures over the course of the resting scan. Future studies might directly evaluate this hypothesis through the use of eye tracking, simultaneous EEG-fMRI, machine learning, or other methods which can provide a continuous index of arousal during the resting state (Chang et al., 2016; Horovitz et al., 2008; Olbrich et al., 2009; Tagliazucchi et al., 2012; Tagliazucchi & Laufs, 2014; Wang et al., 2016).

Methodological considerations

The gradients we identify—their loadings, topography, and associations with other features of cortical organization—are highly similar to those reported by (Shafiei et al., 2020), who undertook a very similar set of analyses to those we present here, but using a much larger set of over 6000 time series features. In this way, our results demonstrate that intrinsic BOLD dynamics can be described using multiple orders of magnitude fewer features than have been previously used to characterize regional time series phenotypes (Fallon et al., 2020; Markicevic et al., 2020, 2022; Sethi et al., 2017; Shafiei et al., 2020). That said, our results must be considered in light of the fact that the gradients we identify necessarily reflect the set of features which define them.

In particular, we caution that our results should not be interpreted as suggesting that autocorrelation is the time series property which best captures how intrinsic BOLD dynamics vary across cortical areas. Instead, the fact that autocorrelation features load strongly on the first principal component (rather than the second) is largely a byproduct of a large number of features sensitive to the same time series property, and the correlation among these features. More specifically, the *catch22* feature set used here is enriched for measures sensitive to autocorrelation and temporal dependence (as is the larger HCTSA feature set from which *catch22* is derived), and these features tend to produce correlated results across a wide range of time series, not just BOLD fMRI data. This can be seen in Figure S19, which visualizes the correlation between features when *catch22* is applied to 1000 diverse time series taken from multiple different fields (B. Fulcher, 2020). Similarly, a PCA on the resulting 22 x 1000 feature matrix identifies a first principal component which has significant loadings from 12 of the 14

features which load significantly on the primary gradient (Fig. S20). Therefore, while the primary gradient is non-trivial insofar as it captures common structure in how autocorrelation features vary across the cerebral cortex, the fact that this is identified as the primary axis of variation is not unique to the case of intrinsic brain dynamics. In contrast, the secondary gradient does not appear to reflect generic feature dependencies, as features which show a significant loading on the secondary gradient exhibit only very weak or near-zero correlations across the 1000 time series (Fig. S19). Likewise, none of the significant principal components from that dataset have a similar pattern of feature loadings to the secondary gradient (Fig. S20). As such, the secondary gradient appears to describe non-trivial structure in the relationships between time series features which may be unique to BOLD fMRI data.

Limitations

This study has at least six limitations. First, while we analyzed fMRI data from two independent samples, these samples were taken from the same larger dataset. Second, we used the same structural connectome and maps of T1w/T2w MRI and cortical thickness in our analysis of both samples. As such, these analyses are not fully independent. Third, our analysis focused on group-level estimates of dynamics, anatomy, and connectivity. It is possible that the effects we observe may not fully generalize to individual participants. Fourth, we used only a single cortical parcellation and denoising strategy, and our results might differ when using alternative region definitions or in the absence of global signal regression. Fifth, recent work suggests that the generative null model we use to account for spatial autocorrelation may not exactly control the false positive rate (Markello & Misic, 2021). Sixth, as noted above, the gradients we identify necessarily reflect the features which define them, and the use of additional or alternative features may produce different results. Our findings should be considered in light of these limitations.

Supplemental Methods

Resting BOLD fMRI data

We analyzed resting BOLD fMRI data from two independent samples of unrelated healthy young individuals (ages 21-35) selected from the Human Connectome Project (Van Essen et al., 2013). Our initial exploratory analysis used data from 95 participants, while our replication analysis used a validation sample of 87 participants. Both of these samples were selected based on subject lists provided by (Shine et al., 2016), and all analyses were repeated separately for each sample. For each individual, we analyzed the first 15 minute resting fMRI scan (TR/TE = 720/33ms, 2mm isotropic voxels) from the first scan session (Smith et al., 2013). We used minimally preprocessed data (Glasser et al., 2013) provided by HCP which had undergone ICA-FIX denoising (Griffanti et al., 2014). To further mitigate the potentially confounding effects of in-scanner head motion (Ciric et al., 2017; Parkes et al., 2018) and aliased physiological signals (Tong et al., 2019), we additionally applied global signal regression and a 0.009 to 0.08 Hz bandpass filter.

Time series phenotyping

Time series features were computed using the '*catch22*' Python package (Lubba et al., 2019). Complete details regarding the calculation of each individual feature is beyond the scope of this article, and readers are encouraged to refer to the original article by Lubba and colleagues, as well as the *catch22* github page[9] which provides additional information about each feature, as well as the underlying code. Due to inaccuracies in the feature descriptions provided by Lubba et al. (which we uncovered during our analysis), some of the feature descriptions used here differ from those in the original *catch22* paper. Sliding-window measures of distributional features (standard deviation and kurtosis) were calculated using custom Python code with a window size of 100 volumes and a step size of 50 volumes. Estimates of linear trend (i.e. slope) for these features were computed by fitting a linear model against time point indices. Given evidence that ROI volume can bias measures of intrinsic dynamics (particularly those based on autocorrelation (Afyouni et al., 2019; Fallon et al., 2019; Sethi et al., 2017; Shinn et al., 2021)), group-level time series features were residualized relative to the number of voxels in each ROI prior to visualization and further analyses.

Hierarchical clustering

We applied agglomerative hierarchical clustering with a Ward linkage and similarity between features defined by Euclidean distance. Feature values were z-scored across regions prior to clustering. Feature clusters were defined based on visualization of the dendrogram and clustered feature matrix.

T1w/T2w MRI and cortical thickness

Group average maps of T1w/T2w MRI and curvature corrected cortical thickness were taken from the Human Connectome Project 1200 Subjects Data Release (Van Essen et al., 2013).

Functional connectivity

For each participant, we estimated functional connectivity as the strength of Pearson correlation between the time series of each pair of ROIs. We then applied the Fisher r-to-z transform to the correlations estimated from each individual before averaging edges across participants to create a group-level network. Due to uncertainties regarding the interpretation of negative correlations in studies of functional connectivity (M. D. Fox et al., 2009; K. Murphy et al., 2009; Rubinov & Sporns, 2010), all edges with negative z-scores were set to zero.

Structural connectivity network construction

We constructed a single structural connectivity network from a publicly available, expert-curated voxelwise "population-average" atlas of the human structural connectome (Yeh et al., 2018). This atlas was derived from high-resolution, multi-shell diffusion MRI images from 842 participants from the Human Connectome Project (Van Essen et al., 2013). Complete details of how the atlas was produced can be found in (Yeh et al., 2018), but we review

[9] https://github.com/DynamicsAndNeuralSystems/catch22

them briefly here. Images for each participant were transformed to MNI space using q-space diffeomorphic registration (Yeh & Tseng, 2011), which preserves spins and fiber geometry and estimates the spin distribution function (SDF) at each voxel. Voxelwise SDFs were averaged across participants to create a group-average template, after which multiple runs of deterministic tractography (Yeh et al., 2013) were used to estimate 550,000 streamlines describing connectivity across the entire brain. All streamlines were then reviewed and labeled by a team of expert neuroanatomists to identify fiber tracts, remove anatomically implausible (i.e. false positive) connections, and manually seed additional streamlines to identify known fascicles which were missing from the initial set of connections. The final atlas contains ~145,000 voxelwise streamlines describing the representative white matter connectivity of cortical and subcortical regions in the human brain. Based on this atlas, we estimated structural connectivity as the number of streamlines connecting each pair of cortical ROIs. Because the distribution of streamline counts can be highly skewed and span several orders of magnitude, we followed the common practice of applying a log transformation to edge weights prior to subsequent analyses (Fornito et al., 2016).

Cortical zones and functional networks

Cortical ROIs were grouped into one of four cortical zones proposed by (M. Mesulam, 2000; M. M. Mesulam, 1998) based on a surface map of these zones provided by (Paquola et al., 2019). ROI assignments were based on the zone which comprised the majority of vertices within each ROI. Functional network memberships for each ROI were provided by (Schaefer et al., 2018).

Statistical testing

The significance of correlations between gradient scores and other continuous measures (e.g. cortical thickness, connectivity strength) were evaluated relative to 10,000 surrogate null gradient maps generated using a spatial-autocorrelation preserving generative model (Burt et al., 2020). We use the method introduced by (Zou, 2007) for comparing correlations. In this approach, a confidence interval is computed for the difference in effects while accounting for dependence (i.e. measures estimated from the same data, such as time series features and functional connectivity strength) and overlapping variables (e.g. X is overlapping in a comparison of $corr_{X,Y}$ and $corr_{X,Z}$). If the confidence interval includes zero, we are unable to reject the null hypothesis for a difference between correlations (and vice versa). The critical value for computing confidence intervals was corrected for selective inference using the False Coverage-statement Rate method from (Benjamini & Yekutieli, 2005). Differences in gradient scores between cortical zones and functional networks were evaluated using a Welch's ANOVA to account for unequal sample sizes and variances across zones/networks, and the significance of the main effect for each model was evaluated relative to a null distribution of F statistics generated using the same 10,000 surrogate maps used for evaluating the significance of correlations. For the same reason, we used Games-Howell tests for post-hoc pairwise comparisons rather than alternatives such as the Tukey HSD. Due to the significant computational resources required for each permutation test and the large number of pairwise comparisons, the significance of each pairwise comparison was evaluated to 1,000 rather than 10,000 surrogate maps.

Supplemental Results

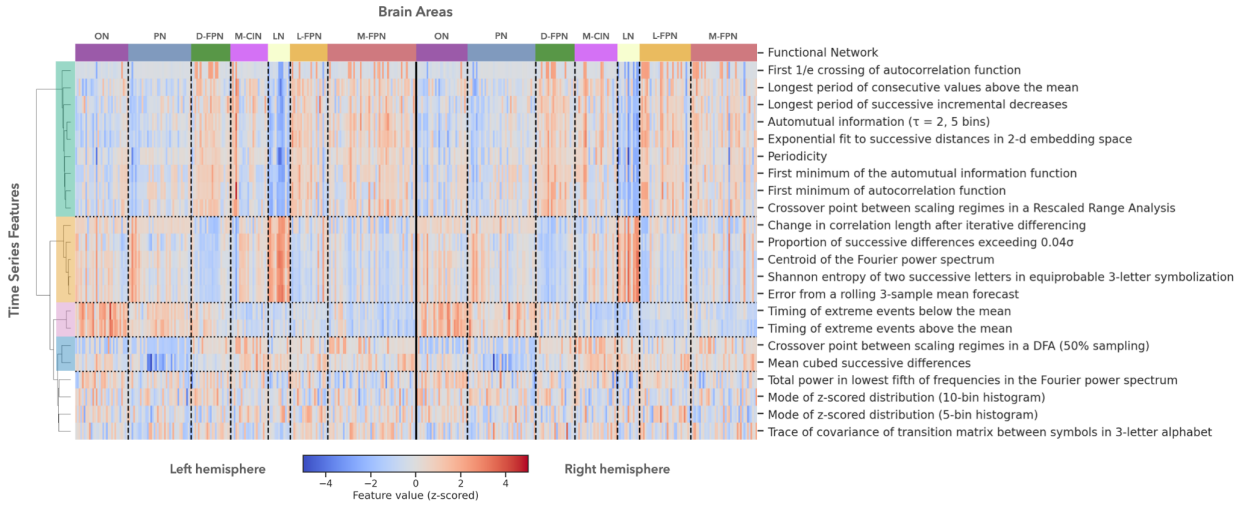


Figure S1: Clustering results in the validation sample.
Dotted horizontal lines delineate the four feature clusters. Left and right hemisphere regions are separated by the solid vertical line, while dashed vertical lines delineate functional connectivity networks. Network definitions are taken from (Yeo et al., 2011) and have been re-labeled using the anatomy-based taxonomy proposed by (Uddin et al., 2019): ON, occipital; PN, pericentral; D-FPN, dorsal frontoparietal; M-CIN, midcingulo-insular; LN, limbic; L-FPN, lateral frontoparietal; M-FPN, medial frontoparietal).

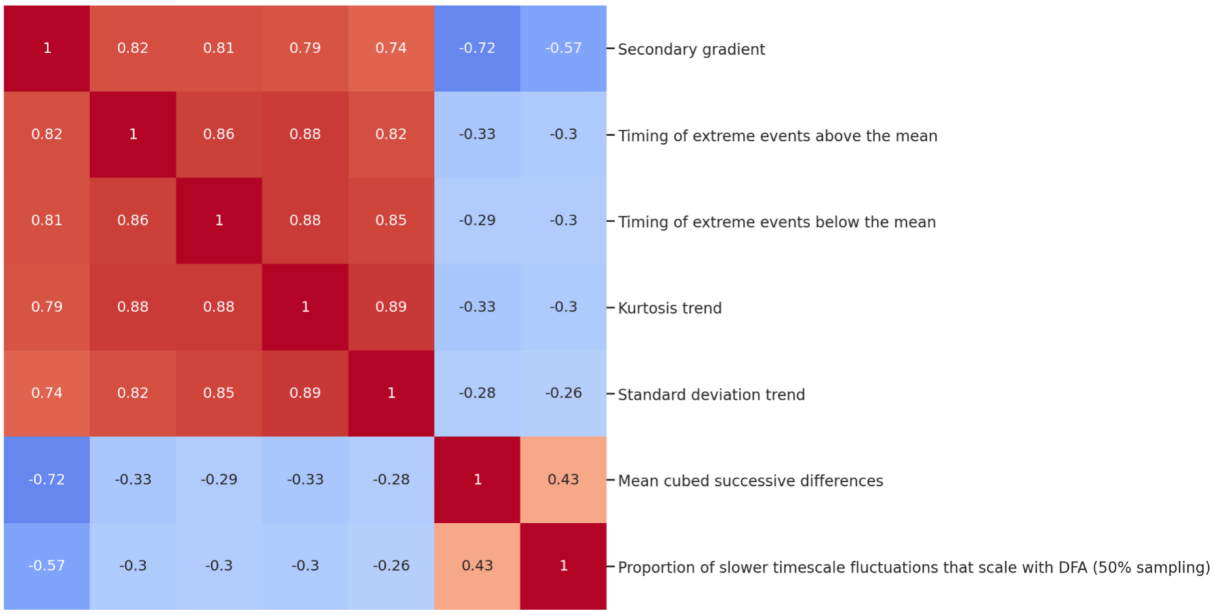


Figure S6: Correlation of m_{SD} and m_K with the secondary gradient and associated features in the validation sample.
The value in each cell is the Pearson correlation coefficient, which is equivalent to PCA feature loading.

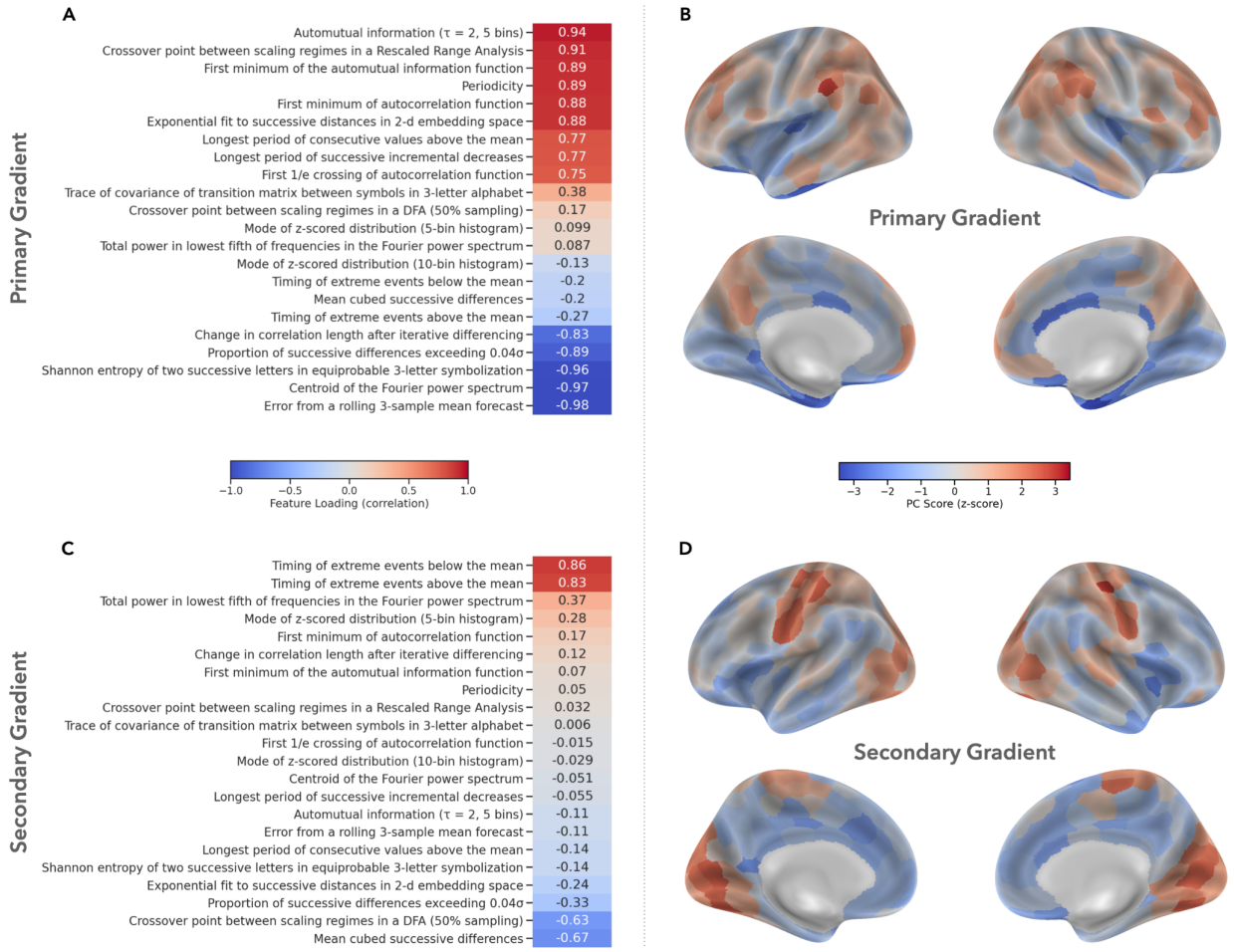


Figure S8: Gradient loadings and scores in the validation sample.

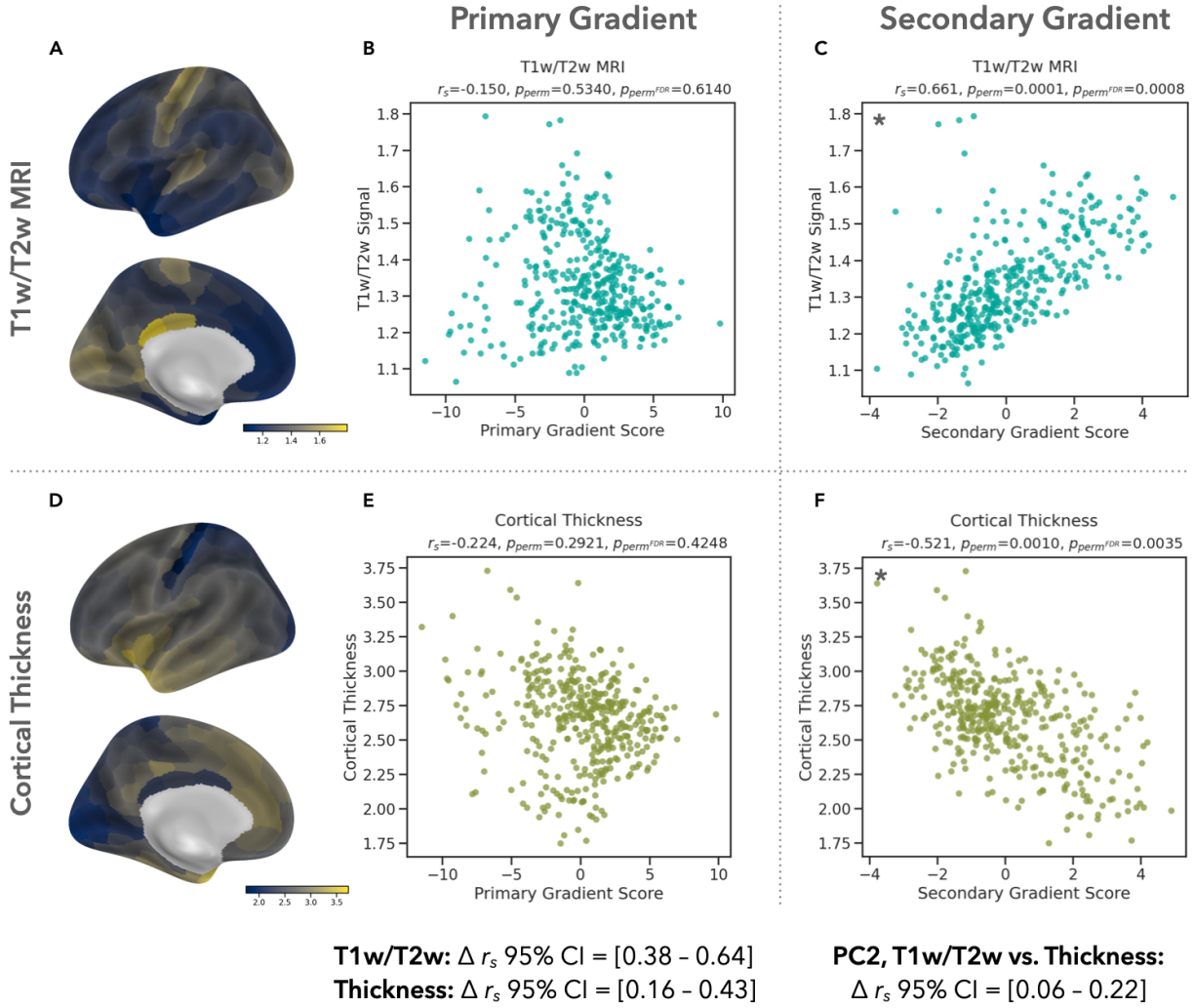


Figure S9: Relationship between gradient scores and anatomical measures in the validation sample. Asterisks indicate correlations which are significant at FDR q ≤ 0.05. Confidence intervals are for the difference in effect size between gradients (left column) and between modalities for the secondary gradient (right column).

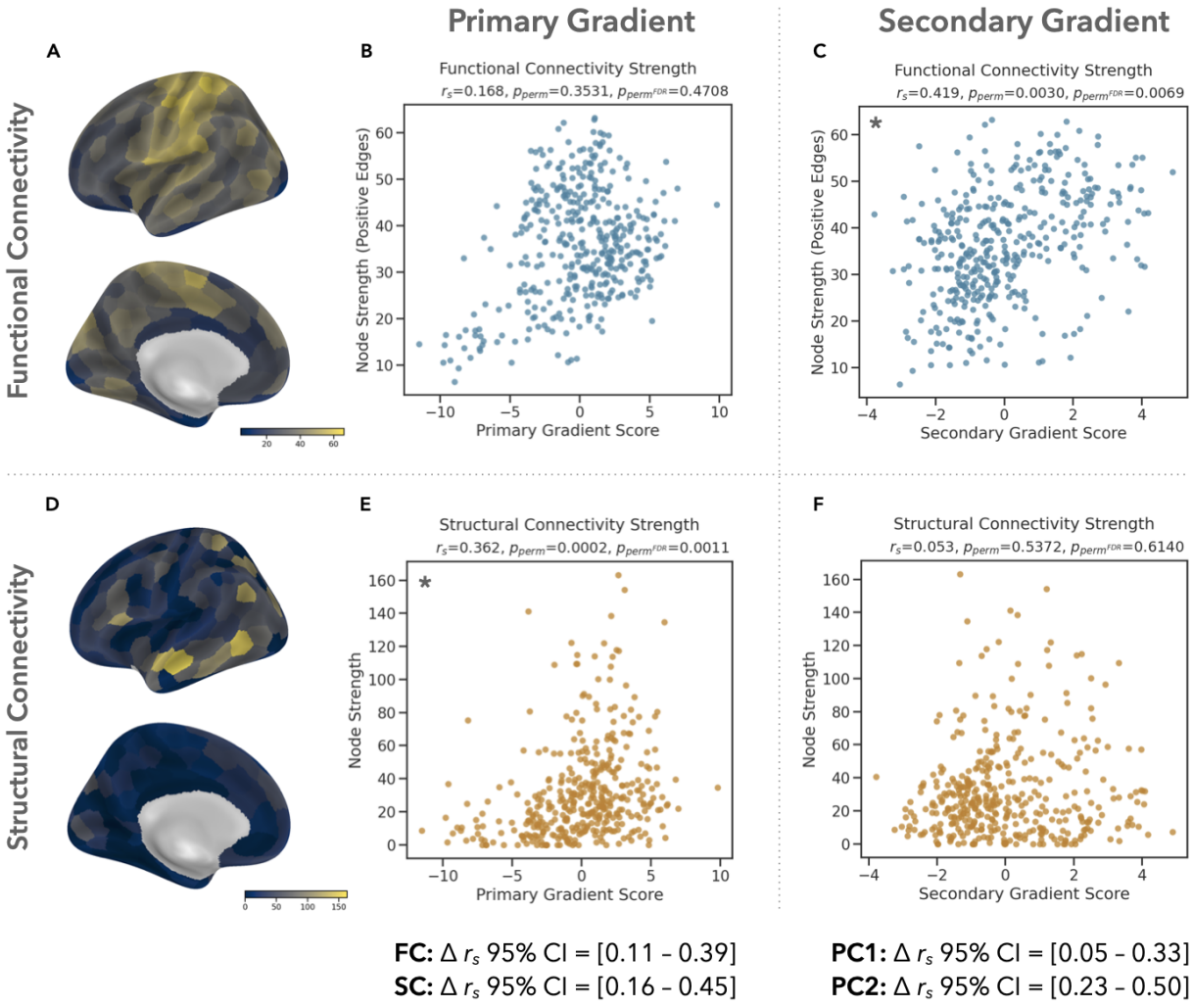


Figure S10: Relationship between gradient scores and connectivity strength in the validation sample. Asterisks indicate correlations which are significant at FDR q ≤ 0.05. Confidence intervals are for the difference in effect size between gradients (left column) and between modalities (right column).

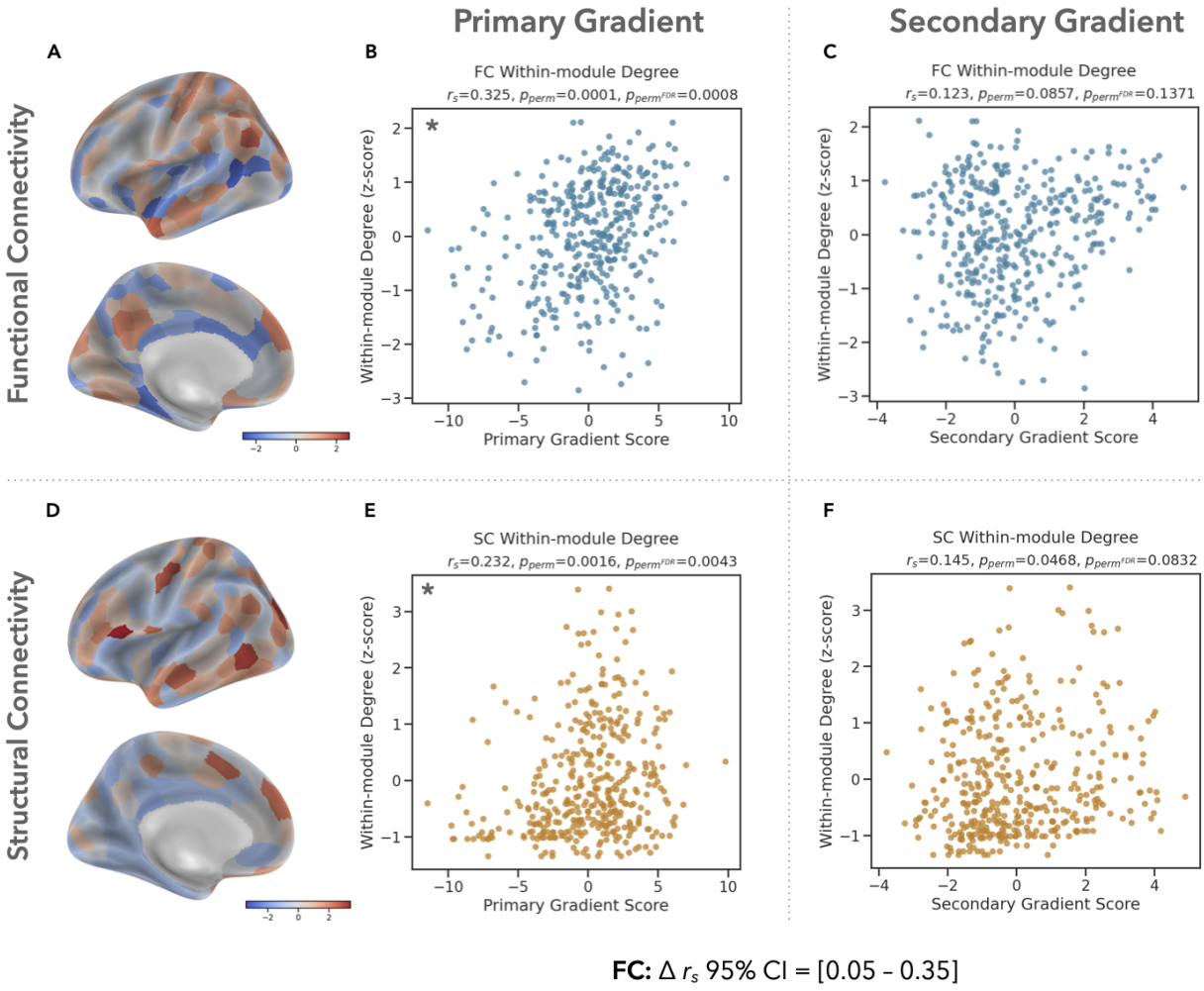


Figure S11: Relationship between gradient scores and within-module degree in the validation sample. Asterisks indicate correlations which are significant at FDR q ≤ 0.05. The confidence interval is for the difference in FC effect size between gradients.

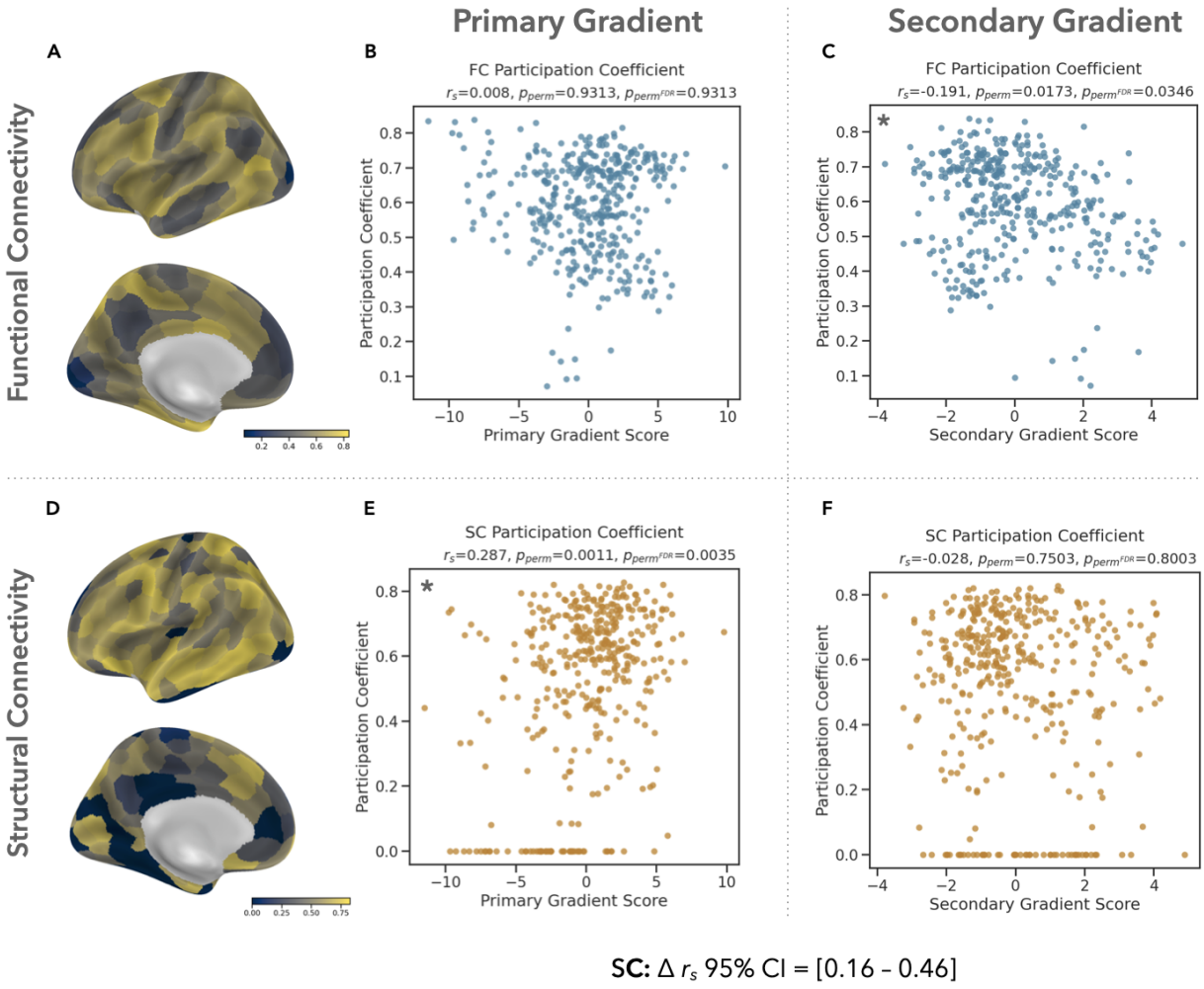


Figure S12: Relationship between gradient scores and participation coefficient in the validation sample.

Asterisks indicate correlations which are significant at FDR q ≤ 0.05. The confidence interval is for the difference in SC effect size between gradients.

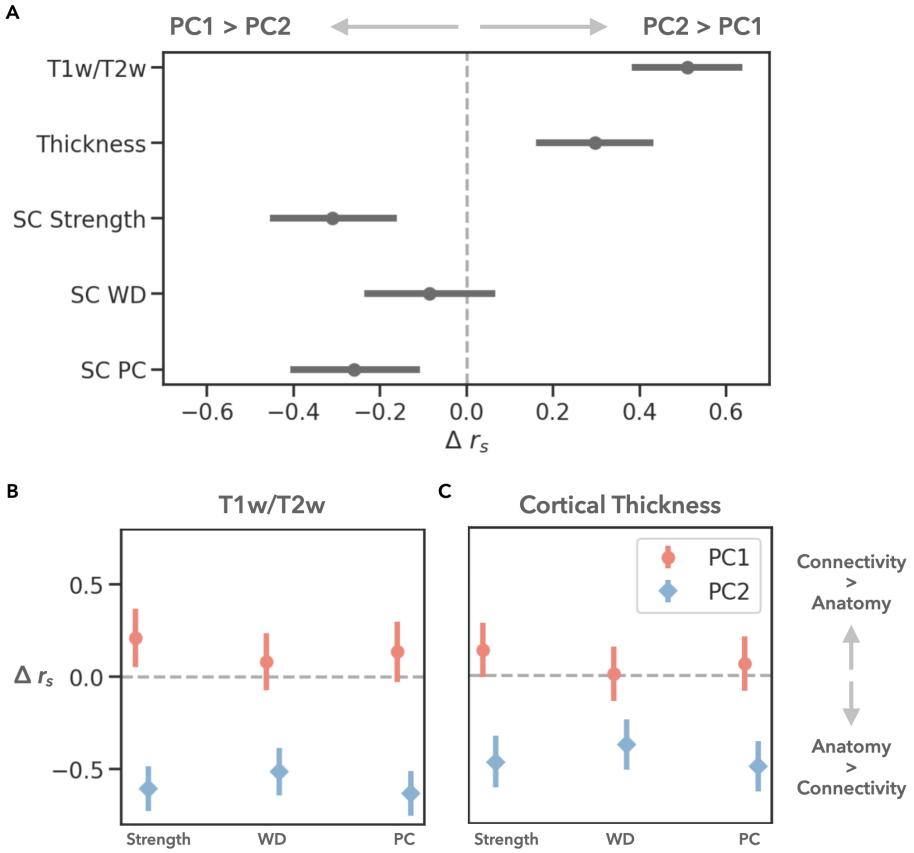
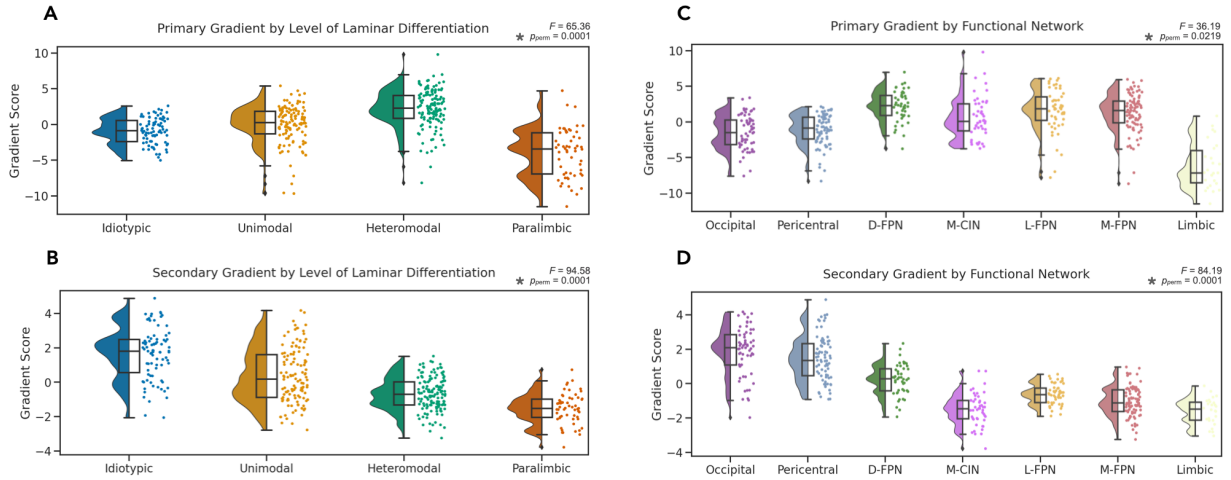


Figure S13: Effect comparisons in the validation sample.



PC1: $\eta^2 = 0.37$
PC2: $\eta^2 = 0.40$

PC1: $\eta^2 = 0.39$
PC2: $\eta^2 = 0.61$

Figure S14: Differences between cortical zones and functional networks in the validation sample.
Asterisks indicate a significant ANOVA main effect. The standardized effect size (η^2) is shown for cortical zones (left)

and functional networks (right).

Table S1: Post-hoc pairwise comparisons of primary gradient scores across cortical zones (validation sample).

A	B	mean(A)	mean(B)	diff	SE	T	df	p_{perm}	Hedges' g
Heteromodal	Idiotypic	2.236	-0.922	3.158	0.300	10.516	216.677	0.001	1.452
Heteromodal	Paralimbic	2.236	-4.002	6.238	0.508	12.284	83.148	0.001	1.935
Heteromodal	Unimodal	2.236	-0.023	2.260	0.336	6.726	248.388	0.011	0.836
Idiotypic	Paralimbic	-0.922	-4.002	3.080	0.497	6.198	76.164	0.019	1.066
Idiotypic	Unimodal	-0.922	-0.023	-0.898	0.319	-2.814	199.627	0.271	-0.401
Paralimbic	Unimodal	-4.002	-0.023	-3.979	0.519	-7.662	89.262	0.003	-1.236

Table S2: Post-hoc pairwise comparisons of secondary gradient scores across cortical zones (validation sample).

A	B	mean(A)	mean(B)	diff	SE	T	df	p_{perm}	Hedges' g
Heteromodal	Idiotypic	-0.739	1.472	-2.211	0.179	-12.323	143.416	0.001	-1.701
Heteromodal	Paralimbic	-0.739	-1.486	0.747	0.146	5.103	132.898	0.041	0.804
Heteromodal	Unimodal	-0.739	0.568	-1.307	0.163	-8.012	218.388	0.001	-0.996
Idiotypic	Paralimbic	1.472	-1.486	2.958	0.190	15.588	135.547	0.001	2.681
Idiotypic	Unimodal	1.472	0.568	0.905	0.203	4.458	181.277	0.070	0.635
Paralimbic	Unimodal	-1.486	0.568	-2.054	0.174	-11.776	165.747	0.001	-1.900

Table S3: Post-hoc pairwise comparisons of secondary gradient scores across functional networks (validation sample).

A	B	mean(A)	mean(B)	diff	se	T	df	p_{perm}	Hedges' g
D-FPN	L-FPN	0.229	-0.623	0.852	0.159	5.367	75.329	0.220	1.078
D-FPN	Limbic	0.229	-1.590	1.819	0.202	9.015	60.413	0.035	2.188
D-FPN	M-CIN	0.229	-1.489	1.717	0.192	8.949	90.991	0.036	1.841
D-FPN	M-FPN	0.229	-1.039	1.268	0.163	7.782	85.351	0.068	1.400
D-FPN	Occipital	0.229	1.881	-1.652	0.227	-7.292	102.924	0.093	-1.414
D-FPN	Pericentral	0.229	1.468	-1.240	0.202	-6.124	117.997	0.158	-1.134
L-FPN	Limbic	-0.623	-1.590	0.967	0.171	5.667	40.709	0.193	1.348
L-FPN	M-CIN	-0.623	-1.489	0.865	0.159	5.448	76.771	0.209	1.088
L-FPN	M-FPN	-0.623	-1.039	0.416	0.122	3.403	135.912	0.435	0.588
L-FPN	Occipital	-0.623	1.881	-2.504	0.199	-12.561	83.151	0.004	-2.355
L-FPN	Pericentral	-0.623	1.468	-2.092	0.171	-12.203	113.350	0.006	-2.177
Limbic	M-CIN	-1.590	-1.489	-0.101	0.202	-0.503	60.819	0.928	-0.122

Limbic	M-FPN	-1.590	-1.039	-0.551	0.175	-3.155	44.952	0.467	-0.697
Limbic	Occipital	-1.590	1.881	-3.471	0.235	-14.767	80.353	0.001	-3.428
Limbic	Pericentral	-1.590	1.468	-3.058	0.212	-14.436	75.704	0.001	-3.250
M-CIN	M-FPN	-1.489	-1.039	-0.449	0.163	-2.755	87.000	0.528	-0.492
M-CIN	Occipital	-1.489	1.881	-3.370	0.227	-14.865	103.614	0.001	-2.865
M-CIN	Pericentral	-1.489	1.468	-2.957	0.203	-14.601	119.333	0.001	-2.686
M-FPN	Occipital	-1.039	1.881	-2.920	0.203	-14.404	89.711	0.001	-2.372
M-FPN	Pericentral	-1.039	1.468	-2.508	0.175	-14.305	126.846	0.001	-2.205
Occipital	Pericentral	1.881	1.468	0.413	0.236	1.752	124.314	0.701	0.299

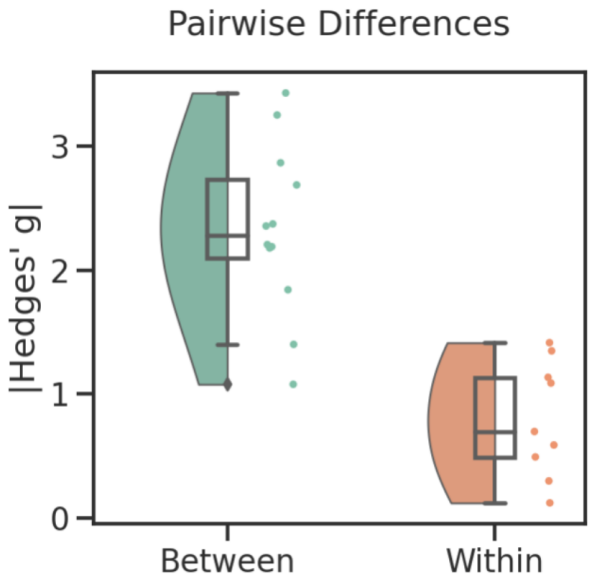


Figure S17: Pairwise differences in secondary gradient scores between functional networks in the validation sample.
Pairwise comparisons within and between the four "higher order" (limbic, mid-cingulo insular, medial and lateral frontoparietal) and three "lower order" (occipital, pericentral, and dorsal frontoparietal) networks.

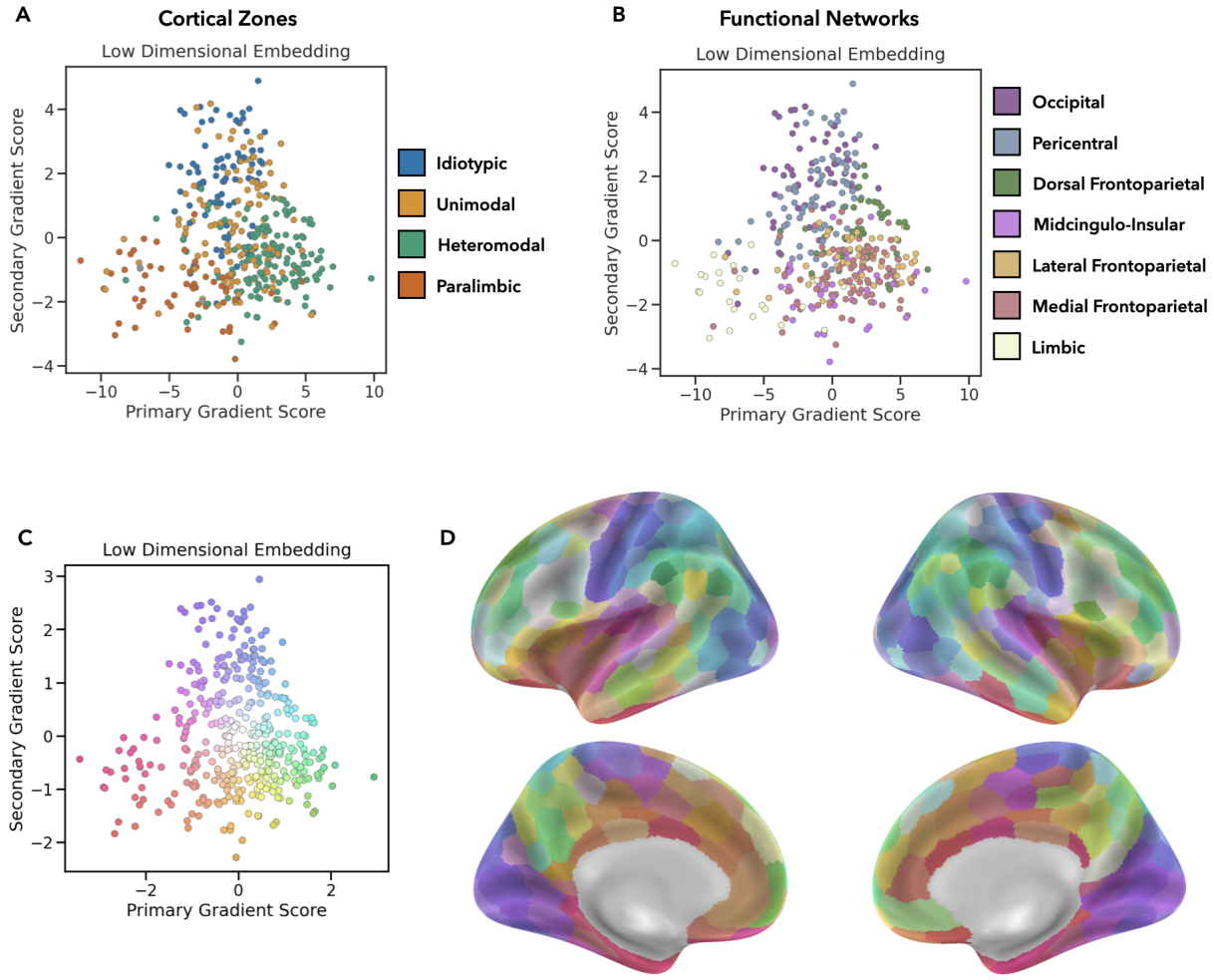


Figure S18: Visualization of low-dimensional embedding in the validation sample.

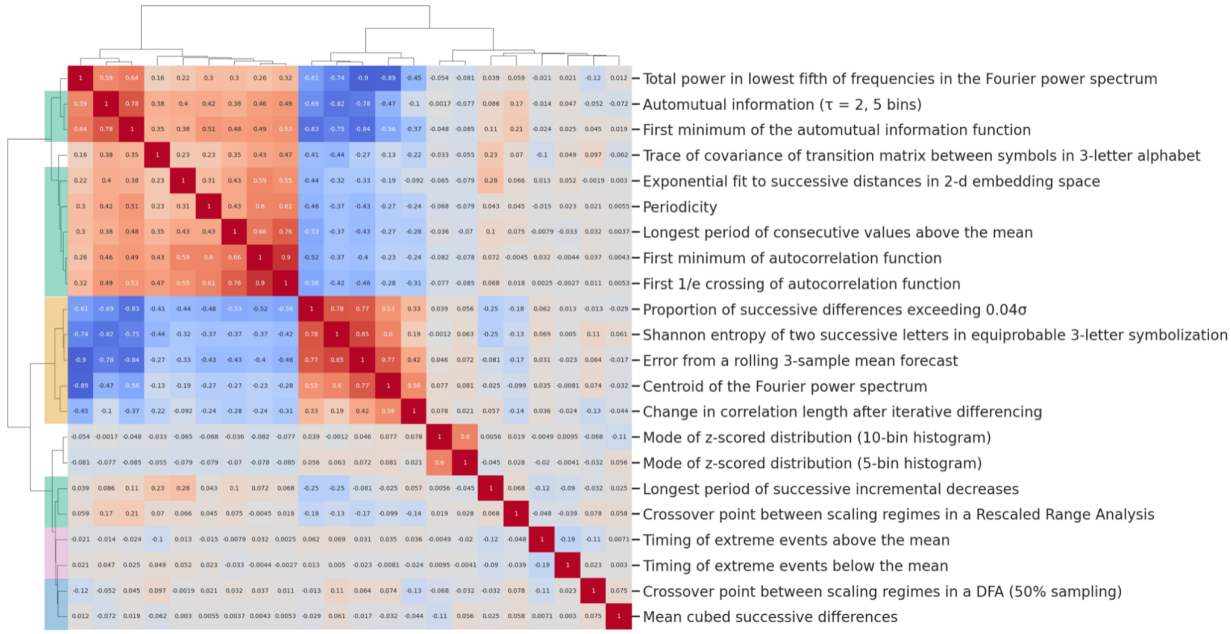


Figure S19: Cluster structure and feature dependencies across 1000 diverse time series.
Rows and columns are clustered based on correlations between features. The colored dendrogram (left) visualizes the cluster structure from Figure 1. The value in each cell is the Pearson correlation coefficient.

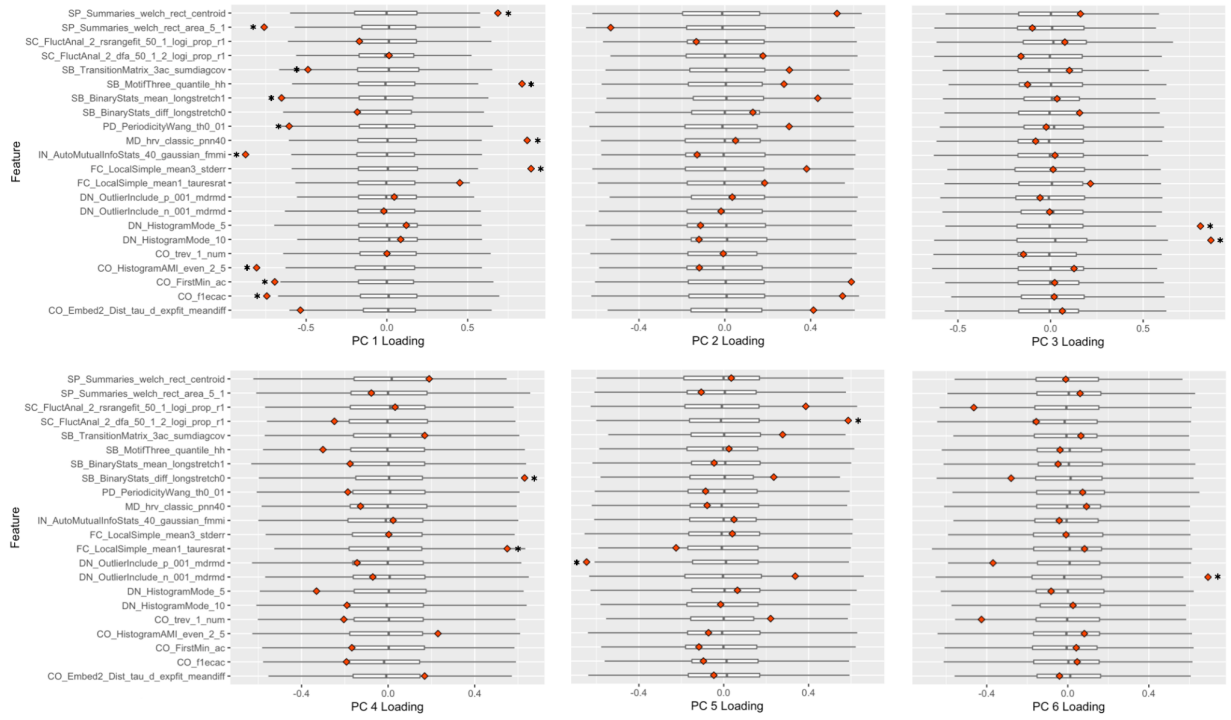


Figure S20: PCA feature loadings for *catch22* features applied to 1000 diverse time series (significant PCs only).

References

Afyouni, S., Smith, S. M., & Nichols, T. E. (2019). Effective degrees of freedom of the Pearson's correlation coefficient under autocorrelation. *NeuroImage*, *199*, 609–625. https://doi.org/10.1016/j.neuroimage.2019.05.011

Alexander-Bloch, A. F., Shou, H., Liu, S., Satterthwaite, T. D., Glahn, D. C., Shinohara, R. T., Vandekar, S. N., & Raznahan, A. (2018). On testing for spatial correspondence between maps of human brain structure and function. *NeuroImage*, *178*, 540–551. https://doi.org/10.1016/j.neuroimage.2018.05.070

Allen, E. A., Damaraju, E., Eichele, T., Wu, L., & Calhoun, V. D. (2018). EEG Signatures of Dynamic Functional Network Connectivity States. *Brain Topography*, *31*(1), 101–116. https://doi.org/10.1007/s10548-017-0546-2

Amunts, K., Lepage, C., Borgeat, L., Mohlberg, H., Dickscheid, T., Rousseau, M.-É., Bludau, S., Bazin, P.-L., Lewis, L. B., Oros-Peusquens, A.-M., Shah, N. J., Lippert, T., Zilles, K., & Evans, A. C. (2013). BigBrain: an ultrahigh-resolution 3D human brain model. *Science*, *340*(6139), 1472–1475. https://doi.org/10.1126/science.1235381

Amunts, K., Mohlberg, H., Bludau, S., & Zilles, K. (2020). Julich-Brain: A 3D probabilistic atlas of the human brain's cytoarchitecture. *Science*, *369*(6506), 988–992. https://doi.org/10.1126/science.abb4588

Amunts, K., & Zilles, K. (2015). Architectonic Mapping of the Human Brain beyond Brodmann. *Neuron*, *88*(6), 1086–1107. https://doi.org/10.1016/j.neuron.2015.12.001

Anderson, K. M., Collins, M. A., Chin, R., Ge, T., Rosenberg, M. D., & Holmes, A. J. (2020). Transcriptional and imaging-genetic association of cortical interneurons, brain function, and schizophrenia risk. *Nature Communications*, *11*(1), 2889. https://doi.org/10.1038/s41467-020-16710-x

Bagnall, A., Lines, J., Bostrom, A., Large, J., & Keogh, E. (2017). The great time series classification bake off: a review and experimental evaluation of recent algorithmic advances. *Data Mining and Knowledge Discovery*, *31*(3), 606–660. https://doi.org/10.1007/s10618-016-0483-9

Baird, B., Smallwood, J., Lutz, A., & Schooler, J. W. (2014). The decoupled mind: mind-wandering disrupts cortical phase-locking to perceptual events. *Journal of Cognitive Neuroscience*, *26*(11), 2596–2607. https://doi.org/10.1162/jocn_a_00656

Baria, A. T., Mansour, A., Huang, L., Baliki, M. N., Cecchi, G. A., Mesulam, M. M., & Apkarian, A. V. (2013). Linking human brain local activity fluctuations to structural and functional network architectures. *NeuroImage*, *73*, 144–155. https://doi.org/10.1016/j.neuroimage.2013.01.072

Benedek, M., Jauk, E., Beaty, R. E., Fink, A., Koschutnig, K., & Neubauer, A. C. (2016). Brain mechanisms associated with internally directed attention and self-generated thought.

Scientific Reports, *6*, 22959. https://doi.org/10.1038/srep22959

Benjamini, Y., & Yekutieli, D. (2005). False Discovery Rate–Adjusted Multiple Confidence Intervals for Selected Parameters. *Journal of the American Statistical Association*, *100*(469), 71–81. https://doi.org/10.1198/016214504000001907

Bertolero, M. A., Yeo, B. T. T., & D'Esposito, M. (2015). The modular and integrative functional architecture of the human brain. *Proceedings of the National Academy of Sciences of the United States of America*, *112*(49), E6798–E6807. https://doi.org/10.1073/pnas.1510619112

Bianciardi, M., Fukunaga, M., van Gelderen, P., Horovitz, S. G., de Zwart, J. A., & Duyn, J. H. (2009). Modulation of spontaneous fMRI activity in human visual cortex by behavioral state. *NeuroImage*, *45*(1), 160–168. https://doi.org/10.1016/j.neuroimage.2008.10.034

Bro, R., Kjeldahl, K., Smilde, A. K., & Kiers, H. A. L. (2008). Cross-validation of component models: a critical look at current methods. *Analytical and Bioanalytical Chemistry*, *390*(5), 1241–1251. https://doi.org/10.1007/s00216-007-1790-1

Bullmore, E., & Sporns, O. (2009). Complex brain networks: graph theoretical analysis of structural and functional systems. *Nature Reviews. Neuroscience*, *10*(3), 186–198. https://doi.org/10.1038/nrn2575

Burt, J. B., Demirtaş, M., Eckner, W. J., Navejar, N. M., Ji, J. L., Martin, W. J., Bernacchia, A., Anticevic, A., & Murray, J. D. (2018). Hierarchy of transcriptomic specialization across human cortex captured by structural neuroimaging topography. *Nature Neuroscience*, *21*(9), 1251–1259. https://doi.org/10.1038/s41593-018-0195-0

Burt, J. B., Helmer, M., Shinn, M., Anticevic, A., & Murray, J. D. (2020). Generative modeling of brain maps with spatial autocorrelation. *NeuroImage*, *220*, 117038. https://doi.org/10.1016/j.neuroimage.2020.117038

Camargo, A. (2022). PCAtest: testing the statistical significance of Principal Component Analysis in R. *PeerJ*, *10*, e12967. https://doi.org/10.7717/peerj.12967

Chang, C., Leopold, D. A., Schölvinck, M. L., Mandelkow, H., Picchioni, D., Liu, X., Ye, F. Q., Turchi, J. N., & Duyn, J. H. (2016). Tracking brain arousal fluctuations with fMRI. *Proceedings of the National Academy of Sciences of the United States of America*, *113*(16), 4518–4523. https://doi.org/10.1073/pnas.1520613113

Chaudhuri, R., Bernacchia, A., & Wang, X.-J. (2014). A diversity of localized timescales in network activity. *eLife*, *3*, e01239. https://doi.org/10.7554/eLife.01239

Chaudhuri, R., Knoblauch, K., Gariel, M.-A., Kennedy, H., & Wang, X.-J. (2015). A Large-Scale Circuit Mechanism for Hierarchical Dynamical Processing in the Primate Cortex. *Neuron*, *88*(2), 419–431. https://doi.org/10.1016/j.neuron.2015.09.008

Christoff, K., Gordon, A. M., Smallwood, J., Smith, R., & Schooler, J. W. (2009). Experience sampling during fMRI reveals default network and executive system contributions to mind wandering. *Proceedings of the National Academy of Sciences*, *106*(21), 8719–8724.

https://doi.org/10.1073/pnas.0900234106

Christoff, K., Irving, Z. C., Fox, K. C. R., Spreng, R. N., & Andrews-Hanna, J. R. (2016). Mind-wandering as spontaneous thought: a dynamic framework. *Nature Reviews. Neuroscience*, *17*(11), 718–731. https://doi.org/10.1038/nrn.2016.113

Churchill, N. W., Spring, R., Grady, C., Cimprich, B., Askren, M. K., Reuter-Lorenz, P. A., Jung, M. S., Peltier, S., Strother, S. C., & Berman, M. G. (2016). The suppression of scale-free fMRI brain dynamics across three different sources of effort: aging, task novelty and task difficulty. *Scientific Reports*, *6*, 30895. https://doi.org/10.1038/srep30895

Ciric, R., Wolf, D. H., Power, J. D., Roalf, D. R., Baum, G. L., Ruparel, K., Shinohara, R. T., Elliott, M. A., Eickhoff, S. B., Davatzikos, C., Gur, R. C., Gur, R. E., Bassett, D. S., & Satterthwaite, T. D. (2017). Benchmarking of participant-level confound regression strategies for the control of motion artifact in studies of functional connectivity. *NeuroImage*, *154*, 174–187. https://doi.org/10.1016/j.neuroimage.2017.03.020

Cohen, D., Nakai, T., & Nishimoto, S. (2022). Brain networks are decoupled from external stimuli during internal cognition. *NeuroImage*, *256*, 119230. https://doi.org/10.1016/j.neuroimage.2022.119230

Cole, M. W., Bassett, D. S., Power, J. D., Braver, T. S., & Petersen, S. E. (2014). Intrinsic and task-evoked network architectures of the human brain. *Neuron*, *83*(1), 238–251. https://doi.org/10.1016/j.neuron.2014.05.014

Crossley, N. A., Mechelli, A., Vértes, P. E., Winton-Brown, T. T., Patel, A. X., Ginestet, C. E., McGuire, P., & Bullmore, E. T. (2013). Cognitive relevance of the community structure of the human brain functional coactivation network. *Proceedings of the National Academy of Sciences of the United States of America*, *110*(28), 11583–11588. https://doi.org/10.1073/pnas.1220826110

Demirtaş, M., Burt, J. B., Helmer, M., Ji, J. L., Adkinson, B. D., Glasser, M. F., Van Essen, D. C., Sotiropoulos, S. N., Anticevic, A., & Murray, J. D. (2019). Hierarchical Heterogeneity across Human Cortex Shapes Large-Scale Neural Dynamics. *Neuron*. https://doi.org/10.1016/j.neuron.2019.01.017

Duff, E. P., Johnston, L. A., Xiong, J., Fox, P. T., Mareels, I., & Egan, G. F. (2008). The power of spectral density analysis for mapping endogenous BOLD signal fluctuations. *Human Brain Mapping*, *29*(7), 778–790. https://doi.org/10.1002/hbm.20601

Fallon, J., Ward, P. G. D., Parkes, L., Oldham, S., Arnatkevičiūtė, A., Fornito, A., & Fulcher, B. D. (2020). Timescales of spontaneous fMRI fluctuations relate to structural connectivity in the brain. *Network Neuroscience (Cambridge, Mass.)*, *4*(3), 788–806. https://doi.org/10.1162/netn_a_00151

Fallon, J., Ward, P., Parkes, L., Oldham, S., Arnatkevičiūtė, A., Fornito, A., & Fulcher, B. D. (2019). Timescales of spontaneous activity fluctuations relate to structural connectivity in the brain. In *bioRxiv* (p. 655050). https://doi.org/10.1101/655050

Fegen, D. (2012). *Cortical mechanisms underlying verbal working memory* (M. D'Esposito (ed.))

[PhD, UC Berkeley]. https://escholarship.org/uc/item/6zp350v9

Fornito, A., Zalesky, A., & Bullmore, E. T. (Eds.). (2016). Chapter 4 - Node Degree and Strength. In *Fundamentals of Brain Network Analysis* (pp. 115–136). Academic Press. https://doi.org/10.1016/B978-0-12-407908-3.00004-2

Fox, K. C. R., Spreng, R. N., Ellamil, M., Andrews-Hanna, J. R., & Christoff, K. (2015). The wandering brain: meta-analysis of functional neuroimaging studies of mind-wandering and related spontaneous thought processes. *NeuroImage*, *111*, 611–621. https://doi.org/10.1016/j.neuroimage.2015.02.039

Fox, M. D., Zhang, D., Snyder, A. Z., & Raichle, M. E. (2009). The global signal and observed anticorrelated resting state brain networks. *Journal of Neurophysiology*, *101*(6), 3270–3283. https://doi.org/10.1152/jn.90777.2008

Froudist-Walsh, S., Xu, T., Niu, M., Rapan, L., Margulies, D. S., Zilles, K., Wang, X.-J., & Palomero-Gallagher, N. (2021). Gradients of receptor expression in the macaque cortex. In *bioRxiv* (p. 2021.02.22.432173). https://doi.org/10.1101/2021.02.22.432173

Fukunaga, M., Horovitz, S. G., van Gelderen, P., de Zwart, J. A., Jansma, J. M., Ikonomidou, V. N., Chu, R., Deckers, R. H. R., Leopold, D. A., & Duyn, J. H. (2006). Large-amplitude, spatially correlated fluctuations in BOLD fMRI signals during extended rest and early sleep stages. *Magnetic Resonance Imaging*, *24*(8), 979–992. https://doi.org/10.1016/j.mri.2006.04.018

Fulcher, B. (2020). *1000 Empirical Time series* [Data set]. figshare. https://doi.org/10.6084/M9.FIGSHARE.5436136.V9

Fulcher, B. D., & Jones, N. S. (2017). hctsa: A Computational Framework for Automated Time-Series Phenotyping Using Massive Feature Extraction. *Cell Systems*, *5*(5), 527–531.e3. https://doi.org/10.1016/j.cels.2017.10.001

Fulcher, B. D., Little, M. A., & Jones, N. S. (2013). Highly comparative time-series analysis: the empirical structure of time series and their methods. *Journal of the Royal Society, Interface / the Royal Society*, *10*(83), 20130048. https://doi.org/10.1098/rsif.2013.0048

Gao, R., van den Brink, R. L., Pfeffer, T., & Voytek, B. (2020). Neuronal timescales are functionally dynamic and shaped by cortical microarchitecture. *eLife*, *9*. https://doi.org/10.7554/eLife.61277

Gaut, G., Turner, B., Lu, Z.-L., Li, X., Cunningham, W. A., & Steyvers, M. (2019). Predicting Task and Subject Differences with Functional Connectivity and Blood-Oxygen-Level-Dependent Variability. *Brain Connectivity*, *9*(6), 451–463. https://doi.org/10.1089/brain.2018.0632

Glasser, M. F., Sotiropoulos, S. N., Wilson, J. A., Coalson, T. S., Fischl, B., Andersson, J. L., Xu, J., Jbabdi, S., Webster, M., Polimeni, J. R., Van Essen, D. C., & Jenkinson, M. (2013). The minimal preprocessing pipelines for the Human Connectome Project. *NeuroImage*, *80*, 105–124. https://doi.org/10.1016/j.neuroimage.2013.04.127

Glasser, M. F., & Van Essen, D. C. (2011). Mapping human cortical areas in vivo based on myelin

content as revealed by T1- and T2-weighted MRI. *The Journal of Neuroscience: The Official Journal of the Society for Neuroscience*, *31*(32), 11597–11616. https://doi.org/10.1523/JNEUROSCI.2180-11.2011

Gollo, L. L., Zalesky, A., Hutchison, R. M., van den Heuvel, M., & Breakspear, M. (2015). Dwelling quietly in the rich club: brain network determinants of slow cortical fluctuations. *Philosophical Transactions of the Royal Society of London. Series B, Biological Sciences*, *370*(1668). https://doi.org/10.1098/rstb.2014.0165

Gomez, J., Zhen, Z., & Weiner, K. S. (2019). Human visual cortex is organized along two genetically opposed hierarchical gradients with unique developmental and evolutionary origins. *PLoS Biology*, *17*(7), e3000362. https://doi.org/10.1371/journal.pbio.3000362

Griffanti, L., Salimi-Khorshidi, G., Beckmann, C. F., Auerbach, E. J., Douaud, G., Sexton, C. E., Zsoldos, E., Ebmeier, K. P., Filippini, N., Mackay, C. E., Moeller, S., Xu, J., Yacoub, E., Baselli, G., Ugurbil, K., Miller, K. L., & Smith, S. M. (2014). ICA-based artefact removal and accelerated fMRI acquisition for improved resting state network imaging. *NeuroImage*, *95*, 232–247. https://doi.org/10.1016/j.neuroimage.2014.03.034

Guimerà, R., & Amaral, L. A. N. (2005). Cartography of complex networks: modules and universal roles. *Journal of Statistical Mechanics* , *2005*(P02001), nihpa35573. https://doi.org/10.1088/1742-5468/2005/02/P02001

Guimerà, R., & Nunes Amaral, L. A. (2005). Functional cartography of complex metabolic networks. *Nature*, *433*(7028), 895–900. https://doi.org/10.1038/nature03288

Gu, Y., Han, F., & Liu, X. (2019). Arousal Contributions to Resting-State fMRI Connectivity and Dynamics. *Frontiers in Neuroscience*, *13*, 1190. https://doi.org/10.3389/fnins.2019.01190

Hardstone, R., Poil, S.-S., Schiavone, G., Jansen, R., Nikulin, V. V., Mansvelder, H. D., & Linkenkaer-Hansen, K. (2012). Detrended fluctuation analysis: a scale-free view on neuronal oscillations. *Frontiers in Physiology*, *3*, 450. https://doi.org/10.3389/fphys.2012.00450

Hasson, U., Chen, J., & Honey, C. J. (2015). Hierarchical process memory: memory as an integral component of information processing. *Trends in Cognitive Sciences*, *19*(6), 304–313. https://doi.org/10.1016/j.tics.2015.04.006

Hasson, U., Yang, E., Vallines, I., Heeger, D. J., & Rubin, N. (2008). A hierarchy of temporal receptive windows in human cortex. *The Journal of Neuroscience: The Official Journal of the Society for Neuroscience*, *28*(10), 2539–2550. https://doi.org/10.1523/JNEUROSCI.5487-07.2008

He, B. J. (2011). Scale-free properties of the functional magnetic resonance imaging signal during rest and task. *The Journal of Neuroscience: The Official Journal of the Society for Neuroscience*, *31*(39), 13786–13795. https://doi.org/10.1523/JNEUROSCI.2111-11.2011

Hilgetag, C. C., & Goulas, A. (2020). "Hierarchy" in the organization of brain networks. *Philosophical Transactions of the Royal Society of London. Series B, Biological Sciences*,

375(1796), 20190319. https://doi.org/10.1098/rstb.2019.0319

Honey, C. J., Thesen, T., Donner, T. H., Silbert, L. J., Carlson, C. E., Devinsky, O., Doyle, W. K., Rubin, N., Heeger, D. J., & Hasson, U. (2012). Slow cortical dynamics and the accumulation of information over long timescales. *Neuron*, *76*(2), 423–434. https://doi.org/10.1016/j.neuron.2012.08.011

Horovitz, S. G., Fukunaga, M., de Zwart, J. A., van Gelderen, P., Fulton, S. C., Balkin, T. J., & Duyn, J. H. (2008). Low frequency BOLD fluctuations during resting wakefulness and light sleep: a simultaneous EEG-fMRI study. *Human Brain Mapping*, *29*(6), 671–682. https://doi.org/10.1002/hbm.20428

Huth, A. G., de Heer, W. A., Griffiths, T. L., Theunissen, F. E., & Gallant, J. L. (2016). Natural speech reveals the semantic maps that tile human cerebral cortex. *Nature*, *532*(7600), 453–458. https://doi.org/10.1038/nature17637

Ito, T., Brincat, S. L., Siegel, M., Mill, R. D., He, B. J., Miller, E. K., Rotstein, H. G., & Cole, M. W. (2020). Task-evoked activity quenches neural correlations and variability across cortical areas. *PLoS Computational Biology*, *16*(8), e1007983. https://doi.org/10.1371/journal.pcbi.1007983

Ito, T., Hearne, L. J., & Cole, M. W. (2020). A cortical hierarchy of localized and distributed processes revealed via dissociation of task activations, connectivity changes, and intrinsic timescales. *NeuroImage*, *221*(117141), 117141. https://doi.org/10.1016/j.neuroimage.2020.117141

Jao, T., Vértes, P. E., Alexander-Bloch, A. F., Tang, I.-N., Yu, Y.-C., Chen, J.-H., & Bullmore, E. T. (2013). Volitional eyes opening perturbs brain dynamics and functional connectivity regardless of light input. *NeuroImage*, *69*, 21–34. https://doi.org/10.1016/j.neuroimage.2012.12.007

Kam, J. W. Y., Dao, E., Farley, J., Fitzpatrick, K., Smallwood, J., Schooler, J. W., & Handy, T. C. (2011). Slow fluctuations in attentional control of sensory cortex. *Journal of Cognitive Neuroscience*, *23*(2), 460–470. https://doi.org/10.1162/jocn.2010.21443

Kiebel, S. J., Daunizeau, J., & Friston, K. J. (2008). A hierarchy of time-scales and the brain. *PLoS Computational Biology*, *4*(11), e1000209. https://doi.org/10.1371/journal.pcbi.1000209

Krienen, F. M., Yeo, B. T. T., & Buckner, R. L. (2014). Reconfigurable task-dependent functional coupling modes cluster around a core functional architecture. *Philosophical Transactions of the Royal Society of London. Series B, Biological Sciences*, *369*(1653). https://doi.org/10.1098/rstb.2013.0526

Krzanowski, W. J. (1987). Cross-Validation in Principal Component Analysis. *Biometrics*, *43*(3), 575–584. https://doi.org/10.2307/2531996

Kucyi, A., Esterman, M., Capella, J., Green, A., Uchida, M., Biederman, J., Gabrieli, J. D. E., Valera, E. M., & Whitfield-Gabrieli, S. (2021). Prediction of stimulus-independent and task-unrelated thought from functional brain networks. *Nature Communications*, *12*(1),

1793. https://doi.org/10.1038/s41467-021-22027-0

Larson-Prior, L. J., Zempel, J. M., Nolan, T. S., Prior, F. W., Snyder, A. Z., & Raichle, M. E. (2009). Cortical network functional connectivity in the descent to sleep. *Proceedings of the National Academy of Sciences of the United States of America*, *106*(11), 4489–4494. https://doi.org/10.1073/pnas.0900924106

Laumann, T. O., Snyder, A. Z., Mitra, A., Gordon, E. M., Gratton, C., Adeyemo, B., Gilmore, A. W., Nelson, S. M., Berg, J. J., Greene, D. J., McCarthy, J. E., Tagliazucchi, E., Laufs, H., Schlaggar, B. L., Dosenbach, N. U. F., & Petersen, S. E. (2017). On the Stability of BOLD fMRI Correlations. *Cerebral Cortex* , *27*(10), 4719–4732. https://doi.org/10.1093/cercor/bhw265

Li, S., & Wang, X.-J. (2022). Hierarchical timescales in the neocortex: Mathematical mechanism and biological insights. *Proceedings of the National Academy of Sciences of the United States of America*, *119*(6). https://doi.org/10.1073/pnas.2110274119

Liu, T. T., & Falahpour, M. (2020). Vigilance Effects in Resting-State fMRI. *Frontiers in Neuroscience*, *14*, 321. https://doi.org/10.3389/fnins.2020.00321

Lubba, C. H., Sethi, S. S., Knaute, P., Schultz, S. R., Fulcher, B. D., & Jones, N. S. (2019). catch22: CAnonical Time-series CHaracteristics. *Data Mining and Knowledge Discovery*, *33*(6), 1821–1852. https://doi.org/10.1007/s10618-019-00647-x

Mahjoory, K., Schoffelen, J.-M., Keitel, A., & Gross, J. (2020). The frequency gradient of human resting-state brain oscillations follows cortical hierarchies. *eLife*, *9*. https://doi.org/10.7554/eLife.53715

Manea, A. M. G., Zilverstand, A., Ugurbil, K., Heilbronner, S. R., & Zimmermann, J. (2022). Intrinsic timescales as an organizational principle of neural processing across the whole rhesus macaque brain. *eLife*, *11*. https://doi.org/10.7554/eLife.75540

Margulies, D. S., Ghosh, S. S., Goulas, A., Falkiewicz, M., Huntenburg, J. M., Langs, G., Bezgin, G., Eickhoff, S. B., Castellanos, F. X., Petrides, M., Jefferies, E., & Smallwood, J. (2016). Situating the default-mode network along a principal gradient of macroscale cortical organization. *Proceedings of the National Academy of Sciences of the United States of America*, *113*(44), 12574–12579. https://doi.org/10.1073/pnas.1608282113

Markello, R. D., & Misic, B. (2021). Comparing spatial null models for brain maps. *NeuroImage*, *236*, 118052. https://doi.org/10.1016/j.neuroimage.2021.118052

Markicevic, M., Fulcher, B. D., Lewis, C., Helmchen, F., Rudin, M., Zerbi, V., & Wenderoth, N. (2020). Cortical Excitation:Inhibition Imbalance Causes Abnormal Brain Network Dynamics as Observed in Neurodevelopmental Disorders. *Cerebral Cortex* , *30*(9), 4922–4937. https://doi.org/10.1093/cercor/bhaa084

Markicevic, M., Sturman, O., Bohacek, J., Rudin, M., Zerbi, V., Fulcher, B. D., & Wenderoth, N. (2022). Neuromodulation of striatal D1 cells shapes BOLD fluctuations in anatomically connected thalamic and cortical regions. In *bioRxiv* (p. 2022.03.11.483972). https://doi.org/10.1101/2022.03.11.483972

Martin, C. G., He, B. J., & Chang, C. (2021). State-related neural influences on fMRI connectivity estimation. *NeuroImage*, *244*, 118590. https://doi.org/10.1016/j.neuroimage.2021.118590

McAvoy, M., Larson-Prior, L., Ludwikow, M., Zhang, D., Snyder, A. Z., Gusnard, D. L., Raichle, M. E., & d'Avossa, G. (2012). Dissociated mean and functional connectivity BOLD signals in visual cortex during eyes closed and fixation. *Journal of Neurophysiology*, *108*(9), 2363–2372. https://doi.org/10.1152/jn.00900.2011

McAvoy, M., Larson-Prior, L., Nolan, T. S., Vaishnavi, S. N., Raichle, M. E., & d'Avossa, G. (2008). Resting states affect spontaneous BOLD oscillations in sensory and paralimbic cortex. *Journal of Neurophysiology*, *100*(2), 922–931. https://doi.org/10.1152/jn.90426.2008

Mesulam, M. (Ed.). (2000). Behavioral Neuroanatomy: Large-Scale Networks, Association Cortex, Frontal Syndromes, the Limbic System, and Hemispheric Specializations. In *Principles of Behavioral and Cognitive Neurology* (pp. 1–94). Oxford University Press. https://cpb-us-e1.wpmucdn.com/sites.northwestern.edu/dist/7/2577/files/2018/08/8-Mesulam-1scdsoy.pdf

Mesulam, M. M. (1998). From sensation to cognition. *Brain: A Journal of Neurology*, *121 (Pt 6)*, 1013–1052. https://doi.org/10.1093/brain/121.6.1013

Millar, P. R., Ances, B. M., Gordon, B. A., Benzinger, T. L. S., Morris, J. C., & Balota, D. A. (2021). Evaluating Cognitive Relationships with Resting-State and Task-driven Blood Oxygen Level-Dependent Variability. *Journal of Cognitive Neuroscience*, *33*(2), 279–302. https://doi.org/10.1162/jocn_a_01645

Müller, E. J., Munn, B., Hearne, L. J., Smith, J. B., Fulcher, B., Arnatkevičiūtė, A., Lurie, D. J., Cocchi, L., & Shine, J. M. (2020). Core and matrix thalamic sub-populations relate to spatio-temporal cortical connectivity gradients. *NeuroImage*, *222*, 117224. https://doi.org/10.1016/j.neuroimage.2020.117224

Murphy, C., Jefferies, E., Rueschemeyer, S.-A., Sormaz, M., Wang, H.-T., Margulies, D. S., & Smallwood, J. (2018). Distant from input: Evidence of regions within the default mode network supporting perceptually-decoupled and conceptually-guided cognition. *NeuroImage*, *171*, 393–401. https://doi.org/10.1016/j.neuroimage.2018.01.017

Murphy, C., Wang, H.-T., Konu, D., Lowndes, R., Margulies, D. S., Jefferies, E., & Smallwood, J. (2019). Modes of operation: A topographic neural gradient supporting stimulus dependent and independent cognition. *NeuroImage*, *186*, 487–496. https://doi.org/10.1016/j.neuroimage.2018.11.009

Murphy, K., Birn, R. M., Handwerker, D. A., Jones, T. B., & Bandettini, P. A. (2009). The impact of global signal regression on resting state correlations: are anti-correlated networks introduced? *NeuroImage*, *44*(3), 893–905. https://doi.org/10.1016/j.neuroimage.2008.09.036

Murray, J. D., Bernacchia, A., Freedman, D. J., Romo, R., Wallis, J. D., Cai, X., Padoa-Schioppa, C., Pasternak, T., Seo, H., Lee, D., & Wang, X.-J. (2014). A hierarchy of intrinsic timescales across primate cortex. *Nature Neuroscience*, *17*(12), 1661–1663.

https://doi.org/10.1038/nn.3862

Olbrich, S., Mulert, C., Karch, S., Trenner, M., Leicht, G., Pogarell, O., & Hegerl, U. (2009). EEG-vigilance and BOLD effect during simultaneous EEG/fMRI measurement. *NeuroImage*, *45*(2), 319–332. https://doi.org/10.1016/j.neuroimage.2008.11.014

Panizzon, M. S., Fennema-Notestine, C., Eyler, L. T., Jernigan, T. L., Prom-Wormley, E., Neale, M., Jacobson, K., Lyons, M. J., Grant, M. D., Franz, C. E., Xian, H., Tsuang, M., Fischl, B., Seidman, L., Dale, A., & Kremen, W. S. (2009). Distinct Genetic Influences on Cortical Surface Area and Cortical Thickness. *Cerebral Cortex* , *19*(11), 2728–2735. https://doi.org/10.1093/cercor/bhp026

Paquola, C., Seidlitz, J., Benkarim, O., Royer, J., Klimes, P., Bethlehem, R. A. I., Larivière, S., Vos de Wael, R., Rodríguez-Cruces, R., Hall, J. A., Frauscher, B., Smallwood, J., & Bernhardt, B. C. (2020). A multi-scale cortical wiring space links cellular architecture and functional dynamics in the human brain. *PLoS Biology*, *18*(11), e3000979. https://doi.org/10.1371/journal.pbio.3000979

Paquola, C., Vos De Wael, R., Wagstyl, K., Bethlehem, R. A. I., Hong, S.-J., Seidlitz, J., Bullmore, E. T., Evans, A. C., Misic, B., Margulies, D. S., Smallwood, J., & Bernhardt, B. C. (2019). Microstructural and functional gradients are increasingly dissociated in transmodal cortices. *PLoS Biology*, *17*(5), e3000284. https://doi.org/10.1371/journal.pbio.3000284

Parkes, L., Fulcher, B., Yücel, M., & Fornito, A. (2018). An evaluation of the efficacy, reliability, and sensitivity of motion correction strategies for resting-state functional MRI. *NeuroImage*, *171*, 415–436. https://doi.org/10.1016/j.neuroimage.2017.12.073

Peng, C. K., Buldyrev, S. V., Havlin, S., Simons, M., Stanley, H. E., & Goldberger, A. L. (1994). Mosaic organization of DNA nucleotides. *Physical Review. E, Statistical Physics, Plasmas, Fluids, and Related Interdisciplinary Topics*, *49*(2), 1685–1689. https://doi.org/10.1103/physreve.49.1685

Peng, C. K., Havlin, S., Stanley, H. E., & Goldberger, A. L. (1995). Quantification of scaling exponents and crossover phenomena in nonstationary heartbeat time series. *Chaos* , *5*(1), 82–87. https://doi.org/10.1063/1.166141

Peres-Neto, P. R., Jackson, D. A., & Somers, K. M. (2003). Giving Meaningful Interpretation to Ordination Axes: Assessing Loading Significance in Principal Component Analysis. *Ecology*, *84*(9), 2347–2363. http://www.jstor.org/stable/3450140

Peres-Neto, P. R., Jackson, D. A., & Somers, K. M. (2005). How many principal components? stopping rules for determining the number of non-trivial axes revisited. *Computational Statistics & Data Analysis*, *49*, 974–997. https://doi.org/10.1016/j.csda.2004.06.015

Raut, R. V., Snyder, A. Z., & Raichle, M. E. (2020). Hierarchical dynamics as a macroscopic organizing principle of the human brain. *Proceedings of the National Academy of Sciences of the United States of America*, *117*(34), 20890–20897. https://doi.org/10.1073/pnas.2003383117

Rieck, J. R., DeSouza, B., Baracchini, G., & Grady, C. L. (2022). Reduced modulation of BOLD

variability as a function of cognitive load in healthy aging. *Neurobiology of Aging*, *112*, 215–230. https://doi.org/10.1016/j.neurobiolaging.2022.01.010

Rubinov, M., & Sporns, O. (2010). Complex network measures of brain connectivity: uses and interpretations. *NeuroImage*, *52*(3), 1059–1069. https://doi.org/10.1016/j.neuroimage.2009.10.003

Schaefer, A., Kong, R., Gordon, E. M., Laumann, T. O., Zuo, X.-N., Holmes, A. J., Eickhoff, S. B., & Yeo, B. T. T. (2018). Local-Global Parcellation of the Human Cerebral Cortex from Intrinsic Functional Connectivity MRI. *Cerebral Cortex* , *28*(9), 3095–3114. https://doi.org/10.1093/cercor/bhx179

Schooler, J. W., Smallwood, J., Christoff, K., Handy, T. C., Reichle, E. D., & Sayette, M. A. (2011). Meta-awareness, perceptual decoupling and the wandering mind. *Trends in Cognitive Sciences*, *15*(7), 319–326. https://doi.org/10.1016/j.tics.2011.05.006

Sethi, S. S., Zerbi, V., Wenderoth, N., Fornito, A., & Fulcher, B. D. (2017). Structural connectome topology relates to regional BOLD signal dynamics in the mouse brain. *Chaos* , *27*(4), 047405. https://doi.org/10.1063/1.4979281

Shafiei, G., Markello, R. D., Vos de Wael, R., Bernhardt, B. C., Fulcher, B. D., & Misic, B. (2020). Topographic gradients of intrinsic dynamics across neocortex. *eLife*, *9*. https://doi.org/10.7554/eLife.62116

Shine, J. M., Bissett, P. G., Bell, P. T., Koyejo, O., Balsters, J. H., Gorgolewski, K. J., Moodie, C. A., & Poldrack, R. A. (2016). The Dynamics of Functional Brain Networks: Integrated Network States during Cognitive Task Performance. *Neuron*, *92*(2), 544–554. https://doi.org/10.1016/j.neuron.2016.09.018

Shinn, M., Hu, A., Turner, L., Noble, S., Achard, S., Anticevic, A., Scheinost, D., Todd Constable, R., Lee, D., Bullmore, E. T., & Murray, J. D. (2021). Spatial and temporal autocorrelation weave human brain networks. In *bioRxiv* (p. 2021.06.01.446561). https://doi.org/10.1101/2021.06.01.446561

Smallwood, J. (2013). Distinguishing how from why the mind wanders: a process-occurrence framework for self-generated mental activity. *Psychological Bulletin*, *139*(3), 519–535. https://doi.org/10.1037/a0030010

Smallwood, J., Beach, E., Schooler, J. W., & Handy, T. C. (2008). Going AWOL in the brain: mind wandering reduces cortical analysis of external events. *Journal of Cognitive Neuroscience*, *20*(3), 458–469. https://doi.org/10.1162/jocn.2008.20037

Smallwood, J., & Schooler, J. W. (2015). The science of mind wandering: empirically navigating the stream of consciousness. *Annual Review of Psychology*, *66*, 487–518. https://doi.org/10.1146/annurev-psych-010814-015331

Smallwood, J., Turnbull, A., Wang, H.-T., Ho, N. S. P., Poerio, G. L., Karapanagiotidis, T., Konu, D., Mckeown, B., Zhang, M., Murphy, C., Vatansever, D., Bzdok, D., Konishi, M., Leech, R., Seli, P., Schooler, J. W., Bernhardt, B., Margulies, D. S., & Jefferies, E. (2021). The neural correlates of ongoing conscious thought. *iScience*, *24*(3), 102132.

https://doi.org/10.1016/j.isci.2021.102132

Smith, S. M., Beckmann, C. F., Andersson, J., Auerbach, E. J., Bijsterbosch, J., Douaud, G., Duff, E., Feinberg, D. A., Griffanti, L., Harms, M. P., Kelly, M., Laumann, T., Miller, K. L., Moeller, S., Petersen, S., Power, J., Salimi-Khorshidi, G., Snyder, A. Z., Vu, A. T., … WU-Minn HCP Consortium. (2013). Resting-state fMRI in the Human Connectome Project. *NeuroImage*, *80*, 144–168. https://doi.org/10.1016/j.neuroimage.2013.05.039

Smith, S. M., Fox, P. T., Miller, K. L., Glahn, D. C., Fox, P. M., Mackay, C. E., Filippini, N., Watkins, K. E., Toro, R., Laird, A. R., & Beckmann, C. F. (2009). Correspondence of the brain's functional architecture during activation and rest. *Proceedings of the National Academy of Sciences of the United States of America*, *106*(31), 13040–13045. https://doi.org/10.1073/pnas.0905267106

Stacklies, W., Redestig, H., Scholz, M., Walther, D., & Selbig, J. (2007). pcaMethods--a bioconductor package providing PCA methods for incomplete data. *Bioinformatics* , *23*(9), 1164–1167. https://doi.org/10.1093/bioinformatics/btm069

Stephens, G. J., Honey, C. J., & Hasson, U. (2013). A place for time: the spatiotemporal structure of neural dynamics during natural audition. *Journal of Neurophysiology*, *110*(9), 2019–2026. https://doi.org/10.1152/jn.00268.2013

Tagliazucchi, E., & Laufs, H. (2014). Decoding wakefulness levels from typical fMRI resting-state data reveals reliable drifts between wakefulness and sleep. *Neuron*, *82*(3), 695–708. https://doi.org/10.1016/j.neuron.2014.03.020

Tagliazucchi, E., von Wegner, F., Morzelewski, A., Borisov, S., Jahnke, K., & Laufs, H. (2012). Automatic sleep staging using fMRI functional connectivity data. *NeuroImage*, *63*(1), 63–72. https://doi.org/10.1016/j.neuroimage.2012.06.036

Talkner, P., & Weber, R. O. (2000). Power spectrum and detrended fluctuation analysis: application to daily temperatures. *Physical Review. E, Statistical Physics, Plasmas, Fluids, and Related Interdisciplinary Topics*, *62*(1 Pt A), 150–160. https://doi.org/10.1103/physreve.62.150

Tong, Y., Hocke, L. M., & Frederick, B. B. (2019). Low Frequency Systemic Hemodynamic "Noise" in Resting State BOLD fMRI: Characteristics, Causes, Implications, Mitigation Strategies, and Applications. *Frontiers in Neuroscience*, *13*, 787. https://doi.org/10.3389/fnins.2019.00787

Turnbull, A., Wang, H. T., Murphy, C., Ho, N. S. P., Wang, X., Sormaz, M., Karapanagiotidis, T., Leech, R. M., Bernhardt, B., Margulies, D. S., Vatansever, D., Jefferies, E., & Smallwood, J. (2019). Left dorsolateral prefrontal cortex supports context-dependent prioritisation of off-task thought. *Nature Communications*, *10*(1), 3816. https://doi.org/10.1038/s41467-019-11764-y

Uddin, L. Q. (2021). Cognitive and behavioural flexibility: neural mechanisms and clinical considerations. *Nature Reviews. Neuroscience*, *22*(3), 167–179. https://doi.org/10.1038/s41583-021-00428-w

Uddin, L. Q., Yeo, B. T. T., & Spreng, R. N. (2019). Towards a Universal Taxonomy of Macro-scale

Functional Human Brain Networks. *Brain Topography*, *32*(6), 926–942. https://doi.org/10.1007/s10548-019-00744-6

van den Heuvel, M. P., & Sporns, O. (2013). Network hubs in the human brain. *Trends in Cognitive Sciences*, *17*(12), 683–696. https://doi.org/10.1016/j.tics.2013.09.012

Van Essen, D. C., Smith, S. M., Barch, D. M., Behrens, T. E. J., Yacoub, E., Ugurbil, K., & WU-Minn HCP Consortium. (2013). The WU-Minn Human Connectome Project: an overview. *NeuroImage*, *80*, 62–79. https://doi.org/10.1016/j.neuroimage.2013.05.041

Vitale, R., Westerhuis, J. A., Naes, T., Smilde, A. K., de Noord, O. E., & Ferrer, A. (2017). Selecting the number of factors in principal component analysis by permutation testing-Numerical and practical aspects. *Journal of Chemometrics*, *31*(12), e2937. https://doi.org/10.1002/cem.2937

von Economo, C. F., & Koskinas, G. N. (1925). *Die cytoarchitektonik der hirnrinde des erwachsenen menschen*. Springer.

Wagstyl, K., Larocque, S., Cucurull, G., Lepage, C., Cohen, J. P., Bludau, S., Palomero-Gallagher, N., Lewis, L. B., Funck, T., Spitzer, H., Dickscheid, T., Fletcher, P. C., Romero, A., Zilles, K., Amunts, K., Bengio, Y., & Evans, A. C. (2020). BigBrain 3D atlas of cortical layers: Cortical and laminar thickness gradients diverge in sensory and motor cortices. *PLoS Biology*, *18*(4), e3000678. https://doi.org/10.1371/journal.pbio.3000678

Wagstyl, K., Ronan, L., Goodyer, I. M., & Fletcher, P. C. (2015). Cortical thickness gradients in structural hierarchies. *NeuroImage*, *111*, 241–250. https://doi.org/10.1016/j.neuroimage.2015.02.036

Wang, C., Ong, J. L., Patanaik, A., Zhou, J., & Chee, M. W. L. (2016). Spontaneous eyelid closures link vigilance fluctuation with fMRI dynamic connectivity states. *Proceedings of the National Academy of Sciences of the United States of America*, *113*(34), 9653–9658. https://doi.org/10.1073/pnas.1523980113

Waschke, L., Kloosterman, N. A., Obleser, J., & Garrett, D. D. (2021). Behavior needs neural variability. *Neuron*, *109*(5), 751–766. https://doi.org/10.1016/j.neuron.2021.01.023

Watanabe, T., Rees, G., & Masuda, N. (2019). Atypical intrinsic neural timescale in autism. *eLife*, *8*. https://doi.org/10.7554/eLife.42256

Wengler, K., Goldberg, A. T., Chahine, G., & Horga, G. (2020). Distinct hierarchical alterations of intrinsic neural timescales account for different manifestations of psychosis. *eLife*, *9*. https://doi.org/10.7554/eLife.56151

Whitaker, K. J., Vértes, P. E., Romero-Garcia, R., Váša, F., Moutoussis, M., Prabhu, G., Weiskopf, N., Callaghan, M. F., Wagstyl, K., Rittman, T., Tait, R., Ooi, C., Suckling, J., Inkster, B., Fonagy, P., Dolan, R. J., Jones, P. B., Goodyer, I. M., NSPN Consortium, & Bullmore, E. T. (2016). Adolescence is associated with genomically patterned consolidation of the hubs of the human brain connectome. *Proceedings of the National Academy of Sciences of the United States of America*, *113*(32), 9105–9110. https://doi.org/10.1073/pnas.1601745113

Winkler, A. M., Kochunov, P., Blangero, J., Almasy, L., Zilles, K., Fox, P. T., Duggirala, R., & Glahn, D. C. (2010). Cortical thickness or grey matter volume? The importance of selecting the phenotype for imaging genetics studies. *NeuroImage*, *53*(3), 1135–1146. https://doi.org/10.1016/j.neuroimage.2009.12.028

Wong, C. W., DeYoung, P. N., & Liu, T. T. (2016). Differences in the resting-state fMRI global signal amplitude between the eyes open and eyes closed states are related to changes in EEG vigilance. *NeuroImage*, *124*(Pt A), 24–31. https://doi.org/10.1016/j.neuroimage.2015.08.053

Yeh, F.-C., Panesar, S., Fernandes, D., Meola, A., Yoshino, M., Fernandez-Miranda, J. C., Vettel, J. M., & Verstynen, T. (2018). Population-averaged atlas of the macroscale human structural connectome and its network topology. *NeuroImage*, *178*, 57–68. https://doi.org/10.1016/j.neuroimage.2018.05.027

Yeh, F.-C., & Tseng, W.-Y. I. (2011). NTU-90: a high angular resolution brain atlas constructed by q-space diffeomorphic reconstruction. *NeuroImage*, *58*(1), 91–99. https://doi.org/10.1016/j.neuroimage.2011.06.021

Yeh, F.-C., Verstynen, T. D., Wang, Y., Fernández-Miranda, J. C., & Tseng, W.-Y. I. (2013). Deterministic diffusion fiber tracking improved by quantitative anisotropy. *PloS One*, *8*(11), e80713. https://doi.org/10.1371/journal.pone.0080713

Yeo, B. T. T., Krienen, F. M., Sepulcre, J., Sabuncu, M. R., Lashkari, D., Hollinshead, M., Roffman, J. L., Smoller, J. W., Zöllei, L., Polimeni, J. R., Fischl, B., Liu, H., & Buckner, R. L. (2011). The organization of the human cerebral cortex estimated by intrinsic functional connectivity. *Journal of Neurophysiology*, *106*(3), 1125–1165. https://doi.org/10.1152/jn.00338.2011

Zou, G. Y. (2007). Toward using confidence intervals to compare correlations. *Psychological Methods*, *12*(4), 399–413. https://doi.org/10.1037/1082-989X.12.4.399

Investigating the impact of focal brain lesions on regional dynamics and functional network topology

Introduction

Previous work from our lab, as well as numerous studies from other groups, has demonstrated that focal brain lesions are associated with widespread alterations of functional connectivity in remote, undamaged brain areas (Blaschke et al., 2021; Froudist-Walsh et al., 2018; Gratton et al., November 9-13 2013, 2012; Grayson et al., 2016; Griffis et al., 2019; Huang et al., 2022; Nomura et al., 2010; Olafson et al., 2021; Ovadia-Caro et al., 2013; Park et al., 2011; Siegel et al., 2018; Termenon et al., 2016; Wang et al., 2014). These changes are a form of diaschisis, and result from multiple interacting factors including the loss of influence from lesioned areas to other parts of the brain, as well as damage to direct and indirect axonal pathways between undamaged brain areas (Carrera & Tononi, 2014; Fornito et al., 2015). While the particular pattern of changes in functional connectivity following a focal insult will inherently depend on the size and location of the lesion, growing work suggests that the magnitude and direction of changes in functional connectivity in undamaged brain areas may also depend on the topology and connectivity of those regions prior to injury. In particular, a number of studies have observed a stereotyped pattern of "hub disruption" in which topologically central brain areas (i.e. those with high degree, participation coefficient, etc.) tend to show the greatest decreases in centrality following focal lesions, while peripheral regions (i.e. those with low degree, PC, etc.) tend to show the greatest increases in centrality (Froudist-Walsh et al., 2018; Gratton et al., November 9-13 2013; Huang et al., 2022; Termenon et al., 2016). The strongest evidence for this phenomenon comes from experimental work by (Froudist-Walsh et al., 2018) and colleagues, who found that cortical areas with high pre-lesion "hubness" (strength and participation coefficient) showed the greatest decreases in participation coefficient and within-module functional connectivity following bilateral hippocampal lesions in macaques, while areas with low pre-lesion hubness tended to increases their PC and WD. In humans, this effect has been observed both when comparing measures of regional topology between patients and healthy participants, as well as when comparing homotopic areas between the ipsilesional and contralesional hemispheres within each patient (Gratton et al., November 9-13 2013; Huang et al., 2022; Termenon et al., 2016).

In light of this literature and prior observations that the timescale of intrinsic regional BOLD activity is correlated with multiple properties of structural and functional network topology (Chapters 1 and 2), we hypothesized that patients with focal subcortical lesions due to stroke would exhibit altered cortical timescales. In particular, given evidence for systematic "hub

disruption"[1] in patients with focal lesions, we predicted that cortical areas in patients would show a stereotyped pattern of increases and decreases in functional connectivity strength, within-module degree, and participation coefficient, and critically, that increases and decreases in within-module degree would be associated with lengthening and shortening of intrinsic timescales in the same cortical areas.

Contrary to our predictions, we did not find evidence for stereotyped hub disruption in stroke patients during the initial weeks of recovery, nor did we find evidence for systematic lengthening and shortening of cortical timescales. We also did not find evidence for idiosyncratic (rather than systematic) alterations in timescales or within-module degree in patients, though we did find preliminary evidence for non-systematic alterations in strength and participation coefficient when comparing patients to healthy participants. Further, while patients tended to exhibit greater individual differences than healthy participants in measures of functional network topology, no such effect was observed for cortical timescales. Together, these results suggest that cortical timescales may be largely preserved following focal brain lesions.

Given that we did not observe the predicted effects of focal lesions on regional dynamics or functional network topology, we re-cast our hypothesis regarding parallel alterations of timescales and within-module degree in stroke patients to instead consider the more general question of whether individual differences in regional dynamics are correlated with individual differences in topology. We found that this is indeed the case, and further, that timescales show distinct associations with different aspects of functional network topology within individual participants.

Methods

Participants

We analyzed data from 23 patients (7 female, ages 19–70; mean/SD = 50/11 years) with focal subcortical lesions due to stroke (Fig. 1), and 17 healthy individuals (7 female, ages 21–83; mean/SD = 56/15 years) recruited as age-matched controls. These participants were selected (see below for selection criteria) from a larger dataset collected at Washington University, which contained imaging data from 136 patients and 31 healthy controls. These data were made available by Corbetta and colleagues, and downloaded from the Washington University Central Neuroimaging Data Archive. We refer readers to (Corbetta et al., 2015) and (Siegel et al., 2016) for complete details regarding recruitment and experimental procedures, but we summarize them briefly below.

[1] As noted in Chapter 1, connector regions (those with high PC) do not necessarily exhibit widespread connectivity, and as such labeling them as hubs is technically a misnomer. That said, we use the term "hub disruption" here as a shorthand, and because it has consistently been applied in the literature to refer to measures of regional topology beyond those which are strictly indicative of "hub" status.

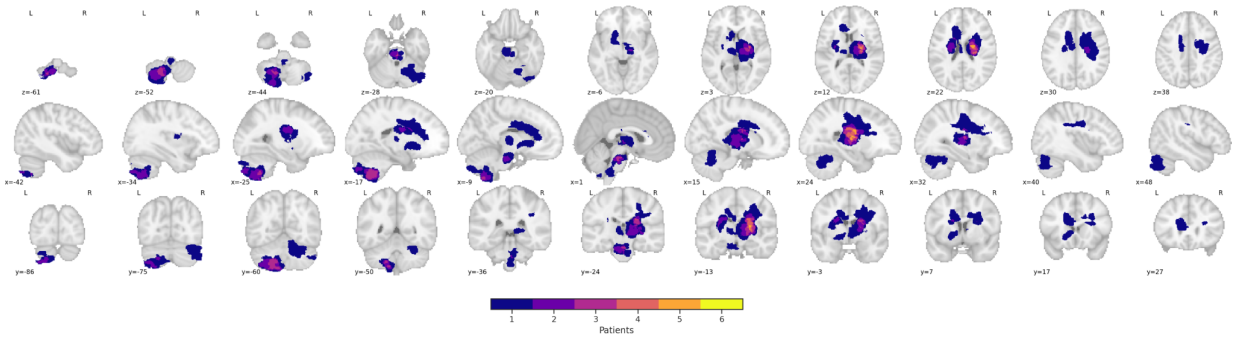


Figure 1: Lesion overlap map for the current sample.
Colors indicate the number of patients with stroke damage to each voxel. Lesion masks for each patient were transformed to the MNI template to facilitate visualization in a common space.

Patients with first time symptomatic stroke were prospectively recruited through the stroke service at Barnes Jewish Hospital in St. Louis, MO. All patients had persistent stroke symptoms at hospital discharge. Patients were excluded from the study if there was evidence of previous stroke on clinical imaging. Healthy control participants were matched to the patient sample for age, gender, and years of education. Both patients and controls were excluded from the study if they had a history of brain injury, other neurological disorder, or major psychiatric illness.

To assess whether patients in our sample were representative of the larger cohort, we used a Wilcoxson-Mann-Whitney U test (MWU) to compare their scores on the NIH Stroke Scale (NIHSS) to both the entire study cohort (136 patients) as well as to all patients from the study who had exclusively subcortical lesions (61 patients).

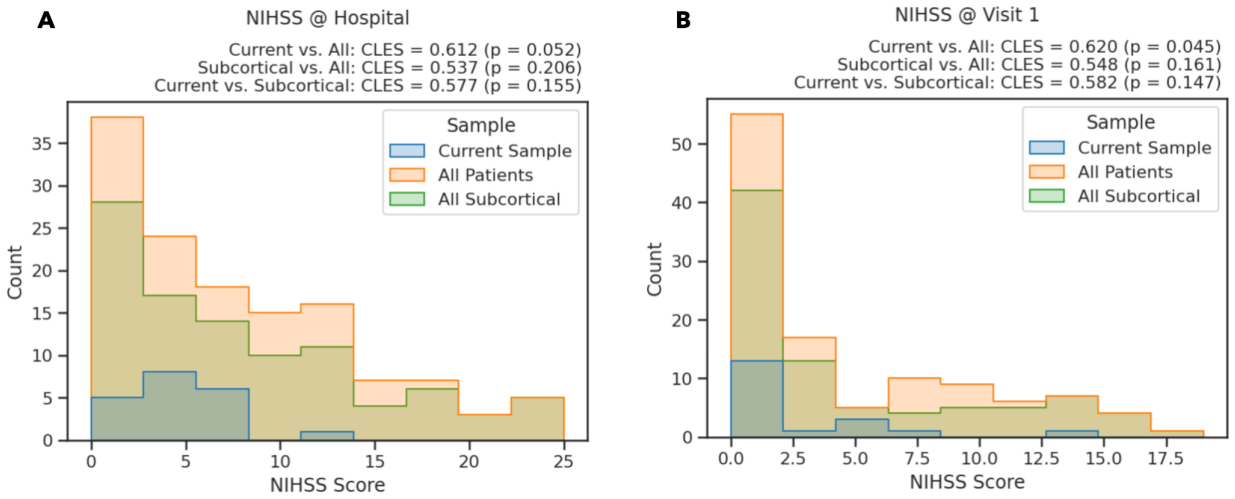


Figure S1: Stroke severity in the current sample compared to the full sample.
(A) Assessment at hospitalization was typically conducted within 24 hours post stroke. (B) The NIHSS was re-administered at study visit 1 (1-2 weeks post stroke), on the same day as scanning. NIHSS; NIH Stroke Scale. CLES; Common Language Effect Size, the probability that a randomly selected patient in each subset will have a lower NIHSS score than a randomly selected patient from the larger set to which it is being compared.

When assessed in the hospital (usually within 24 hours post stroke), NIHSS scores in our sample were not significantly different from the larger cohort (CLES = 0.612, p = 0.052) or the set of all patients with exclusively subcortical lesions (CLES = 0.577, p = 0.155) (Fig. S1A). When assessed at the study visit (1-2 weeks post stroke), NIHSS scores in the current sample were marginally lower than in the larger cohort (CLES = 0.620, p = 0.045), but did not differ from the full set of patients with subcortical lesions (CLES = 0.582, p = 0.147) (Fig. S1B). Together, these results suggest that stroke severity at the time of scanning in our sample is representative of the larger cohort of patients with subcortical lesions.

MRI acquisition

Patients were scanned 1–2 weeks, 3 months, and 1 year post-stroke. Here, we focus on the first scan session. MRI images were collected using a Siemens 3T Tim-Trio scanner, and included high resolution (1mm isotropic) T1w MPRAGE and T2w TSE images in addition to 6–8 ~4.25 minute "resting" fMRI scans (TR/TE = 2000/27ms, 4mm isotropic, 128 volumes per scan) during which patients were instructed to fixate on a small cross. Control participants underwent an identical imaging protocol.

Lesion segmentation

Lesion masks were provided by Corbetta and colleagues, and were manually traced on T1w and T2w images from the first study visit (1-2 weeks post stroke) which had been registered to a study-specific template in 711-2B space. Masks were transformed to native T1w space by first using ANTs (Avants et al., 2014) to register the MPRAGE image from each patient to the 2mm 711-2B study-specific template via an affine transform, and then applying the inverse transform to the mask image. Because this transformation is imperfect, we used the ITK-SNAP (Yushkevich et al., 2006) Convert3D tool to apply a 2mm morphological dilation and 1mm morphological erosion to the binary mask images to ensure coverage at the borders of the lesion. All original masks were reviewed and approved by two board-certified neurologists, and transformed masks for patients in the final sample were additionally reviewed by the first author of this paper.

Preliminary identification of patients with subcortical lesions

To identify patients with subcortical lesions, we first visually inspected the lesion mask of each patient overlaid on the study-specific template used by the original authors. We excluded 75 patients whose masks extended into the cerebral cortex.

Data quality control

Imaging data for the remaining 61 patients and 31 healthy control participants underwent quantitative quality control using MRIQC (Esteban et al., 2017). This allowed us to identify and exclude any resting fMRI scans with excessive head motion, which we defined as a mean FD > 0.4mm. We acknowledge that this threshold is double the commonly recommended maximum of 0.2mm (Power et al., 2012, 2014; Satterthwaite et al., 2012; Yan et al., 2013), but was necessary due to the high levels of in-scanner head motion present in both patients and control participants (patient average = 0.48mm, control average = 0.51mm). To ensure sufficient data was available to reliably characterize brain connectivity and dynamics, we excluded any patient with fewer than 3 scans (12.8 minutes) of fMRI data remaining after motion QC. Control participants were included as long as they had one passing scan. Thirty-one patients and 17 healthy controls met these initial QC criteria. Levels of head motion remained well matched between groups following motion QC (patient average = 0.25mm, control average = 0.27mm; $t = -1.20$, $p = 0.230$).

Following motion QC, we used ITK-SNAP to closely inspect the T1w and T2w images for each remaining patient. Based on these inspections, we excluded 3 patients whose stroke lesions extended into cortex, as well as 4 patients with highly progressed white matter disease (Fazekas grade > 2.5; (Fazekas et al., 1987)), and one patient for whom no lesion or pathology was visible on any of the structural images (including supplemental FLAIR, DWI, and DIR scans). Twenty-three patients remained in the final sample (Fig. S2).

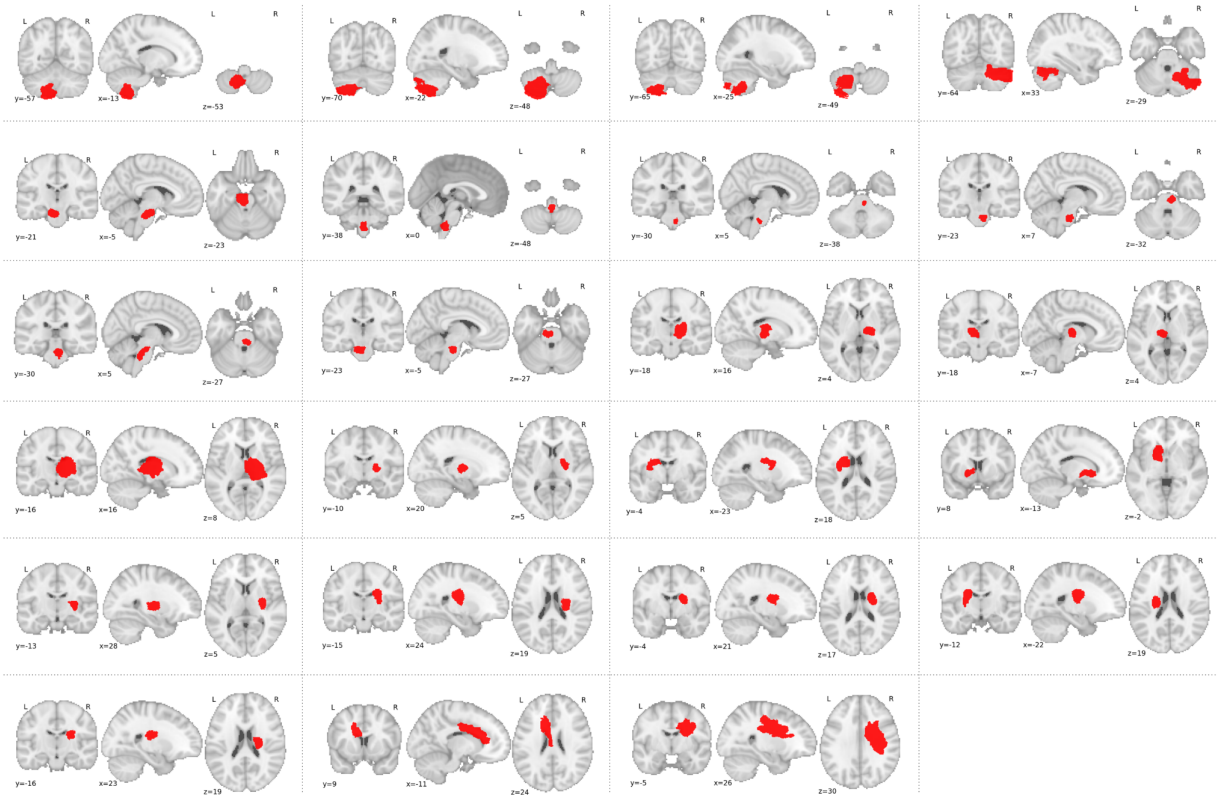


Figure S2: Stroke lesion location and extent for each patient in the final sample.
Lesion masks for each patient were transformed to the MNI template to facilitate visualization in a common space.

Preprocessing

MRI data for patients and controls were reconstructed from DICOM images and organized as per the BIDS specification (K. J. Gorgolewski et al., 2016) using BIDScoin (Zwiers et al., 2021). T1w and BOLD images were preprocessed using FMRIPREP (Esteban et al., 2019) version 1.3.2 run via Singularity (Kurtzer et al., 2017). This process was identical to that described in Chapter 1, with the following additions: 1) The binary lesion mask for each patient was used for constrained cost-function masking (Kim et al., 2008) during nonlinear registration of the T1w image to the MNI template. Cost-function masking is necessary to avoid warping healthy tissue into the lesioned area (and vice-versa) (Andersen et al., 2010; Brett et al., 2001; Crinion et al., 2007), and this feature is provided in the official release of FMRIPREP (having been contributed by the first author of this paper). 2) We re-calculated nuisance regressors after subtracting the lesion mask from the combined white matter + CSF aCompCor ROI. This was accomplished using a custom Nipype workflow (K. Gorgolewski et al., 2011) and is necessary to ensure that our nuisance regressors did not include signals from stroke-damaged gray matter regions which may have been misclassified as WM or CSF.

Denoising

We used GLM-based denoising with a model that included 24 motion parameters (6 rigid body parameters estimated during volume realignment, plus their Volterra series expansion), 6 aCompCor components (Behzadi et al., 2007) estimated from a combined white matter + CSF mask, plus the global mean signal and its Volterra series expansion. This combination of regressors was chosen based on the results of prior studies which evaluated the effectiveness of a wide range of denoising approaches for minimizing the confounding effects of in-scanner head motion (Ciric et al., 2017; Lydon-Staley et al., 2019; Parkes et al., 2018). We additionally applied a 0.009–0.1 Hz bandpass filter.

Cortical timescales

Timescales were estimated as the lag-1 autocorrelation of the denoised BOLD time series from each of 400 cortical regions defined by (Schaefer et al., 2018). Timescales were estimated separately for each scan and then averaged across scans for each patient and healthy participant. Group-average timescale maps were highly similar between patients and healthy controls (Fig. S3), and are consistent with the results we present in Chapters 1 and 2.

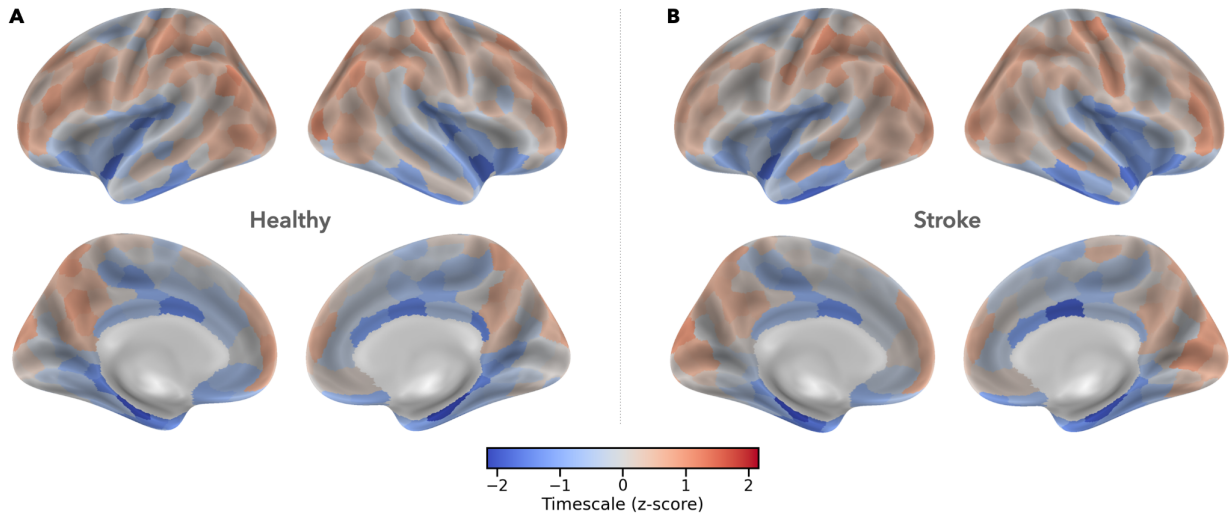


Figure S3: Group-average timescales in healthy participants and stroke patients.
We did not test for parcel-wise group differences in timescales, as this was beyond the scope of our study.

Static functional connectivity

For each scan, we estimated the static functional connectivity (Pearson correlation) between each pair of cortical regions. Functional connectivity estimates were then averaged across scans

for each patient and control participant to create an individualized average functional connectivity network. Negative edges were set to zero.

Topological roles

We calculated the strength (weighted degree) of each cortical region as the sum of all positive edges in each individual's average static functional connectivity network. To calculate participation coefficient and within-module degree, we first used consensus clustering (Lancichinetti & Fortunato, 2012) to identify a stable community partition for each individual's average static functional connectivity network based on 250 runs of the Louvain community detection algorithm (Blondel et al., 2008) with a resolution of $\gamma = 1.5$. We then calculated PC and WD relative to these individualized network partitions. Our use of individualized network partitions rather than a single common partition follows previous work from our lab on the impact of focal lesions on functional connectivity (Gratton et al., November 9-13 2013, 2012), and allows our analyses to respect individual differences in functional network organization (Gordon, Laumann, Adeyemo, & Petersen, 2017; Gordon, Laumann, Adeyemo, Gilmore, et al., 2017; Gordon, Laumann, Gilmore, et al., 2017; Kong et al., 2019; Seitzman et al., 2019).

Hemisphere-level analyses

Given predominantly contralateral projections between the cortex and cerebellum (Schmahmann & Pandya, 1997), cerebellar lesions were reverse-coded (e.g. right hemisphere ipsilesional for a lesion in the left cerebellum). Following (Siegel et al., 2018), patients with brainstem lesions were excluded from all hemisphere-level analyses due to the possibility of projection fibers which cross the midline.

Results

No evidence for stereotyped "hub disruption" in patients

To assess whether patients in our sample exhibited alterations in regional topology which follow the predicted stereotyped pattern of "hub disruption", we first computed difference scores between the median value of each topological measure for each region in patients (<stroke>) and the median values for the same region in healthy controls (<healthy>). We then plotted these difference scores (<stroke> – <healthy>; y-axis) against the median values from the control group (<healthy>; x-axis). This allowed us to visualize the extent to which topological measures for each region in patients are higher ($y > 0$), lower ($y < 0$), or roughly similar to ($y \sim 0$) the same region in controls. If regions with high values show the greatest decrease, and regions with low values show the greatest increase, we would expect to see a negative relationship between difference scores and the healthy group median. Following (Achard et al., 2012), we defined a "disruption index" (K_i) as the slope of a linear fit to this data. To evaluate the possibility that timescales also exhibit a stereotyped pattern of increases and decreases, we repeated this process for timescale estimates. At the group level, we observed weakly negative slopes for all three measures of regional topology, as well as for cortical timescales (Fig. 2). However, due to the significant heterogeneity among patients in lesion size

and location, it is possible that this effect only exists for group-median values (which may fail to reflect the particular patterns of topology and timescales present in any individual patient). As such, we also calculated disruption indices for each patient and healthy individual relative to the healthy group median. Critically, we used a "Leave One Out" strategy when computing K_i for individuals in the control group, such that the each healthy participant was compared to a group median computed from all *other* controls. This approach stands in contrast to how individual K_i values were computed for healthy participants in (Achard et al., 2012), as well as in the papers by (Gratton et al., November 9-13 2013), (Termenon et al., 2016), and (Huang et al., 2022), all of whom compared each control participant to the mean of *all* controls. This modification is necessary because comparing an individual to reference values which are based in part on their own data (i.e. a healthy individual compared to the mean of all healthy individuals) will *necessarily* result in greater similarity (less "disruption") than when comparing values for an individual whose data did not contribute to the reference template.

We used a Wilcoxon-Mann-Whitney (WMW) test to compare the distribution of K_i values between patients and healthy participants. The WMW tests the null hypothesis that a randomly selected observation from one sample will be equally likely to be larger or smaller than a randomly selected observation from a second sample, and as a non-parametric test it is more robust to (and more powerful in the presence of) deviations from normality than a t-test (Fay & Proschan, 2010). However, like an F statistic, the WMW U statistic does not provide information about the direction of departure from the null hypothesis (i.e. whether an observation from X is likely to be larger or smaller than an observation from Y). As such, we focus on the Common Language Effect Size (CLES) (McGraw & Wong, 1992), which gives the probability that a randomly selected patient will have a lower K_i value than a randomly selected healthy individual. We computed the CLES using the brute-force method proposed by (Vargha & Delaney, 2000), which does not assume normally distributed data. To evaluate the significance of group differences, we compared the observed CLES to a null distribution generated by randomly permuting group labels 1000 times.

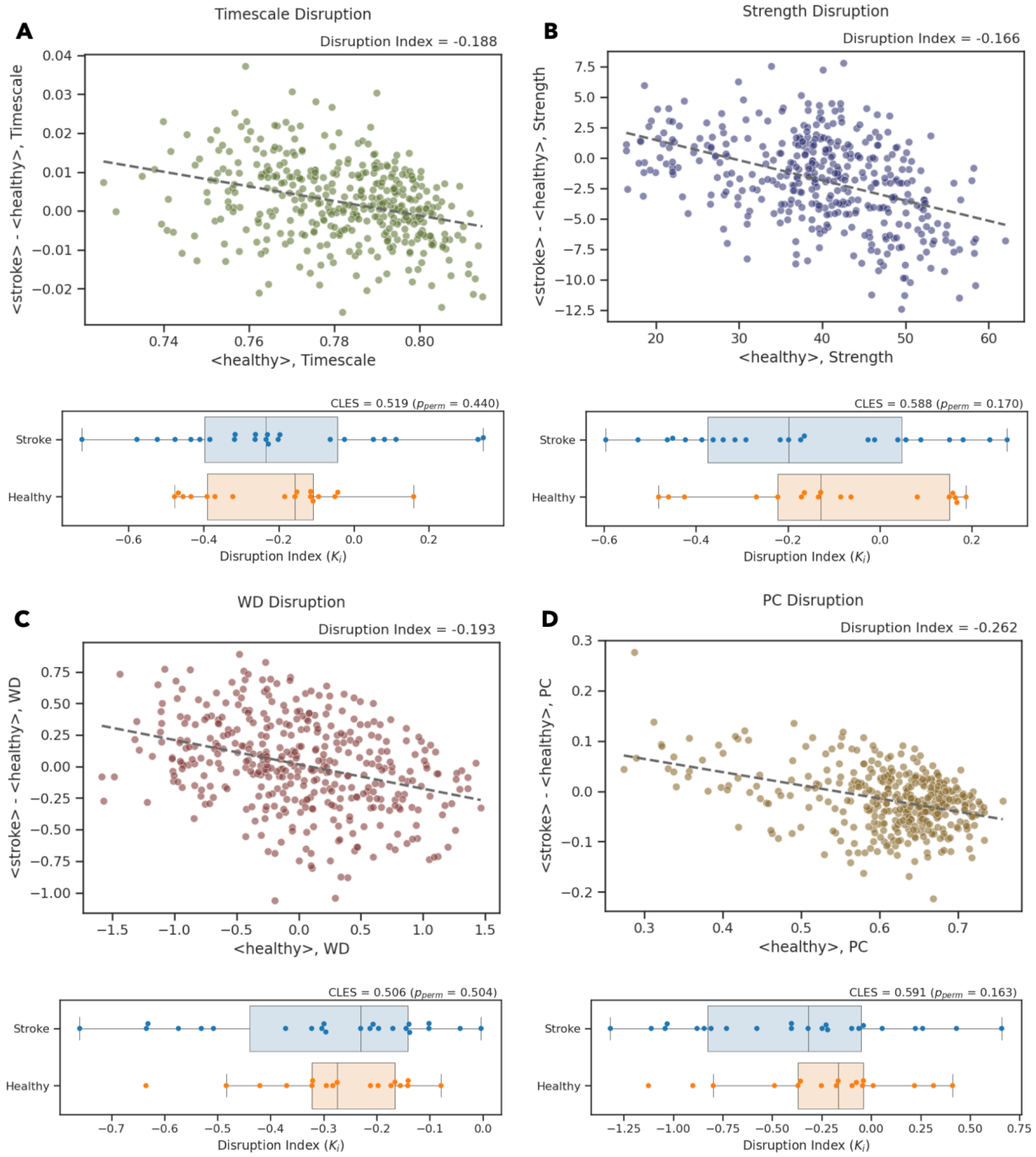


Figure 2: Cortex-wide disruption index analysis.
The top plot in each panel shows group level disruption plots for Timescale, Strength, WD, and PC. The disruption index K_i (e.g. K_T, K_{WD}) is the slope of a linear fit to the data points (dashed lines). We observed weakly negative slopes for each measure at the group level, but found no significant group differences in individual K_i values (bottom of each panel). CLES is the probability that a randomly selected patient will have a lower K_i than a randomly selected healthy participant.

In our initial analysis, we computed K_i values across all cortical regions in both hemispheres (Fig. 2). While we observed negative K_i values for topological properties and timescales at the group level (K_S = -0.166; K_{WD} = -0.193; K_{PC} = -0.262; K_T = -0.188) we found no significant group differences in individual K_i values for any measure (K_S: CLES = 0.588, p = 0.170; K_{WD}: CLES = 0.506, p = 0.504; K_{PC}: CLES = 0.591, p = 0.163; K_T: CLES = 0.519, p = 0.440). However, it is possible that disruptions due to stroke may be limited to the injured hemisphere. To evaluate this possibility, we conducted two complementary analyses.

First, we computed inter-hemispheric K_i values by comparing topological properties and timescales in the ipsilesional hemisphere of each patient to homotopic areas in the contralesional hemisphere. Because topological properties and timescales may differ between hemispheres even in healthy brains, we conducted this analysis separately for patients with lesions in the left and right hemisphere. We found a significant difference in inter-hemispheric K_S values for patients with left hemisphere lesions (CLES = 0.775, p_{perm} = 0.025; Fig. 3B), though we note that this comparison included data from only six patients and that the effect would not survive correction for multiple comparisons. We did not observe any significant differences in inter-hemispheric disruption indices for timescale, within-module degree, or participation coefficient (Fig. 3, A/C/D).

Second, we re-computed K_i values for each patient's ipsilesional hemisphere relative to the same hemisphere in healthy participants, and compared these to the distribution of single-hemisphere K_i values in controls. We did not observe any significant group differences in ipsilesional K_i values for any measure (Fig. 4). We repeated this analysis for the contralesional hemisphere and found a significant group difference in contralesional K_S values (CLES = 0.671, p_{perm} = 0.025; Fig. 5B), though this effect would also not survive correction for multiple comparisons.

Together, the results of our disruption index analysis fail to provide evidence for the predicted stereotyped pattern of increases and decreases in topological measures or timescales in patients with subcortical stroke, either relative to healthy participants, or when comparing measures between hemispheres in each patient.

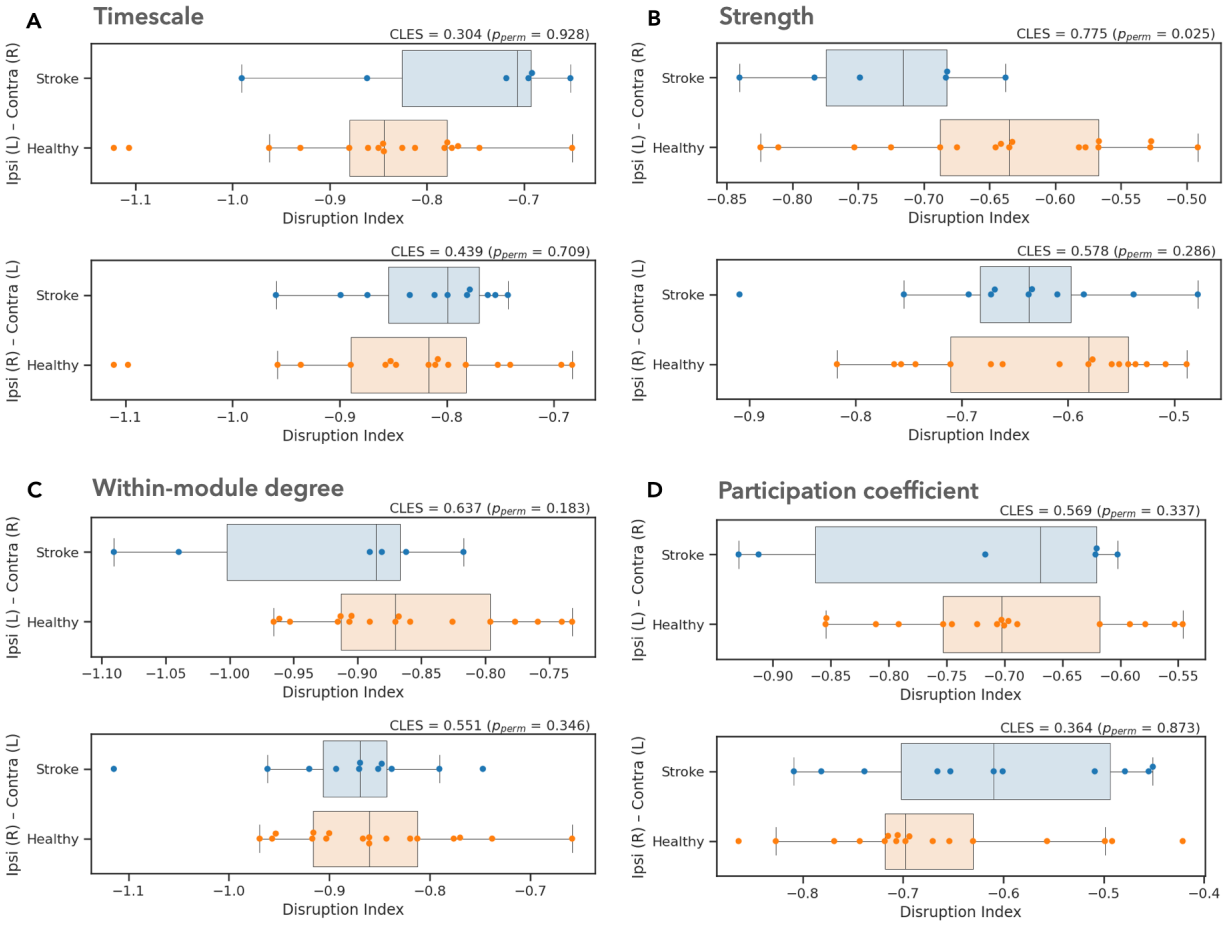


Figure 3: Inter-hemispheric disruption index analysis.
When comparing timescales and topological properties between hemispheres in each individual, patients with left hemisphere stroke lesions tended to have lower K_s values than healthy individuals, though we caution that only six patients were included in that comparison, and that the effect would not survive correction for multiple comparisons. We did not observe any other significant group differences in inter-hemispheric K_i values. CLES is the probability that a randomly selected patient will have a lower K_i than a randomly selected healthy participant.

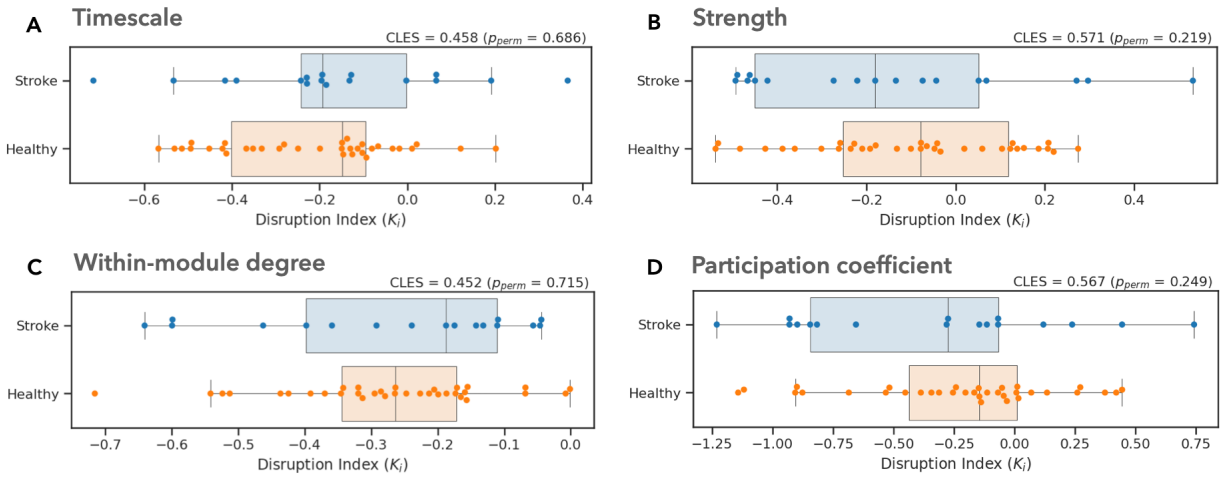


Figure 4: Ipsilesional disruption index analysis.
We did not observe a significant group difference in ipsilesional K_i values for any measure. CLES is the probability that a randomly selected patient will have a lower K_i than a randomly selected healthy participant.

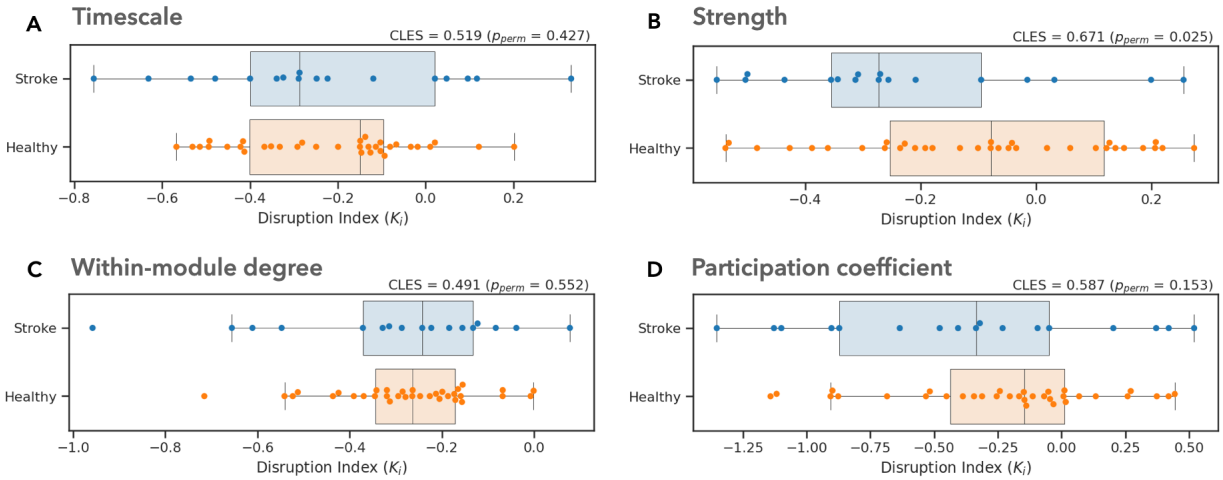


Figure 5: Contralesional disruption index analysis.
When considering only regions in the contralesional hemisphere, patients tended to have lower K_s values than healthy individuals, though we note that this effect would not survive correction for multiple comparisons. We did not observe any other significant group differences in contralesional K_i values. CLES is the probability that a randomly selected patient will have a lower K_i than a randomly selected healthy participant.

Similarity and normative deviation of regional dynamics and topology

Given the null results of our disruption index analysis, we conducted two exploratory follow-up analyses to test whether timescales or topological properties show other types of differences between patients and control participants. The "disruption index" pre-supposes a particular,

distributed pattern of lesion-induced disruption (i.e. the greatest decrease in regions with high values, and the greatest increase in regions with low values), but it is possible that differences in timescales or topological properties between patients and control participants do not follow this pattern, or that differences in patients are relatively circumscribed rather than distributed across many areas.

First, we computed the Euclidean distance between timescales and topological properties in each patient, and the median of each measure in control participants. Lower Euclidean distance indicates greater similarity. Euclidean distance, like correlation, is agnostic to the particular pattern of differences between two vectors. However, unlike correlation, Euclidean distance is also sensitive to the scaling of values, and has recently been used to study changes in functional connectivity following stroke (Branscheidt et al., 2022). If timescales or topological properties are disrupted in multiple brain areas following subcortical stroke, patients should be less similar to the healthy median than control participants, regardless of the particular pattern of disruptions. Second, we adopted a "normative modeling" approach (Marquand et al., 2016) to identify cortical areas in each patient where timescales or topological properties were significantly different than those in healthy participants. For each cortical area in each patient, we computed a z-score relative to the distribution of values for the same area in healthy participants. Then, following (Lv et al., 2021), we defined extreme deviations as regions with an absolute z-score of at least 1.96, and counted the number of such deviations for each measure. Assuming that individual differences in timescales and topology are normally distributed in the larger population, patients with stroke-related disruptions in these measures should have a higher number of extreme deviations than healthy participants, even if disruptions are limited to a small number of areas, and even if no two patients show extreme deviations in the same regions. Euclidean distances and normative deviations were both calculated in healthy participants using the "leave one out" strategy described above, and we used the same permutation testing approach to evaluate the significance of group differences (with the exception that the alternative hypothesis was that patients exhibit higher rather than lower values compared to controls). Because these were exploratory follow-up analyses, we did not correct for multiple comparisons, and our results should be considered in light of this decision.

Cortex-wide patterns of strength and participation coefficient in patients tended to be less similar to the healthy median than in control participants (strength: CLES = 0.714, p_{perm} = 0.017; PC: CLES = 0.670, p_{perm} = 0.035; Fig. 6B/D). Patients also tended to have a greater number of cortical areas where strength showed a large deviation from the normative distribution (CLES = 0.666, p_{perm} = 0.048; Fig. 6B). We found similar results in each cortical hemisphere. In the ipsilesional hemisphere, distributed patterns of strength and participation coefficient in patients tended to be less similar to the healthy median than in controls (strength: CLES = 0.730, p_{perm} = 0.003; PC: CLES = 0.671, p_{perm} = 0.024; Fig. 7B/D), and patients tended to have a greater number of extreme normative deviations in these measures (strength: CLES = 0.683, p_{perm} = 0.014; PC: CLES = 0.650, p_{perm} = 0.047; Fig. 7B/D). In the contralesional hemisphere, distributed patterns of strength and participation coefficient in patients tended to be less similar to the healthy median than in controls (strength: CLES = 0.692, p_{perm} = 0.019; PC: CLES = 0.666, p_{perm} = 0.030; Fig. 8B/D), and patients tended to have a greater number of extreme normative deviations in participation coefficient (CLES = 0.654, p_{perm} = 0.034; Fig. 8D). We did

not observe any group differences in Euclidean distance or the number of normative deviations for timescale or within-module degree at any level of analysis. Similarly, we did not find any evidence that patients showed greater inter-hemispheric differences than healthy participants (Fig. 9). Together, these results provide preliminary evidence that patients with subcortical stroke exhibit both distributed and localized differences in regional functional connectivity strength and participation coefficient during the sub-acute stage of recovery.

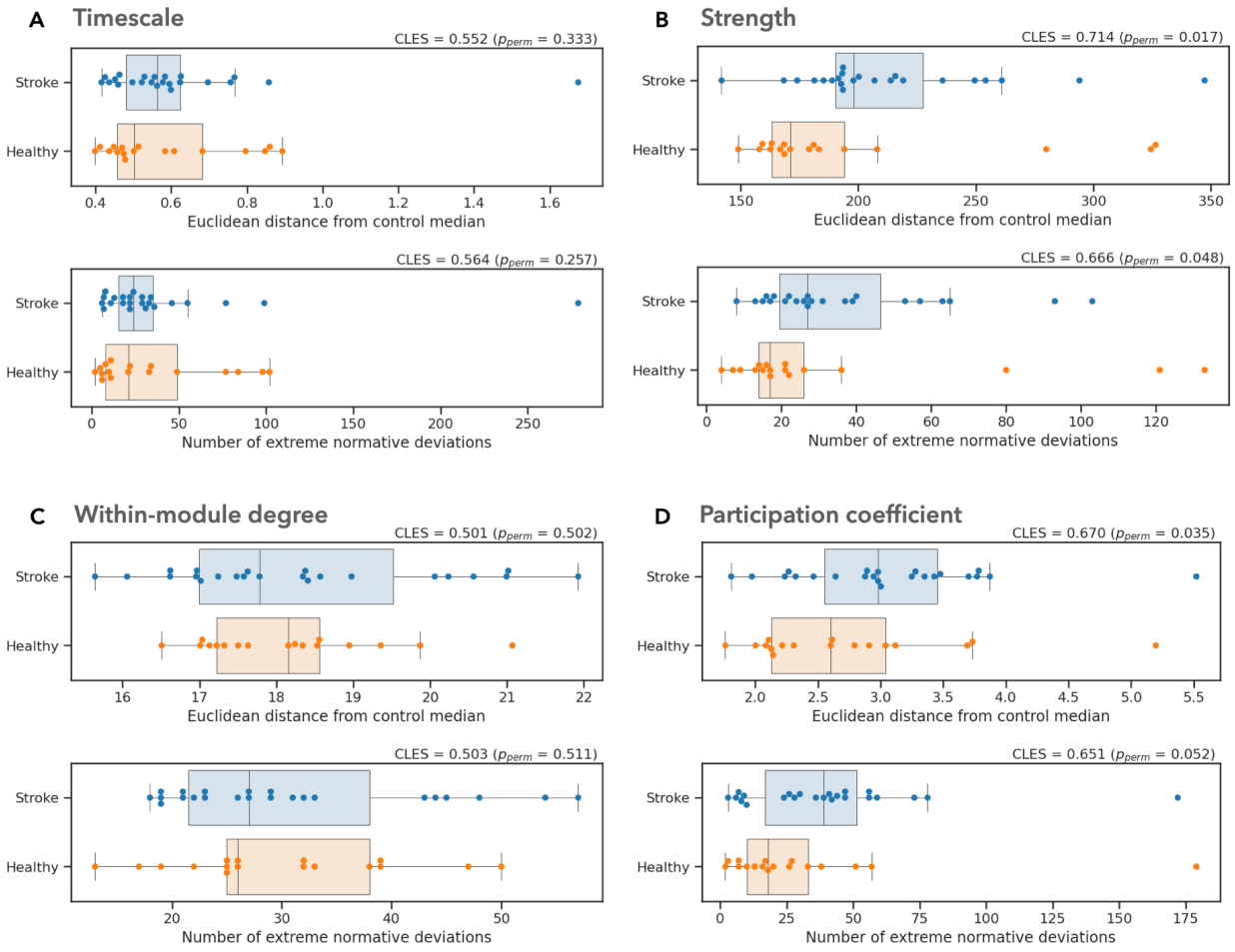


Figure 6: Similarity and normative deviation of timescales and topology across all cortical areas. Euclidean distance (top of each panel) quantifies the similarity of timescales and topological properties across all cortical areas in each individual relative to the median in healthy participants. Higher distance indicates lower similarity. In contrast, normative modeling (bottom of each panel) allows us to count the number of individual regions in each participant which differ significantly from the healthy distribution. Strength and participation coefficient in patients were both significantly less similar to the healthy median than in controls, and patients also had significantly more extreme normative deviations in strength than controls. CLES is the probability that a randomly selected patient will have a higher Euclidean distance or greater number of extreme deviations than a randomly selected healthy participant.

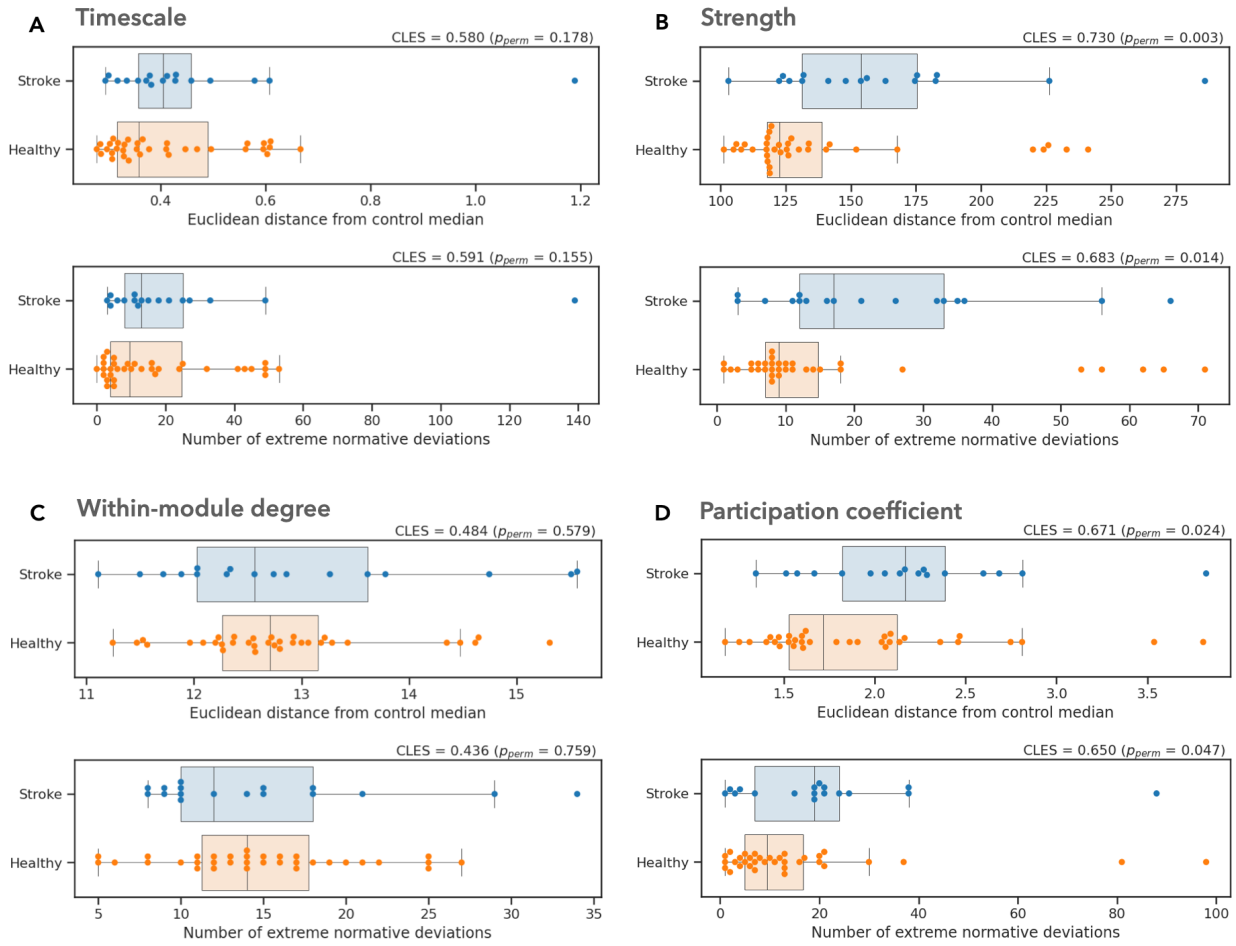


Figure 7: Similarity and normative deviation of timescales topology in the ipsilesional hemisphere. Patients tended to show greater differences in strength and participation coefficient (relative to the expected value in healthy individuals) than control participants, both in terms of the similarity of the pattern of strength and PC values across regions, as well as in the number of regions which show an extreme deviation from the distribution of healthy values. CLES is the probability that a randomly selected patient will have a higher Euclidean distance or greater number of extreme deviations than a randomly selected healthy participant.

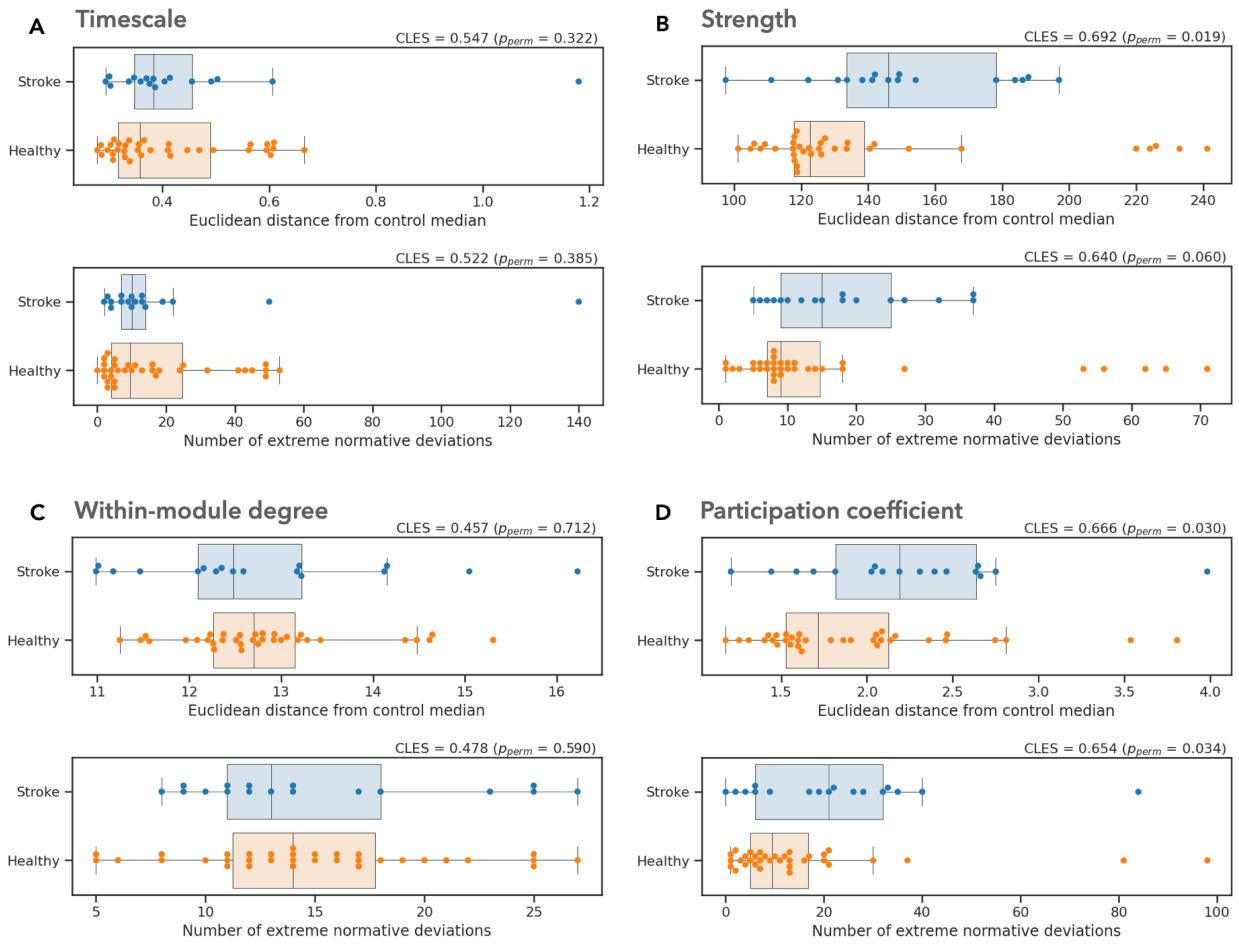


Figure 8: Similarity and normative deviation of timescales and topology in the contralesional hemisphere.

Patients tended to show lower similarity in strength and participation coefficient (relative to the healthy median) than controls. Patients also tended to have a greater number of extreme deviations in participation coefficient than controls. CLES is the probability that a randomly selected patient will have a higher Euclidean distance or greater number of extreme deviations than a randomly selected healthy participant.

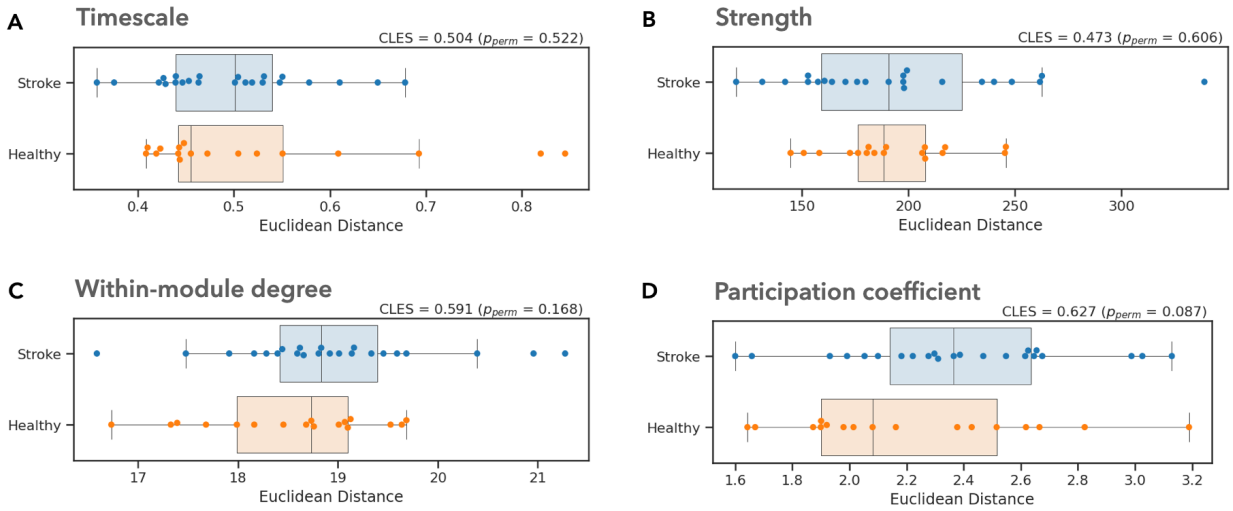


Figure 9: Inter-hemispheric similarity of timescales and topology.
We did not observe a significant group difference in inter-hemispheric similarity for any measure. CLES is the probability that a randomly selected patient will have a higher Euclidean distance than a randomly selected healthy participant.

Finally, given recent evidence that patients exhibit greater inter-individual variability in functional connectivity patterns (Branscheidt et al., 2022), we additionally computed the similarity in cortex-wide timescales and topological properties between each pair of patients and each pair of controls. For each measure, this produced a distribution of Euclidean distances which quantifies the similarity of regional dynamics and topological properties within each group. As above, we used a WMW test to compare these distributions, and evaluated significance relative to 10,000 random permutations of group labels. Consistent with the results of our other analyses, while patients did not show greater inter-individual variability in timescales than healthy participants (CLES = 0.540, pperm = 0.0951), they did show greater variability in strength (CLES = 0.619, pperm = 0.0002) and participation coefficient (CLES = 0.570, pperm = 0.0130), as well as within-module degree (CLES = 0.640, pperm = 0.0001). These results suggest that in addition to showing greater deviations in strength and participation coefficient relative to healthy individuals, patients also show more idiosyncratic patterns of regional topology than healthy individuals.

Individual differences in topology correlate with individual differences in timescale

While we did not find evidence for stereotyped disruption of timescales or topological properties in patients, it is clear from our results that these measures do differ between individuals. As such, while our failure to observe alterations in timescales or within-module degree in patients means that we are unable to test our a priori hypothesis that these alterations will be correlated, the same analysis can be re-framed as asking the more general question of whether individual differences in topological properties are related to individual differences in regional dynamics. In particular, given our prior observations of a robust positive correlation

between cortical timescales and within-module functional connectivity degree (Chapters 1 and 2), we predicted (post-hoc) that normative deviations in timescales would be positively correlated with normative deviations in within-module degree. Thus, for each individual patient and healthy participant, we calculated the Spearman correlation between normative deviations in timescale and normative deviations in each of the three measures of regional topology (strength, WD, and PC). As a reminder, the normative deviation of each cortical area in an individual is the z-score of that region relative to the distribution of values for that region in healthy individuals. Because spatial autocorrelation can inflate measures of association when comparing brain maps, we evaluated the significance of these correlations using spin testing (Alexander-Bloch et al., 2018) and 1000 permutations. For each topological measure, we counted the number of participants exhibiting a significant correlation, and estimated the 95% confidence interval for the mean correlation using the bias-corrected and accelerated bootstrap confidence interval method (which corrects for both the bais and skewness of bootstrapped parameter estimates) (Davison & Hinkley, 1997).

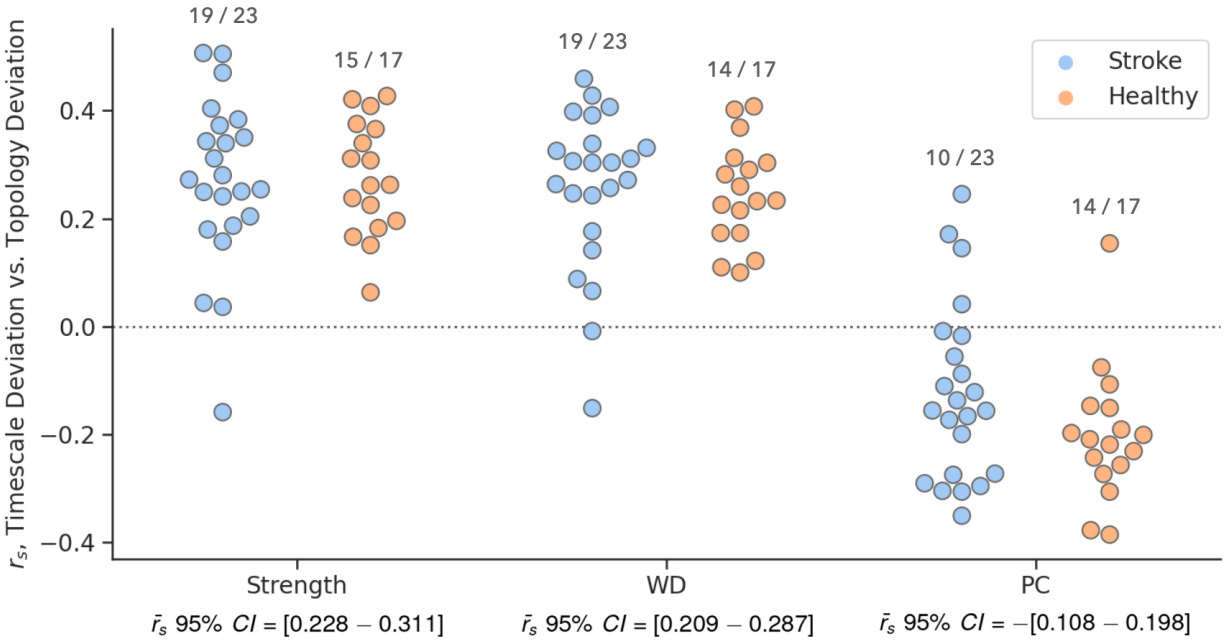


Figure 10: Correlation between timescale deviations and topology deviations within each individual. To investigate whether individual differences in regional dynamics were correlated with individual differences in topological properties, we computed, within each participant, the Spearman correlation between timescale deviations and deviations in each of the three measures of regional topology. We found that cortical areas in patients and healthy participants which exhibit higher than average strength and within-module degree also tend to exhibit longer than average timescales, and that a similar (but opposite) relationship exists for participation coefficient in most healthy individuals. The fractions above each set of data points is the proportion of individuals showing a significant correlation. Significance was determined using spin-based permutation testing and an alpha of p = 0.0167 (i.e. 0.05 / 3 measures of topology), though we note that the majority of significant p-values were less than 0.005 (Fig. S4). Bootstrapped 95% confidence intervals for the mean correlation (across all participants) are shown at the bottom of the figure.

We found robust evidence for a relationship between individual differences in regional dynamics and hub properties (Fig. 10). As predicted, timescale deviations exhibited a significant positive correlation with within-module degree deviations in the majority of individuals (19 of 23 patients and 15 of 17 healthy participants; bootstrapped 95% CI = [0.209 – 0.287]). Most individuals also had a significant positive correlation between timescale deviations and strength deviations (19 of 23 patients and 14 of 17 healthy participants; 95% CI = [0.228 – 0.311]). Just over half of individuals showed a significant negative correlation between timescale deviations and PC deviations (10 of 23 patients and 14 of 17 healthy participants; 95% CI = -[0.108 – 0.198]). These findings indicate that cortical areas in patients and healthy participants which exhibit greater than average global (strength) and within-module (WD) functional connectivity (relative to the same region in other individuals) are also likely to exhibit longer than average timescales, and that a similar (though opposite) relationship exists for participation coefficient.

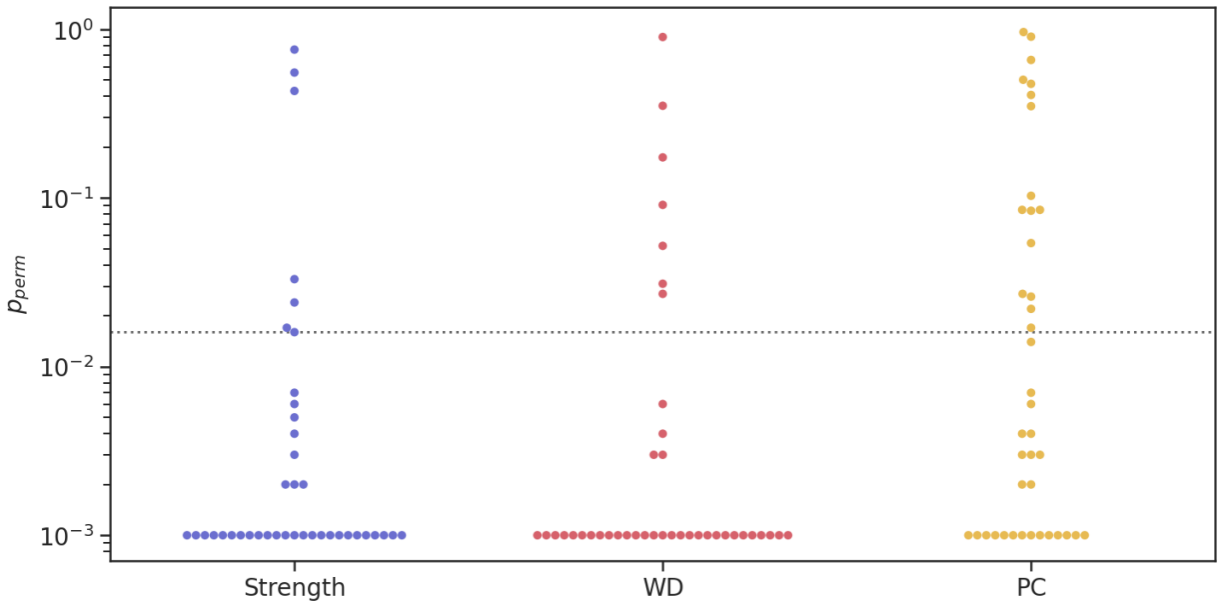


Figure S4: P-values for correlations between timescale deviations and topology deviations within individuals.
The horizontal dotted line shows the p = 0.0167 threshold for significance.

Timescales are correlated with topology at the level of individual participants

Given our novel finding that timescale deviations are correlated with deviations in multiple topological properties in the majority of individual participants, we additionally investigated whether the group-level relationship between timescales and within-module degree which we observed in previous chapters also exists within each individual. This analysis was nearly identical to that presented in the previous section, except we evaluated the relationship

between "raw" values of timescale and topology in each participant rather than normative deviations in these measures.

As in our analysis of correlated individual differences, we found robust evidence for a relationship between timescales and topology at the level of individual participants (Fig. 11). In particular, timescales exhibited a significant positive correlation with within-module degree in a large majority of individuals (20 of 23 patients and 14 of 17 healthy participants; 95% CI = [0.247 – 0.361]). Just over half of individuals also showed a significant positive correlation between timescales and strength (15 of 23 patients and 10 of 17 healthy participants; 95% CI = [0.239 – 0.359]), and a significant negative correlation between timescales and participation coefficient (11 of 23 patients and 15 of 17 healthy participants; 95% CI = -[0.141 – 0.274]). These results suggest that the positive correlation between timescales and within-module degree—which we observed in previous chapters at the group level—also exists at the level of individuals. Further, they suggest that analyses undertaken at the group level may obscure relationships between timescale and other features of regional topology (i.e. strength and participation coefficient) which exist in many individual participants.

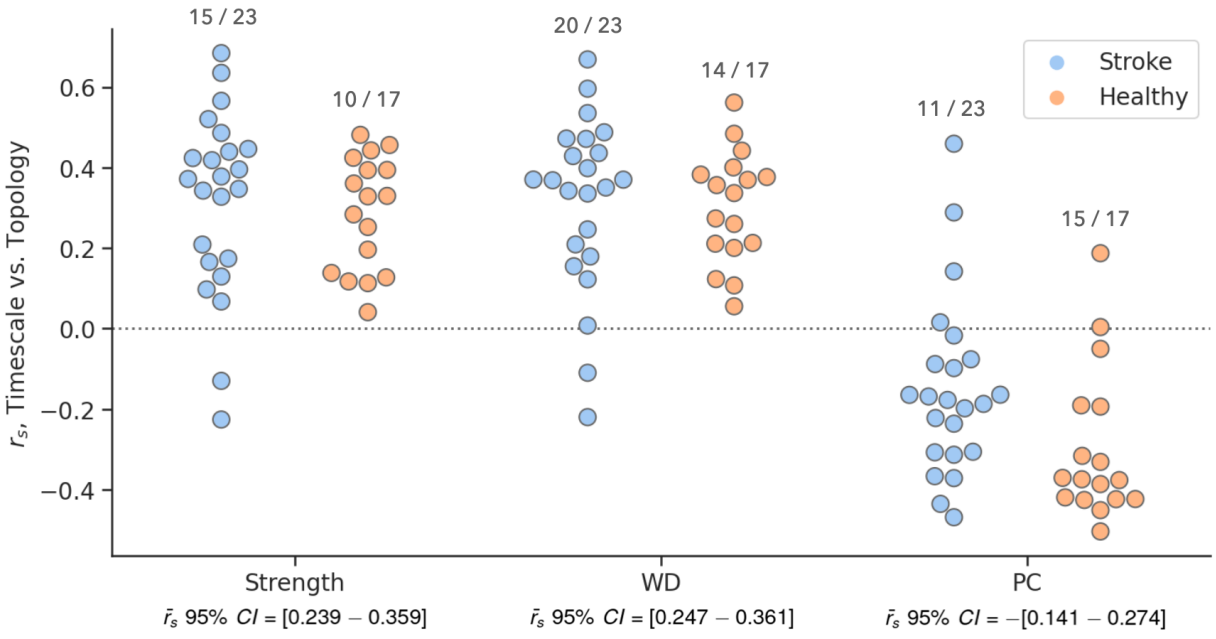


Figure 11: Correlation between timescales and topology within each individual.
Consistent with the results of our group-level analyses from previous chapters, we found that the majority of individuals showed a significant positive correlation between timescales and within-module degree. Further, we found that over half of participants also exhibited a significant positive correlation between timescales and strength, and a significant negative correlation between timescales and participation coefficient. The fractions above each set of data points is the proportion of individuals showing a significant correlation. Significance was determined using spin-based permutation testing and an alpha of p = 0.0167 (i.e. 0.05 / 3 measures of topology), though we note that the majority of significant p-values were below 0.005 (Fig. S5). Bootstrapped 95% confidence intervals for the mean correlation (across all participants) are shown at the bottom of the figure.

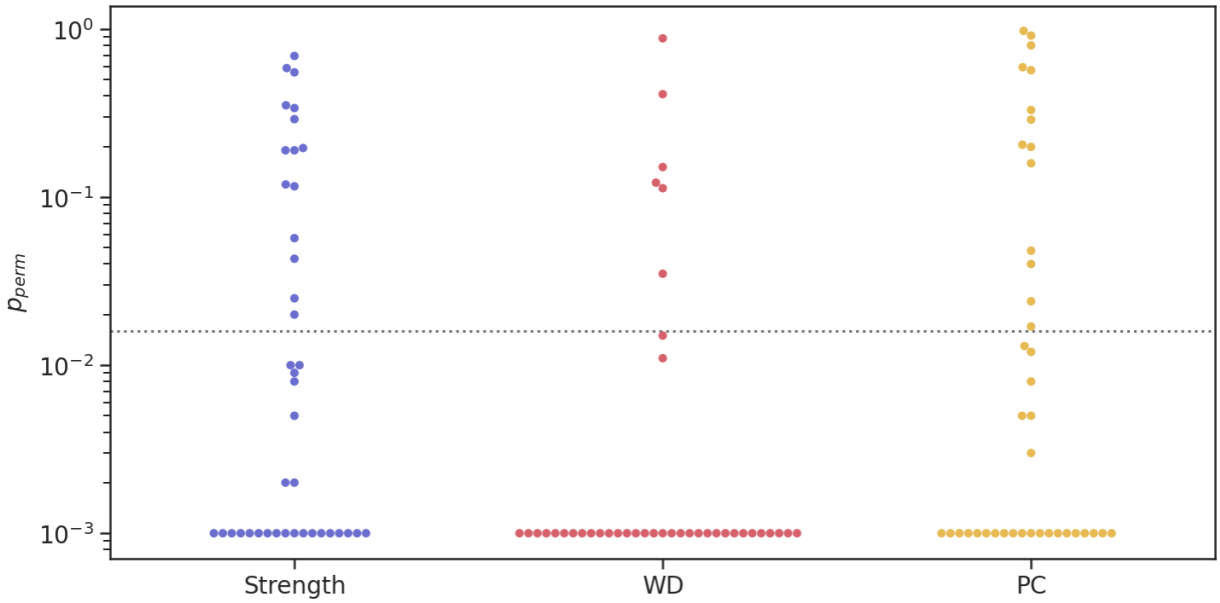


Figure S5: P-values for correlations between timescales and topology within individuals.
The horizontal dotted line shows the p = 0.0167 threshold for significance.

Timescales are correlated with topology across participants

Our previous analyses have provided evidence for relationships between timescales and topology *within* individuals. However, a stronger test of the hypothesis that these features are related is to assess whether timescales and topological features are correlated *across* individuals. As such, in our final analysis, we computed the Spearman correlation between timescale and each of the three topological features in each cortical area across patients and healthy individuals. Consistent with both our group-level analyses in previous chapters—as well as the single-subject analyses presented in previous sections of this chapter—we found that timescales were positively correlated with within-module degree in most cortical areas (95% CI = [0.181 – 0.219]; Fig. 12B). Timescales were also positively correlated with strength (95% CI = [0.241 – 0.274]; Fig. 12A) and negatively correlated with participation coefficient (95% CI = -[0.181 – 0.214]; Fig. 12C) in most cortical areas. Further, each of these effects was independently significant in dozens of individual regions, even after using the False Discovery Rate (FDR) method (Benjamini & Hochberg, 1995) to correct for multiple comparisons (Fig. S6).

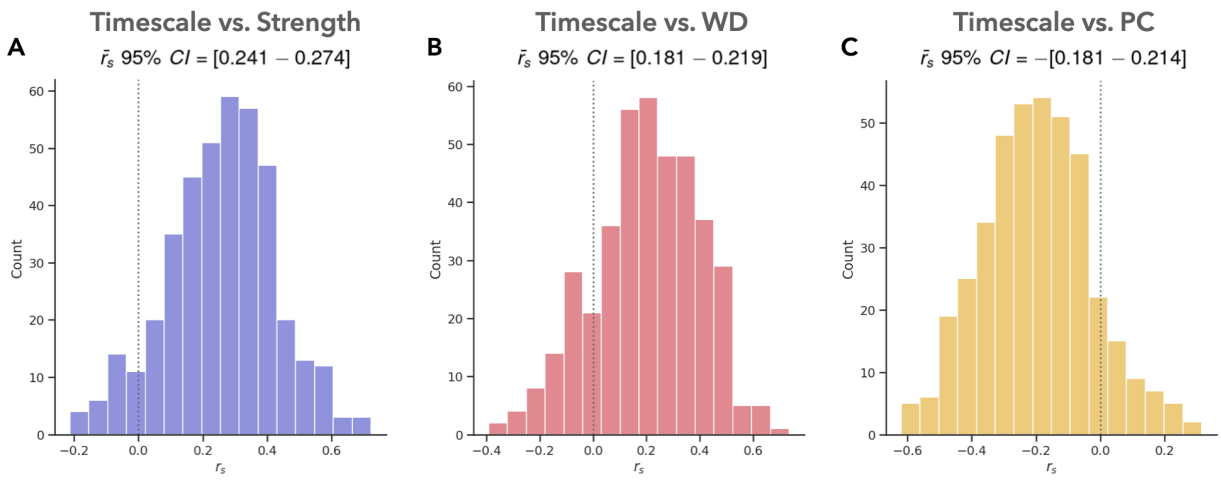


Figure 12: Correlations between timescales and topology across individuals.
Distributions show the Spearman correlation between timescale and each topological feature calculated across all 40 participants for each of the 400 cortical regions. Bootstrapped 95% confidence intervals are for the mean correlation across cortical areas.

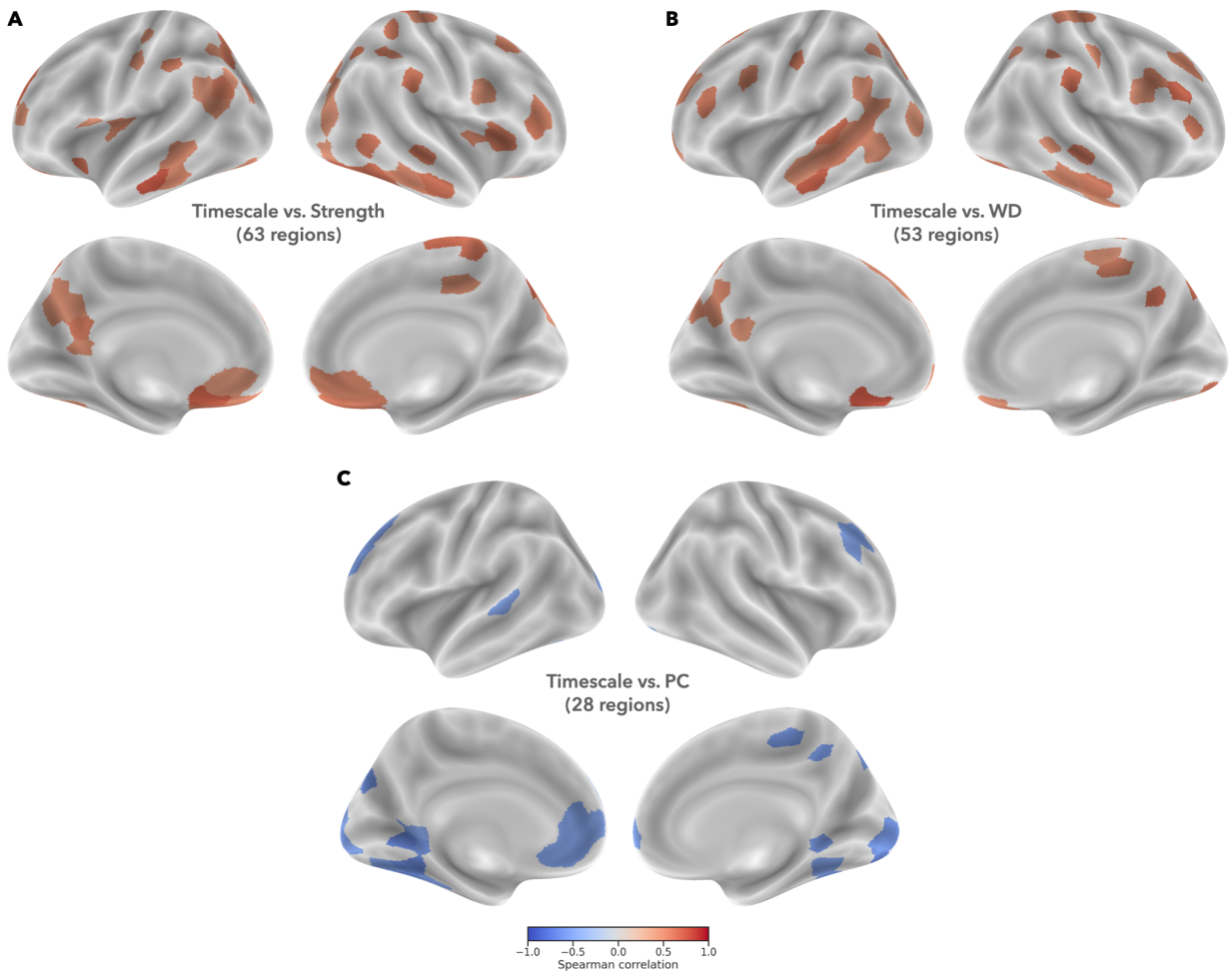


Figure S6: Cortical areas showing a significant correlation between timescale and topology.
Surface maps are thresholded to show only regions where the Spearman correlation between timescale and each topological measure was significant at FDR $q \leq 0.05$.

Discussion

Previous studies from our group and others have found both robust evidence for alterations of functional connectivity in patients with focal brain lesions, as well as a relationship between the timescale of intrinsic regional BOLD activity and the topological role of each brain area. As such, we predicted that cortical timescales would be altered in patients with subcortical lesions due to stroke, and more specifically, that these alterations would parallel a stereotyped pattern of topology-dependent increases and decreases in within-module degree. Contrary to our predictions, we did not find evidence for stereotyped alterations timescale or within-module degree, nor strength or participation coefficient. Similarly, neither did we find evidence for non-systematic alterations in timescales or within-module degree, though we did find preliminary evidence for idiosyncratic, non-systematic alterations in strength and participation coefficient in patients, both in terms of the similarity of distributed patterns of these features compared to a healthy template, as well as the number of individual regions

which exhibited a large normative deviation from the healthy distribution. Patients also tended to show greater individual differences in the three topological measures than healthy participants, though we found no such effect for timescales. Together, these results suggest that some aspects of regional functional network topology are altered in patients with focal subcortical lesions due to stroke, but fail to replicate prior observations of a stereotyped pattern of "hub disruption" in these patients. Further, they suggest that cortical timescales may be largely preserved during the early stages of stroke recovery.

In contrast, we found robust evidence that individual differences in timescales are correlated with individual differences in regional topology. Within individuals, normative deviations in timescale were positively correlated with normative deviations in strength and within-module degree, and negatively correlated with normative deviations in participation coefficient. Across individuals, cortical areas with longer timescales tended to have higher strength and within-module degree, and lower participation coefficient. Additionally, we extend our prior work on group-level associations between timescales and within-module degree by demonstrating that the same relationship exists at the level of individual participants, and further, that timescales are also correlated with strength and participation coefficient in single-subject analyses. Together, these results contribute to the growing literature on the relationship between regional connectivity and intrinsic dynamics, and suggest that BOLD timescales show distinct associations with the extent to which each brain area acts as a hub (strength, WD) or connector (participation coefficient) within cortical functional connectivity networks.

While we did not find evidence for altered timescales in our sample of stroke patients, a number of recent studies have reported localized alterations in other properties of intrinsic dynamics in undamaged brain areas during the initial stages of recovery after stroke, and further, that these alterations are related to the degree of behavioral impairment (Guo et al., 2019; Liang et al., 2020; Tian et al., 2022; Xie et al., 2022). In particular, (Guo et al., 2019) found that patients with post-stroke aphasia had significantly lower variability in the amplitude of low-frequency fluctuations (dALFF) in the left inferior frontal gyrus and middle temporal gyrus compared to healthy individuals, and that dALFF in the IFG was correlated with aphasia severity. Similarly, (Liang et al., 2020) and (Tian et al., 2022) found that the entropy of intrinsic dynamics in the supplementary motor area of patients with post-stroke motor impairment was associated with the severity of that impairment. Notably, like the analysis we present here, the study by Tian and colleagues focused exclusively on patients with subcortical lesions. Together, these studies suggest that focal lesions due to stroke may be associated with relatively circumscribed alterations in the intrinsic dynamics of remote brain areas. Given that our analyses were not designed to identify spatially localized group differences, it remains possible that timescales show similar alterations, and future work is needed to evaluate this hypothesis.

Our results fail to replicate the findings of three prior studies which have reported evidence for stereotyped hub disruption in patients with focal brain lesions. In particular, an unpublished analysis from our group (Gratton et al., November 9-13 2013) found evidence for stereotyped disruption of within-module degree and participation coefficient (relative to healthy individuals) in patients during the chronic stage recovery from stroke, traumatic brain injury,

and tumor resection. Gratton and colleagues also found evidence for stereotyped disruption of participation coefficient when comparing the ipsilesional and contralesional hemisphere within each patient, and their study was the primary inspiration for the current analysis. In similar work, (Termenon et al., 2016) found stereotyped disruption of local and global efficiency, degree, and clustering coefficient in stroke patients relative to healthy controls, and disruption of local and global efficiency, degree, and betweenness centrality when comparing the ipsilesional to contralesional hemisphere in patients. More recently, (Huang et al., 2022) reported that stroke patients show stereotyped disruption in degree, betweenness centrality, clustering coefficient, local efficiency, and participation coefficient relative to healthy individuals. Together, these studies suggest that functional connectivity networks in stroke patients show stereotyped disruption in a wide range of topological measures. Stereotyped hub disruption has also been observed across a wide range of psychiatric and neurological disorders, including epilepsy (Banjac et al., 2021; Ridley et al., 2015; Roger et al., 2020; Song et al., 2015), dementia (Baggio et al., 2014), autism (Itahashi et al., 2014), schizophrenia (Lo et al., 2015), chronic pain (Barroso et al., 2021; Mano et al., 2018; Mansour et al., 2016) and disorders of consciousness (Achard et al., 2012; Malagurski et al., 2019; Sinitsyn et al., 2018).

While methodological differences do exist between the current study and those undertaken by Gratton, Termonon, and Huang, we believe we are able to rule out three key factors which might otherwise offer an explanation for our failure to replicate their results. First, hub disruption in stroke patients has been observed at both the sub-acute (Huang, Termenon) and chronic stages of recovery (Gratton). As such, our failure to find evidence for hub disruption is unlikely to be due to our focus on data collected from patients in the first few weeks after stroke. Second, while both Gratton and Termenon included patients with both cortical and subcortical lesions, Huang and colleagues (like the current analysis) focused exclusively on patients with subcortical lesions. Third, it is unlikely that our null findings result from a small sample size or lack of power. In particular, while the studies by Gratton and Huang both included more than twice the number of patients than we analyzed here, Termenon et al. analyzed data from slightly less patients than in our sample. Further, while neither Gratton or Termeon reported effect sizes for the difference in disruption indices between patients and healthy participants, Huang et al. report an effect size of $d = 1.27$ for PC disruption, and $d = 0.95$ for degree disruption. In a post-hoc power analysis, we found that our study was powered at 0.985 (PC) and 0.885 (degree) to detect these effects. As such, further work is needed to identify the factors which led to our divergent results.

More generally, our finding that strength and participation coefficient in patients exhibit reduced similarity to the healthy median—as well as a greater number of extreme normative deviations—is consistent with prior work showing that focal brain lesions are associated with alterations of functional connectivity in remote brain areas (Gratton et al., 2012; Grayson et al., 2016; Griffis et al., 2019; Nomura et al., 2010; Ovadia-Caro et al., 2013; Park et al., 2011; Siegel et al., 2018; Wang et al., 2014), and in particular, their topological properties (Blaschke et al., 2021; Froudist-Walsh et al., 2018; Gratton et al., November 9-13 2013; Huang et al., 2022; Li et al., 2020; Olafson et al., 2021). Similarly, our observation that patients exhibit greater inter-individual variability in topological measures is consistent with a recent study by (Branscheidt et al., 2022), who also found increased inter-individual variability in functional

connectivity patterns following subcortical stroke. Notably, however, patients in the study by Branscheidt and colleagues all had unilateral upper extremity weakness due to subcortical lesions to the corticospinal tract, and the researchers focused their analysis exclusively on regions of interest in the motor cortex. This suggests that while our findings of increased inter-individual variability are likely due at least in part to heterogeneity in lesion location, such heterogeneity is not necessary to produce these effects.

In previous chapters, we found (in group level analyses) that functional connectivity within-module degree—but not strength or participation coefficient[2]—was positively correlated with cortical timescales. Here, we show that the relationship between timescales and within-module degree also exists both across cortical areas within individual participants, as well as in individual cortical areas across participants. Further, we find that in contrast to the results of our prior group-level analyses, timescales are also correlated with strength and participation coefficient when studied within and across individuals. These results emphasize the importance of studying functional brain organization at the level of the individual, and build on past work suggesting that timescales are correlated with regional degree in the structural and functional connectivity networks of many individuals (Fallon et al., 2020; Shinn et al., 2021). More generally, they provide additional evidence that hub regions with extensive connectivity tend to have long timescales, consistent with their putative role in integrating information from diverse brain areas both within their own network modules and across the brain as a whole. In contrast, our new results indicate that diverse functional connectivity may be associated with shorter timescales. This suggests that connector regions—which have previously been suggested to play an important role in coordinating activity and shaping functional interactions among other brain areas (Bertolero et al., 2015, 2018)—may have relatively less stable dynamics. That said, we note that while the positive correlation between timescales and within-module degree has now been replicated in three different datasets (and in both group-level and single subject analyses), our finding that timescales are correlated with strength and participation coefficient should be considered preliminary until these relationships can be replicated in a second dataset.

This study has limitations. First, while we did find preliminary evidence that stroke patients exhibit non-systematic alterations in strength and participation coefficient relative to healthy individuals, we have no way to know whether these differences are actually the result of focal damage to subcortical gray matter and axonal pathways. For example, these differences might be due to other types of pathology which are common in stroke patients, such as hypertension, diabetes, high cholesterol, or chronic ischemia due to cerebrovascular disease. Put crudely, the fact that we observe differences in neurophysiological measures between neurological patients and healthy individuals should not come as a surprise, and additional work is needed to establish precisely which factors contribute to these differences. Second, the absence of evidence must not be taken as evidence of absence. Many of our analyses produced null effects,

[2] As noted in Chapter 1: "the relationship between timescale and FC PC was significantly weaker than the relationship with FC WD at multiple scales" (pg. 19). Similarly, unreported effect comparisons for the results from Chapter 2 found that the relationship between the primary gradient and FC WD was significantly stronger than the relationship with strength or FC PC.

but additional work is needed to establish whether, for example, there is truly no difference in timescale disruption indices between patients and healthy individuals. Similarly, formal effect comparisons would be needed to determine whether strength and participation coefficient show greater alterations than timescale and within-module degree, and so we are unable to say that patients show differences in some measures but not others (only that we find evidence for some effects, but not others). Third, we did not account for differences in age or sex when comparing timescales or topological properties between patients and healthy participants, though we note that ages are relatively well matched between groups.

References

Achard, S., Delon-Martin, C., Vértes, P. E., Renard, F., Schenck, M., Schneider, F., Heinrich, C., Kremer, S., & Bullmore, E. T. (2012). Hubs of brain functional networks are radically reorganized in comatose patients. *Proceedings of the National Academy of Sciences of the United States of America*, *109*(50), 20608–20613. https://doi.org/10.1073/pnas.1208933109

Alexander-Bloch, A. F., Shou, H., Liu, S., Satterthwaite, T. D., Glahn, D. C., Shinohara, R. T., Vandekar, S. N., & Raznahan, A. (2018). On testing for spatial correspondence between maps of human brain structure and function. *NeuroImage*, *178*, 540–551. https://doi.org/10.1016/j.neuroimage.2018.05.070

Andersen, S. M., Rapcsak, S. Z., & Beeson, P. M. (2010). Cost function masking during normalization of brains with focal lesions: still a necessity? *NeuroImage*, *53*(1), 78–84. https://doi.org/10.1016/j.neuroimage.2010.06.003

Avants, B. B., Tustison, N. J., Stauffer, M., Song, G., Wu, B., & Gee, J. C. (2014). The Insight ToolKit image registration framework. *Frontiers in Neuroinformatics*, *8*, 44. https://doi.org/10.3389/fninf.2014.00044

Baggio, H.-C., Sala-Llonch, R., Segura, B., Marti, M.-J., Valldeoriola, F., Compta, Y., Tolosa, E., & Junqué, C. (2014). Functional brain networks and cognitive deficits in Parkinson's disease. *Human Brain Mapping*, *35*(9), 4620–4634. https://doi.org/10.1002/hbm.22499

Banjac, S., Roger, E., Pichat, C., Cousin, E., Mosca, C., Lamalle, L., Krainik, A., Kahane, P., & Baciu, M. (2021). Reconfiguration dynamics of a language-and-memory network in healthy participants and patients with temporal lobe epilepsy. *NeuroImage. Clinical*, *31*, 102702. https://doi.org/10.1016/j.nicl.2021.102702

Barroso, J., Wakaizumi, K., Reis, A. M., Baliki, M., Schnitzer, T. J., Galhardo, V., & Apkarian, A. V. (2021). Reorganization of functional brain network architecture in chronic osteoarthritis pain. *Human Brain Mapping*, *42*(4), 1206–1222. https://doi.org/10.1002/hbm.25287

Behzadi, Y., Restom, K., Liau, J., & Liu, T. T. (2007). A component based noise correction method (CompCor) for BOLD and perfusion based fMRI. *NeuroImage*, *37*(1), 90–101. https://doi.org/10.1016/j.neuroimage.2007.04.042

Benjamini, Y., & Hochberg, Y. (1995). Controlling the false discovery rate: A practical and

powerful approach to multiple testing. *Journal of the Royal Statistical Society*, *57*(1), 289–300. https://doi.org/10.1111/j.2517-6161.1995.tb02031.x

Bertolero, M. A., Yeo, B. T. T., Bassett, D. S., & D'Esposito, M. (2018). A mechanistic model of connector hubs, modularity and cognition. *Nature Human Behaviour*, *2*(10), 765–777. https://doi.org/10.1038/s41562-018-0420-6

Bertolero, M. A., Yeo, B. T. T., & D'Esposito, M. (2015). The modular and integrative functional architecture of the human brain. *Proceedings of the National Academy of Sciences of the United States of America*, *112*(49), E6798–E6807. https://doi.org/10.1073/pnas.1510619112

Blaschke, S. J., Hensel, L., Minassian, A., Vlachakis, S., Tscherpel, C., Vay, S. U., Rabenstein, M., Schroeter, M., Fink, G. R., Hoehn, M., Grefkes, C., & Rueger, M. A. (2021). Translating Functional Connectivity After Stroke: Functional Magnetic Resonance Imaging Detects Comparable Network Changes in Mice and Humans. *Stroke; a Journal of Cerebral Circulation*, *52*(9), 2948–2960. https://doi.org/10.1161/STROKEAHA.120.032511

Blondel, V. D., Guillaume, J. L., & Lambiotte, R. (2008). Fast unfolding of communities in large networks. *Journal of Statistical.* https://iopscience.iop.org/article/10.1088/1742-5468/2008/10/P10008/meta

Branscheidt, M., Ejaz, N., Xu, J., Widmer, M., Harran, M. D., Cortés, J. C., Kitago, T., Celnik, P., Hernandez-Castillo, C., Diedrichsen, J., Luft, A., & Krakauer, J. W. (2022). No evidence for motor-recovery-related cortical connectivity changes after stroke using resting-state fMRI. *Journal of Neurophysiology*, *127*(3), 637–650. https://doi.org/10.1152/jn.00148.2021

Brett, M., Leff, A. P., Rorden, C., & Ashburner, J. (2001). Spatial normalization of brain images with focal lesions using cost function masking. *NeuroImage*, *14*(2), 486–500. https://doi.org/10.1006/nimg.2001.0845

Carrera, E., & Tononi, G. (2014). Diaschisis: past, present, future. *Brain: A Journal of Neurology*, *137*(9), 2408–2422. https://doi.org/10.1093/brain/awu101

Ciric, R., Wolf, D. H., Power, J. D., Roalf, D. R., Baum, G. L., Ruparel, K., Shinohara, R. T., Elliott, M. A., Eickhoff, S. B., Davatzikos, C., Gur, R. C., Gur, R. E., Bassett, D. S., & Satterthwaite, T. D. (2017). Benchmarking of participant-level confound regression strategies for the control of motion artifact in studies of functional connectivity. *NeuroImage*, *154*, 174–187. https://doi.org/10.1016/j.neuroimage.2017.03.020

Corbetta, M., Ramsey, L., Callejas, A., Baldassarre, A., Hacker, C. D., Siegel, J. S., Astafiev, S. V., Rengachary, J., Zinn, K., Lang, C. E., Connor, L. T., Fucetola, R., Strube, M., Carter, A. R., & Shulman, G. L. (2015). Common behavioral clusters and subcortical anatomy in stroke. *Neuron*, *85*(5), 927–941. https://doi.org/10.1016/j.neuron.2015.02.027

Crinion, J., Ashburner, J., Leff, A., Brett, M., Price, C., & Friston, K. (2007). Spatial normalization of lesioned brains: performance evaluation and impact on fMRI analyses. *NeuroImage*, *37*(3), 866–875. https://doi.org/10.1016/j.neuroimage.2007.04.065

Davison, A. C., & Hinkley, D. V. (1997). Confidence Intervals. In *Bootstrap Methods and their Application* (pp. 191–255). Cambridge University Press. https://doi.org/10.1017/CBO9780511802843.006

Esteban, O., Birman, D., Schaer, M., Koyejo, O. O., Poldrack, R. A., & Gorgolewski, K. J. (2017). MRIQC: Advancing the automatic prediction of image quality in MRI from unseen sites. *PloS One*, *12*(9), e0184661. https://doi.org/10.1371/journal.pone.0184661

Esteban, O., Markiewicz, C. J., Blair, R. W., Moodie, C. A., Isik, A. I., Erramuzpe, A., Kent, J. D., Goncalves, M., DuPre, E., Snyder, M., Oya, H., Ghosh, S. S., Wright, J., Durnez, J., Poldrack, R. A., & Gorgolewski, K. J. (2019). fMRIPrep: a robust preprocessing pipeline for functional MRI. *Nature Methods*, *16*(1), 111–116. https://doi.org/10.1038/s41592-018-0235-4

Fallon, J., Ward, P. G. D., Parkes, L., Oldham, S., Arnatkevičiūtė, A., Fornito, A., & Fulcher, B. D. (2020). Timescales of spontaneous fMRI fluctuations relate to structural connectivity in the brain. *Network Neuroscience (Cambridge, Mass.)*, *4*(3), 788–806. https://doi.org/10.1162/netn_a_00151

Fay, M. P., & Proschan, M. A. (2010). Wilcoxon-Mann-Whitney or t-test? On assumptions for hypothesis tests and multiple interpretations of decision rules. *Statistics Surveys*, *4*, 1–39. https://doi.org/10.1214/09-SS051

Fazekas, F., Chawluk, J. B., Alavi, A., Hurtig, H. I., & Zimmerman, R. A. (1987). MR signal abnormalities at 1.5 T in Alzheimer's dementia and normal aging. *American Journal of Roentgenology*, *149*(2), 351–356. https://www.ajronline.org/doi/abs/10.2214/ajr.149.2.351

Fornito, A., Zalesky, A., & Breakspear, M. (2015). The connectomics of brain disorders. *Nature Reviews. Neuroscience*, *16*(3), 159–172. https://doi.org/10.1038/nrn3901

Froudist-Walsh, S., Browning, P. G. F., Young, J. J., Murphy, K. L., Mars, R. B., Fleysher, L., & Croxson, P. L. (2018). Macro-connectomics and microstructure predict dynamic plasticity patterns in the non-human primate brain. *eLife*, *7*, e34354. https://doi.org/10.7554/eLife.34354

Gordon, E. M., Laumann, T. O., Adeyemo, B., Gilmore, A. W., Nelson, S. M., Dosenbach, N. U. F., & Petersen, S. E. (2017). Individual-specific features of brain systems identified with resting state functional correlations. *NeuroImage*, *146*, 918–939. https://doi.org/10.1016/j.neuroimage.2016.08.032

Gordon, E. M., Laumann, T. O., Adeyemo, B., & Petersen, S. E. (2017). Individual Variability of the System-Level Organization of the Human Brain. *Cerebral Cortex* , *27*(1), 386–399. https://doi.org/10.1093/cercor/bhv239

Gordon, E. M., Laumann, T. O., Gilmore, A. W., Newbold, D. J., Greene, D. J., Berg, J. J., Ortega, M., Hoyt-Drazen, C., Gratton, C., Sun, H., Hampton, J. M., Coalson, R. S., Nguyen, A. L., McDermott, K. B., Shimony, J. S., Snyder, A. Z., Schlaggar, B. L., Petersen, S. E., Nelson, S. M., & Dosenbach, N. U. F. (2017). Precision Functional Mapping of Individual Human Brains.

Neuron, *95*(4), 791–807.e7. https://doi.org/10.1016/j.neuron.2017.07.011

Gorgolewski, K., Burns, C. D., Madison, C., Clark, D., Halchenko, Y. O., Waskom, M. L., & Ghosh, S. S. (2011). Nipype: a flexible, lightweight and extensible neuroimaging data processing framework in python. *Frontiers in Neuroinformatics*, *5*, 13. https://doi.org/10.3389/fninf.2011.00013

Gorgolewski, K. J., Auer, T., Calhoun, V. D., Craddock, R. C., Das, S., Duff, E. P., Flandin, G., Ghosh, S. S., Glatard, T., Halchenko, Y. O., Handwerker, D. A., Hanke, M., Keator, D., Li, X., Michael, Z., Maumet, C., Nichols, B. N., Nichols, T. E., Pellman, J., … Poldrack, R. A. (2016). The brain imaging data structure, a format for organizing and describing outputs of neuroimaging experiments. *Scientific Data*, *3*, 160044. https://doi.org/10.1038/sdata.2016.44

Gratton, C., Gallen, C., & D'Esposito, M. (November 9-13 2013). *Focal lesions lead to functional plasticity in the roles of individual brain regions within large-scale networks*. 43rd annual meeting of the Society for Neuroscience, San Diego, California.

Gratton, C., Nomura, E. M., Pérez, F., & D'Esposito, M. (2012). Focal brain lesions to critical locations cause widespread disruption of the modular organization of the brain. *Journal of Cognitive Neuroscience*, *24*(6), 1275–1285. https://doi.org/10.1162/jocn_a_00222

Grayson, D. S., Bliss-Moreau, E., Machado, C. J., Bennett, J., Shen, K., Grant, K. A., Fair, D. A., & Amaral, D. G. (2016). The Rhesus Monkey Connectome Predicts Disrupted Functional Networks Resulting from Pharmacogenetic Inactivation of the Amygdala. *Neuron*, *91*(2), 453–466. https://doi.org/10.1016/j.neuron.2016.06.005

Griffis, J. C., Metcalf, N. V., Corbetta, M., & Shulman, G. L. (2019). Structural Disconnections Explain Brain Network Dysfunction after Stroke. *Cell Reports*, *28*(10), 2527–2540.e9. https://doi.org/10.1016/j.celrep.2019.07.100

Guo, J., Biswal, B. B., Han, S., Li, J., Yang, S., Yang, M., & Chen, H. (2019). Altered dynamics of brain segregation and integration in poststroke aphasia. *Human Brain Mapping*, *40*(11), 3398–3409. https://doi.org/10.1002/hbm.24605

Huang, Q., Lin, D., Huang, S., Cao, Y., Jin, Y., Wu, B., Fan, L., Tu, W., Huang, L., & Jiang, S. (2022). Brain Functional Topology Alteration in Right Lateral Occipital Cortex Is Associated With Upper Extremity Motor Recovery. *Frontiers in Neurology*, *13*, 780966. https://doi.org/10.3389/fneur.2022.780966

Itahashi, T., Yamada, T., Watanabe, H., Nakamura, M., Jimbo, D., Shioda, S., Toriizuka, K., Kato, N., & Hashimoto, R. (2014). Altered network topologies and hub organization in adults with autism: a resting-state fMRI study. *PloS One*, *9*(4), e94115. https://doi.org/10.1371/journal.pone.0094115

Kim, J., Avants, B., Patel, S., & Whyte, J. (2008). *Spatial normalization of injured brains for neuroimaging research: An illustrative introduction of available options* (NCRRN Methodology Papers). Moss Rehabilitation Research Institute.

Kong, R., Li, J., Orban, C., Sabuncu, M. R., Liu, H., Schaefer, A., Sun, N., Zuo, X.-N., Holmes, A. J., Eickhoff, S. B., & Yeo, B. T. T. (2019). Spatial Topography of Individual-Specific Cortical Networks Predicts Human Cognition, Personality, and Emotion. *Cerebral Cortex (New York, N.Y. : 1991)*, *29*(6), 2533–2551. https://doi.org/10.1093/cercor/bhy123

Kurtzer, G. M., Sochat, V., & Bauer, M. W. (2017). Singularity: Scientific containers for mobility of compute. *PloS One*, *12*(5), e0177459. https://doi.org/10.1371/journal.pone.0177459

Lancichinetti, A., & Fortunato, S. (2012). Consensus clustering in complex networks. *Scientific Reports*, *2*, 336. https://doi.org/10.1038/srep00336

Liang, L., Hu, R., Luo, X., Feng, B., Long, W., & Song, R. (2020). Reduced Complexity in Stroke with Motor Deficits: A Resting-State fMRI Study. *Neuroscience*, *434*, 35–43. https://doi.org/10.1016/j.neuroscience.2020.03.020

Li, Q.-G., Zhao, C., Shan, Y., Yin, Y.-Y., Rong, D.-D., Zhang, M., Ma, Q.-F., & Lu, J. (2020). Dynamic Neural Network Changes Revealed by Voxel-Based Functional Connectivity Strength in Left Basal Ganglia Ischemic Stroke. *Frontiers in Neuroscience*, *14*, 526645. https://doi.org/10.3389/fnins.2020.526645

Lo, C.-Y. Z., Su, T.-W., Huang, C.-C., Hung, C.-C., Chen, W.-L., Lan, T.-H., Lin, C.-P., & Bullmore, E. T. (2015). Randomization and resilience of brain functional networks as systems-level endophenotypes of schizophrenia. *Proceedings of the National Academy of Sciences of the United States of America*, *112*(29), 9123–9128. https://doi.org/10.1073/pnas.1502052112

Lv, J., Di Biase, M., Cash, R. F. H., Cocchi, L., Cropley, V. L., Klauser, P., Tian, Y., Bayer, J., Schmaal, L., Cetin-Karayumak, S., Rathi, Y., Pasternak, O., Bousman, C., Pantelis, C., Calamante, F., & Zalesky, A. (2021). Individual deviations from normative models of brain structure in a large cross-sectional schizophrenia cohort. *Molecular Psychiatry*, *26*(7), 3512–3523. https://doi.org/10.1038/s41380-020-00882-5

Lydon-Staley, D. M., Ciric, R., Satterthwaite, T. D., & Bassett, D. S. (2019). Evaluation of confound regression strategies for the mitigation of micromovement artifact in studies of dynamic resting-state functional connectivity and multilayer network modularity. *Network Neuroscience (Cambridge, Mass.)*, *3*(2), 427–454. https://doi.org/10.1162/netn_a_00071

Malagurski, B., Péran, P., Sarton, B., Vinour, H., Naboulsi, E., Riu, B., Bounes, F., Seguin, T., Lotterie, J. A., Fourcade, O., Minville, V., Ferré, F., Achard, S., & Silva, S. (2019). Topological disintegration of resting state functional connectomes in coma. *NeuroImage*, *195*, 354–361. https://doi.org/10.1016/j.neuroimage.2019.03.012

Mano, H., Kotecha, G., Leibnitz, K., Matsubara, T., Sprenger, C., Nakae, A., Shenker, N., Shibata, M., Voon, V., Yoshida, W., Lee, M., Yanagida, T., Kawato, M., Rosa, M. J., & Seymour, B. (2018). Classification and characterisation of brain network changes in chronic back pain: A multicenter study. *Wellcome Open Research*, *3*(19), 19. https://doi.org/10.12688/wellcomeopenres.14069.2

Mansour, A., Baria, A. T., Tetreault, P., Vachon-Presseau, E., Chang, P.-C., Huang, L., Apkarian, A. V., & Baliki, M. N. (2016). Global disruption of degree rank order: a hallmark of chronic pain. *Scientific Reports*, *6*, 34853. https://doi.org/10.1038/srep34853

Marquand, A. F., Rezek, I., Buitelaar, J., & Beckmann, C. F. (2016). Understanding Heterogeneity in Clinical Cohorts Using Normative Models: Beyond Case-Control Studies. *Biological Psychiatry*, *80*(7), 552–561. https://doi.org/10.1016/j.biopsych.2015.12.023

McGraw, K. O., & Wong, S. P. (1992). A common language effect size statistic. In *Psychological Bulletin* (Vol. 111, Issue 2, pp. 361–365). https://doi.org/10.1037/0033-2909.111.2.361

Nomura, E. M., Gratton, C., Visser, R. M., Kayser, A., Perez, F., & D'Esposito, M. (2010). Double dissociation of two cognitive control networks in patients with focal brain lesions. *Proceedings of the National Academy of Sciences of the United States of America*, *107*(26), 12017–12022. https://doi.org/10.1073/pnas.1002431107

Olafson, E. R., Jamison, K. W., Sweeney, E. M., Liu, H., Wang, D., Bruss, J. E., Boes, A. D., & Kuceyeski, A. (2021). Functional connectome reorganization relates to post-stroke motor recovery and structural and functional disconnection. *NeuroImage*, *245*, 118642. https://doi.org/10.1016/j.neuroimage.2021.118642

Ovadia-Caro, S., Villringer, K., Fiebach, J., Jungehulsing, G. J., van der Meer, E., Margulies, D. S., & Villringer, A. (2013). Longitudinal effects of lesions on functional networks after stroke. *Journal of Cerebral Blood Flow and Metabolism: Official Journal of the International Society of Cerebral Blood Flow and Metabolism*, *33*(8), 1279–1285. https://doi.org/10.1038/jcbfm.2013.80

Park, C.-H., Chang, W. H., Ohn, S. H., Kim, S. T., Bang, O. Y., Pascual-Leone, A., & Kim, Y.-H. (2011). Longitudinal changes of resting-state functional connectivity during motor recovery after stroke. *Stroke; a Journal of Cerebral Circulation*, *42*(5), 1357–1362. https://doi.org/10.1161/STROKEAHA.110.596155

Parkes, L., Fulcher, B., Yücel, M., & Fornito, A. (2018). An evaluation of the efficacy, reliability, and sensitivity of motion correction strategies for resting-state functional MRI. *NeuroImage*, *171*, 415–436. https://doi.org/10.1016/j.neuroimage.2017.12.073

Power, J. D., Barnes, K. A., Snyder, A. Z., Schlaggar, B. L., & Petersen, S. E. (2012). Spurious but systematic correlations in functional connectivity MRI networks arise from subject motion. *NeuroImage*, *59*(3), 2142–2154. https://doi.org/10.1016/j.neuroimage.2011.10.018

Power, J. D., Mitra, A., Laumann, T. O., Snyder, A. Z., Schlaggar, B. L., & Petersen, S. E. (2014). Methods to detect, characterize, and remove motion artifact in resting state fMRI. *NeuroImage*, *84*, 320–341. https://doi.org/10.1016/j.neuroimage.2013.08.048

Ridley, B. G. Y., Rousseau, C., Wirsich, J., Le Troter, A., Soulier, E., Confort-Gouny, S., Bartolomei, F., Ranjeva, J.-P., Achard, S., & Guye, M. (2015). Nodal approach reveals differential impact of lateralized focal epilepsies on hub reorganization. *NeuroImage*, *118*, 39–48. https://doi.org/10.1016/j.neuroimage.2015.05.096

Roger, E., Pichat, C., Torlay, L., David, O., Renard, F., Banjac, S., Attyé, A., Minotti, L., Lamalle, L., Kahane, P., & Baciu, M. (2020). Hubs disruption in mesial temporal lobe epilepsy. A resting-state fMRI study on a language-and-memory network. *Human Brain Mapping*, *41*(3), 779–796. https://doi.org/10.1002/hbm.24839

Satterthwaite, T. D., Wolf, D. H., Loughead, J., Ruparel, K., Elliott, M. A., Hakonarson, H., Gur, R. C., & Gur, R. E. (2012). Impact of in-scanner head motion on multiple measures of functional connectivity: Relevance for studies of neurodevelopment in youth. *NeuroImage*, *60*(1), 623–632. https://doi.org/10.1016/j.neuroimage.2011.12.063

Schaefer, A., Kong, R., Gordon, E. M., Laumann, T. O., Zuo, X.-N., Holmes, A. J., Eickhoff, S. B., & Yeo, B. T. T. (2018). Local-Global Parcellation of the Human Cerebral Cortex from Intrinsic Functional Connectivity MRI. *Cerebral Cortex* , *28*(9), 3095–3114. https://doi.org/10.1093/cercor/bhx179

Schmahmann, J. D., & Pandya, D. N. (1997). The Cerebrocerebellar System. In J. D. Schmahmann (Ed.), *International Review of Neurobiology* (Vol. 41, pp. 31–60). Academic Press. https://doi.org/10.1016/S0074-7742(08)60346-3

Seitzman, B. A., Gratton, C., Laumann, T. O., Gordon, E. M., Adeyemo, B., Dworetsky, A., Kraus, B. T., Gilmore, A. W., Berg, J. J., Ortega, M., Nguyen, A., Greene, D. J., McDermott, K. B., Nelson, S. M., Lessov-Schlaggar, C. N., Schlaggar, B. L., Dosenbach, N. U. F., & Petersen, S. E. (2019). Trait-like variants in human functional brain networks. *Proceedings of the National Academy of Sciences of the United States of America*, *116*(45), 22851–22861. https://doi.org/10.1073/pnas.1902932116

Shinn, M., Hu, A., Turner, L., Noble, S., Achard, S., Anticevic, A., Scheinost, D., Todd Constable, R., Lee, D., Bullmore, E. T., & Murray, J. D. (2021). Spatial and temporal autocorrelation weave human brain networks. In *bioRxiv* (p. 2021.06.01.446561). https://doi.org/10.1101/2021.06.01.446561

Siegel, J. S., Ramsey, L. E., Snyder, A. Z., Metcalf, N. V., Chacko, R. V., Weinberger, K., Baldassarre, A., Hacker, C. D., Shulman, G. L., & Corbetta, M. (2016). Disruptions of network connectivity predict impairment in multiple behavioral domains after stroke. *Proceedings of the National Academy of Sciences of the United States of America*, *113*(30), E4367–E4376. https://doi.org/10.1073/pnas.1521083113

Siegel, J. S., Seitzman, B. A., Ramsey, L. E., Ortega, M., Gordon, E. M., Dosenbach, N. U. F., Petersen, S. E., Shulman, G. L., & Corbetta, M. (2018). Re-emergence of modular brain networks in stroke recovery. *Cortex; a Journal Devoted to the Study of the Nervous System and Behavior*, *101*, 44–59. https://doi.org/10.1016/j.cortex.2017.12.019

Sinitsyn, D. O., Legostaeva, L. A., Kremneva, E. I., Morozova, S. N., Poydasheva, A. G., Mochalova, E. G., Chervyakova, O. G., Ryabinkina, J. V., Suponeva, N. A., & Piradov, M. A. (2018). Degrees of functional connectome abnormality in disorders of consciousness. *Human Brain Mapping*, *39*(7), 2929–2940. https://doi.org/10.1002/hbm.24050

Song, J., Nair, V. A., Gaggl, W., & Prabhakaran, V. (2015). Disrupted brain functional organization in epilepsy revealed by graph theory analysis. *Brain Connectivity*, *5*(5), 276–283. https://doi.org/10.1089/brain.2014.0308

Termenon, M., Achard, S., Jaillard, A., & Delon-Martin, C. (2016). The "Hub Disruption Index," a Reliable Index Sensitive to the Brain Networks Reorganization. A Study of the Contralesional Hemisphere in Stroke. *Frontiers in Computational Neuroscience*, *10*, 84. https://doi.org/10.3389/fncom.2016.00084

Tian, N., Liang, L.-K., Luo, X.-M., Hu, R.-L., Long, W.-S., & Song, R. (2022). More than just statics: altered complexity of dynamic amplitude of low-frequency fluctuations in the resting brain after stroke. *Journal of Neural Engineering*, *19*(3). https://doi.org/10.1088/1741-2552/ac71ce

Vargha, A., & Delaney, H. D. (2000). A Critique and Improvement of the "CL" Common Language Effect Size Statistics of McGraw and Wong. *Journal of Educational and Behavioral Statistics: A Quarterly Publication Sponsored by the American Educational Research Association and the American Statistical Association*, *25*(2), 101–132. https://doi.org/10.2307/1165329

Wang, C., Qin, W., Zhang, J., Tian, T., Li, Y., Meng, L., Zhang, X., & Yu, C. (2014). Altered functional organization within and between resting-state networks in chronic subcortical infarction. *Journal of Cerebral Blood Flow and Metabolism: Official Journal of the International Society of Cerebral Blood Flow and Metabolism*, *34*(4), 597–605. https://doi.org/10.1038/jcbfm.2013.238

Xie, X., Zhang, T., Bai, T., Chen, C., Ji, G.-J., Tian, Y., Yang, J., & Wang, K. (2022). Resting-State Neural-Activity Alterations in Subacute Aphasia after Stroke. *Brain Sciences*, *12*(5). https://doi.org/10.3390/brainsci12050678

Yan, C.-G., Cheung, B., Kelly, C., Colcombe, S., Craddock, R. C., Di Martino, A., Li, Q., Zuo, X.-N., Castellanos, F. X., & Milham, M. P. (2013). A comprehensive assessment of regional variation in the impact of head micromovements on functional connectomics. *NeuroImage*, *76*, 183–201. https://doi.org/10.1016/j.neuroimage.2013.03.004

Yushkevich, P. A., Piven, J., Hazlett, H. C., Smith, R. G., Ho, S., Gee, J. C., & Gerig, G. (2006). User-guided 3D active contour segmentation of anatomical structures: significantly improved efficiency and reliability. *NeuroImage*, *31*(3), 1116–1128. https://doi.org/10.1016/j.neuroimage.2006.01.015

Zwiers, M., Moia, S., & Oostenveld, R. (2021). BIDScoin: A user-friendly application to convert source data to the Brain Imaging Data Structure. *Frontiers in Neuroinformatics*, *15*, 65. https://doi.org/10.3389/fninf.2021.770608

Conclusion

Across three chapters, I used both hypothesis-based and data-driven analyses to investigate how intrinsic dynamics vary across different areas of the human brain, as well as how different aspects of these dynamics are related to other features of brain structure and function. While the results of these studies provide new insight into multiple aspects of functional brain organization, together they suggest three broad conclusions.

First, I demonstrate that while cortical timescales estimated from resting BOLD fMRI are largely consistent across datasets and analytic methods, they depart at least to some extent from canonical axes of cortical organization. In particular, while timescales do appear to lengthen from primary sensorimotor areas to heteromodal association regions, limbic and paralimbic areas actually exhibit the shortest rather than longest timescales. This raises important questions about whether regional differences in BOLD timescales reflect underlying differences in neural timescales versus other factors (neurophysiological or artefactual). Studies which have directly compared BOLD timescales to electrophysiological timescales have generally found good correspondence, but more work is needed on this topic, especially as an increasing number of studies seek to use BOLD timescales to study individual differences in functional brain organization. Additional work is also needed to further establish the relevance of BOLD timescales to cognition and behavior in health and disease.

Second, I demonstrate that regardless of their correspondence with underlying electrophysiological dynamics, BOLD timescales show robust relationships to multiple features of structural and functional network topology. In particular, I replicate prior reports that regions with extensive structural connectivity tend to exhibit longer timescales, consistent with their putative role in integrating signals across many other brain areas. I show for the first time that BOLD timescales are also correlated with topological measures which consider the modular organization of brain networks. In group-level analyses, I find that longer timescales are associated with extensive functional connectivity to other areas in the same network module, and diverse structural connectivity to regions in other modules. These effects replicate across multiple data sets. I additionally show that the relationship between timescales and within-module functional connectivity also exists within individual participants and in individual cortical areas across participants. Further, single-subject analyses suggest that timescales are also associated with global connectivity and the degree to which each cortical area acts as a "connector" between network modules. These latter results should be considered preliminary until they are replicated, but emphasize the importance of studying functional brain organization at the level of the individual. More generally, however, these results make a significant contribution to our understanding of the relationship between brain connectivity and dynamics.

Finally (but no less significantly), I demonstrate the importance of considering the myriad ways in which intrinsic dynamics can vary between brain areas. In particular, I show that in addition to varying in the timescale over which their intrinsic activity fluctuates, cortical areas also differ

in the extent to which distributional features (variance and kurtosis) tend to increase (or to a lesser extent, decrease) over the course of a resting scan. Further, I show that this novel axis of dynamical variation is more strongly associated with anatomical and information processing hierarchies, while timescales—in line with the results from my other analyses—show a stronger association with the connectomic properties of each region. Critically, the changes in variance and kurtosis I identify in my data-driven analysis are fundamentally different from timescale insofar as they capture a particular pattern of change over time, whereas timescales are agnostic to the arrow of time. As such, we hypothesize that they may reflect the dynamics of arousal and cognition during the resting state. Further work is needed to evaluate this hypothesis.